UTS UNIVERSITY OF TECHNOLOGY SYDNEY

Developing an Efficiency Relationship for Tapered Pile Groups in Sand Using Analytical and 3D Numerical Analysis

by Amin Shafaghat

Thesis submitted in fulfilment of the requirements for the degree of

Doctor of Philosophy (PhD)

under the supervision of A/Prof. Hadi Khabbaz and A/Prof Behzad Fatahi

University of Technology Sydney
Faculty of engineering and information technology (FEIT)

January 2022

CERTIFICATE OF ORIGINAL AUTHORSHIP

I, Amin Shafaghat, declare that this thesis, is submitted in fulfilment of the requirements for the award of Doctor of Philosophy (PhD), in the School of civil and environmental engineering, faculty of engineering and information technology (FEIT) at the University of Technology Sydney.

This thesis is wholly my own work unless otherwise referenced or acknowledged. In addition, I certify that all information sources and literature used are indicated in the thesis. This document has not been submitted for qualifications at any other academic institution. This research is supported by the Australian Government Research Training Program.

Signature:

Production Note:
Signature removed prior to publication.

Date: 22/01/2022

Abstract

It is remarkable that a small tapering angle can boost the bearing capacity of a pile foundation notably. It implies that a pile with a small tapering angle, resembling a truncated cone, can approximately accommodate up to 40% more structural loading than its counterpart same volume cylindrical pile.

This study aims to establish an equation for obtaining the optimum tapering angle of bored tapered piles correlated to the pile geometry and sand properties varying with the relative density. The optimum tapering angle corresponds to the maximum axial bearing capacity, while keeping the volume of material in the tapered pile the same as the counterpart straight cylindrical pile.

Firstly, analytical formulations are developed to estimate the axial bearing capacity of bored tapered piles embedded in sand. The proposed governing equations capture the shaft vertical bearing component of the tapered pile, which is unique to tapered piles and varies nonlinearly with the tapering angle. By differentiating the obtained bearing capacity equation with respect to the tapering angle, an optimum tapering angle is achieved. The finite element method, mostly using PLAXIS, is also adopted to conduct the numerical modelling and to calibrate the model parameters of the proposed analytical equation, considering the soil nonlinearities and interaction between the tapered pile and the surrounding soil subjected to axial loading. UBC sand constitutive model is used to simulate the soil response in the vicinity of the tapered pile; and the model parameters are calibrated against laboratory test results for sandy soils with different relative densities. However, due to the complexity of the proposed differentiation and inverse calculation, a numerical solution is used to obtain the results. Consequently, the load-displacement curves of the tapered piles are attained numerically, and the optimum tapering angle, resulting in the maximum axial capacity of the pile, is determined. Results exhibit a good agreement between the analytically determined axial bearing capacity for the tapered pile and the corresponding numerical modelling predictions. Furthermore, a simplified empirical equation is established to select the optimum tapering angle, which can readily be

used by practicing engineers. On the other hand, a new simple equation for prediction of pile group efficiency considering the effect of tapering angle in cohesionless soil under vertical loading condition is developed. Firstly, a simple analytical relationship based on the mathematical definition of the pile group efficiency is developed. However, the effect of tapering angle is captured by defining a new geometry efficiency coefficient related to the shaft vertical bearing component of tapered piles. Thereafter, this new mathematical equation is developed, considering the shaft vertical bearing ratio and the new geometry efficiency coefficient. Furthermore, a numerical analysis is performed for modelling single cylindrical and tapered piles as well as pile groups to validate the proposed mathematical equation. Subsequently, the load-displacement diagrams for a single pile and group of piles are obtained. Then, the bearing capacities of cylindrical and tapered bored piles both as single and group are computed and compared using specific settlement criterion. Besides, the friction resistance ratio and the shaft vertical bearing ratio are separated using existing numerical methods. Having the ratios of various components of bearing capacity, pile group efficiencies can be obtained from both the numerical and mathematical models. The results show that the proposed equation can predict the pile group efficiency by considering the tapering angle as well as other affecting parameters as a simple and novel relationship.

Finally, step-tapered piles (those with a larger top diameter, and a smaller diameter at lower sections) are analysed numerically. In this study the behaviour of step-tapered piles having only one step under axial loading condition is investigated. Three series of piles embedded in sand are examined numerically using the three-dimensional finite element method. Each set consists of five piles, including one reference straight sided wall pile and four step-tapered piles having the same volume. Different internal friction angles (to represent loose, medium and dense sands) and corresponding elastic modulus and lateral earth pressure coefficients are considered to observe their effect on the bearing capacity and settlement of piles. The load-displacement diagram of each pile is obtained, and accordingly, the frictional and end bearing resistances are calculated. Some MATLAB codes are developed to get the numerical data and carry out the calculations. Moreover, the normal and shear stress states, plastic points, and deformations around the step and toe of piles are

computed and compared. According to the results, the advantages of step-tapered piles over their counterpart cylindrical ones in terms of bearing capacity and settlement are discussed. Finally, the optimum stepped length of the pile is determined.

To my late father,

My lovely mother,

My wise brother

And

My supportive fiancé whose love and encouragements have always been with me throughout this journey.

Acknowledgement

During this challenging and pleasant journey, I learned many things beyond my specific area of expertise from some nice people around me. Therefore, I would like to mention some of them below and to appreciate them as I definitely owe them this achievement.

I am very grateful to my very knowledgeable supervisors, Associate Professor Hadi Khabbaz and Associate Professor Behzad Fatahi, who guided me throughout this journey. Unquestionably, I will always be appreciable to them and owe both of them a very big thank you. Thanks to their supervision during my research at UTS, I could develop my research professionally in several good journal papers as well as prestigious conferences and book chapters. On the other hand, now that I am comparing myself to where I was standing before starting the PhD at UTS, I can see how I have been developed myself as well. Therefore, I believe this approximately four years of my life that I dedicated to my research at UTS as a PhD student, was a very right time and right place that I was standing in. I also thank Miss Van Le, the school academic officer, who dedicatedly supported me during my research at UTS.

I should confess that my mother and my brother, Amirhosein, played a significant role in my success to reach to this current point. Although, spending about four years far away from them as an overseas PhD student made this research journey rather difficult, they both covered me from long distance and encouraged me with their positive attitude and constructive advices. I am very grateful to them both and will never take their existence in my life as granted, particularly after losing my late father.

My best ever gift in my life, my lovely fiancé Sahar who supported me every day and every moment. I truly don’t know which word I should use to describe her significant role on my success. Having a supportive, kind, understanding, energetic, funny, generous, creative, loyal and diligent person by my side, made it much easier for me

to overcome the difficulties of this journey. I am grateful for having her in my life and do appreciate her support during this time.

Moreover, my friends whose existence around me was full of positive energy and motivation, particularly in tough situations. I am grateful to Danon and Sasan as two of my best friends who encouraged me during this journey. Having you lovely friends around me is one of the reasons for where I am standing.

I am also grateful to Australian Government research program and university of technology Sydney for supporting my PhD studies with a full scholarship. Many thanks to the Graduate Research School (GRS) and Faculty of Engineering and Information Technology (FEIT) for providing financial assistance for me to attend conferences and to be able to present my work for my peers from all over the world.

Finally, this thesis has been completed during the pandemic of Covid-19, which was a big challenge for humankind. Hence, as a researcher, I appreciate all the scientists who are working on novel methods to manufacture effective vaccines and medications to break off the pandemic.

List of publications extracted from this thesis

Journal papers:

Shafaghat, A., & Khabbaz, H. (2020). Recent advances and past discoveries on tapered pile foundations: a review. Geomechanics and Geoengineering, 1-30.

Shafaghat, A., Khabbaz, H., Fatahi, B. (2021). Analytical and Numerical Approaches to Attain the Optimum Tapering Angle for Axially Loaded Bored Piles in Sandy Soils. International Journal of Geomechanics, ASCE, DOI: 10.1061/ (ASCE) GM.1943-5622.0002056

Shafaghat, A., Khabbaz, H., Fatahi, B. (2021). Axial and Lateral Efficiency of Tapered Pile Groups in Sand Using Mathematical and Three-Dimensional Numerical Analyses, Published in the journal of Performance of Constructed Facilities, ASCE

Book chapters and conference papers:

Shafaghat, A. and Khabbaz, H., 2021. Numerical Evaluation of Bearing Capacity of Step-Tapered Piles Using P-Y Curves Analysis. In Advancements in Geotechnical Engineering (pp. 200-212). Springer, Cham.

Shafaghat, A., Khabbaz, H., Fatahi, B. (2021). Developing an Efficiency Equation for Tapered Pile Groups in Sand Using Mathematical and Numerical Analyses (Sustainable Civil Infrastructures)

Table of Contents

Abstract ii

Acknowledgement vi

List of extracted publications viii

1 Chapter 1: Inroduction 1

1.1 Introduction 1

1.2 History and development of tapered piles 2

1.3 Problem statement 5

1.4 Objectives 7

1.5 Scope and limitations of the work 7

1.6 Structure of the thesis 7

2 Chapter 2: Literature Review 9

2.1 Introduction 9

2.2 Past experiences and recent discoveries 10

2.3 Statically axial and lateral loading conditions 11

2.3.1 Experimental investigations 11

2.3.2 Analytical investigations 37

2.3.3 Numerical investigations 41

2.4 Dynamic axial and lateral loading conditions 44

2.4.1 A brief review of experimental, numerical and theoretical models 44

2.4.2 Tapering angle, slenderness ratio and stiffness effects 45

2.4.3 Load-displacement behaviour 47

2.4.4 Mathematical developments 49

2.5 Case history on tapered piles application 50

2.6 Pile group 51

2.6.1 Efficiency of pile groups 52

2.7 Summary and gap identification 59

3 Chapter 3: Methodology of the Numerical Modelling and Soil Calibration Exercise 62

3.1 Introduction 62

3.2 Adopted soil constitutive model 62

3.3 Overview of the model 64

3.4 Soil calibration exercise 68

4 Chapter 4: Analytical and Numerical Approaches to Attain the Optimum Tapering Angle for Axially Loaded Bored Piles in Sandy Soils 73

4.1 Introduction 73

4.2 Analytical development for ultimate axial bearing capacity of bored tapered piles in sand 75

4.3 Numerical results and discussion 89

4.4 Simplified equation for selecting optimum tapering angle 110

4.5 Validation of the numerical model with field test results 113

4.6 Summary 116

5 Chapter 5: Developing an Efficiency Equation for Tapered Pile Groups in Sand Using Mathematical and Numerical Analyses 118

5.1 Introduction 118

5.2 Existing group efficiency equations 120

5.3 Analytical approach 121

5.4 Three-dimensional finite element modelling and overview of the numerical models 125

5.5 Validation of the obtained efficiency equation using 3D FEM numerical analysis 129

5.6 Validation of the obtained efficiency equation using field test data 135

5.7 Summary 136

6 Chapter 6: Numerical Evaluation of Bearing Capacity of Step-tapered Piles Using p-y Curves Analysis 137
6.1 Introduction 137
6.2 Modelling in PLAXIS 2D 138
6.3 Calculation of bearing capacity of piles 139
6.4 Model properties selection 141
6.5 The properties of used soil 144
6.6 Results and discussion 145
6.6.1 Results of bearing capacity and settlement 145
6.6.2 Stress states and plastic points around piles 146
6.6.3 The state of stress on the end surface of the pile (base) 149
6.7 Summary 150
7 Chapter 7: Conclusions and Ideas for Future Research on Tapered Piles .. 151
7.1 Summary 151
7.2 Concluding remarks 152
7.3 New directions and ideas for future research on tapered pile foundations . 154
References 158
Appendix A – Differentiations with respect to tapering angle 169
Appendix B – Developed MATLAB codes 172

List of Figures

Figure 1.1. Common types of cast-in-place (patented) piles: (a) Commonly used uncased pile; (b) Franki uncased pedestal pile; (c) Franki cased pedestal pile; (d) welded or seamless pipe; (e) Western cased pile; (f) Union or monotube pile (tapered); (g) Raymon pile (h) step-tapered pile (modified after Bowles (1996)) 3

Figure 2.1. Variation of shaft resistance coefficient Kt with lateral stress (after El Naggar and Wei, 1999a) 17

Figure 2.2. Taper coefficient values Kt obtained from the laboratory experiments and the theoretical values in different overburden pressures (after El Naggar and Sakr, 2000; Sakr and El Naggar, 2003) 18

Figure 2.3. Effects of tapering angle on (a) the base taper coefficient (TFb); (b) the shaft taper coefficient (TFs) for different lateral earth pressures (after Paik et al., 2013) 20

Figure 2.4. Effects of K_0 for the tapering angle of 1° in different relative densities 22

Figure 2.5. Comparing different taper coefficients with different confining pressures presented by different researchers (data are taken from Naggar & Sakr, 2000; Paik et al., 2013; Sakr & El Naggar, 2003) 23

Figure 2.6. Effect of tapering angle on the normalized pile capacity using cavity expansion theory (any reference?) 24

Figure 2.7. Decreasing trend of the horizontal subgrade modulus reaction with deflection (any reference?) 25

Figure 2.8. Distribution of the ultimate load by pile point for various applied confining pressures (after Wei and El Naggar, 1998) 27

Figure 2.9. Shaft friction of tapered and straight-sided wall pile in-depth under various confining pressures in medium-dense sand (after El Naggar and Wei, 2000b) 28

Figure 2.10. Measured stresses variation at different applied confining pressure levels (after El Naggar and Wei, 1999a) 28

Figure 2.11. Distribution of moment along pile shaft subjected to ultimate pile load using toe driving under 30 and60kPa confining pressures (after Sakr et al., 2005) 29

Figure 2.12. Comparative moment diagrams of both analyses at a confining pressure of 60kPa 30

Figure 2.13. Load-displacement curves for piles (a) base load and (b) shaft load (after Paik et al., 2010) 31

Figure 2.14. Load-settlement curves for piles tested using the head driving method at (a) low confining pressures (b) high confining pressure (after Sakr et al., 2004) 32

Figure 2.15. Load-settlement diagrams for piles embedded in soil with different confining pressures (a) tapered pile in dense sand (b) straight side pile in dense sand (c) tapered pile in loose sand (d) straight side pile in loose sand (after Wei, 1998) 33

Figure 2.16. Variation of lateral earth pressure coefficient surrounding the pile body vs tapering angle (after Nordlund, 1963) 35

Figure 2.17. Comparative p-y diagrams of piles under static lateral loading condition at zero confining pressure 37

Figure 2.18. The schematic of complete tapered pile and its element (complete tapered pile; and the element at depth x) (after Kodikara and Moore, 1993) 38

Figure 2.19. Schematic diagram of a single tapered pile and the element forces (after Liu et al., 2012) 39

Figure 2.20. Optimum tapering angles of piles in sand with various friction angles (a) Loose sand, (b) Medium sand, (c) Dense sand (after Hataf and Shafaghat, 2015) 43

Figure 2.21. Effect of tapering angle on resonant frequency and amplitude (a) $\vartheta = 0.33; vs = 105 ft/sec$; l/r=20; r=3.94in. b) $\vartheta = 0.33; vs = 315 ft/sec$; l/r=20; r=5.91in (after Saha and Ghosh, 1986) 45

Figure 2.22. Dimensionless amplitude vs. vibration frequency for (a) end-bearing piles (b) floating piles (after Bryden et al., 2018) 47

Figure 2.23. Load-settlement diagrams of piles having different tapering angles at no confining pressure (a) the first load cycles (b) the last (10th) load cycles (after El Naggar and Wei 2000a) 48

Figure 2.24. Measured versus Calculated Load-Settlement Curves for JFKIA (after Horvath and Trochalides, 2004) 50

Figure 2.25. Stresses surrounding a pile and the summing effects of a pile group (after Bowles 1996) 51

Figure 2.26. Distribution of vertical stress under individual pile and pile group (pressure-area formula, after Chellis 1969)..... 56

Figure 2.27. The diagram of group efficiency coefficient (after Kishida 1965). 57

Figure 2.28. Group efficiency diagrams for various S/D ratios (after Vesic 1967) 58

Figure 3.1. The methodology to design tapered pile models used in the numerical analysis based on the cylindrical reference pile with constant volume, b) The shear stress bulbs beneath the toe and surrounding the pile shaft (i.e. cylindrical pile, loose sand, L/D=10)..... 66

Figure 3.2. Elements utilized by adopted finite-element model, a) Nodes, b) Stress points..... 66

Figure 3.3. Axisymmetry model of a tapered pile along with the interfaces and the meshed model..... 67

Figure 3.4. Comparison of (deviatoric stress vs axial strain) data and numerical calibration for various confining pressures of drained triaxial compression tests on isotropically consolidated, (a) Loose Cambria sand, data taken from Lade & Bopp (2005), (b) Medium Toyoura sand, data taken from Fukushima & Tatsuoka (1984), (c) Dense Sacramento River sand, data taken from Lee & Seed (1967) 70

Figure 3.5. Comparison of (volumetric strain vs axial strain) data and numerical calibration for various confining pressures of drained triaxial compression tests on isotropically consolidated, (a) Loose Cambria sand, data taken from Lade & Bopp (2005), (b) Medium Toyoura sand, data taken from Fukushima & Tatsuoka (1984), (c) Dense Sacramento River sand, data taken from Lee & Seed (1967) 71

Figure 4.1. Free body diagram of shaft resistance force component of an element 75

Figure 4.2. Schematic diagram of the stress state for an element adjacent to pile shaft for both bored cylindrical and tapered piles embedded in sand (before and after loading) 76

Figure 4.3. The schematic shape of a tapered pile divided into segments and the ledge force component (rc,Dc are radius and the diameter of the reference cylindrical pile with the same volume) 78

Figure 4.4. Schematic bottom perspective of a step-tapered pile with six ledges 79

Figure 4.5. Correlation between the assumed simplified equation for the taper coefficient (kt) and the equation proposed by El Naggar and Sakr (2000) (Assuming Sr=Up/D=0.1) 83

Figure 4.6. Correlation between the assumed simplified equation for the bearing capacity factor and the equation proposed by Paik et al. (2013) 85

Figure 4.7. Schematic load transfer curve, the failure wedges beneath cylindrical and tapered piles and the ψ definition used in Nq factor (modified after Janbu 1976) 86

Figure 4.8. Flow chart of the applied algorithm in numerical solution based on Cauchy method (after Baesso et al. 2007) 88

Figure 4.9. Variation of optimum tapering angle of piles having different L/D ratios embedded in different sands obtained from numerical solution 89

Figure 4.10. Load-displacement diagrams of tapered and straight-sided piles with L/D=10 in loose (Cambria), medium (Toyoura) and dense (Sacramento River) sands 90

Figure 4.11. Load-displacement diagrams of tapered and straight-sided piles with L/D=20 in loose (Cambria), medium (Toyoura) and dense (Sacramento River) sands 90

Figure 4.12. Load-displacement diagrams of tapered and straight-sided piles with L/D=30 in loose (Cambria), medium (Toyoura) and dense (Sacramento River) sands 91

Figure 4.13. Load-displacement diagrams of tapered and straight-sided piles with L/D=40 in loose (Cambria), medium (Toyoura) and dense (Sacramento River) sands 91

Figure 4.14. Variation of different components of ultimate bearing capacity for different tapering angels (L/D=10 & L/D=20) a) Total bearing (QT) b) Base resistance (BRT) c) Frictional resistance (FRT) d) Shaft Vertical resistance (SVRT) 96

Figure 4.15. Variation of different components of ultimate bearing capacity for different tapering angels (L/D=30 & L/D=40) (a) Total bearing (QT) (b) Base resistance (BRT) (c) Frictional resistance (FRT) (d) Shaft Vertical resistance (SVRT) 100

Figure 4.16. Relative shear stress distribution around piles with different slenderness ratios in sand with various relative densities (Loose Cambria sand,

Medium Toyoura sand, and Dense Sacramento River sand), (C: Cylindrical, T: Tapered) 107

Figure 4.17. Validation of the proposed analytical model for obtaining the bearing capacity with numerical results for various L/D ratios and different types of sand (a) L/D=10, (b) L/D=20, (c) L/D=30, (d) L/D=40..... 109

Figure 4.18. Variation of optimum tapering angel versus length to diameter ratio for loose sand (Cambria), medium sand (Toyoura), dense sand (Sacramento River) obtained from numerical analysis 111

Figure 4.19. Schematic of bored piles along with the manufactured augers by Lee et al. (2009) for installing and testing piles at Iksan City in the southern region of the Republic of Korea..... 114

Figure 4.20. Comparison between the load-displacement diagrams obtained from numerical modelling and pile load tests conducted by Lee et al. (2009)..... 115

Figure 5.1. Tapered pile group and the separated resistance forces..... 121

Figure 5.2. Bottom view of a typical pile group pattern and the geometry efficiency coefficients definition a) shaft geometry efficiency ($\eta s'$) b) shaft vertical bearing geometry efficiency (ηsv) 123

Figure 5.3. Enhanced meshed system used for piles in 3D numerical analyses, (a) Single pile and group of four piles, (b) Pile group along with the adjacent soil used in numerical analysis..... 126

Figure 5.4. Interfaces surrounding the individual piles and at the lateral and bottom faces of pile blocks (a) Pile block along with the single pile and the interfaces (b) The interface of pile group below the pile block (bottom view) (c) Pile toe interfaces (bottom view) 128

Figure 5.5. Load-displacement curves for single and group of cylindrical pile modellings, (Loose Cambria sand) 131

Figure 5.6. Load-displacement curves for single and group of tapered pile modellings, (Loose Cambria sand) 131

Figure 5.7. Relative shear stress state on the end surface of the block of pile groups (bottom view), (a) Cylindrical pile group, (b) Tapered pile group (α=1.4°)..... 133

Figure 5.8. Vertical displacement state on the end surface of the block of pile groups (bottom view), (a) Cylindrical pile group, (b) Tapered pile group (α=1.4°) 134

Figure 6.1. The schematic shape of a step-tapered pile and the failure zone beneath the ledge 140

Figure 6.2. The schematic shape of step-tapered along with their cylindrical reference pile 143

Figure 6.3. Step-tapered pile model in Plaxis 2D along with the pile-soil interface 144

Figure 6.4. The P-Y curves of cylindrical reference pile and step-tapered piles in sand with Φ=33º 146

Figure 6.5. Distribution of plastic points around the piles (a) Cylindrical pile, 147

Figure 6.6. Principal stress directions around (a) Cylindrical pile (b) Step-tapered pile ST1 147

Figure 6.7. Relative shear stress distribution on the pile shaft 149

List of Tables

Table 1.1. Summary of several pile tests for estimating the lateral earth pressure coefficient (LEPC) (after Bowles, 1996) 4

Table 2.1. Summary of the experimental investigations conducted on tapered piles 13

Table 2.2. Comparison of the capacity of tapered and straight piles (after Khan et al., 2008)..... 34

Table 2.3. Bearing capacity of straight and tapered piles with 0.73 m length (after Spronken, 1998)..... 36

Table 2.4. The geometry properties of the modelled tapered pile (Hataf & Shafaghat, 2015)..... 42

Table 3.1. Geometry of all piles with various slenderness ratios used in numerical analysis..... 65

Table 3.2. Sandy soil properties obtained from soil calibration exercise using UBC sand model..... 72

Table 4.1. Compared optimum tapering angels obtained from analytical and numerical methods..... 112

Table 4.2. Soil properties at the site of Iksan City in the southern region of the Republic of Korea (after Lee et al. 2009) 114

Table 4.3. Comparison of bearing capacity results obtained from various methods 116

Table 5.1. Geometry of the piles used in the numerical analyses..... 125

Table 5.2. Pile material parameters..... 129

Table 5.3. Sandy soil properties adopted for numerical analysis based on UBC sand model (loose Cambria sand)..... 130

Table 5.4. Bearing capacity ratios of a single same volume cylindrical and tapered piles..... 132

Table 5.5. Comparison between pile group efficiencies achieved from the proposed model of this study and values obtained from other sources, including numerical, theoretical and experimental investigations 135

Table 6.1. Meshing properties used in modelling 138

Table 6.2. Different considered conditions for modelling in sand 141

Table 6.3. Properties of step-tapered piles having the same volume as cylindrical reference piles 142

Table 6.4. Properties of used concrete in modelling 143

Table 6.5. Properties of used sand in modelling 145

Table 6.6. Comparison between the bearing capacities of same volume piles in loose sand (Set 1) 148

Table 6.7. Comparison between the bearing capacities of same volume piles in medium sand (Set 2) 148

Table 6.8. Comparison between the bearing capacities of same volume piles in dense sand (Set 3) 149

List of Notations

English letters

A_b: Pile toe area;

A_{bn}: Projected area of the ledge of a segment;

A_{p-bot}: Step-tapered pile toe area;

A_{p-top}: Step-tapered pile top cross-section area;

A_s: Pile lateral surface area;

A_{sn}: Lateral surface area of an element;

D_{av}: Average diameter of a tapered pile;

D_b : Base diameter of a tapered pile;

D_{top} : Top diameter of a tapered pile;

E_{50}: Young's modulus (The secant modulus in drained triaxial test);

E_{oed}: Young's modulus (Tangent modulus for primary oedometer loading);

E_{ur}: Young's modulus (Unloading-Reloading);

K: Lateral earth pressure coefficient;

K_0: At rest lateral earth pressure coefficient;

K_t: Taper factor for the shaft resistance of tapered piles;

L: Length of pile;

m: Number of piles in each row;

n: Number of piles in each column;

N_t: Bearing capacity factor for tapered piles;

P_g: Perimeter of a group of piles;

P_s: Perimeter of a single of piles;

Q_b: Base bearing capacity of a single pile;

Q_f: Frictional bearing capacity of a single pile;

Q_g: Total bearing capacity of a pile group;

Q_s: Total bearing capacity of a single pile;

Q_{sv}: Shaft Vertical bearing capacity of a single pile;

r: Radius of the pile's nth segment;

R_f: Failure ratio;

R_{inter}: Interface coefficient;

S: Spacing between piles in a group;

S_g: Settlement of a pile group;

S_s: Settlement of a single pile;

V_c: Volume of a cylindrical pile;

V_t: Volume of a tapered pile;

q_{bt}: Toe resistance of a single pile;

q_{st}: Shaft resistance of a single pile;

q_{sv}: Vertical bearing resistance stemming from the body of a tapered pile;

r_b: Bottom radius of the pile;

r_c: Radius of the counterpart same volume cylindrical pile;

r_t: Top radius of the pile;

η'_s: Geometric efficiency coefficient (Shaft resistance);

η'_{sv}: Geometric efficiency coefficient (Shaft vertical resistance);

ϕ_i: Internal friction angle of the interface;

Greek letters

α: Tapering angle;

α_{max}: Maximum tapering angle for a pile with constant volume;

α_{opt}: Optimum tapering angle;

α_r: Ratio of optimum tapering angle to the maximum tapering angle;

β: Correlation coefficient;

γ: Soil unit weight;

γ^p: Plastic shear strain increment;

η_f: Stress ratio at failure;

ν_i: Poisson's ratio of the interface;

σ': Mean stress in the plane of loading;

σ'_b: Effective stresses at pile toe and mid-length of the pile;

σ'_{bn}: Effective normal stress (at the middle of the nth pile element);

σ'_m: Effective stresses at mid-length of the pile;

ϕ_i: Internal friction angle of the interface;

$d\varepsilon_v^p$: Increment of plastic volumetric strain;

$d\eta$: Change in shear stress ratio;

δ: Pile-soil interface friction angle;

ζ: A correlation coefficient controls the approaching rates of assumed functions for parameters;

η: Shear stress ratio;

η_g: Pile group efficiency;

λ: Correlation coefficient;

μ: A coefficient corresponding to the portion of mobilized Passive earth pressure coefficient;

τ: Shear stress;

ψ: A coefficient in bearing capacity factor suggested by Janbu corresponding to relative density;

ψ': Dilation angle of soil;

ϕ: Internal friction angle of soil;

ϕ': Effective soil friction angle;

Chapter 1

Introduction

1.1 Introduction

Due to the increasing demand for more efficient and cost-effective foundations in the construction sector, geotechnical engineers are pursuing research on finding novel ideas to design foundations providing higher bearing capacities, while using less or eco-friendly materials. Many investigations have been conducted into understanding the behaviour of tapered piles. Some of them are indicating the advantages of this kind of piles compared to their counterpart cylindrical ones, and some of them are presenting specific circumstances wherein the advantages of tapered piles can far outweigh the straight-sided wall piles. However, it seems that there are some gaps for appraising whether using such piles are adequately beneficial to be substituted with the cylindrical ones.

Besides, finding the theory behind the idea of tapered piles can be of considerable significance to make a decision. The question arises from the point that what happens when the shaft of a straight-sided wall pile get inclined and by increasing this inclination which aspects of the pile change. Moreover, finding the answer to the

question whether any specific tapering angle for these piles reported enhancing the bearing capacity while being in the allowable settlement zone, may contribute to a much sound judgment regarding their advantages. Many previously published investigations have introduced tapered piles as effective replacements for conventional cylindrical piles. However, one of the main objectives of this study is to shed light on the conditions and aspects that can make these piles more beneficial in the construction of deep foundations.

This study is presenting a comprehensive review on tapered pile foundations comprising experimental, analytical and numerical investigations in Chapter 2. This includes both axial and lateral behaviour of tapered piles for static and dynamic loading conditions. Moreover, this study mainly focuses on studying the behaviour of bored tapered piles embedded in sandy soil.

1.2 History and development of tapered piles

Tapered piles are one of the first human-made piles since they were from timber materials, which were available easily for construction purposes. Various geometrical shapes and pile materials have frequently been implemented in the construction of structures. Concrete, steel, and timber piles are more commonly employed in building foundations. Piles with different cross-sectional shapes such as square, circular or H shape are regularly used, which are commonly straight in length with a small number of exclusions (i.e., timber tapered piles, monotube piles, Raymond step-tapered piles, and taper-tube piles). Figure 1.1 demonstrates different kinds of piles embedded in soil.

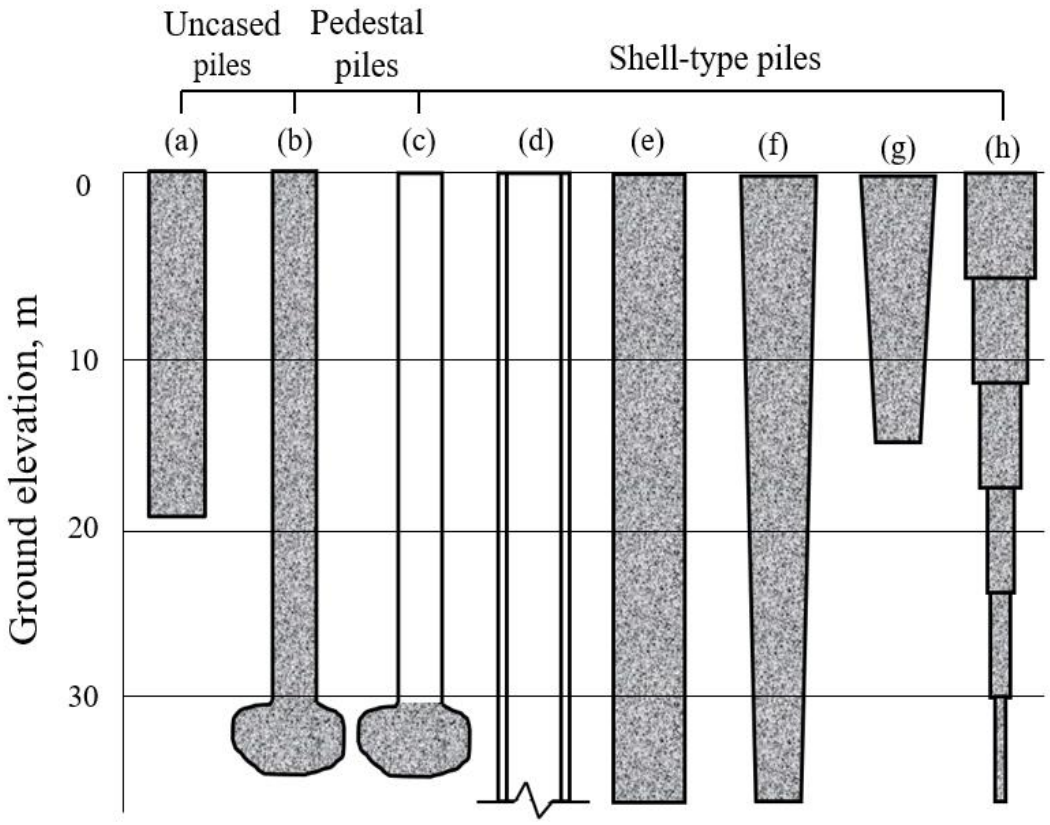

Figure 1.1. Common types of cast-in-place (patented) piles: (a) Commonly used uncased pile; (b) Franki uncased pedestal pile; (c) Franki cased pedestal pile; (d) welded or seamless pipe; (e) Western cased pile; (f) Union or monotube pile (tapered); (g) Raymon pile (h) step-tapered pile (modified after Bowles (1996))

Depths shown indicate usual ranges for the various piles. Due to the inclined body of tapered piles, the soil surrounding the piles are compacted during pile driving (ASCE 1984; Dougherty 2017; Poulos 1979). This issue can contribute to a higher lateral earth pressure coefficient in the adjacent soil. Table 1.1 illustrates some estimations for the lateral earth pressure coefficient (LEPC) based on several pile tests. The tapered piles used for tests were made of timber material. However, the values obtained in tension tests for step-tapered piles were not accepted since tests were performed in saturated soil, and the values might have resulted from water suction in the point region. In other words, the negative pressure in soil can increase the effective stress and consequently intensify the lateral earth pressures. Due to this reason, the obtained lateral earth pressures cannot be precise and reliable.

Table 1.1. Summary of several pile tests for estimating the lateral earth pressure coefficient (LEPC) (after Bowles, 1996)

Reference	H piles	Pipe	Precast concrete	Timber	Tapered	Tension tests
Mansur and Hunter (Mansur, 1970)	1.4-1.9	1.2-1.3	1.45-1.6	1.25	-	0.4-09 All types
Tavenas (Tavenas, 1971)	0.5	-	0.7	-	1.25	-
Ireland (Ireland, 1957)	-	-	-	-	-	1.11-3.64
API (American Petroleum Institute, 1984)	-	1.0-0.8	1.0	-	-	-

Referring to Table 1.1, the lateral earth pressure coefficient (LEPC) estimated for timber tapered piles is about 1.25. However, other studies suggested different values for this coefficient, which is discussed in this study in Chapter 2. Once the applied lateral load pushes the pile head, the transferred force to soil by the pile decreases from pile head to its bottom, which proves the beneficial effects of material distribution in tapered piles (Kurian & Srinivas 1995). Since a substantial number of surveys on piles and related published papers are associated with cylindrical piles, in this study, it is planned to investigate various features of tapered piles.

The current building codes and design techniques are generally inclined towards cylindrical piles (Livneh & El Naggar 2008). Reinforced concrete tapered piles are regularly precast with desired shapes of cross-section (PETAJA 1981). When they are used as driven piles, they are categorised as ‘displacement' piles. Thus, they move a volume of soil equivalent to the pile volume. In loose sand, this movement even by a straight-sided wall pile results in soil compaction around the pile, which enhances the frictional bearing noticeably owing to the significant increase in stresses acting perpendicularly to the pile side surface. Besides, tapered piles have an added advantage about their vertical load-carrying capacity. This transmits from a part of load, which is transmitted by vertical bearing on the sides due to the inclination of

the body. This component leads to an increase in the pile bearing capacity when compared to straight-sided wall piles, which in turn increases the frictional component of the pile resistance.

1.3 Problem statement

The author believes that even though tapered piles are generally cost-effective, particularly as driven piles, experience suggests they are underutilized in practice. This issue appears to be due to the following factors:

A. Lack of knowledge and insufficient information about their existence.
B. Lack of a reliable and straight forward analytical technique for estimating their axial compressive capacity.
C. Insufficient marketplace competition to minimize their costs.

On the other hand, most of the relationships, developed for predicting the behaviour of piles, are associated with the conventional cylindrical piles or prismatic ones. However, for tapered and step-tapered piles, there are limited analytical solutions. By and large, in the last three decades, the growing tendency to investigate the behaviour of tapered and step-tapered piles has made it inevitable to conduct more research in this area. Figure 1.1 demonstrates some different bored cast piles having various shapes (Bowles, 1996). Referring to Figure 1.1 (h), a step-tapered pile is demonstrated schematically. This study aims to investigate the behaviour of these piles installed in sand. The load-displacement diagram of each model is obtained separately, and a detailed comparison is made to quantify the behaviour of piles with different shapes, but having the same volume. By altering the stepped length of the pile, the stress contours developed around the shaft will change due to changes in the stress level and the lateral earth pressures.

Furthermore, this study aims to find a rather simple set of equations for axial bearing capacity of tapered piles and also investigate whether an optimum tapering angle resulting in maximised bearing capacity exits or not. For this purpose, since this study investigates the behaviour of bored tapered piles, the mechanism of failure for the

base resistance is assumed to follow the Prandtl-type punching failure (Terzaghi 1943). However, the two important coefficients of k_t (taper factor), and bearing capacity factor N_t, are considered as functions of tapering angle α.

Several researchers have developed different mathematical equations for prediction of the bearing capacity equations of tapered piles, where most were developed based on the cavity expansion theory, applicable to tapered driven piles. However, for the tapered bored piles, a few equations were established based on experimental results by representing a taper coefficient (El Naggar & Sakr 2000; Lee et al. 2009; Paik et al. 2010, 2013).

Indeed, most of the previous analytical, numerical and experimental studies, investigating the response of tapered piles, had considered an arbitrary tapering angle (El Naggar & Wei 1999a, 2000b; Lee et al. 2009; Paik et al. 2010, 2013; Spronken 1998; Wei & El Naggar 1998). Although Horvath (2004b) by referring to Nordlund (1963) mentioned that there should be a limiting value for the tapering angle, other researchers such as Kodikara & Moore (1993) did not discuss the possibility of such limit in their mathematical derivations. On the other hand, Hataf & Shafaghat (2015b) have performed several numerical modellings and compared the load-displacement curves to show that there is an optimum tapering angle for piles based on hardening soil model. However, their numerical modelling has considered a constant lateral earth pressure coefficient for all cases of cylindrical and tapered piles. In addition, they have adopted several assumptions such as a constant stiffness for three different cases of soil types, which is not a practical condition. Hence, in this study it is tried to clarify the concept of optimum tapering angle and its relationship with the sandy soil properties, using analytical and numerical analyses. Afterwards, the behaviour of tapered piles in a group is investigated to estimate the bearing capacity of tapered pile groups using group efficiency concept. Finally, step-tapered piles with one ledge were analysed numerically and their load-displacement diagrams were compared to gain a clearer understanding of the behaviour of these type of deep foundations.

1.4 Objectives

The main goal of this study is to investigate the behaviour of tapered and step-tapered piles under axial and lateral loads. Four specific objectives of this research are as follows:

- Developing new equations to obtain the bearing capacity of piles considering the tapering angle.
- Finding an optimum tapering angle for different types of sand, through analytical approach and using the developed bearing capacity equations.
- Developing an efficiency relationship for tapered pile groups.
- Investigating the effectiveness of step-tapered piles in terms of bearing capacity through load-displacement curves.

1.5 Scope and limitations of the work

In this study, concrete bored piles embedded in sandy soil under axial static loading condition are investigated through analytical and numerical modellings. Two different constitutive models are used to capture different aspects of each one for the purpose of tapered and step-tapered pile modelling (UBC sand model and hardening soil HS model). The water table is considered below the pile toe for all models. In addition, the behaviour of bored piles is investigated in this study, where the simulations represent the construction stages of soil excavation and casting the concrete piles in the bored hole.

1.6 Structure of the thesis

Chapter 2 of the current study describes the past studies which have been performed on tapered piles. In that chapter it is attempted to extract the most important findings of the previous studies on tapered piles, and present them as a critical review. The behaviour of tapered piles under different types of loading are investigated and the knowledge gap in the area is clarified. The methodology of the research, including the adopted soil behavioural models and the soil calibration exercise, is presented in

Chapter 3. It should be mentioned that the soil calibration exercise, which has been used in finding the best soil strength parameters in numerical analyses, is summarised in Chapter 3.

In Chapter 4, an analytical approach is adopted to find the optimum tapering angle of piles in which piles can provide the maximum bearing capacity with identical volume of material. This research also contributes to an efficiency equation in Chapter 5, to predict the bearing capacity of group of tapered piles. Hence, the ratio of the bearing capacity of a pile group to the summation of bearing capacities of single piles in the group, known as the pile group efficiency, is investigated. In the new developed efficiency equations, the effect of tapering angle is considered, as the practical usefulness of tapered piles has been enlightened by the course of time. Particularly, the cylindrical pile groups have the potential to be substituted with same volume tapered pile groups in some projects, which in turn it can considerably save cost and time.

In Chapter 6, the behaviour of step-tapered piles having one ledge and embedded in sand is investigated. Step-tapered piles can provide bearing capacity through their shaft, base, and the end surface of stepped section. This specific kind of deep foundation has a larger upper diameter (for an assigned pile length) and smaller diameters in the lower parts. Step-tapered piles have an effective material distribution through their body. As the upper sections endure higher forces compared to the lower parts, accumulation of material distribution in the upper part is more efficient to resist against greater forces.

Finally, in Chapter 7, a brief summary of the acquired results is presented, comprising some recommendations for future researchers who are interested in pursuing investigation on tapered pile foundations. Chapter 7 also portrays new directions and ideas for future research on step-tapered piles.

Chapter 2

Literature Review

2.1 Introduction

The growing tendency to study the behaviour of tapered piles in the last two decades has made it necessary to gain a deeper insight into this specific kind of deep foundation. Tapered piles have been investigated through analytical, experimental, and numerical studies. These piles have revealed different behaviour under various loading conditions. Hence, reviewing and assessing these efforts to comprehend their response can be of great significance. In this chapter firstly, it is attempted to go over the previous experimental studies, conducted on tapered piles. Then, the proposed analytical and mathematical solutions, employed to calculate the bearing capacity of single tapered piles are compared to have a better vision of how these piles behave. In the third section of this chapter, the numerical modelling studies are brought together to make a comparison between the optimum tapering angle in loose, medium and dense sand.

Finally, all the efforts are investigated technically to find the advantages, disadvantages and the research gaps for this specific kind of piles. In addition to the comparison of different methods toward understanding the behaviour of tapered pile foundations, a section, entitled the directions and ideas for future research on tapered

piles, is provided at the end of this study (Chapter 7) comprising the most recent achievements in this area. Moreover, the implementation of tapered piles in a significant project as a case study is discussed. The efforts made in this study can give an enhanced perspective to the practitioners and researchers to investigate the behaviour of tapered piles professionally.

2.2 Past experiences and recent discoveries

Due to the increasing demand for more efficient and cost-effective resolutions in construction industries, geotechnical engineers are pursuing research on finding novel ideas to design foundations providing more bearing capacities using less material. Many investigations have been conducted to deeply understand the behaviour of tapered piles employed in different conditions. Some of them have revealed the advantages of this kind of piles in comparison to their counterpart cylindrical ones, and some of them are presenting specific circumstances wherein the advantages of tapered piles can far outweigh straight sided wall piles. However, it seems that there are some gaps for deciding whether using such piles is reasonably beneficial to be employed in place of the cylindrical piles. Furthermore, finding the theoretical reasons behind the idea of tapered piles can be of great importance to make a decision. Finding the answer to the question whether any specific tapering angle for these piles reported (in allowable settlement zone) to provide maximum bearing capacity, may contribute to a much logical judgment regarding their advantages. Due to a wide range of parameters linked to the performance of tapered piles, categorizing the main factors affecting the results can be of great significance. Hence, in this study, categorization is carried out firstly based on the loading conditions. A comprehensive overview of axial and lateral static loading conditions is presented in the first part. Then the special effects of the taper coefficient (K_t), the effective overburden pressure (σ_V'), the confining pressure (σ_h') and the load-displacement curves (p-y) of piles are studied and compared. The second part is allocated to study the response of tapered piles under axial and lateral dynamic loading condition. In the second part, similar to the first one, in three separate sections the effects of various parameters such as the tapering angle, the slenderness ratio and the stiffness will be discussed. The load-displacement diagrams of tapered piles subjected to axial harmonic loading is discussed. Finally, the

mathematical developments for predicting the response of non-uniform cross-section piles subjected to axial and lateral harmonic loading are collected as a comprehensive assessment.

In next section, the main findings acquired based on experimental investigations on vertically loaded tapered piles, are presented. The results of these investigations can be divided into three parts. The first part consists of studying the parameters, which directly play an essential role in the behaviour of tapered piles. Based on the conducted studies, these parameters are the taper coefficient (which has been used widely in attaining knowledge regarding the behaviour of these kinds of deep foundations), the effective overburden pressure, and the relative density of sand. The second part is allocated to studying the load-displacement behaviour of tapered piles. Particularly, comparing the tapered piles' load-displacement curves with their counterpart cylindrical piles can gain a deeper insight into their usefulness. Moreover, the inclination body of this kind of pile can make the surrounding soil be compacted, which in turn can contribute to the enhancement of the lateral earth pressure coefficients significantly. Hence, the third part of this section discusses the effect of confining pressure on tapered piles performance.

2.3 Statically axial and lateral loading conditions

2.3.1 Experimental investigations

2.3.1.1 A brief review of experimental literature

The axial capacity of tapered piles has been investigated under compression and uplift loading conditions by many researchers (Bakholdin 1971; El Naggar & Wei 1999a, 2000b; Fahmy & El Naggar 2017; Fellenius 2017; Khan et al. 2008; Livneh & El Naggar 2008; Manandhar & Yasufuku 2013; Paik et al. 2010, 2013; Rybnikov 1990; Sakr et al. 2004; Society 1978; Spronken 1998; Wei & El Naggar 1998; Wei 1998). Ismael (2003, 2006, 2009) investigated the behaviour of step-tapered bored piles in calcareous and cemented sand under static lateral loading. Horvath & Trochalides (2004) presented a report for the evaluation of used tapered piles at the John F. Kennedy international airport as a case study. The behaviour of tapered piles driven

into sand using centrifuge equipment has been studied by (El Naggar & Sakr 2000; Sakr & El Naggar 2003). El Naggar & Wei (1999b) conducted a vast range of tests on realistic scale steel piles to obtain the response of cone shaped piles subjected to lateral loading.

Fellenius et al. (2000) analysed the effect of soil set-up, concrete stiffness, and residual stress for tapered piles in sand. Nordlund (1963) studied the load-carrying capacity of tapered piles and proposed design curves to determine the coefficient of earth pressure taking into account the effect of the tapering angle. D'Appolonia & Hribar (1963) studied the behaviour of step-tapered piles with a corrugated surface considering its load transfer mechanism and an analytical method has been presented accordingly to obtain the load transfer curves of these piles. Based on the test proposed results the bearing capacity of tapered piles is the sum of the tip resistance and the side resistance, the latter having two components, (1) skin friction, and (2) vertical component of wedge reaction. Jain et al. (2013) studied the comparative behaviour of tapered and uniform piles driven in loose sands and discussed the dependability of N, (bearing capacity factor) and K_h (the coefficient of lateral earth pressure) values. Dutta (1986) conducted model pile load tests to study the effect of the tapered shape of pile with variable cross-section on the ultimate bearing and uplift capacities. Dutta (1986) found that the tapering angle was a key parameter influencing the load capacity of the pile and figured out that geometrically the triangular pile carried the maximum load.

Around three decades ago, Meyerhof et al. (1988) have examined the response of single cylindrical piles embedded in sand by performing lateral load tests. They found that the relative stiffness of piles (the ratio of pile stiffness to soil stiffness) plays a significant role on the lateral performance of piles. The importance of the pile geometry factor have been highlighted by Mahmoud & Burley (1994), who have conducted lateral load tests on a series of square and circular short pile models.

The behaviour of the cone shaped piles under static lateral loading condition has been investigated by El Naggar & Wei (1999b), including a vast range of tests on large-scale steel piles. Sakr et al. (2005) have conducted some pressure chamber tests on composite tapered and cylindrical piles subjected to static lateral loading using the

conventional head and toe driving methods. Sakr et al. (2005) have compared their proposed model for the p-y curves with the strain wedge model proposed by Norris (1986), which considers the interaction between the structure (pile) and the adjacent soil. Table 2.1 presents a summary of the experimental investigations, including the applied apparatuses, pile materials, dimensions, and the methods used for each experiment on tapered piles.

Table 2.1. Summary of the experimental investigations conducted on tapered piles

Reference	Pile material	pile Length (m)	Tapering angles (degree)	Soil	Method	Apparatus
Livneh and El Naggar (2008)	Steel, square shaft helical pile	1.5	2.12°, 5.33°	Sand with silty clay	Screw into the ground by pile helix of a screw thread	Field test
El Naggar and Wei (1999a)	Steel	1.524	0°, 0.6°, 0.95°	Coarse angular air-dried sand (loose and medium)	Raining technique	Chamber VLPSC
Fahmy and El Naggar (2017)	Hollow close-ended helical pile, ductile iron with a very rough external surface and steel with a smooth surface (t=5.5mm)	3.1	0, 0.46°	Silty Sand	ASTM D1143	Field test
Paik et al. (2013))	Steel pipes	0.9	0, 1°, 1.5°	Jumoonjin sand	Pluviation	Calibration chamber test

Khan et al. (2008)	Concrete	1.524, 3.048	0, 0.95°, 1.91°	Layered soil consisted of sand and clay	Cast-in-place piles using a tapered auger	Field test
Rybnikov (1990)	Steel	4.5	0, 1.2°, 2°, 2.4°	Sandy loam, ordinary loam, and sand	Bored cast-in-place piles	Field test
Wei and El Naggar (1998)	Steel	1.524	0, 0.6°, 0.95°	Coarse angular air-dried sand (medium and dense)	Raining technique	Chamber (VLPSC)
Paik et al. (2010)	Steel pipes with a smooth surface	0.9	0, 1°, 1.5°	Jumoonjin sand (SP)	Raining technique	Calibration chamber
Sakr et al. (2004)	Steel and FRP (fibre-reinforced polymer using GFW (Glass Filament Wound) filled with self-consolidated concrete (SCC)	1.524	0, 0.53°, 0.71°, 1.13°	Sand	Toe driving technique	Pressure chamber
Wei (1998)	Steel	1.52	0, 0.6°, 0.95°	Coarse angular air-dried sand	Raining technique	Chamber (VLPSC)
Spronken (1998)	Steel pipe	0.362	0, 0.5°, 1°, 2°	Sand (SP)	Pluviation	Pluviation tank
El Naggar and Wei (2000)	Steel	1.52	0, 0.6°, 0.95°	Loose and medium sand	Pouring with no densification	Chamber (VLPSC)
Manandhar and Yasufuku (2013)	Chromium-plated steel	0.5	0, 0.7°, 1.4°	TO sand K-7 sand FB sand	Speed control driving method	Chamber

Ismael (2009)	Concrete	5	Step-Tapered	Medium-Dense sand with wick cementation	Bored Piles	Field test
Horvath and Trochalides (2004)	Close-ended steel pipe piles filled with concrete	30	0.33°, 0.57°, 0.95°	Sand	Pile driving	Field test
Sakr and El Naggar (2003)	Cold drawn steel tubing with a thickness of 0.88	0.452	0, 0.35°, 0.54°, 1.02°	Medium angular dried sand	Sand falling	Centrifuge
Naggar and Sakr (2000)	Cold drawn steel tubing with a thickness of 0.88mm	0.452	0, 0.35°, 0.54°, 1.02°	Medium angular dried sand	Driving (pile pushed into the soil)	Centrifuge
El Naggar and Wei (1999b)	Steel	1.524	0, 0.6°, 0.95°	Sand	Raining technique	Chamber (VLPSC)
Fellenius et al. (2000)	Closed-end monotube filled with concrete	21m long with 7.6m tapered	0.58°	Layered soil (Marsh, sand, and clay	Driving	Field test
Lee et al. (2009)	Steel pipes	0.9	0, 1°, 1.5°	Jumoonjin sand	Raining technique	Calibration chamber CPT
El Naggar and Wei (1999)	Steel piles	1.524	0, 0.6°, 0.95°	Sand	Rain technique	Chamber (VLPSC)
Sakr et al. (2005)	FRP shell and steel piles	1.524	0, 0.53°, 0.71°, 1.13°	Dense sand	Conventionl pile head and pile toe driving	Pressure chamber

Referring to Table 2, most of the experiments conducted on small scale model tests on tapered piles using chamber apparatus and a pluviation technique; while the pile

material used were steel pipes. The air-pluviation is a technique that dry sand particles are poured into the chamber through the air from a certain height with a constant velocity (Tabaroei et al. 2017). According to Table 2, a wide range of tapering angles have been used in the experiments (from 0° to 2.5°) and most of the tests performed in sand. However, to the best of authors' knowledge, a limited number of laboratory and field tests have been conducted to investigate the lateral behaviour of tapered and step-tapered piles.

2.3.1.2 Tapering angle, overburden and relative density effects

A wide range of experiments has been performed to inspect the effectiveness of tapered piles compared with constant cross-section piles with the same material input by El Naggar & Wei (1999a). Besides, a taper coefficient was introduced to calculate the shaft resistance of tapered piles. Equation 2.1 is used to obtain the shaft bearing of tapered piles.

$$Q_S = \int_0^L K_t \, K_s \sigma_v P . tan\delta . dz \qquad 2.1$$

Where K_s is the at rest earth pressure coefficienct, σ_v is the vertical effective stress at depth z, P is the perimeter of the pile section, δ is the soil-pile interaction friction angle, and K_t is the taper coefficient which is suggested by Figure 2.1 and defined as Equation 2.2:

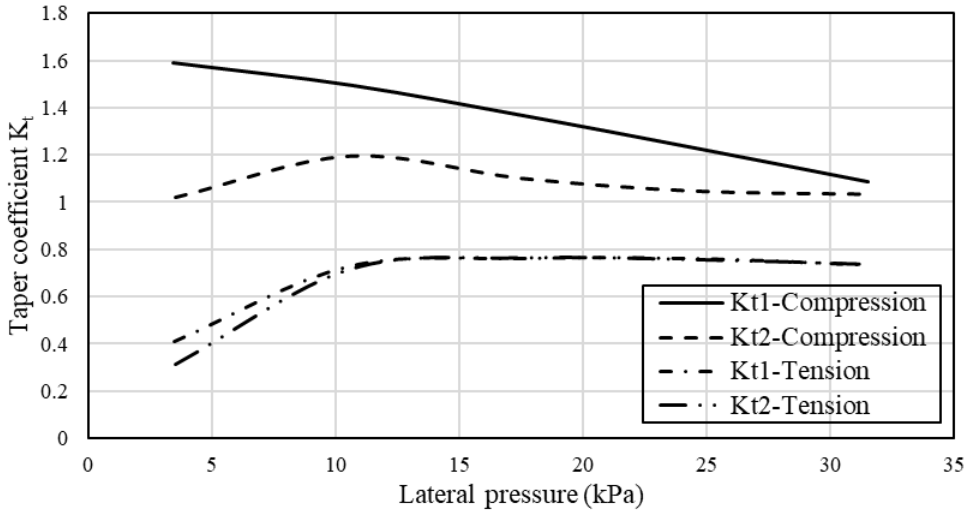

Figure 2.1. Variation of shaft resistance coefficient Kt with lateral stress (after El Naggar and Wei, 1999a)

$$K_t = \frac{\text{unit shaft friction of tapered pile}}{\text{unit shaft friction of cylindrical pile}} \qquad 2.2$$

The remaining parameters are the same as those are used for estimating the shaft resistance of straight-sided wall piles. According to El Naggar & Wei (1999a) test results, the tapering effect is significantly beneficial for a depth of approximately 20 pile diameters. According to Figure 2.1, higher lateral pressures may contribute to lower shaft resistance coefficient values.

The axial performance of tapered piles in compressive loading condition was studied by El Naggar & Sakr (2000) using centrifuge model tests. As a result of their research, an approach for designing tapered piles was developed. El Naggar & Sakr (2000) recommended the ratio of the pile top section diameter to its length should be in the range of 20–25 for having the optimum efficiency. However, their small scale prototype piles were limited to only three different values of length to diameter ratios of 14, 18 and 26. In addition, the tested models were prepared in reduced scale of the prototypes; hence, proper field load tests need to be conducted to examine the optimum efficiency range of *l/d* ratio of the tapered piles. Figure 2.2 demonstrates the values of the taper coefficient, K_t, obtained from the experimental outcomes and the theoretical calculations. It indicates the influence of the rate of changing taper coefficient in different effective overburden pressures for three different lengths to

diameter ratios and tapering angles of piles. Figure 2.2 suggests the values for taper coefficient for *L/D* ratios of 14, 18 and 26, which relates to tapering angles of 1.02°, 0.54°, and 0.35°, respectively.

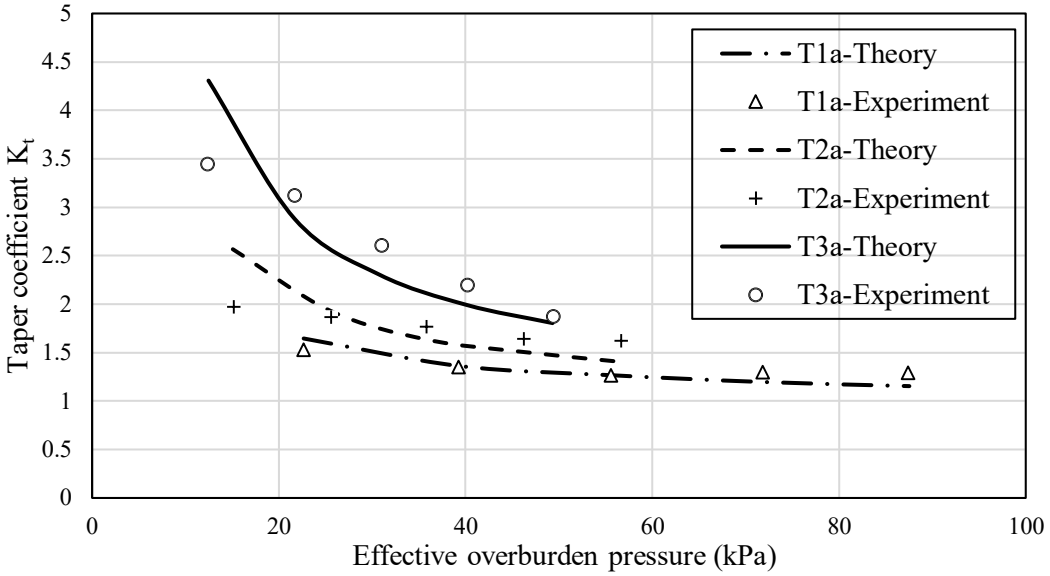

Figure 2.2. Taper coefficient values Kt obtained from the laboratory experiments and the theoretical values in different overburden pressures (after El Naggar and Sakr, 2000; Sakr and El Naggar, 2003)

Taper coefficient values for lower effective overburden pressures are much greater than 1, and by increasing the tapering angle from 0.35° to 1.02°, K_t can raise from 1.6 to 4.3 at its maximum value, where the effective overburden pressure is less than 25 kPa. Equation 2.3 is used as a theoretical relationship for obtaining K_t (El Naggar & Sakr 2000).

$$K_t = \frac{\tan(\theta+\delta)\cot(\delta)}{1+2\ln(\frac{r_1}{r_m})\tan(\theta)\tan(\theta+\delta)} + \frac{4G\tan(\theta)\tan(\theta+\delta)\cot(\delta)}{(1+2\ln(\frac{r_1}{r_m})\tan(\theta)\tan(\theta+\delta))K_s\sigma_v} S_r \qquad 2.3$$

Where, θ is the tapering angle, δ is the pile-soil interface friction angle, K_s is the coefficient of lateral earth pressure of the soil and G is the elastic shear modulus of soil. Besides, σ'_v is the effective vertical stress, and S_r is the settlement ratio (=*Up* /*d*). These experiments were conducted in sand with a relative density of 35% only. Therefore, the effect of relative density in Equation 2.3 has not been considered. In this equation, the lateral earth pressure of the soil assumed to be constant. However, it

is known that by each incremental settlement of the tapered piles, this coefficient can increase in the adjacent soil. The reason for this increase is associated with the soil densification adjacent to the pile wall that can be similar to the compacting process of the surrounding soil. Due to the wide range of K_s values, proposed in various sources for tapered piles (Bowles 1996; Nordlund 1963; Paik et al. 2013), and the key role of this parameter in obtaining the shaft capacity of tapered piles, it is recommended to consider K_s as a function of the relative density and the over-consolidation ratio of the soil. Although Fellenius (2017) mentioned that the concept of "critical depth" is a misconception and is based on incorrect understanding of test data and should not be considered, investigating the critical depth of tapered piles at which shaft resistance may reach a constant value relative to the initial sand density is of considerable significance in taper coefficient. Hence, field testing is of great significance to be carried out and also to analyse tapered piles behaviour with different *l/d* ratios to obtain the potential influence of critical depth for the tapered pile capacity.

Experimental studies were performed by El Naggar & Sakr (2000) and Sakr & El Naggar (2003) to inspect the behaviour of tapered and straight-sided wall piles driven into loose sand using centrifuge tests. According to their study, the shaft resistance amplified by increasing the tapering angle, and the shaft bearing of the tapered pile reached to 1.85 times of its comparable straight-sided wall pile. However, it has not been stated that increasing the tapering angle should be limited to a specific value. They also compared the values with those calculated based on the theory by changing the effective overburden pressure, as shown in Figure 2.3.

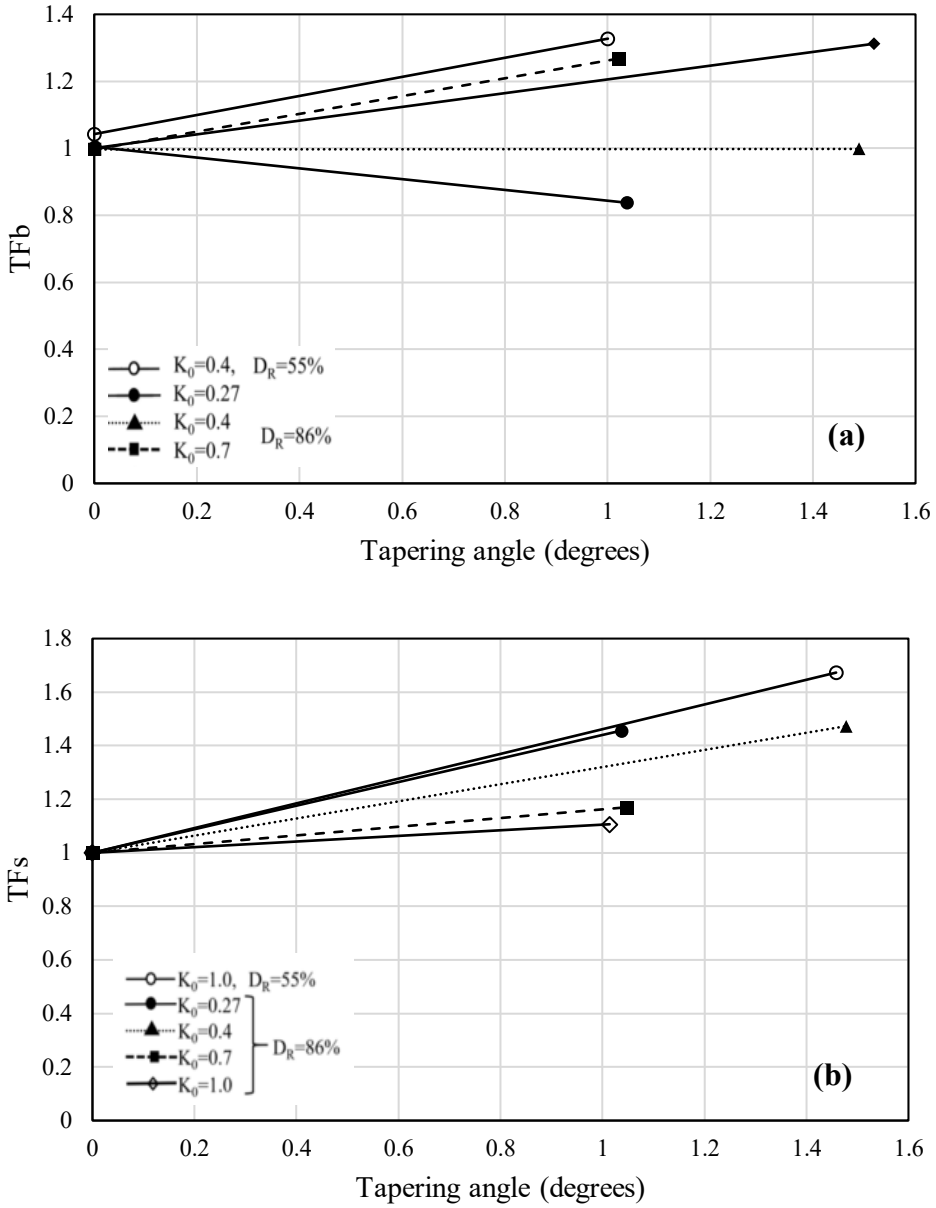

Figure 2.3. Effects of tapering angle on (a) the base taper coefficient (TFb); (b) the shaft taper coefficient (TFs) for different lateral earth pressures (after Paik et al., 2013)

Paik et al. (2013) investigations also demonstrate that the ultimate unit base bearing of a tapered pile increases when the mean stress, the relative density and the tapering angle of a pile magnifies. Nevertheless, the effect of critical depth in shaft capacity calculation was not considered by Paik et al. (2013). Moreover, based on their research, it is comprehended that the ultimate unit shaft bearing of a pile increases as the stress components, the relative density and the tapering angle increase. Figure 2.3 indicates the relationship between the tapering angle of piles and the taper coefficients,

which are defined in Equations 2.4 and 2.5. Referring to these figures, by increasing the tapering angle, the base taper coefficient increases but only for lateral earth pressure coefficients greater than 0.4. However, shaft taper coefficient increases for all lateral earth pressure coefficients up to 1.8 for a tapering angle of 1.5°.

Equations 2.4 and 2.5 are used to calculate the taper coefficients for the base and shaft resistance of tapered piles, respectively (Paik et al. 2013). The coefficients A and B in Figure 2.3 are functions of the relative density, at rest lateral earth pressure coefficient and the pile tapering angle, which have been substituted in Equations 2.4 and 2.5.

$$TF_b = 1 + [0.0005(D_R)^{1.5}\ln(K_0) + 0.359]\theta \quad 2.4$$

$$TF_s = 1 + [6.3 - 22.6\ln(K_0)]\frac{\theta}{D_R} \quad 2.5$$

where, D_R is the relative density of soil, K_0 is the lateral earth pressure coefficient of soil at rest, and θ is the tapering angle of pile. Equations 2.4 and 2.5 can be questioned, since by increasing the relative density of soil, the lateral earth pressure coefficient increases. However, in the proposed model by Paik et al. (2013) for a constant relative density of 86% a wide range for lateral earth pressure coefficients is assumed. In Equations 2.4 and 2.5, by increasing the tapering angle, the base and shaft taper coefficients increase, while the tapering angle should be limited to a certain value. Besides it is recommended that other affecting parameters such as the geometry of piles, the overconsolidation ratio of soil, the pile-soil interaction friction angle and the settlement of piles to be considered for obtaining the shaft taper coefficient. Figure 2.4 demonstrates the effect of lateral earth pressure on the taper coefficient for an ultimate unit base and shaft resistance by different relative densities for a tapering angle of 1 degree, respectively.

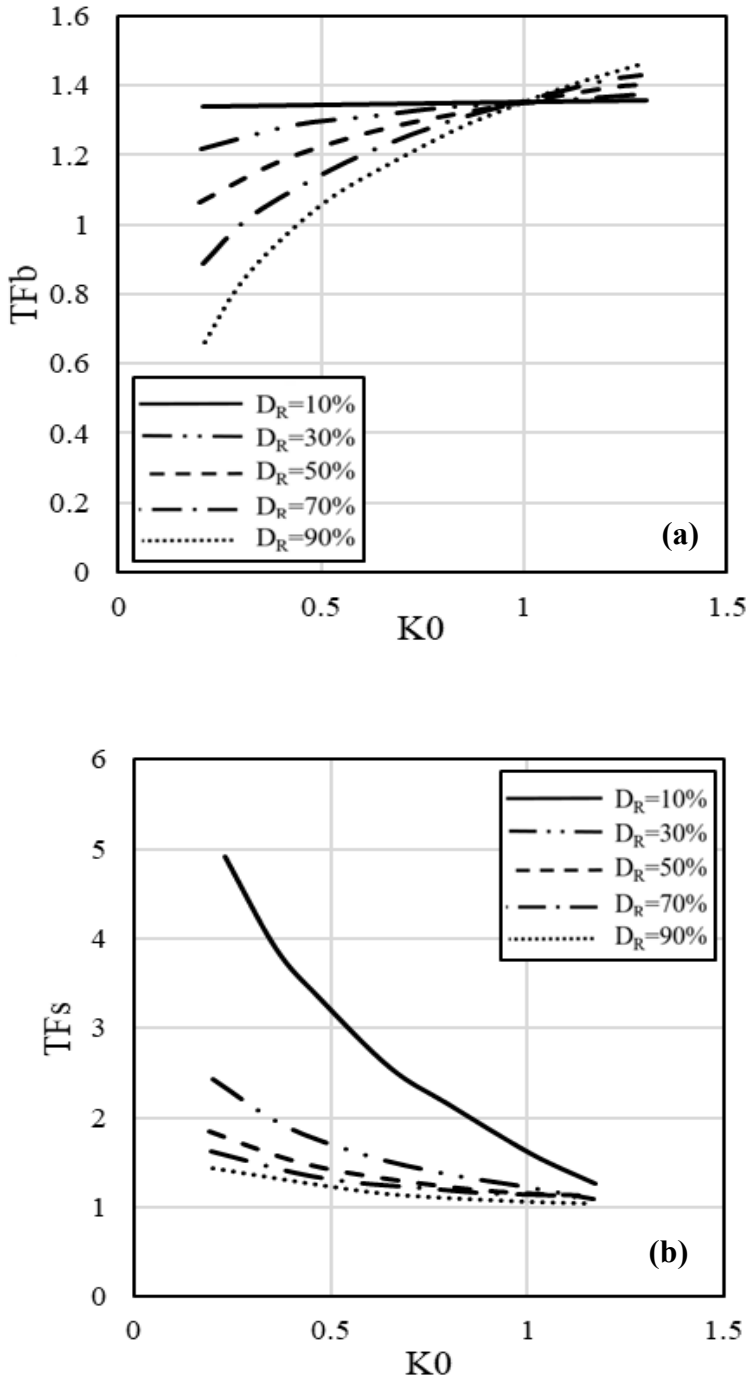

Figure 2.4. Effects of K_0 for the tapering angle of 1° in different relative densities (a) Effect on the base taper coefficient (TFb); (b) Effect on the shaft taper coefficient (TFs) (after Paik et al., 2013)

Figure 2.4 suggests that by increasing at rest lateral earth pressure of the soil, the effect of relative density on taper coefficients of both shaft and base decreases.

Almost all of the efforts, performed to propose a taper coefficient in predicting the shaft resistance of tapered piles, have recommended value in the range of 1 to 4.5, which attributed to a tapering angle approximately between 0º and 1º, respectively. The conceptual three-dimensional diagram in Figure 2.5 illustrates different taper coefficients against confining pressures.

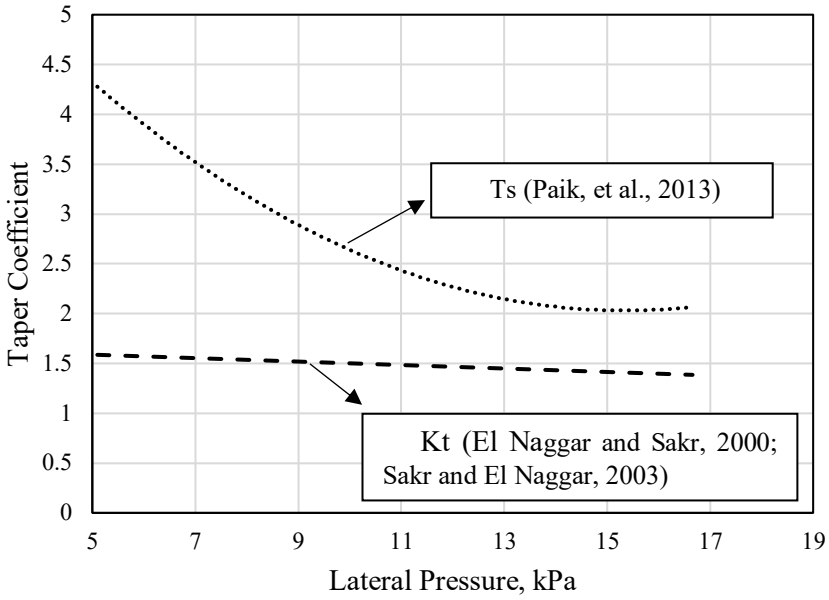

Figure 2.5. Comparing different taper coefficients with different confining pressures presented by different researchers (data are taken from Naggar & Sakr, 2000; Paik et al., 2013; Sakr & El Naggar, 2003)

As can be seen in Figure 2.5, the variation of taper coefficient suggested by El Naggar & Sakr (2000) and Sakr & El Naggar (2003) is negligible in lateral pressure ranging from 5 kPa to 15 kPa. However, the effect of confining pressure on the model presented by Paik et al. (2013) is significant. This comparative diagram confirms that more investigations are required to quantify the taper coefficient value for obtaining the shaft capacity of a cone shaped pile. It should be remarked that the presented equations are developed only based on small scale models. Hence, it is recommended to validate these equations using field test results and rigorous numerical analysis.

The Canadian Geotechnical Society Committee (1978), also suggests employing Equation 2.3 for determination of taper coefficient without considering the relative density of the soil, which can significantly affect the lateral earth pressure coefficient.

Manandhar & Yasufuku (2013) evaluated the skin resistance using cavity expansion theory and stress–dilatancy relationship. Besides, the base resistance of tapered piles assessed by defining a taper coefficient. Their results of experiments have illustrated that a slight increase in the tapering angle contributes to a higher skin resistance and affects the end bearing capacity in comparison with conventional cylindrical piles embedded in various types of sands and relative densities. Figure 2.6 illustrates the increasing shaft and point resistance of tapered piles up to the tapering angle of 1.4° comparing to the straight-sided wall pile.

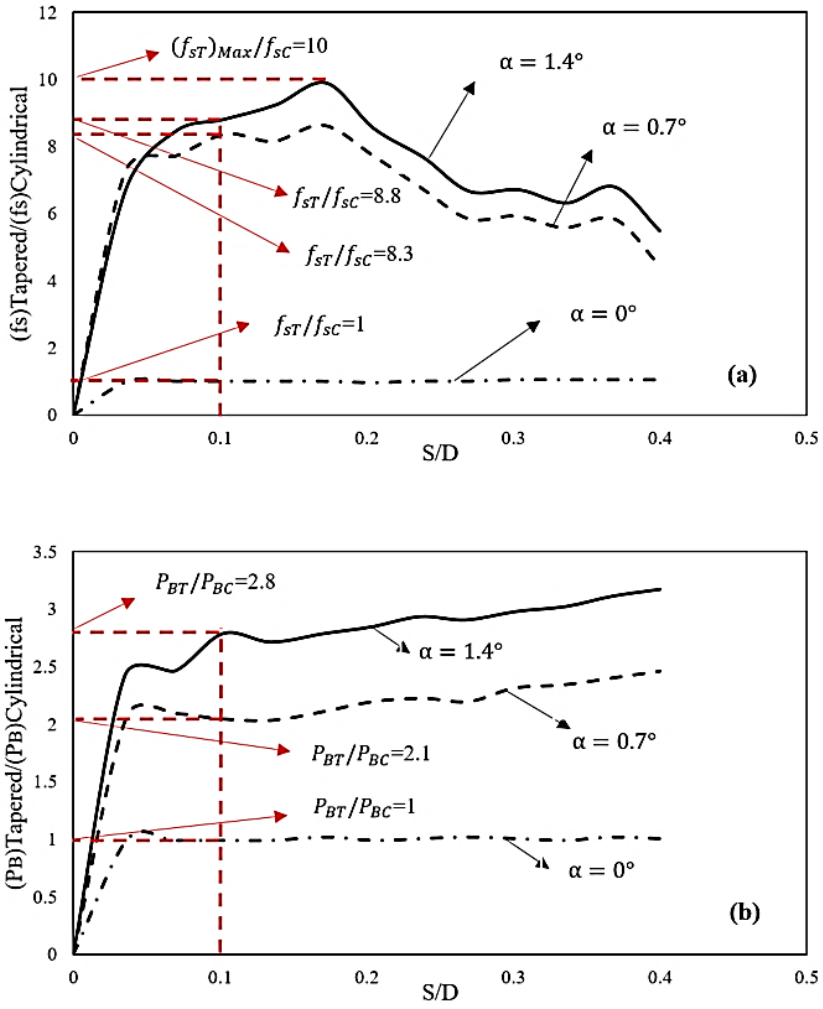

Figure 2.6. Effect of tapering angle on the normalized pile capacity using cavity expansion theory (any reference?)

As shown in Figure 2.6, for a tapered pile having 1.4° tapering angle, the ratio of shaft friction capacity to its counterpart straight sided wall pile reaches to 10 at about 0.2 of

settlement to diameter ratio of the pile. This value for the base capacity in its maximum value is about 3. Hence, taper coefficients defined based on Figure 2.6 enlightenments are proving the effectiveness of tapered piles in both side and base resistance.

On the other hand, the response of laterally loaded piles have been evaluated based on theory of elasticity (Budhu & Davies 1987; Pise 1984; Poulos 1971; Randolph 1981). Although, in order to consider the soil non-linearity, Poulos & Davis (1980) and Budhu & Davies (1987) have proposed some modifications based on yield factors, the effect of tapering angle has not been taken into account for their proposed model. The inclined body of tapered piles can affect the lateral earth pressure coefficient by mobilising a portion of passive pressure (K_p) and subsequently the lateral performance.

Under the lateral loading condition and according to El Naggar & Wei (1999b), the term subgrade reaction modulus deflection is defined as $K_h = p/y$, representing the equivalent spring stiffness used as the elastic medium for the soil, where p is the soil resistance and y is the pile lateral deflection. Although this reaction modulus increases with increasing the tapering angle, it decreases with increasing of the pile lateral deflection, particularly for lesser confining pressures, as shown in Figure 2.7 (El Naggar & Wei 1999b).

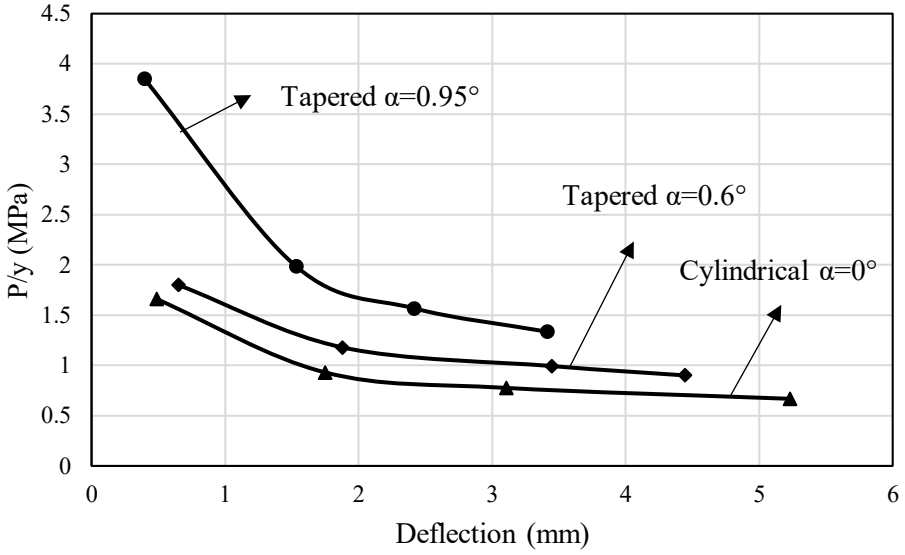

Figure 2.7. Decreasing trend of the horizontal subgrade modulus reaction with deflection (any reference?)

On the other hand, Sakr et al. (2005) have defined a taper coefficient for evaluating the lateral resistance of the piles. This factor has been defined as K_{tl}, which refers to the ratio of the lateral resistance of a tapered pile to its counterpart cylindrical pile, and is defined in Equation 2.6 (Sakr et al. 2005).

$$K_{tl} = e^{0.45\alpha} \quad for \quad (0° \leq \alpha \leq 1.13°) \tag{2.6}$$

Although Equation 2.6 can be used for flexible piles, it is limited to tapering angles in the range of $0° \leq \alpha \leq 1.13°$. Hence, additional centrifuge tests or field tests are required to capture the effect of vertical and radial stress variations with depth on the aforementioned factor.

2.3.1.3 Effect of confining pressure

Wei & El Naggar (1998) found that the skin friction of tapered piles is capable of being 40% greater than their same volume conventional cylindrical piles. Based on their research, it is comprehended that for both pile types, the distribution of load along the pile shafts had a similar pattern, and that is a function of confining pressure. In addition, it is presumed that tapered piles can provide higher resistances than the straight-sided wall piles. On the other hand, they recommend using tapered piles with specific geometry properties (i.e. with a slenderness ratio less than 20). Figure 2.8 illustrates the ultimate point load carrying capacity for various applied confining pressures.

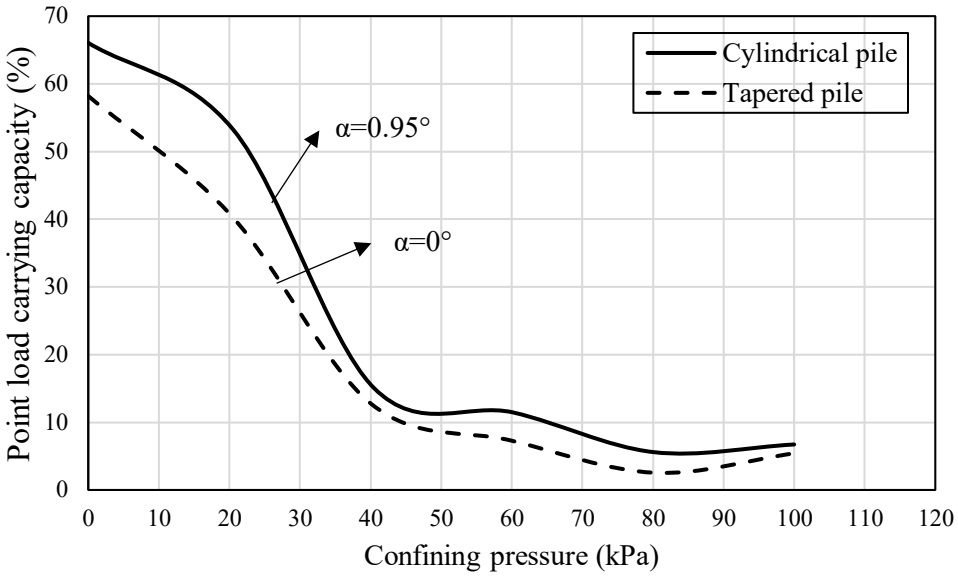

Figure 2.8. Distribution of the ultimate load by pile point for various applied confining pressures (after Wei and El Naggar, 1998)

As can be observed in Figure 2.8, in lower confining pressure levels, the point load-carrying capacity of the cylindrical pile is higher than tapered piles. In higher confining pressures, the difference between the point load-carrying capacities of these piles is not significant. However, it should be noticed that the cross-section area of the cylindrical pile tip is larger than that of a tapered pile, which in turn proves the effectiveness of tapered piles.

The results of El Naggar & Wei (2000b) study indicates that by increasing the confining pressure, the axial uplift resistance of a tapered pile increases. However, it is expected that by increasing the confining pressure, the vertical upside component of the force along the pile shaft will increase and push the pile in the upward direction. Accordingly, it can significantly decrease the uplift capacity of these piles. Figure 2.9 demonstrates the influence of confining pressure on the shaft friction of two piles (S: Straight-sided wall pile, T1: Tapered pile with a tapering angle of 5º) under various confining pressures.

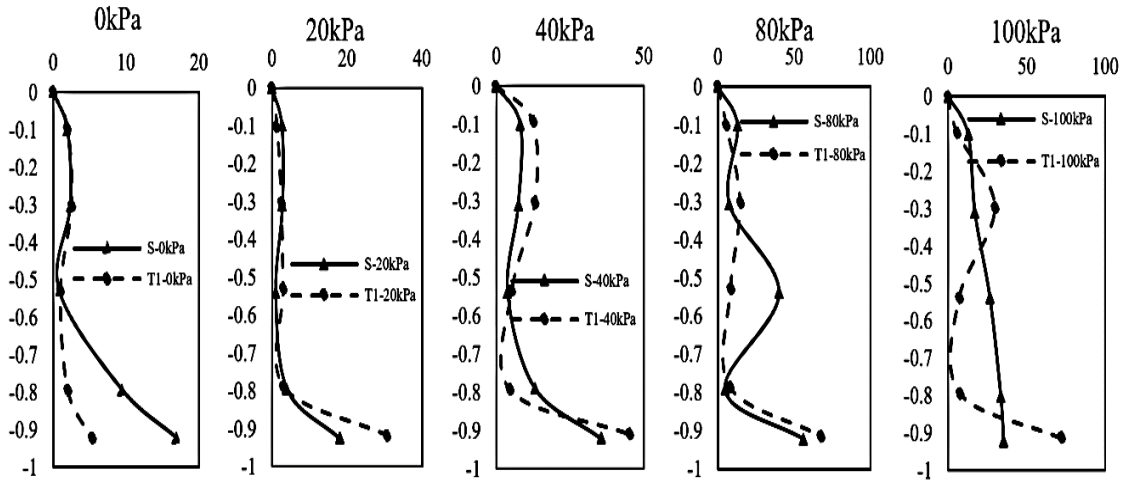

Figure 2.9. Shaft friction of tapered and straight-sided wall pile in-depth under various confining pressures in medium-dense sand (after El Naggar and Wei, 2000b)

Although, the observed trend is similar to the cylindrical piles, reported by De Nicola & Randolph (1993), the ratios of the uplift load to compressive load which has been reported approximately between 0.6 and 0.7 are less matched for tapered piles. This discrepancy is probably due to the higher capacity of tapered piles under compressive loading and less under uplift loading. The relationship between the measured stress and the applied confining pressure is shown in Figure 2.10 (El Naggar & Wei 1999a).

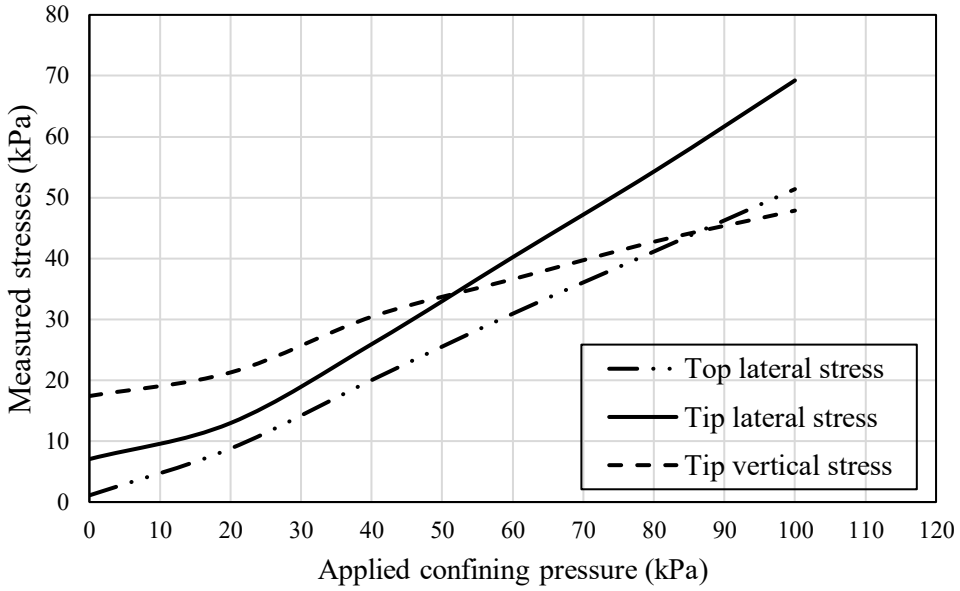

Figure 2.10. Measured stresses variation at different applied confining pressure levels (after El Naggar and Wei, 1999a)

El Naggar & Wei (1999a) employed transducers in their study to compute the average lateral stress at different confining pressure levels applied to the soil chamber. Their efforts, however, can be criticized since the values of the shaft resistance at the boundaries were neglected in their calculations due to the boundary effects. Since the behaviour of soil adjacent to the pile shaft is nearly plastic and for the accuracy and reliability of the results, the effect of boundaries, particularly at pile-soil interfaces, should be taken into consideration. According to their assumption, the shaft friction curve was found to be approximately uniform. However, the average might not represent an accurate estimation for the unit load transfer along the pile shaft.

The confining pressure also plays a significant role in the lateral performance of truncated cone-shaped piles. As reported by Sakr et al. (2005), the moment distribution diagrams for piles having different tapering angles of 0°, 0.53°, 0.71° and 1.13° indicate that the maximum moment increases as the radial/vertical confining pressure increases. Figure 2.11 illustrates that the maximum moment also has a direct relationship with the tapering angle; as can be seen in Figure 2.11, under confining pressures of 30kPa and 60kPa, and from tapering angles from 0° (cylindrical pile) to 1.13°, the moment increases more than 90%.

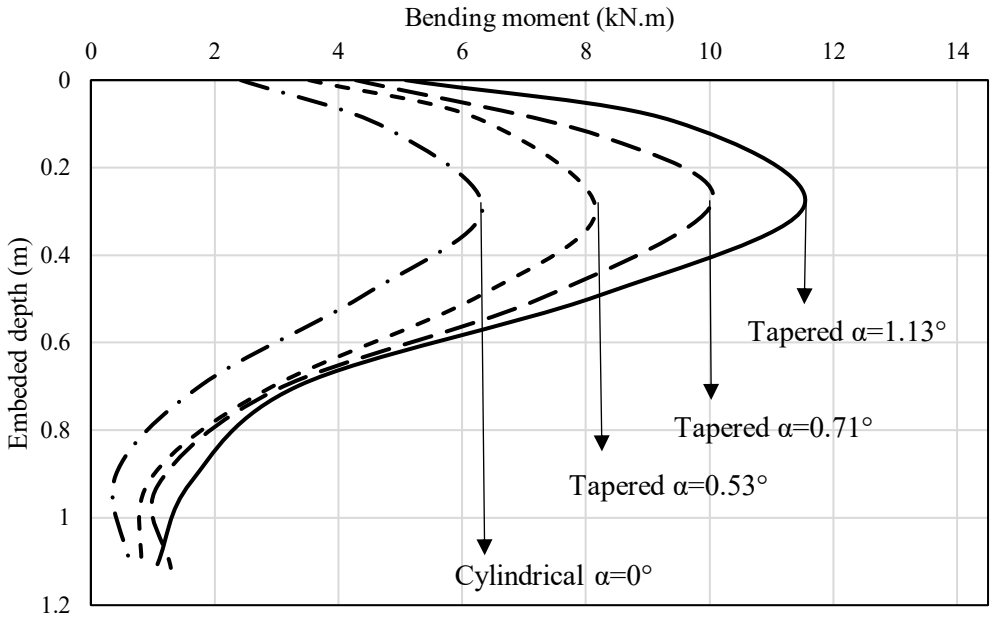

Figure 2.11. Distribution of moment along pile shaft subjected to ultimate pile load using toe driving under 30 and60kPa confining pressures (after Sakr et al., 2005)

This change of moment distribution was also discussed by (El Naggar & Wei 1999b), where three different piles with tapering angles of 0°, 0.6° and 0.95° were tested under static lateral loading condition. According to El Naggar & Wei (1999b), under a zero confining pressure condition and the ultimate lateral loading capacity, the maximum moment of a tapered pile with 0.95° increases approximately 30%. However, under the same condition of loading and confining pressure of 100kPa, this increase is limited to around 20%. Figure 2.12 illustrates a comparative moment diagrams of both analyses performed by El Naggar & Wei (1999b) and Sakr et al. (2005) under a confining pressure of 60kPa.

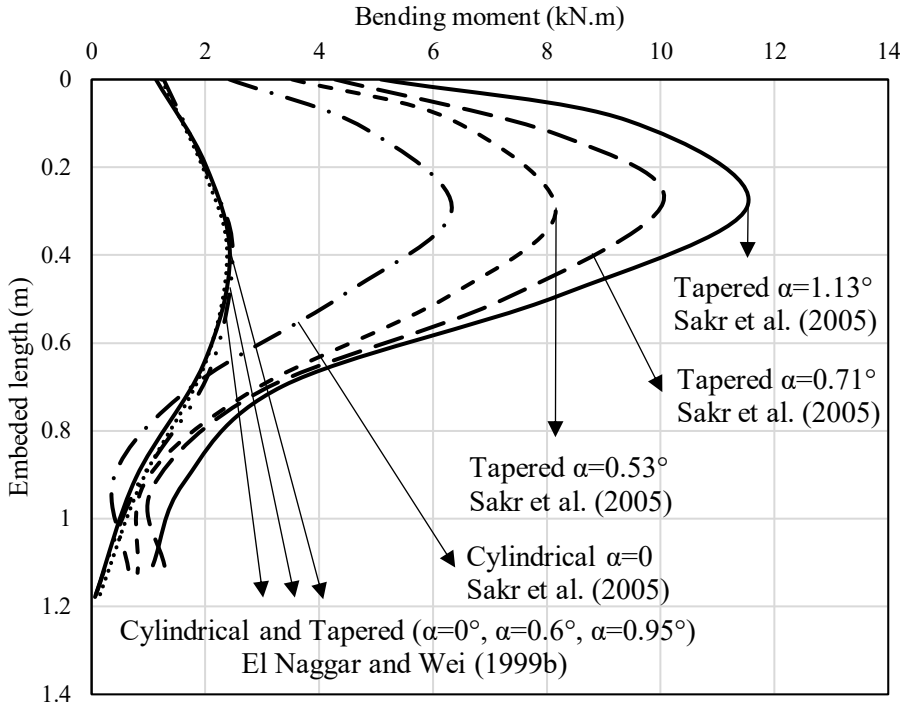

Figure 2.12. Comparative moment diagrams of both analyses at a confining pressure of 60kPa

2.3.1.4 Load-settlement behaviour

Results of pile load tests obtained by Paik et al. (2010) indicated that the frictional resistance of tapered piles continuously increases with pile settlement. However, straight-sided wall piles reach the ultimate frictional bearing at a settlement of 2% of their diameter. According to their study, the ratio of the load-carrying capacity of tapered piles to their counterpart cylindrical ones was found to vary with both the

tapering angle and the sandy soil condition. It has been suggested that for all sandy soil conditions, the ultimate unit shaft resistance of cylindrical piles is generally less than that of tapered piles (Paik et al. 2010). However, in terms of the unit base load carrying capacity, tapered piles only provide higher base resistance in dense sand with lateral earth pressure coefficients more than 0.4. Furthermore, taper coefficients are proposed to estimate the shaft and base resistances of tapered piles, but not considering the effect of overburden pressure or pile-soil interaction effect. Figure 2.13 is depicting the variation of base and shaft loads against the settlement of the piles. Each test is recognized by three symbolic letters (L for low, M for medium and H for high). The first letter designates the level of the relative density D_R of the sample (H for 86% and M for 55%), and the second and third letters designate the levels of the initial vertical and horizontal stresses ($\sigma_V' \; and \; \sigma_h'$) at the mid-depth of the test piles, respectively.

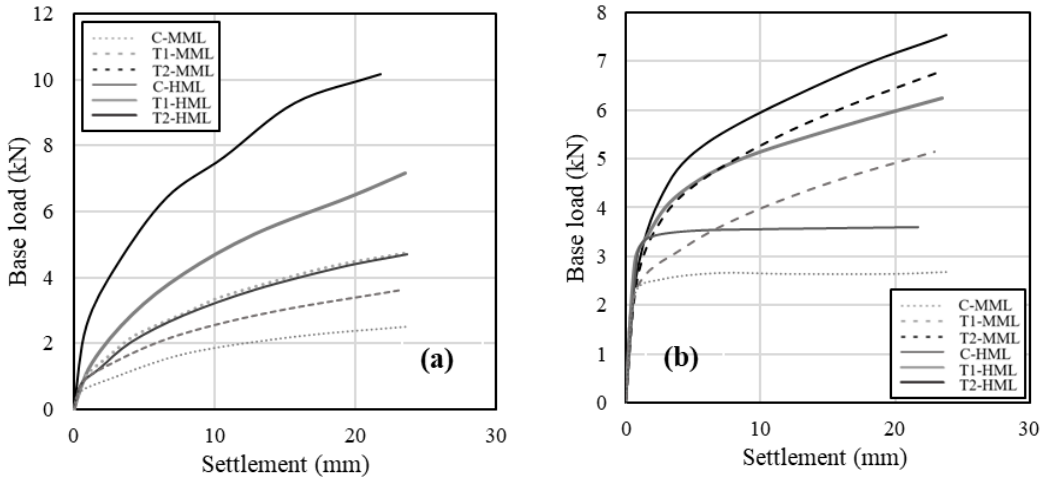

Figure 2.13. Load-displacement curves for piles (a) base load and (b) shaft load (after Paik et al., 2010)

Figure 2.13 suggests that as tapering angle increases, regardless of the sandy soil stress state and relative density, the ultimate unit shaft resistance of piles increases, while the unit base resistance of piles increases in medium sand and decreases in dense sand.

An experimental study has been conducted by Sakr et al. (2004) to inspect different parts of a pile at various stress levels. The load-transfer mechanism of tapered piles was observed in the axial compression loading condition. Moreover, pile performance characteristics evaluated considering the effect of pile material. Figure 2.14 illustrates

the load-displacement behaviour of tapered and straight-sided wall piles at low and high confining pressures using the head driving method.

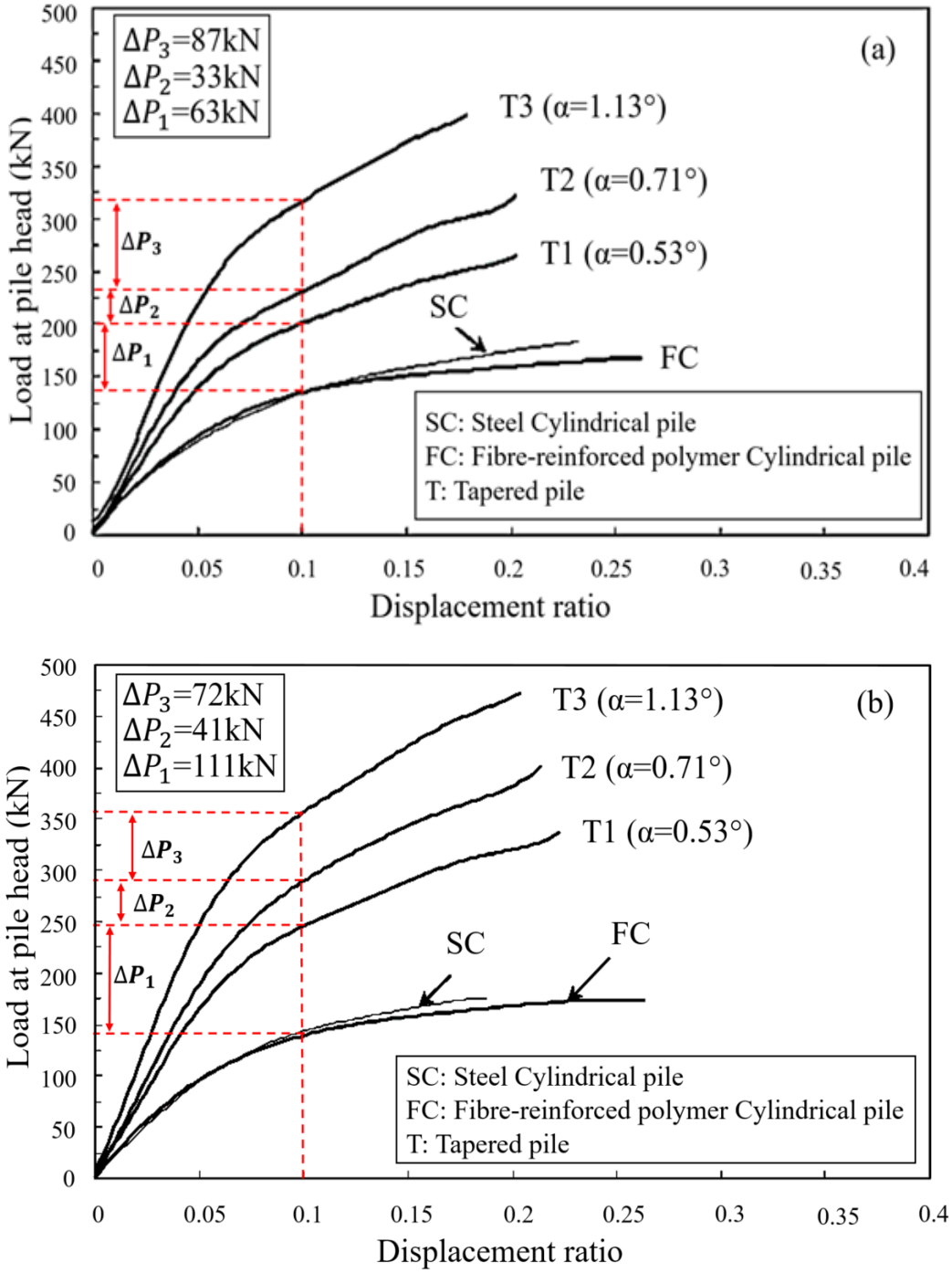

Figure 2.14. Load-settlement curves for piles tested using the head driving method at (a) low confining pressures (b) high confining pressure (after Sakr et al., 2004)

Referring to Figure 2.14, by increasing the tapering angle of piles, the load-carrying capacity of piles increases. The results of the study of Wei (1998) has confirmed the

efficiency of tapered piles comparing to straight-sided wall piles with the same material and in all loading conditions. It is determined that tapered piles indicate a more reasonable distribution of pile material in a number of aspects. As can be observed in Figure 2.15, tapered piles can present more efficient behaviour in terms of bearing capacity and settlement, compared to their counterpart cylindrical piles. However, in dense sand, the amount of bearing capacity enhancement is not significant.

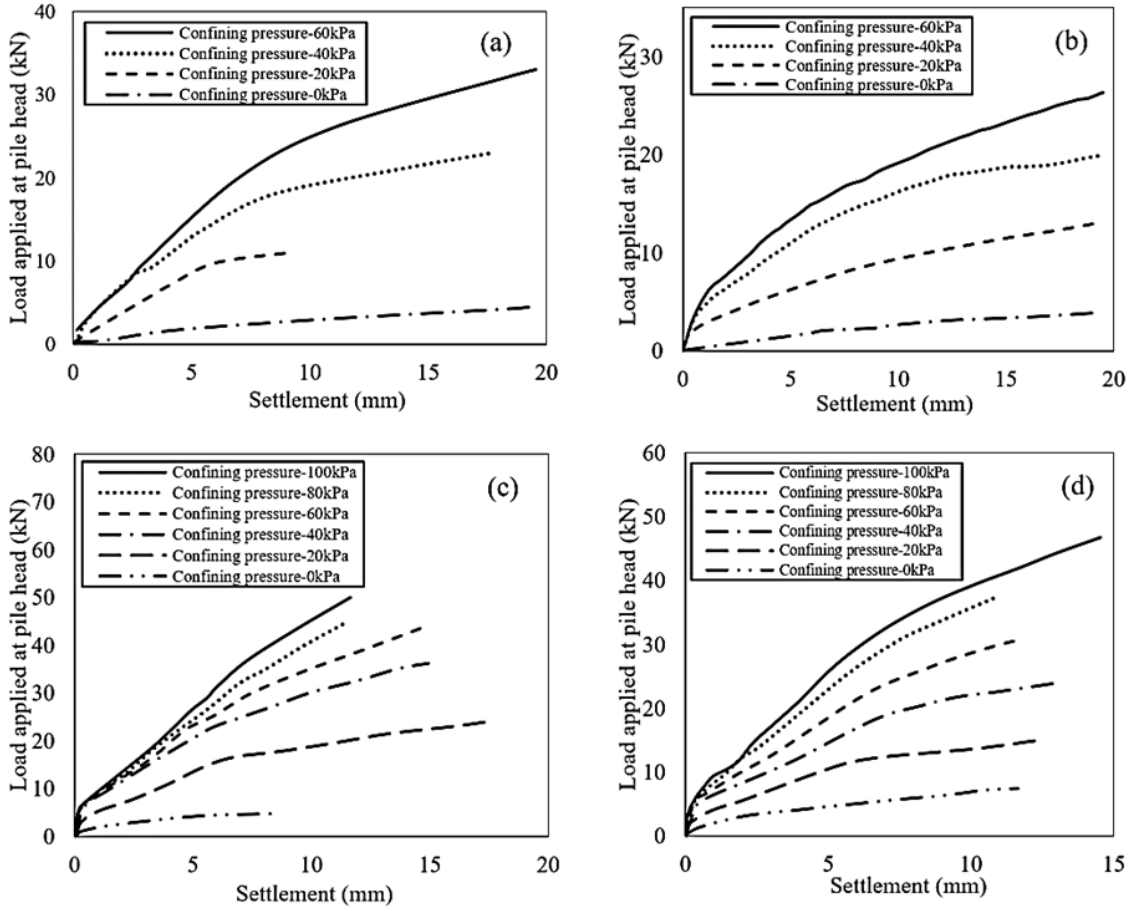

Figure 2.15. Load-settlement diagrams for piles embedded in soil with different confining pressures (a) tapered pile in dense sand (b) straight side pile in dense sand (c) tapered pile in loose sand (d) straight side pile in loose sand (after Wei, 1998)

Khan et al. (2008) investigated the construction and performance of bored tapered piles (made from concrete material) in frictional-cohesive soil. Their (Khan et al. 2008) report illustrates that tapered piles having a tapering angle of 0.96 to 1.92 can provide a load-carrying capacity about1.5 times of their counterpart same volume

cylindrical piles. However, the obtained lab results from experiments are dependent on the specific site characteristics. Table 2.2 presents a comparison between tapered and same volume cylindrical piles based on unit capacity (capacity per unit volume) (Khan et al. 2008).

Table 2.2. Comparison of the capacity of tapered and straight piles (after Khan et al., 2008)

No.	Tapering angle	Length	Concrete volume (m^3)	Volume difference (%)	Axial Capacity (kN)	Capacity increase (%)	Unit capacity (kN/m^3)	Increase in unit capacity (%)
1	0.95°	1.524	0.062	24% more	287	61	4629	30
2	0.95°	1.524	0.038	24% less	205	15	5395	51.50
3	1.91°	1.524	0.05	same	271	52	5420	52
4	0°	1.524	0.05	-	178	-	3560	-
5	0.95°	3.048	0.1	same	412	28	4120	28
6	0°	3.048	0.1	-	321	-	3210	-

According to the data summarised in Table 2.2, for piles having approximately 3m length, tapering effect contributed up to 28% in the unit capacity. This value for piles with 1.5 length reaches to 30% and 52% at tapering angles of 0.95° and 1.91°, respectively. According to Rybnikov (1990), the reason behind the increase in bearing capacity of a tapered pile (per m^3 of material) is the wedge effect under loading. It is revealed that the practical benefit of bored cone shaped piles in non-saturated cohesive soils is obvious. In addition, it is clarified that they are specifically effective under highly confined pressures in reconstruction projects. However, the prime reason for not widely applying tapered piles in practice can be associated with insufficient investigations on their operating characteristics and lack of confidence in practising engineers.

Fahmy & El Naggar (2017), investigated the axial capacity of spun-cast ductile iron (SCDI) tapered pile combined with a lower helical plate. Besides a 3D finite element analysis has been conducted in their effort to evaluate the axial performance of the system. According to their report, tapered helical piles demonstrated a stiffer response

and yielded higher capacities compared to the straight-sided ones. Livneh & El Naggar (2008) found that the load transfers in soil mainly through a cylindrical shear failure adjacent to the tapered profile. Test results of the study conducted by Spronken (1998) have shown that bearing capacity increases as volumetric displacement, confining pressure, tapering angle, and depth of driving increase. Consequently, tapered piles provided significantly greater bearing capacity under high confining pressure conditions. Figure 2.16 presents the variation of the lateral earth pressure coefficient surrounding the pile body by changing the tapering angle (Nordlund 1963).

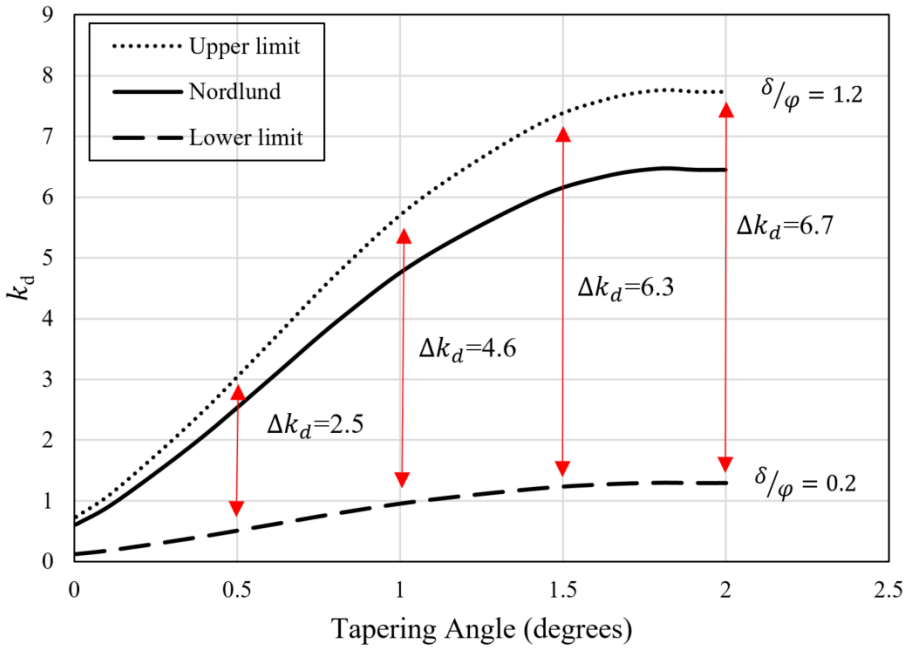

Figure 2.16. Variation of lateral earth pressure coefficient surrounding the pile body vs tapering angle (after Nordlund, 1963)

Referring to Figure 2.16, the lateral earth pressure coefficient increases until the tapering angle reaches to 2°, which can prove the effectiveness of tapered piles. Table 2.3 presents the bearing capacity of straight and tapered piles in the laboratory with a length of 0.73 m (Spronken 1998).

Table 2.3. Bearing capacity of straight and tapered piles with 0.73 m length (after Spronken, 1998)

Capacity	0°	0.5°	1°	2°
Total (N)	1,009	968	757	1,116
Tip (N)	938	403	111	233
Tip (kPa)	463	855	235	494
Settlement (mm)	7.9	7.7	8.2	7.5
Volume (cm^3)	1,480	583	863	1,171
%age of str. Vol.	100 %	39.4 %	58.3 %	79.1 %

The analysis conducted by Fellenius et al. (2000) has determined the magnitude and distribution of the real shaft and base resistances along with the residual load. It is proving that most of the pile capacity has been developed in the base section of the pile approving with effective stress principles. At the maximum applied load, in the tapered section, the resistance has been provided by fully mobilized positive shaft resistance and the toe resistance component that is movement dependant.

Gupta (2015) integrated some of the efforts related to tapered and step-tapered piles as a review report. Other studies have been conducted including field tests on single and group of step-tapered piles in cemented sand as well as pile load tests in clay under axial loading condition (Ismael 2001, 2003, 2006, 2009; Majumder & Chakraborty 2018).

The load-settlement behaviour of tapered piles under lateral loading is obtained for piles having the same length and volume of 1.524m and $0.033m^3$, respectively, and various tapering angles of 0°, 0.53°, 0.71° and 1.13° (Sakr et al. 2005) and 0°, 0.6° and 0.95° (El Naggar & Wei 1999b). For predicting the p-y curves of tapered piles, Sakr et al. (2005) suggested using a taper coefficient in the model proposed by Bhushan & Askari (1984); Bhushan & Haley (1980); Bhushan et al. (1981); Meyer & Reese (1979) based on full-scale load test results in sand as presented in Equation 2.7.

$$p = KzF_1F_2K_{tl}.y \qquad 2.7$$

where, k is a function of the lateral deflection (y), F_1 and F_2 are two factors dependent on the groundwater location and soil relative density, K_{tl} is defined in Equation 2.6, and z is the depth where the p-y curve is generated. While Sakr et al. (2005) have shown using a taper coefficient directly in Equation 2.7 can lead to reasonable results, the proposed model has not been accounted for pile geometry and material properties such as tapering angle and stiffness as well as soil continuity and homogeneity. Figure 2.17 illustrates the p-y curves of the tested piles under the static lateral loading condition as a comparative diagram between the obtained results by Sakr et al. (2005) and El Naggar & Wei (1999b) at zero confining pressure.

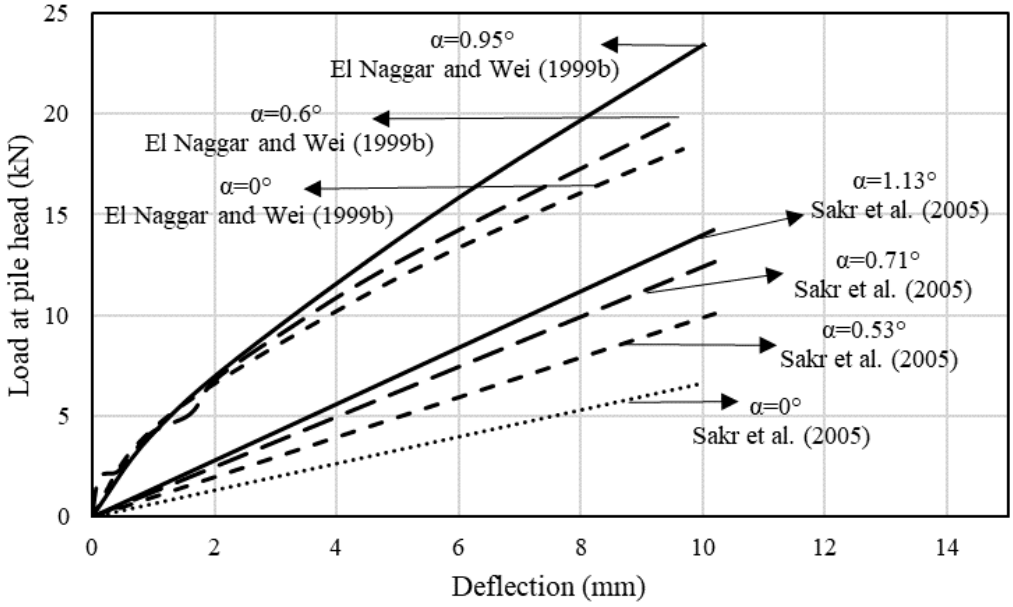

Figure 2.17. Comparative p-y diagrams of piles under static lateral loading condition at zero confining pressure

2.3.2 Analytical investigations

Many researchers have carried out a wide range of analytical investigations on tapered piles axially loaded. Some of them have considered the plastic behaviour of the soil near the ground surface into account or used the finite element method (Gotman 2000; Kurian & Srinivas 1995; Reddy & Ramasamy 1973). Some researchers used the cavity expansion theory to propose analytical models for predicting the end resistance or investigated the buckling and load distribution pattern of a tapered pile (Lee et al. 2018; Liu et al. 2012; Manandhar & Yasufuku 2012). A well-known study carried out

by Kodikara & Moore (1993) employing the axial behaviour of tapered piles in a cohesive-frictional ground. Based on their work, Equations 2.8 to 2.11 are presented for calculating the axial deformation of a tapered pile using Figure 2.18, which can illustrate the geometry of a complete tapered pile and its segment.

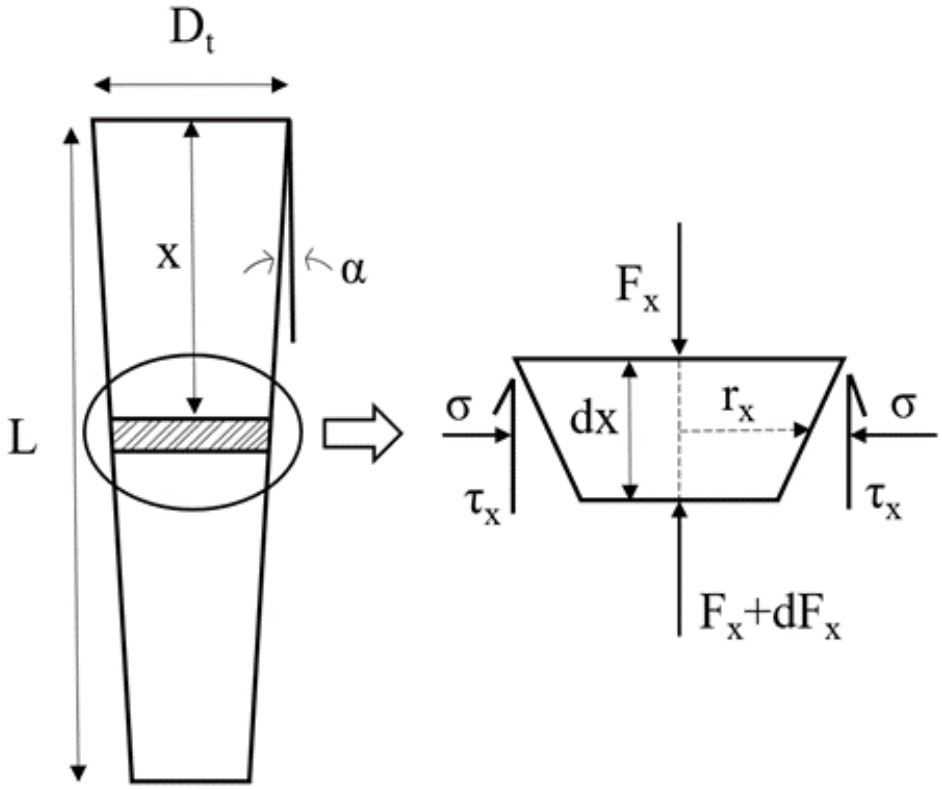

Figure 2.18. The schematic of complete tapered pile and its element (complete tapered pile; and the element at depth x) (after Kodikara and Moore, 1993)

$$\frac{dF_x}{dx} = 2\tau_x \pi r_x \qquad 2.8$$

$$r_x = r_m + \left(\frac{L}{2} - x\right)\tan\alpha \qquad 2.9$$

$$\frac{du_p}{dx} = \frac{F_x}{AE_p} \qquad 2.10$$

$$\frac{d^2u_p}{dx^2} - \frac{2\tan\alpha}{\left[r_m+\left(\frac{L}{2}-x\right)\tan\alpha\right]}\frac{du_p}{dx} = \frac{2\tau_x}{\left[r_m+\left(\frac{L}{2}-x\right)\tan\alpha\right]E_p} \qquad 2.11$$

In the above equations and at depth x, A is the area of the pile cross-section; E_p is elastic modulus of the pile material; F_x is the axial force; τ_x is a function of pile

deformation and u_p denotes the vertical component of the stress at the pile-soil interface. Moreover, r_x is the pile radius for a pile of embedded length L; α is the tapering angle, and r_m is the mean pile radius along the embedded length.

2.3.2.1 Axial force distribution law

The load transfer mechanism in a tapered rigid pile based on Mohr-Coulomb theory is presented by Liu et al. (2012). Based on their model, a tapered pile is divided into M segments. A local coordinate system H_i (for i = 1, 2. . . M) is defined for each segment, as shown in Figure 2.19, where L_i is the length of the i^{th} element, and α is the tapering angle.

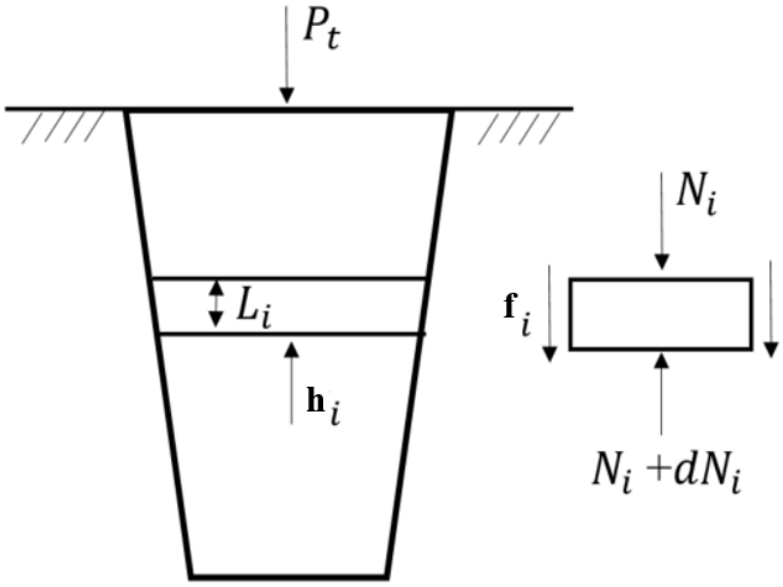

Figure 2.19. Schematic diagram of a single tapered pile and the element forces (after Liu et al., 2012)

A segment of length dh_i (which has been selected from the i^{th} element) is considered. According to Hooke's law and the vertical equilibrium state of this element, the controlling differential equations for the i^{th} element are obtained as:

$$\frac{\partial^2 p_i(h_i)}{\partial h_i^2} = \frac{2}{E_p r_i} f_i(h_i) \qquad 2.12$$

$$N_i(h_i) = -E_p \pi r_i^2 \frac{\partial p_i(h_i)}{\partial h_i} \quad 2.13$$

where $f_i(h_i)$ and $p_i(h_i)$ are the skin friction resistance and vertical displacement for section h_i of the i^{th} pile, respectively, E_p is the pile elastic modulus, and r_i is the average radius of the i^{th} element. It is presumed that $p_i(h_i)$ is the settlement of the i^{th} element under the pile-top load. Based on the geometrical relationships, the soil radial displacement adjacent to the pile can be given by Equation 2.14:

$$d_{ci} = p_i(h_i) tan\alpha \quad 2.14$$

The pile lateral pressure increment produced due to the settlement of the pile is defined as ζ_{ri}, the corresponding soil radial displacement adjacent to the pile, based on elastic theory, can be yield acquired by Equation 2.15:

$$d_{ri} = \zeta_{ri} \frac{(1+\upsilon_{si}) r_i}{E_{si}} \quad 2.15$$

where υ_{si} and E_{si} are the Poisson's ratio and Young's modulus of the i^{th} layer of soil, respectively. Finally, based on the displacement compatibility condition, $d_{ci}=d_{ri}$, and pile lateral pressure increment produced due to the settlement of the pile can be determined by Equation 2.16:

$$\zeta_{ri} = \frac{E_{si}\, tan\alpha}{(1+\upsilon_{si}) r_i} p_i(h_i) \quad 2.16$$

The limitation of Equation 2.16 for calculating the pile lateral pressure increment can be associated with some simplifications based on elastic theories, which may not lead to accurate results. Besides, according to Equation 2.16, the pile lateral pressure increment is not dependent on three key parameters of soil namely, the relative density, the lateral earth pressure coefficient and the overburden pressure, which still proves the insufficiency of the presented equation.

2.3.2.2 Analytical discussion

Fellenius & Altaee (1999) generated an analytical discussion about the behaviour of tapered piles conducted by Wei & El Naggar (1999). The main part of the discussion is about enabling the lateral stress to be increased as the cylindrical test chamber lined with an "air bladder". The discussers stated their disagreement for the claiming that the lateral stress state of the model pile can be comparable to the real stress state of the prototype. Wei & El Naggar (1999) have replied by referring to Vesic (1977), amid others, who have recommended that unit shaft capacity for piles in sand is measured using the lateral effective soil stress, volumetric variations in soil, and the grain crushability and re-arrangement. Wei & El Naggar (1999) have also mentioned that the lateral pressure in the chamber test at the tip of the pile model was a suitable illustrative of the lateral effective pressure in the prototype at the pile tip.

2.3.3 Numerical investigations

Several researchers performed numerical analysis to investigate the behaviour of tapered piles under different loading conditions. Most of the studies conducted using the finite element method (FEM) and different commercially available software packages. In some studies a two-dimensional or three-dimensional numerical modelling has been applied to compare the bearing capacity and settlement of foundations with different geometries such as tapered and under-reamed piles (Hataf & Shafaghat 2015a, 2015b; Kong et al. 2013; Paik et al. 2013; Shafaghat 2013; Shafaghat et al. 2018; Vali et al. 2019; Zhan et al. 2012). Other studies performed to investigate the axial performance of square shaft helical tapered piles in sand under compressive and tensile loading (Fahmy & El Naggar 2017; Livneh & El Naggar 2008). Similar to the well-known analytical equations proposed by Kodikara & Moore (1993), a numerical analysis has been performed by Kodikara et al. (2006). According to their study, the side resistance of tapered piles in mudstone has been evaluated, which clearly illustrates the beneficial effects of these kinds of piles comparing to cylindrical ones in mudstone.

As mentioned above, the bearing capacity of tapered pile groups has been numerically compared using 3D FEM, and a study has been performed on optimizing the resistance of tapered piles in large scale (Hataf & Shafaghat 2015a, 2015b). Based on their

studies, to consider a foundation as a pile, it is usually conventional that the ratio of the pile depth to its width be greater than 6. According to this definition, the maximum tapering angle is 9.468 that can be considered for a tapered pile. The geometry of piles that have been investigated by (Hataf & Shafaghat 2015a, 2015b) are illustrated in Table 2.4.

Table 2.4. The geometry properties of the modelled tapered pile (Hataf & Shafaghat, 2015)

Pile	α (degree)	L (m)	R_T (m)	R_B (m)	V (m^3)
Cylindrical	0°	10	0.3	0.3	2.83
Tapered1	0.4°	10	0.33	0.26	2.83
Tapered2	0.8°	10	0.37	0.23	2.83
Tapered3	1.2°	10	0.4	0.19	2.83
Tapered4	1.6°	10	0.43	0.15	2.83

In Table 2.4, α is tapering angle, L is the pile length, V is the volume of pile and R_B and R_T are the bottom and top radius of pile, respectively. Figure 2.20 illustrates the calculated optimum tapering angles of piles in three different relative densities of sand.

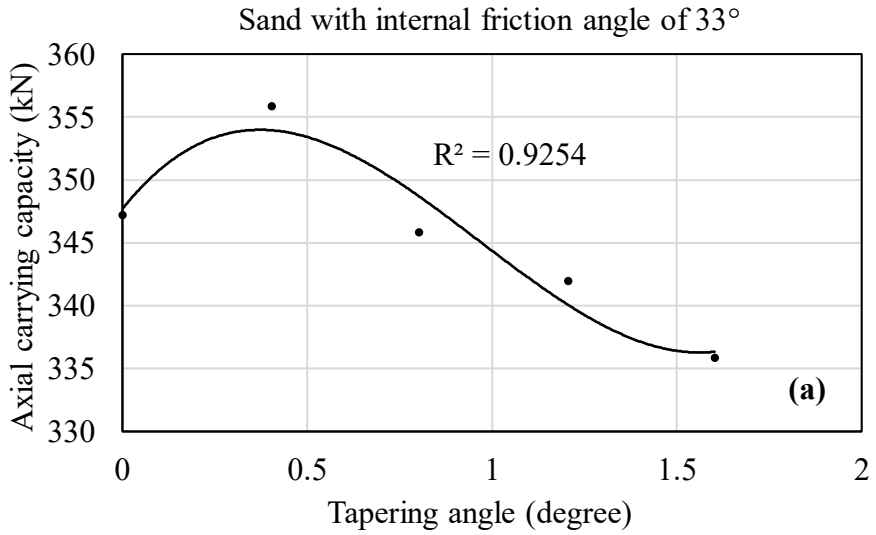

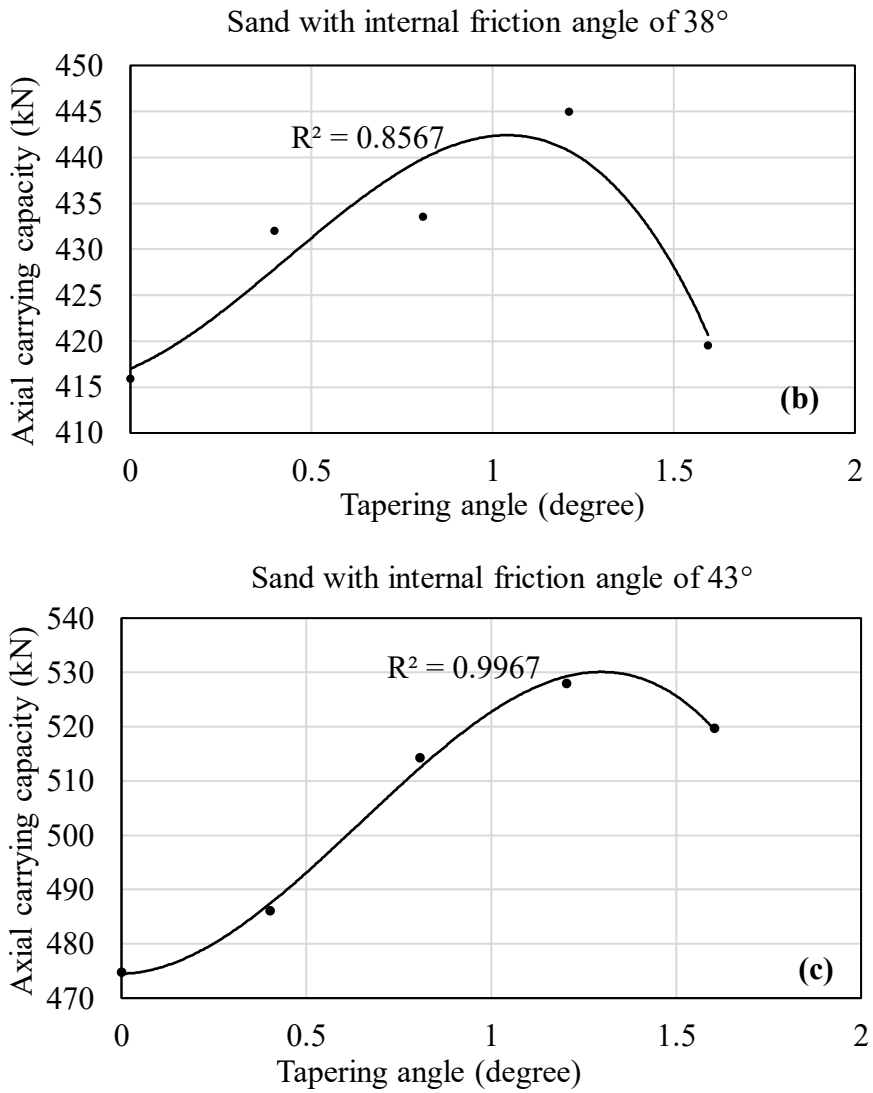

Figure 2.20. Optimum tapering angles of piles in sand with various friction angles (a) Loose sand, (b) Medium sand, (c) Dense sand (after Hataf and Shafaghat, 2015)

Figure 2.20 suggests that by increasing the relative density of sand, the optimum tapering angle increases. Further numerical analysis is required to find the relation of the optimum tapering angle of piles with strength characteristics of soils as well as pile-soil interface properties. Besides to the above investigations, there are several studies around the tapered pile foundations under dynamic loading conditions and also around the bearing capacity behaviour of conventional cylindrical piles which is out of the scope of this research.

2.4 Dynamic axial and lateral loading conditions

2.4.1 A brief review of experimental, numerical and theoretical models

In order to pertain the axial and lateral dynamic response of cylindrical piles a limited number of experimental tests have been conducted. Some experimental investigations reported in the literature are related to the behaviour of full-scale single prototype piles (Elkasabgy & El Naggar 2013; Manna & Baidya 2009; Puri 1988). Some other laboratory tests have been performed to assess the response of small-scale pipes (open ended hollow piles) (El-Marsafawi et al. 1992; Han & Novak 1988; Novak & F. Grigg 1976). However, based on the literature surveys, there are a limited number of experimental tests and numerical surveys have been performed to evaluate the axial and lateral response of tapered piles under dynamic loading conditions. Although some of the efforts in evaluating the response of tapered pile models under cyclic loading have been conducted by El Naggar & Sakr (2002) and El Naggar & Wei (2000a), the loading type has been categorised as nondynamic cyclic loading case similar to wave and wind loads or tidal effects where the load is applied with slow variations.

Generally, several theoretical studies have been performed including developed models for investigating the dynamic axial and lateral behaviour of piles having a non-uniform cross-section (Bryden et al. 2018a, 2020; Dehghanpoor & Ghazavi 2012; Ghazavi 2000a, 2000b, 2003, 2006; Ghazavi 2007, 2008; Ghazavi et al. 2003; Ghazavi et al. 2007; Ghazavi & Dehghanpour 2010; Ghazavi & Etaati 2001; Saha & Ghosh 1986; Tavasoli & Ghazavi 2018, 2020; Xie & Vaziri 1991). Some of the proposed theoretical models have been incorporated the geometric damping, which is a governing form of energy dissipation and attributes to the deformed surface area during the wave propagation (Bryden et al. 2018a; Novak 1977). Other studies have not included the material damping, which according to Bryden et al. (2018b) can affect the dynamic response of piles (Ghazavi 2008; Saha & Ghosh 1986; Xie & Vaziri 1991). Among the proposed models for examining the dynamic response of tapered piles, Ghazavi (2008) has developed a method which its fundamental concept is based on the elastodynamic model proposed by Novak (1974, 1977) using a segment by segment (SSM) method.

2.4.2 Tapering angle, slenderness ratio and stiffness effects

Saha & Ghosh (1986) have presented an approximate method to analyse tapered piles under vertical vibration and account for soil-pile interaction. According to their model, with an increase in the tapering angle, the resonant amplitude decreases and the resonant frequency increases (Figure 2.21).

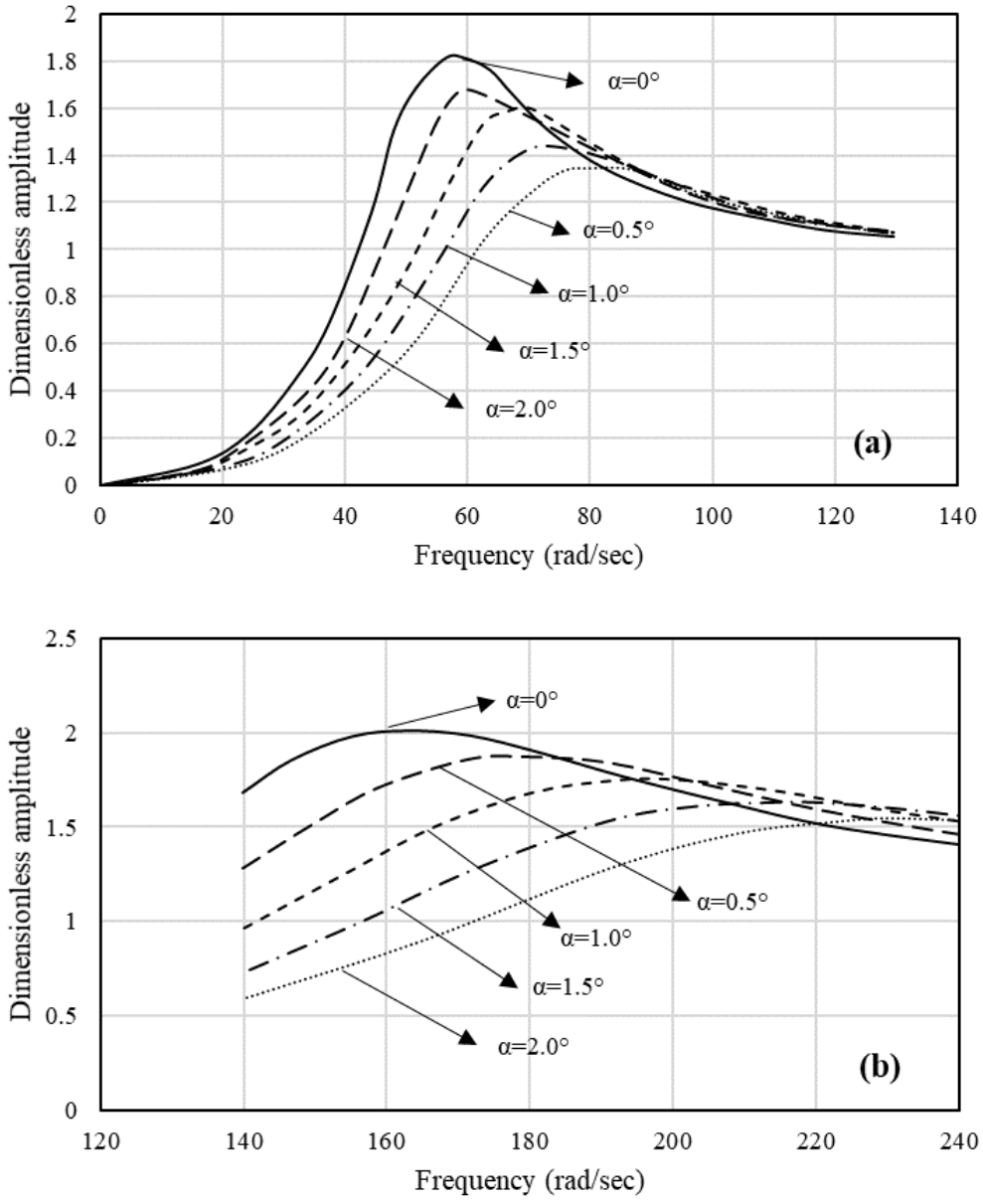

Figure 2.21. Effect of tapering angle on resonant frequency and amplitude (a) $\vartheta = 0.33; v_s = 105 ft/sec$; l/r=20; r=3.94in. b) $\vartheta = 0.33; v_s = 315 ft/sec$; l/r=20; r=5.91in (after Saha and Ghosh, 1986).

This increase in the resonant frequency is dependent on two important parameters of soil stiffness and slenderness ratio (Saha & Ghosh 1986). This means for piles embedded in stiffer soil and having same slenderness ratio, the increasing resonant frequency with increasing tapering angle is more significant. According to Saha & Ghosh (1986), with an increase in the tapering angle, the stiffness of tapered piles increases and the damping decreases. The slenderness ratio also has similar effect on the stiffness and damping parameters of tapered piles with respect to tapering angle; however, for *l/r* ratios of less than 30, where l is the length and *r* is the mean radius of piles, the damping parameters have an increasing trend. In another survey, the response of elastic tapered piles to harmonic vibration loading condition has been predicted through a mathematical method (Ghazavi 2008). It is worth mentioning that the use of tapered piles is superior comparing to their counterpart cylindrical piles as dynamically loaded piles (Ghazavi 2008). This conclusion routes from the geometrical aspect of cone-shaped piles, which can compact the adjacent soil due to their inclined body. This advantage is even more highlighted when the pile has an optimum tapering angle as can be seen in Figure 2.20 (Hataf & Shafaghat 2015a, 2015b; Shafaghat 2013).

The lateral movement of tapered piles to seismic loading has been evaluated using the wave propagation theory (Ghazavi 2007). It has been found that tapered piles show more flexibility comparing to their same volume straight side piles under the same frequency (Ghazavi 2007). Hence, it is expected that due to the concentration of material around the top portion of tapered piles a greater base shear can be induced. Bryden et al. (2018a, 2020) have developed a theoretical model, which does not incorporate the segment by segment method (SSM), to obtain the damping and stiffness parameters of tapered piles. According to Bryden et al. (2018a), as the tapering angle increases, particularly under axial vibration loading condition, the resonant amplitude of tapered piles decreases (Figure 2.22). This advantage can make tapered piles more beneficial for dynamic design applications.

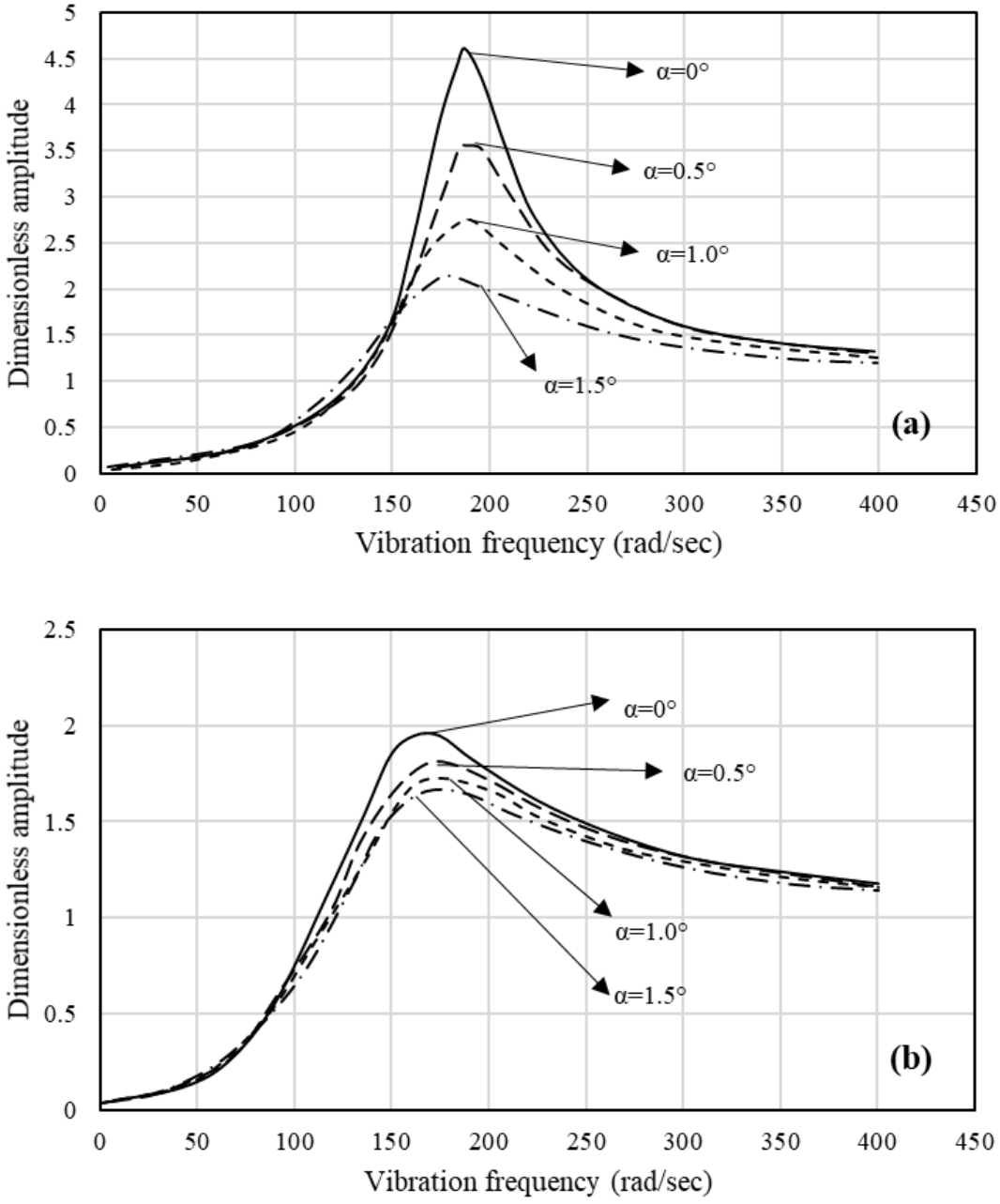

Figure 2.22. Dimensionless amplitude vs. vibration frequency for (a) end-bearing piles (b) floating piles (after Bryden et al., 2018)

2.4.3 Load-displacement behaviour

The load-displacement behaviour of tapered piles under cyclic loading condition has been obtained through several experimental tests and using chamber and centrifuge facilities (El Naggar & Sakr 2002; El Naggar & Wei 2000a). According to the results obtained from centrifuge tests, there is a degradation in shaft resistance of tapered piles in small settlements, while piles show a stiffer behaviour after cyclic loading in larger

settlement levels (El Naggar & Sakr 2002). Another important result is that due to the "shake down" phenomenon reported by Poulos (1982), and due to the considerable small amplitude of loading (comparing to the load capacity of pile), the deflection of tapered piles in the tests has been stabilized, particularly for the tapering of 0.35°. This phenomenon is due to the fact that the pile reaches to the state of residual stresses and permanent strains, which makes the pile to respond elastically to further loading cycles. A possible reason of the "shake down" phenomenon for tapered piles can be referred to the soil densification adjacent to their shaft because of their inclined body. The load-settlement diagrams of piles with different tapering angles embedded in sand with no confining pressure are illustrated in Figure 2.23, depicting the first and last load cycles (El Naggar & Wei 2000a).

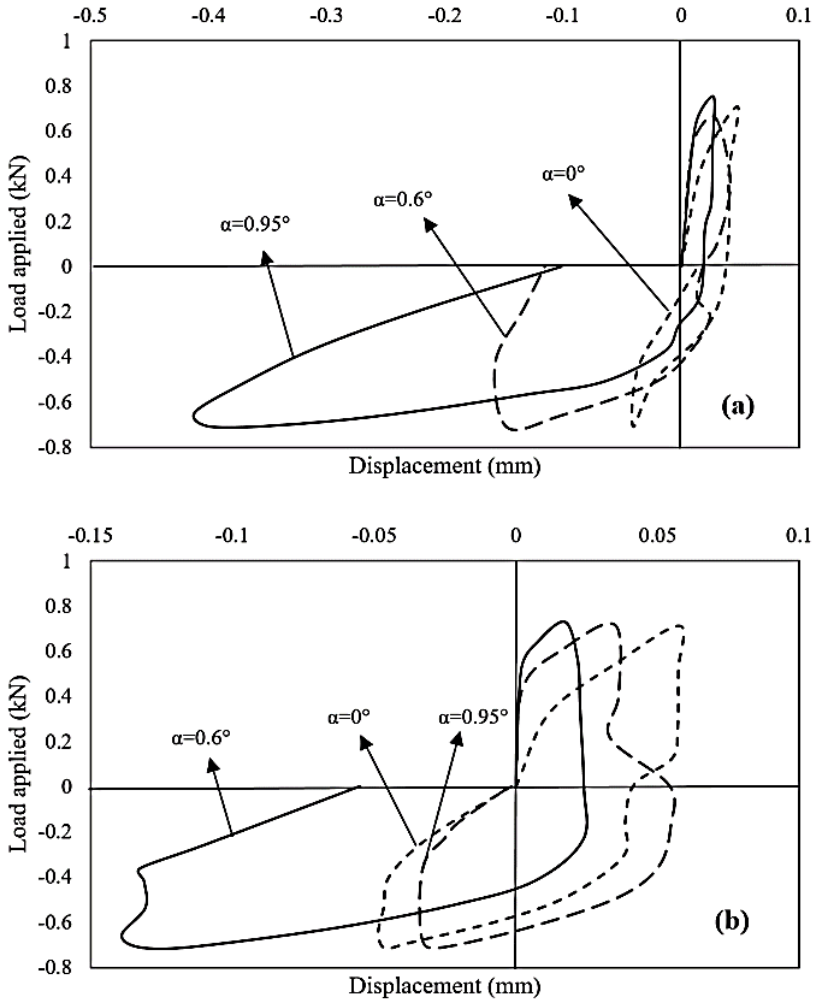

Figure 2.23. Load-settlement diagrams of piles having different tapering angles at no confining pressure (a) the first load cycles (b) the last (10th) load cycles (after El Naggar and Wei 2000a)

2.4.4 Mathematical developments

Several mathematical relationships have been developed to obtain the dynamic response of tapered piles using various assumptions such as segment by segment method (Ghazavi 2003; Ghazavi 2007, 2008; Ghazavi et al. 2003; Ghazavi & Etaati 2001), or by finite difference method (Saha & Ghosh 1986), or even the recent advanced computational method, which accounts for pile material damping (Bryden et al. 2018a, 2020). According to Saha & Ghosh (1986), the differential equation for damped vibration of a tapered pile is as follow:

$$m(z)\frac{\partial^2 W(z,t)}{\partial t^2} + c\frac{W(z,t)}{\partial t} - EA(z)\frac{\partial^2 W(z,t)}{\partial z^2} + S_w(z,t) + S_R(z,t) = 0 \qquad 2.17$$

where, $m(z)$=pile mass (per unit length at depth z), c is coefficient for damping of pile material, E is the Young's modulus, $A(z)$ is the area of pile cross-section at z elevation, $S_w(z,t)$ is the shaft reaction on the projected vertical surface at depth z (per unit length), and $S_R(z,t)$ is the soil reaction on the projected horizontal circular surface at depth z (per unit length). Ghazavi (2008) developed another mathematical method, using the segment by segment method (SSM), which assumes that the pile is embedded in an isotropic, homogeneous, and linearly viscoelastic media. The governing differential equation used by Ghazavi (2008) is inspired from the one represented by Novak & Aboul-Ella (1978) and similar to the abovementioned relationship (Equation 2.17). The only difference is that instead of considering the assumed vertical and horizontal projected planes and considering the forces on those planes, it accounts for the shear modulus of the surrounding soil and the time-dependant complex amplitude at any z level, and a dimensionless parameter of soil resistance. Moreover, Bryden et al. (2018a) have considered the inertial and damping forces within the tapered piles as well as shear modulus of the adjacent soil.

On the other hand, for predicting the response of tapered piles under lateral harmonic loading condition Dehghanpoor & Ghazavi (2012) have developed a method which assumes the linear-elastic behaviour for tapered piles. This method is based on the governing differential equation, which has been proposed by Novak (1974) and is given as:

$$m_{pj}\frac{\partial^2 u_j(z,t)}{\partial t^2} + c_{pj}\frac{\partial^2 u_j(z,t)}{\partial t} + E_{pj}I_{pj}\frac{\partial^4 u_j(z,t)}{\partial z^4} + G_{sj}S_{uj}u_j(z,t) = 0 \qquad 2.18$$

where, m_{pj} denotes the mass (per unit length), c_{pj} is the coefficient of damping, $E_{pj}I_{pj}$ refers to the bending stiffness of the j^{th} segment, G_{sj} denotes the soil shear modulus, $u_j(z,t)$ is the time-dependant complex amplitude at any z level, and S_{uj} is a dimensionless parameter related to soil resistance. As can be seen, the existing equations are based on the assumptions that presume a linear-elastic behaviour for pile material embedded in a homogeneous isotropic soil layer. Hence, further analytical analysis highly seems demanding to observe the response of tapered piles subjected to dynamic axial and lateral loading conditions. Besides, the proposed analytical equations need to be validated with experimental test results or field measured data, which is a notable knowledge gap in this field.

2.5 Case history on tapered piles application

The application, behaviour and capacity of tapered steel pipe piles based on the load testing at John F. Kennedy International Airport (JFKIA) in the United States of America has been surveyed (Horvath 2004a, 2004b; Horvath & Trochalides 2004; Horvath et al. 2004a, 2004b). Figure 2.24 demonstrates the measured versus calculated load-settlement curves at JFKIA after approximately half a century.

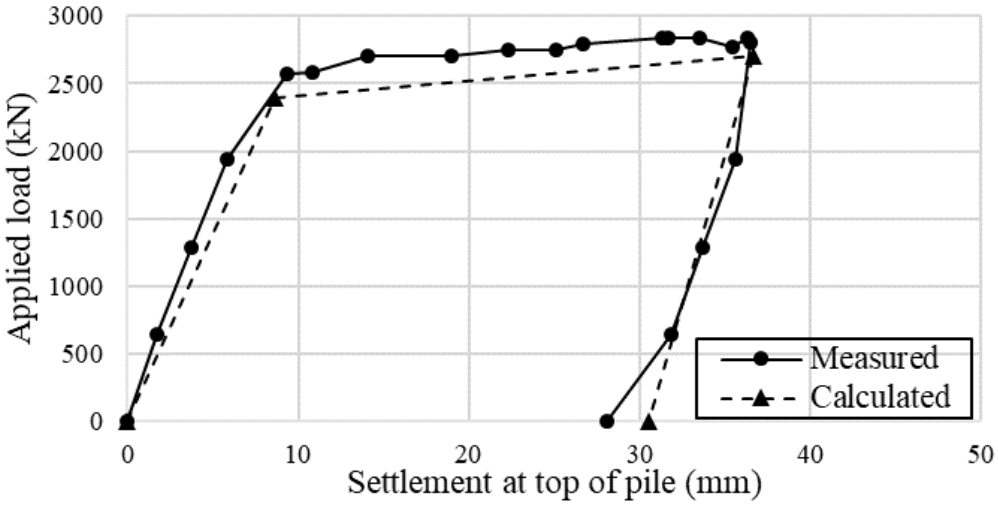

Figure 2.24. Measured versus Calculated Load-Settlement Curves for JFKIA (after Horvath and Trochalides, 2004)

Implementation of tapered piles has proven their reliability for use in significant projects. For instance, their wide implementation at JFKIA has confirmed their ability to bear the total spectrum of axial and lateral loadings due to transportation applications.

2.6 Pile group

When a number of piles are close enough together, it is expected that the soil stresses created from either point bearing or side friction of adjacent piles overlap as illustrated in Figure 2.25. The amount of additional stress depends on the piles' spacing, geometry, pattern, and other parameters related to the pile geometry or the soil properties. If these stresses sufficiently grow, the soil may fail in shear or additional settlements may take place. Hence, piles interact with each other in groups through the surrounding soil, resulting in what is called the group action or pile-soil-pile interaction. Obviously, as spacing of piles increases, stress in overlapped zones noticeably decreases.

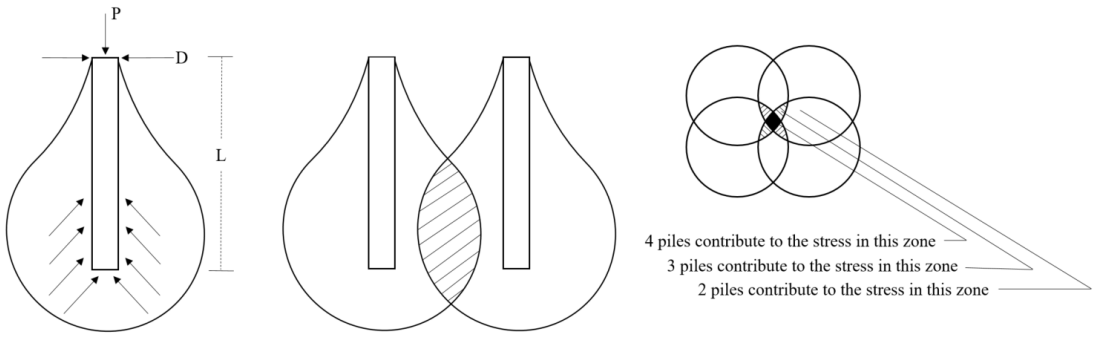

Figure 2.25. Stresses surrounding a pile and the summing effects of a pile group (after Bowles 1996)

In practice, piles are usually used in groups so as to transfer the structural burden to a stronger, and deeper soil strata and also to reinforce the surrounding soil. The other characteristic of a pile group is the cap which connects all piles together through their heads to act as a group. Usually the cap of a pile group is constructed to support structure columns and also to distribute load on piles evenly.

2.6.1 Efficiency of pile groups

Most of the established analytical methods are presented for isolated single piles rather than pile groups; the complication assessment of pile group behaviour may be the reason of it. Concerning pile group design the two main problems are pile group efficiency (η) and the group settlement factor (S_f) as follows:

$$\eta = \frac{Q_g}{\sum Q_s} \qquad 2.19$$

$$S_f = \frac{S_g}{S_S} \qquad 2.20$$

where, Q_g is the capacity of the pile group, Q_s is the capacity of a single pile, S_g is the settlement of the pile group and S_s is the settlement of an individual pile.

If the group capacity is the sum of all individual pile contributions, the group efficiency will be then $\eta = 1$. The ASCE Committee on Deep Foundations report (CDF) suggests that friction piles in cohesionless soils at the usual spacing of $s = 2D$ to 3D will have a group efficiency $\eta > 1$. The reason assumed is that in frictional soil the pile displacement along with driving vibrations increases the soil density in a vicinity zone of the pile, which is further increased as other adjacent piles are driven. Considering friction piles in cohesive soils, the point bearing along with block shear of the group is used as the group capacity, but in this condition, rarely the group capacity is to be considered more than the single pile capacity times the number of piles. However, if the cap is laying on the ground, only the block bearing capacity should be involved. In this case the pile group will settle with the soil as the piles will also settle that much. For free standing cap, the group bearing capacity would be sum of the individual point capacities and block perimeter shear. According to the pile survey conducted by Focht and O'Neill (year?), basically the CDF recommendations for pile groups were being used.

2.6.1.1 Existing group efficiency formulas

There are several relations to predict the group efficiency for conventional cylindrical piles. Some of the relations concerning group of piles in sand and some can predict

the efficiency in clay. Besides, based on cap condition of the group, the efficiency relations are divided into two categories as blow:

a) Pile group with cap laying on the ground

b) Pile group with free-standing cap

Most of the efficiency relations presented and applied for pile groups using below methods.

A. Terzaghi and Peck method

In this method and in case of block failure, a mathematical model is developed in order to estimate the ultimate capacity of pile groups. This equation can be expressed as follows:

$$Q_g = q_b BL + D_f(2B + 2L)s \qquad 2.21$$

where q_b is ultimate capacity per unit area of a rectangular loaded area with dimensions $B.\ L.\ D_f$, Q_g is the ultimate capacity of pile group, B is width of pile group, L is length of pile group, and s is average shearing resistance of soil per unit area. It has been revealed that block failure does not take place unless the number of piles in group are pretty large and they are embedded in soft clay or silt. Furthermore, a pile group is considered safe against block failure if the total design load does not exceed $Q_g/3$. The total design load can be determined through the number of piles multiplied by the ultimate bearing capacity per pile.

B. Converse-Labarre method

According to Chellis (1961) one of the most primitive formulas for predicting the group efficiency used is Converse-Labarre formula (contained in the Uniform Building Code of the International Conference of Building Officials and Specifications of the American Association of State Highway Officials). In this method the efficiency of a pile group η_g is expressed as:

$$\eta_g = 1 - \frac{\xi}{90^\circ} \cdot \left[\frac{(n-1)\cdot m + (m-1)\cdot n}{m \cdot n}\right] \qquad 2.22$$

where, m is number of rows, n is number of piles in a row, $\xi = \arctan(\frac{d}{s})$ in degrees, d is the pile diameter, and s is the centre-to-centre pile spacing. Converse-Labarre formula assumes the group action based on the pile diameter and the spacing between piles. It considers neither the pile length nor the soil properties for predicting the efficiency of pile groups.

C. Los Angeles Group Action method

This method considers another additional term that considers the influence of diagonal piles and it can be expressed as follows:

$$\eta = 1 - \frac{d[m(n-1)+n(m-1)+\sqrt{2}(n-1)(m-1)]}{\pi S m n} \quad 2.23$$

D. Master's method

In this method, the length of piles embedded in frictional soil is taken into consideration. This method is based on Boussinesq equations to predict the transferred load in soil. As Boussinesq method assumes only point load applying on plane boundary of a semi-infinite elastic isotropic solids, Master's method validity is questionable.

E. Feld method

Feld proposed a rule of thumb to estimate the pile group efficiency. In this method, the summation of the capacities of individual piles multiplied by a coefficient (based on the number of piles) ranging between 0.72 and 0.94, is the capacity of the group. This method considers reducing the bearing capacity of single piles in the group by 1/16 so that the effect of each neighbouring pile in the same row is considered. According to this method, different loads will be assigned to the piles based on their placement in a group, while in other revealed equations piles will bear equal loads.

F. Seiler & Kenney method

An empirical equation was offered by Seiler & Kenney (1944) based on the assumptions of Converse-Labarre theory. The relation can be expressed as:

$$\eta = 1 - \frac{11S(n+m-2)}{7(S^2-1)(n+m-1)} + \frac{0.3}{n+m} \quad 2.24$$

where, S denotes spacing in feet (ft) and the definition of other parameters are similar to the Converse-Labarre equation.

G. Whitaker method

Design diagrams are presented by Whitaker to estimate the efficiency of a pile group in clayey soil based on experimental results. These charts are used by U.S. Army Corps of Engineers and the U.S. Navy as the design manuals.

H. Poulos and Davis method

The pile group efficiency is defined as:

$$\frac{1}{\eta_g^2} = 1 + \left[\frac{(n \cdot m)^2 \cdot Q_O^2}{Q_B^2}\right] \quad 2.25$$

where, Q_B is the ultimate load capacity of the block of pile and Q_O is the ultimate load capacity of a single pile.

I. Pressure-area method

Chellis (1969) proposed a formula to predict the pile group efficiency. However, its application is only for the end bearing piles, since it assumes that the load is only transferred in vicinity of pile end surfaces and in a specific defined area of $2S' * 2S'$ in plan as Figure 2.26. This relation, for a square pattern of piles in a group is expressed as:

$$\eta = 1 - \frac{(2k+n)[2-(2k+n)]}{(2kn)^2} \quad 2.26$$

where, n is the number of piles in each row, k is defined as:

$$k = \frac{S'}{S} \quad 2.27$$

where, S is the pile spacing and S' is defined in Figure 2.26.

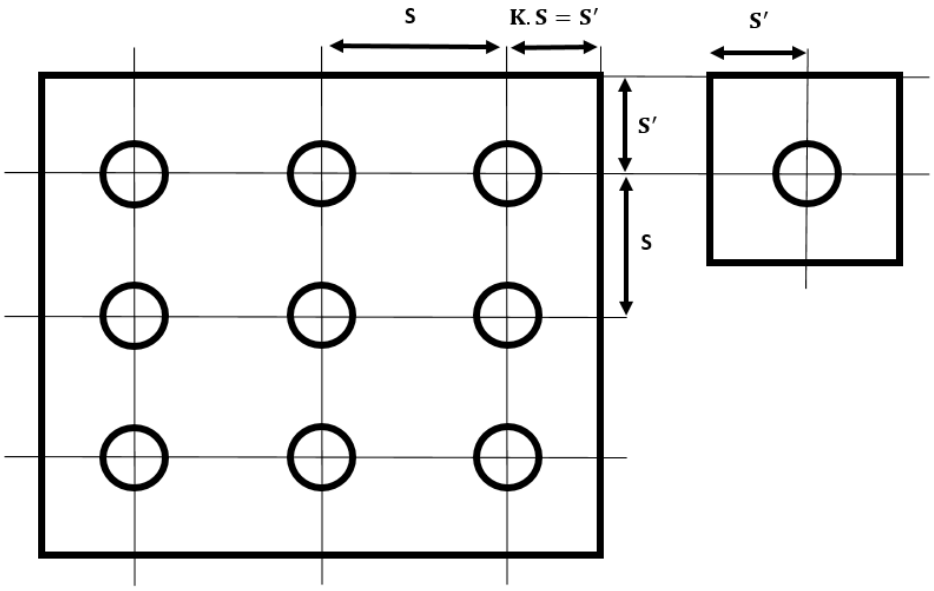

Figure 2.26. Distribution of vertical stress under individual pile and pile group (pressure-area formula, after Chellis 1969)

Figure 2.26 shows the vertical stress distributions under a 3x3 pile group and a single pile. It also demonstrates the definition of the parameter s' in the efficiency equation proposed by Chellis (1969).

J. Kishida and Meyerhof method

Kishida and Meyerhof proposed a diagram to predict the pile group efficiency based on different internal friction angles of soils and S/D ratio, where S is the pile spacing and D is the diameter of piles. The diagram is presented in Figure 2.27.

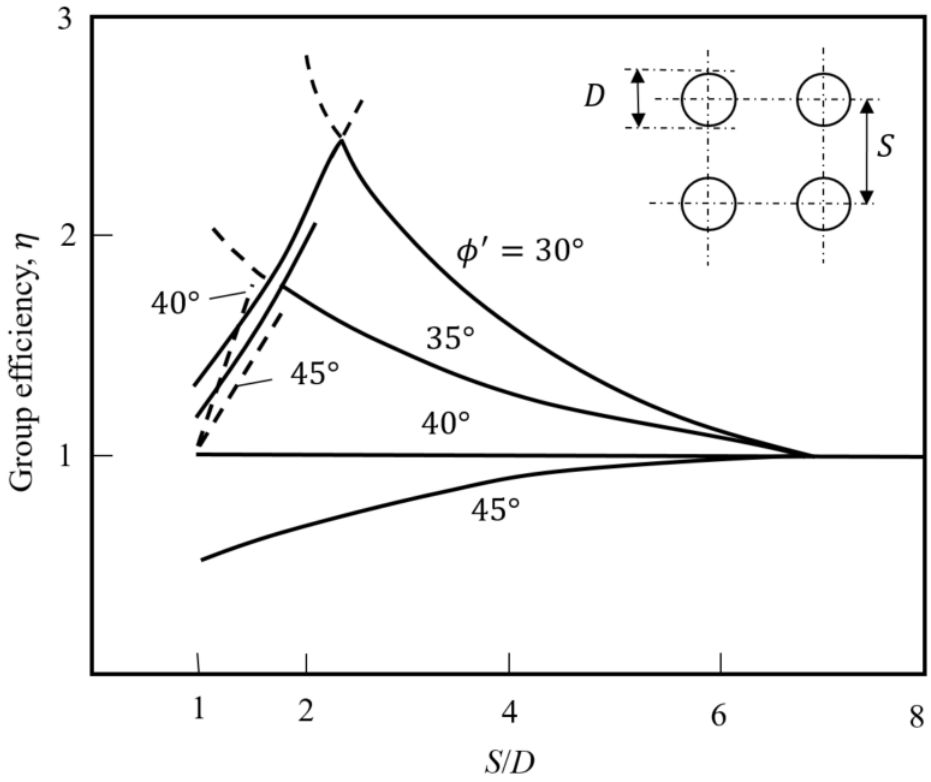

Figure 2.27. The diagram of group efficiency coefficient (after Kishida 1965)

K. Vesic method

According to this method, some diagrams are presented to evaluate the efficiency of pile groups. In this method, only the 4 and 9 pile groups are considered and the efficiency factors are obtained by piles spacing and diameter. However, this method considers the pile cap laying on the ground. The diagrams are illustrated in Figure 2.28.

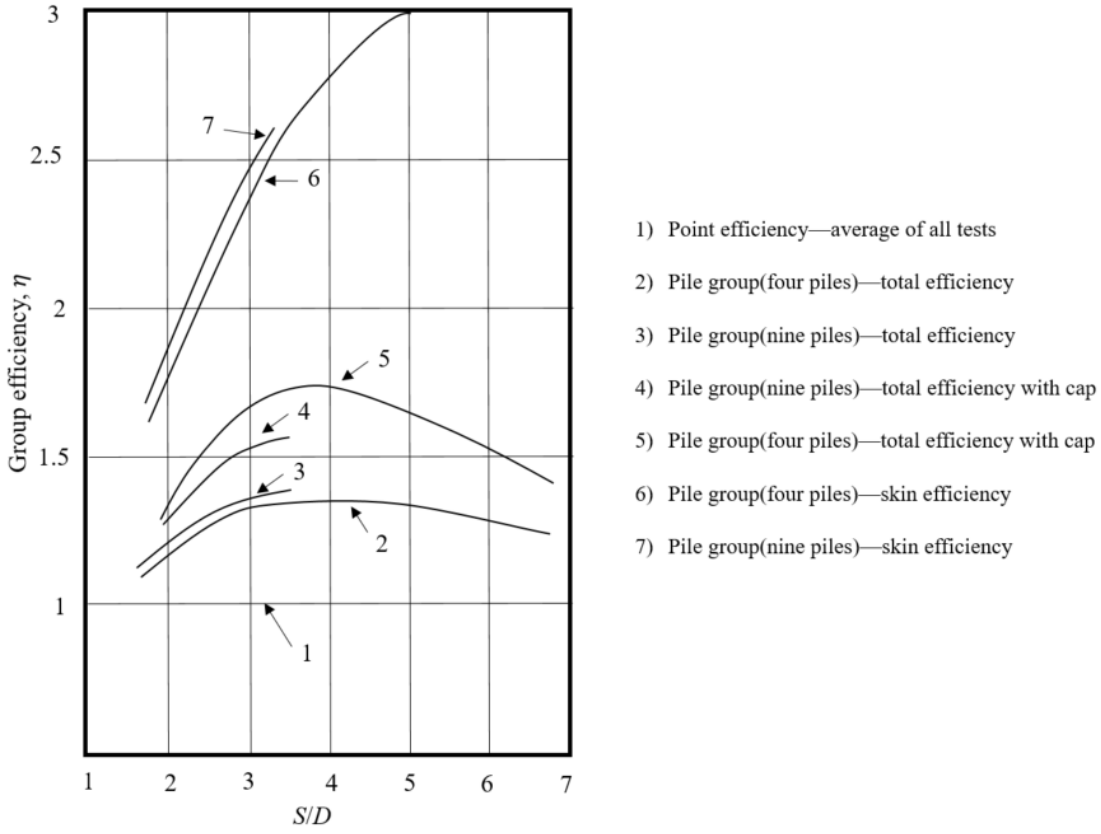

Figure 2.28. Group efficiency diagrams for various S/D ratios (after Vesic 1967)

L. Sayed and Bakeer method

Another relation has been developed to evaluate the group efficiency of pile groups under axially loaded conditions. This relation is based on the premise that only the shaft component should be taken into consideration. The equation is expressed as:

$$\eta = 1 - (1 - \eta' \cdot K) \cdot \rho \qquad 2.28$$

where, η is the group efficiency, ρ is the friction factor, K is the interaction factor, η' is the geometric efficiency and is defined as:

$$\eta' = \frac{P_g}{\sum P_p} \qquad 2.29$$

where, P_g is the perimeter of the pile group, and $\sum P_p$ is the sum of perimeters of individual piles. Hence η' can be written as:

$$\eta' = \frac{2*[(n-1)S+D]+[(m-1)S+D]}{\pi nmD} \quad 2.30$$

M. Das method

An empirical model is proposed by Das to estimate the group efficiency of frictional piles subjected to axial force. The equation can be expressed as:

$$\eta = \frac{2S(n+m-2)+4D}{nm} \quad 2.31$$

where, n is the number of piles in each row, m is the number of piles in each column, s is the spacing of piles, and D is the diameter of a pile. As it can be observed, this method doesn't consider the effect of cap, soil, loading conditions, and pile's length to diameter ratio (L/D), which is of great significance.

Several other equations have been proposed to predict the efficiency of pile groups considering different parameters. However, these relations are only for straight sided wall pile group foundations and none of the above equations considers all the parameters affecting efficiency coefficient simultaneously.

2.7 Summary and gap identification

In most of the equations proposing a taper coefficient, the lateral earth pressure of the soil has been assumed to be constant, while this coefficient will increase by each incremental settlement of a tapered pile. The reason for this increase is soil densification adjacent to the pile wall as plie installation can compact the surrounding soil. Due to the wide range of *Ks* values, which have been proposed in various sources for tapered piles (Bowles 1996; Nordlund 1963; Paik et al. 2013), and the key role of this parameter in obtaining the shaft capacity of tapered piles, it is recommended to consider *Ks* as a function of relative density and the over consolidation ratio of soil. For this purpose, insufficient field test results can be regarded as a limitation of the equations predicting taper coefficient for calculation of shaft capacity of tapered piles.

According to most of the studies, tapered piles are an efficient pile type for increased load-carrying capacity in compression, but less effective under uplift loads. In fact, the performed studies to survey the uplift capacity of tapered piles were under a maximum confining pressure of 60 kPa. Since the confining pressure significantly can affect the uplift resistance of tapered piles, therefore, for higher confining pressures, the uplift capacity should be obtained from uplift load tests, particularly in the field. Although there might be uncertainty that additional efforts in understanding the behaviour of these types of piles are of limited practical use, only limited studies have proven the substantial benefits of the axial and lateral capacity of step-tapered piles (Ismael 2003, 2006, 2009). Since, these piles might be efficient in terms of material usage in some layered soils, which need to be optimised in terms of length and diameter in each layer to have an economical, effective, sustainable design.

Substantial benefits of tapered piles installed in granular soil can be rendered, due to their significant shaft capacity increase. This is also because with increasing the relative stiffness of the surrounding soil, the bearing capacity of a tapered pile increases. Thus, it is more beneficial to construct tapered piles using stiff material such as high-strength concrete penetrated into sandy soils for the purpose of efficient densification.

According to the literature, tapering angle has a significant effect on the stiffness and damping parameters of tapered piles. Besides, the “shake down” phenomenon due to a noticeably small loading amplitude (when compared to the pile load capacity), the deflection of tapered piles can reach to an approximately steady state. This phenomenon happens when the pile reaches to permanent strains and experiences the state of residual stresses, which makes the pile to react elastically to extra loading phases. The reason of the abovementioned phenomenon for tapered piles can be referred to soil densification around the tapered piles.

Lack of experimental investigations for obtaining the response of tapered piles under axial and lateral dynamic loading condition is evident. These experimental and field test data are highly needed for validation of several complex mathematical models, which have been proposed to capture the behaviour of non-uniform cross-section piles.

In addition, numerical modelling of tapered piles under seismic loadings or even cyclic loadings have not been developed adequately. It seems to be a knowledge gap in comparing the dynamic aspects of tapered and cylindrical piles using numerical modelling.

Chapter 3

Methodology of the Numerical Modelling and Soil Calibration Exercise for Finding the Optimum Tapering Angle

3.1 Introduction

In this chapter, firstly, the adopted soil behavioural model in finding the optimum tapering angle is introduced. In this section, the advantages and drawbacks of the adopted constitutive model is explained. Thereafter an overview of the model is discussed and the geometrical properties of the model piles were elaborated. Finally, the soil calibration exercise is explained and the calibrated diagrams (deviatoric stress vs. axial strain and the volumetric strain vs. axial strain) are presented. At the end of the last section of this chapter, table of the soil properties for the numerical analyses is presented.

3.2 Adopted soil constitutive model

UBC sand constitutive model developed by Beaty & Byrne (2011), which is a plasticity based model based on effective stresses in the granular materials such as sands capturing nonlinear stress-strain relationship, was used in this study. This model captures the impacts of soil compression adjacent to the tapered piles, which is a key

feature to analyse the realistic response of tapered piles subjected to axial loading in the numerical modelling. Indeed UBC sand constitutive model assumes a hyperbolic correlation between stresses and strains in the soil and can predict the associated volumetric variation of the soil skeleton by a flow rule, which is a function of the stress ratio. The elastic component of response is assumed to be isotropic and specified by a shear modulus, G^e as follows (Byrne et al. 2004):

$$G^e = K_G^e P_a \left(\frac{\sigma'}{P_a}\right)^{ne} \quad 3.1$$

where, K_G^e is the shear modulus which depends on the relative density, P_a is the reference atmospheric pressure, σ' is the mean stress in the plane of loading equal to $(\sigma'_x + \sigma'_y)/2$, n_e is a model parameter, which varies between 0.2 and 0.6 as reported by Beaty & Byrne (2011); Brinkgreve et al. (2002); Byrne et al. (2004).

In the adopted constitutive model, the yield surface and flow rule control the plastic strains. The plastic shear strain increment, γ^p, is associated with the change in the shear stress ratio, $d\eta$ (where $\eta = {}^{\tau}/_{\sigma'}$), and can be written as:

$$d\gamma^p = \frac{1}{G^p/\sigma'} d\eta \quad 3.2$$

where, G^p is representing the plastic shear modulus. Assuming a hyperbolic relationship between η and γ^p as recommended by Beaty & Byrne (2011), the adopted G^p in the model can be written as:

$$G^p = G_i^p . (1 - \frac{\eta}{\eta_f} . R_f)^2 \quad 3.3$$

where, G_i^p is the plastic modulus at zero stress ratio (i.e. $\eta = 0$), η_f is the stress ratio at failure, which is equal to $sin(\phi_f)$, ϕ_f is the peak friction angle and R_f is the failure ratio used to truncate the best fit hyperbolic correlation and avoid the over-prediction of strength at failure. Referring to Beaty & Byrne (2011); Byrne et al. (2004), the

associated increment of plastic volumetric strain, ε_v^p , is correlated to the plastic shear strain increment, $d\gamma^p$, through the flow rule as follows:

$$d\varepsilon_v^p = \left(sin\,\phi_{cv} - \frac{\tau}{\sigma'}\right).d\gamma^p \qquad 3.4$$

where, ϕ_{cv} is the constant volume friction angle or phase transformation angle.

This constitutive model is one of the recent soil models that has been added to Plaxis available soil model types. The soil calibration exercise is performed using Plaxis virtual lab and the data obtained from triaxial tests on three different soil types (Fukushima & Tatsuoka 1984; Lade & Bopp 2005; Lee & Seed 1967). Similar to other constitutive models, this model also has some advantages and drawbacks. This behavioural model is less common to be used in static conditions. However, as mentioned before, since this model considers the effects of soil densification in the vicinity of tapered piles, which is a key element to analyse the behaviour of this type of pile subjected to axial loading more accurately, this model was selected for this study (Brinkgreve et al. 2002).

3.3 Overview of the model

An array of numerical modelling for tapered piles capturing different tapering angles and soil characteristics were performed using the finite element method in this study. Piles with different geometries but identical volume of material were modelled and the load-settlement curves of each pile were extracted and compared. The geometrical properties of all piles used in the numerical modellings are presented in Table 3.1.

In this study, piles with common slenderness ratios (L/D) of 10, 20, 30 and 40 were modelled and analysed in numerical simulations, which is a typical range for using piles in practice. For piles with L/D=10, which have the largest diameter compared to other models of this study, a radius of 0.75 m was selected for the cylindrical reference pile with a total length of 15m. After selecting the reference cylindrical piles dimensions for each set of analyses with a specific L/D ratio, tapered models were designed. For a given L/D, to keep the volume of all piles the same, the top radius of

the pile should increase while the bottom radius should decrease (as shown in Figure 3.1). On the other hand, in order to reduce the influence of model size on results, based on suggestions in the literature (Khan et al. 2008), dimensions of more than $2.5L(1-\nu)$ were used for the soil model in the numerical analyses, which covers the distance in which the shear stress develops. Hence, the shear stress bulbs (beneath the toe and surrounding the shaft) could be captured in the output results (as shown in Figure 3.1), and the inaccuracies due to the boundary effects could be minimised.

Table 3.1. Geometry of all piles with various slenderness ratios used in numerical analysis

			L/D					L/D		
			10	20	30	40	10	20	30	40
Pile	α	L (m)	Top radius (mm)				Bottom radius (mm)			
C	0°	15	750	375	250	187	750	375	250	187
T1	0.1°	15	763	388	263	200	736	362	236	173
T2	0.2°	15	776	400	275	212	723	348	223	160
T3	0.3°	15	789	413	288	224	710	335	209	146
T4	0.4°	15	801	426	300	237	697	321	196	132
T5	0.5°	15	814	438	312	248	683	307	181	117
T6	0.6°	15	827	450	324	260	670	293	167	102
T7	0.7°	15	839	463	335	271	656	279	152	87
T8	0.8°	15	852	474	347	281	642	265	137	72
T9	0.9°	15	864	486	358	292	629	251	122	56
T10	1.0°	15	877	498	369	301	615	236	107	40
T11	1.1°	15	889	509	379	-	601	221	91	-
T12	1.2°	15	901	521	390	-	587	206	75	-
T13	1.3°	15	913	532	400	-	573	191	59	-
T14	1.4°	15	925	543	409	-	559	176	43	-
T15	1.5°	15	937	553	419	-	545	161	26	-
T16	1.6°	15	949	564	-	-	530	145	-	-
T17	1.7°	15	961	574	-	-	516	129	-	-
T18	1.8°	15	973	585	-	-	501	113	-	-
T19	1.9°	15	984	595	-	-	487	97	-	-
T20	2.0°	15	996	605	-	-	472	81	-	-
T21	2.1°	15	1008	-	-	-	458	-	-	-
T22	2.2°	15	1019	-	-	-	443	-	-	-
T23	2.3°	15	1030	-	-	-	428	-	-	-
T24	2.4°	15	1042	-	-	-	413	-	-	-
T25	2.5°	15	1053	-	-	-	398	-	-	-
T26	2.6°	15	1064	-	-	-	383	-	-	-
T27	2.7°	15	1075	-	-	-	368	-	-	-
T28	2.8°	15	1086	-	-	-	352	-	-	-
T29	2.9°	15	1097	-	-	-	337	-	-	-
T30	3.0°	15	1107	-	-	-	321	-	-	-
Volume of piles (m^3)			26.5	6.6	2.9	1.6	26.5	6.6	2.9	1.6

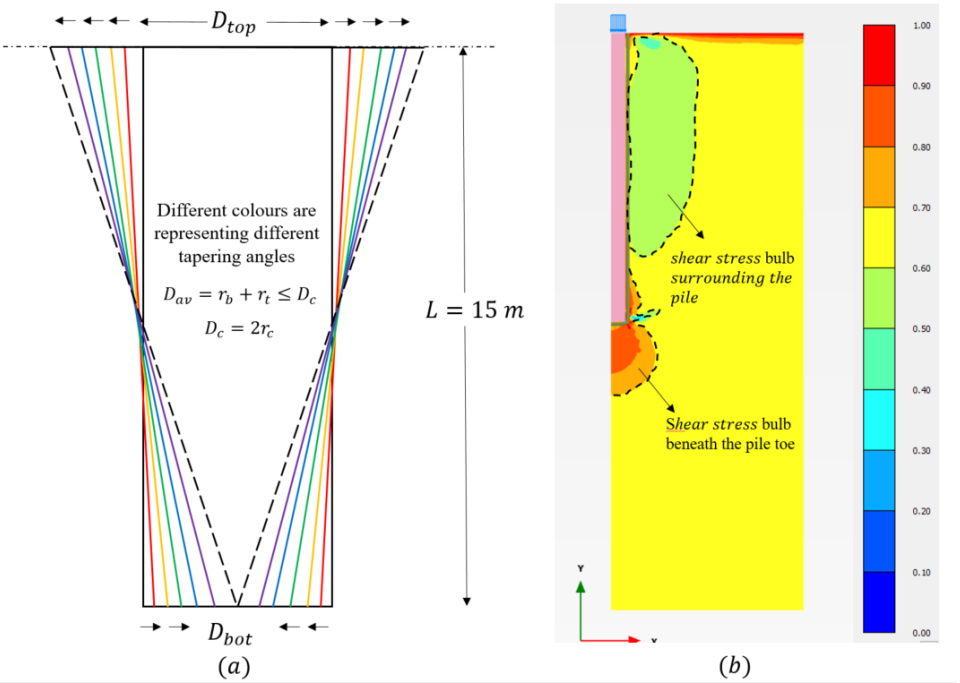

Figure 3.1. The methodology to design tapered pile models used in the numerical analysis based on the cylindrical reference pile with constant volume, b) The shear stress bulbs beneath the toe and surrounding the pile shaft (i.e. cylindrical pile, loose sand, L/D=10)

In this analysis, tapered piles having circular cross-section were modelled and analysed. The pile element was embedded in an elasto-plastic ground and a monotonic compressive axial load was applied on the head of the pile. An axisymmetric model type was selected for the numerical modelling as well as 15-noded element type. The enhanced meshing method was applied surrounding the pile for more accurate results (Figure 3.2 andFigure 3.3).

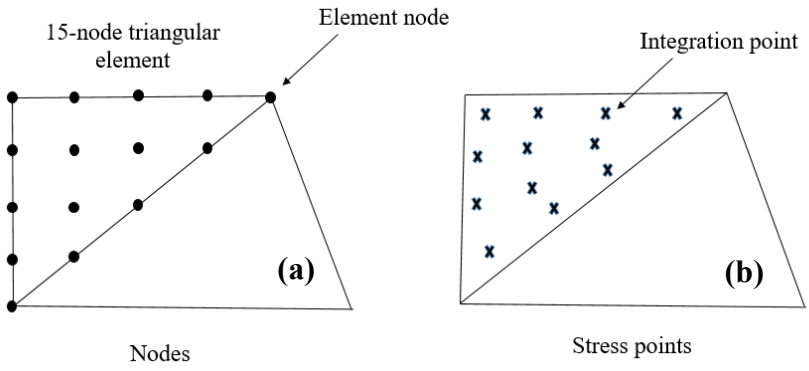

Figure 3.2. Elements utilized by adopted finite-element model, a) Nodes, b) Stress points

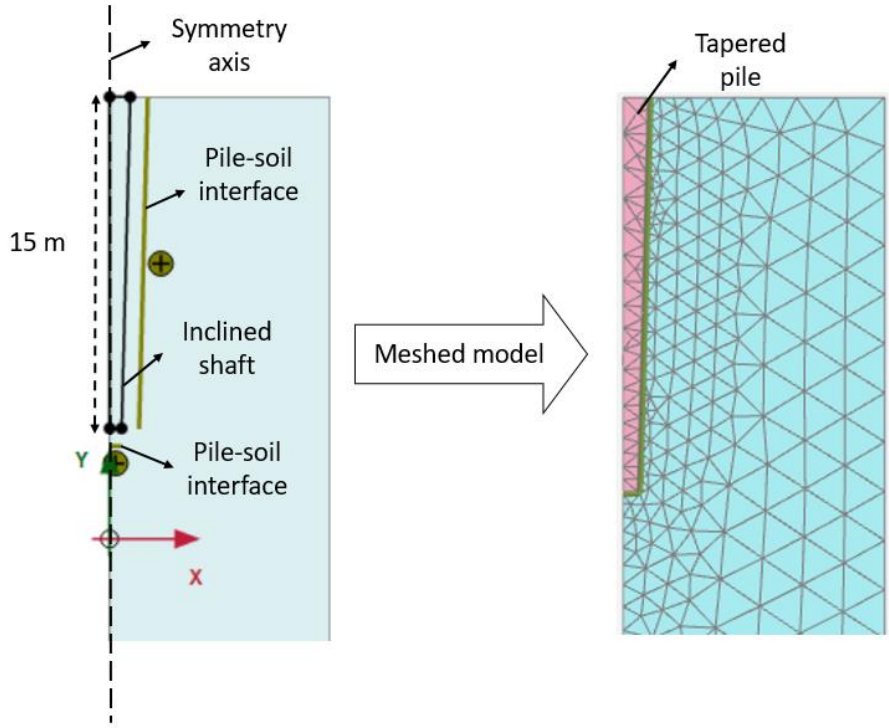

Figure 3.3. Axisymmetry model of a tapered pile along with the interfaces and the meshed model

The mesh refinement was considered around the structural elements, where the pile and soil are in contact through the interface plane. Figure 3.3 also illustrates the axisymmetric model of a tapered pile and the interfaces for shaft and toe of the pile along with the enhanced meshed system used for the analysis using PLAXIS 2D (Brinkgreve et al. 2002). This refinement could improve the mesh quality and hence more accurate predictions. For the purpose of modelling of the pile and the soil cluster, solid elements were used. The pile was modelled as a volumetric object to consider the tapering effect and capturing the stress states adjacent to the pile.

The interface elements between pile and the adjacent soil were considered and the reduction factor (R_f) of 0.7 was used. This factor applies to the strength and stiffness parameters of soil as shown in Equations 3.5 and 3.6.

$$tan\phi_i = R_{inter}\, tan\phi_{soil} \tag{3.5}$$

$$G_i = R^2{}_{inter}.\, G_{soil} \tag{3.6}$$

where, ν_i is the Poisson's ratio of the interface, G_i is the shear modulus of the interface, $E_{oed,i}$ denotes the Young's modulus of the interface, G_{soil} is the shear modulus of the soil and ϕ_i is the internal friction angle of the interface.

3.4 Soil calibration exercise

In this study, sandy soils with different relative densities were selected to assess axial load-displacement of tapered piles. Experimental results for loose, medium dense and dense sand samples, obtained from (Lade & Bopp 2005), (Fukushima & Tatsuoka 1984) and (Lee & Seed 1967) corresponding to relative densities of 30%, 40% and 90%, respectively, were used for the model calibration. Therefore, before conducting the numerical analysis, the triaxial test results for three types of sands each subjected to three different confining pressures were used to obtain the required model parameters. Figure 3.4 illustrates diagrams of deviatoric stress versus axial strain of the soil samples from experimental tests in comparison to numerical predictions adopting calibrated model parameters for loose, medium and dense sand, respectively. Moreover, Figure 3.5 shows the volumetric strain changes with axial strain variations for the abovementioned soils.

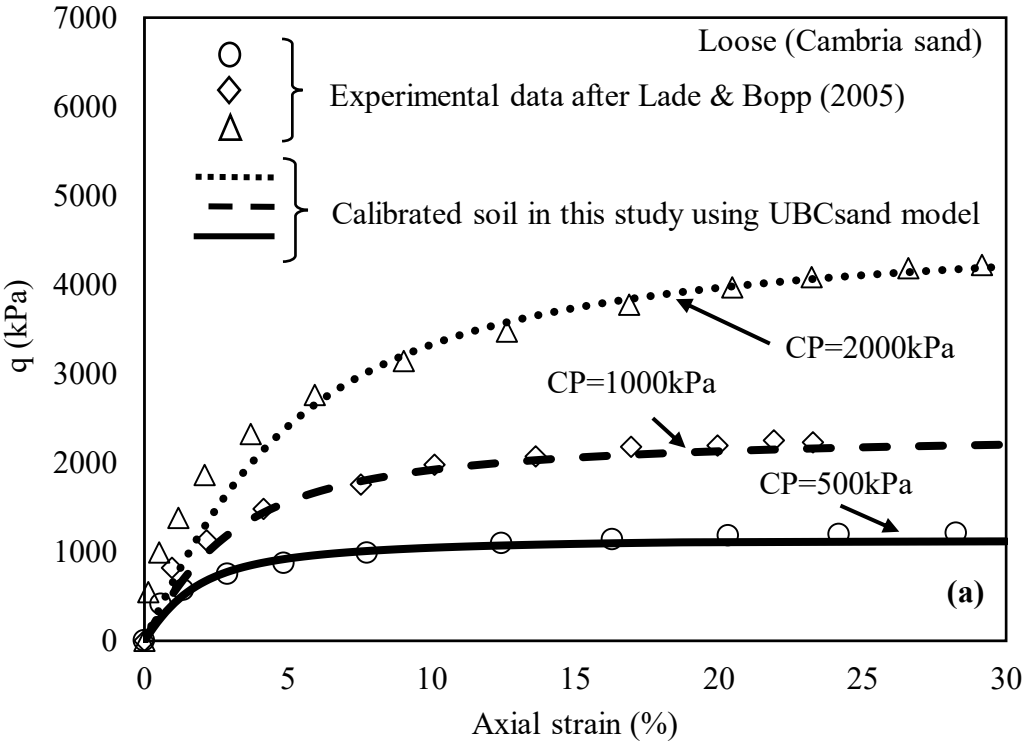
Loose (Cambria sand)
Experimental data after Lade & Bopp (2005)
Calibrated soil in this study using UBCsand model
CP=2000kPa
CP=1000kPa
CP=500kPa
(a)
q (kPa)
Axial strain (%)
0
1000
2000
3000
4000
5000
6000
7000
0
5
10
15
20
25
30

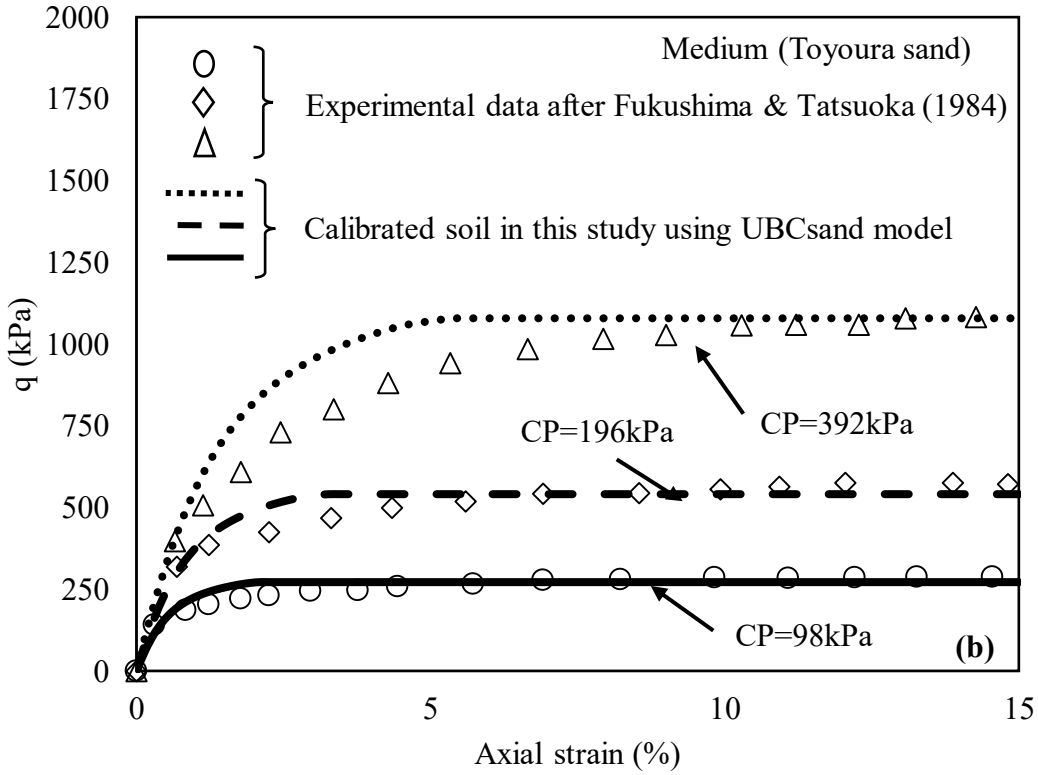
Medium (Toyoura sand)
Experimental data after Fukushima & Tatsuoka (1984)
Calibrated soil in this study using UBCsand model
CP=392kPa
CP=196kPa
CP=98kPa
(b)
q (kPa)
Axial strain (%)
0
250
500
750
1000
1250
1500
1750
2000
0
5
10
15

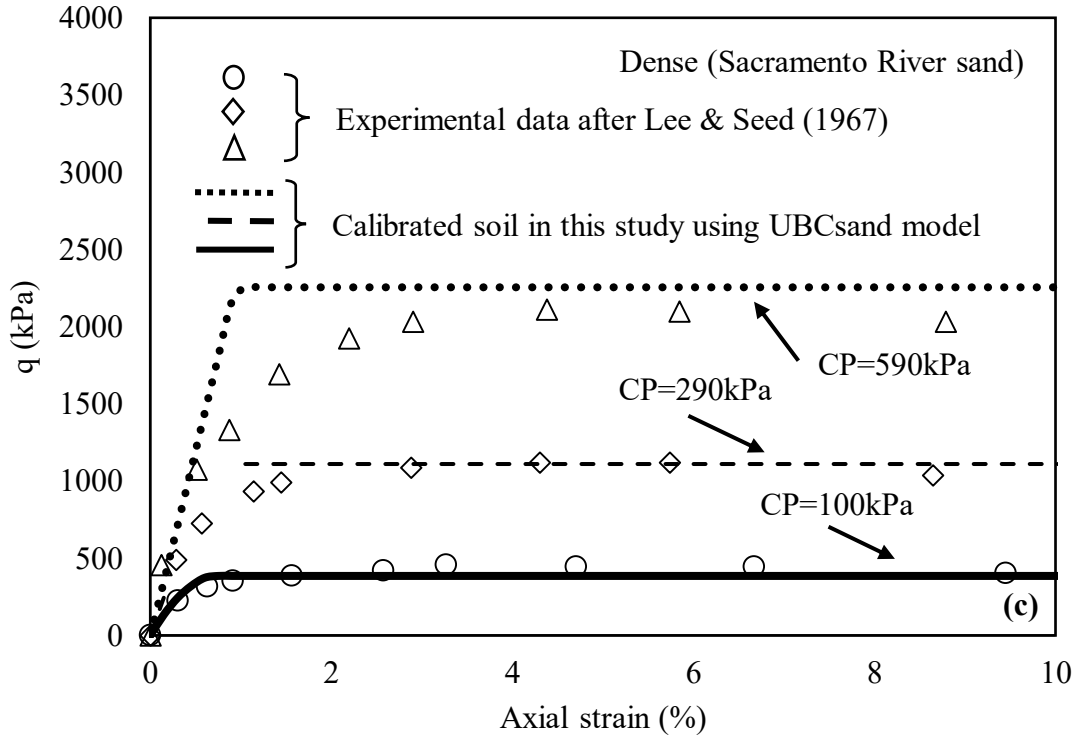

Figure 3.4. Comparison of (deviatoric stress vs axial strain) data and numerical calibration for various confining pressures of drained triaxial compression tests on isotropically consolidated, (a) Loose Cambria sand, data taken from Lade & Bopp (2005), (b) Medium Toyoura sand, data taken from Fukushima & Tatsuoka (1984), (c) Dense Sacramento River sand, data taken from Lee & Seed (1967)

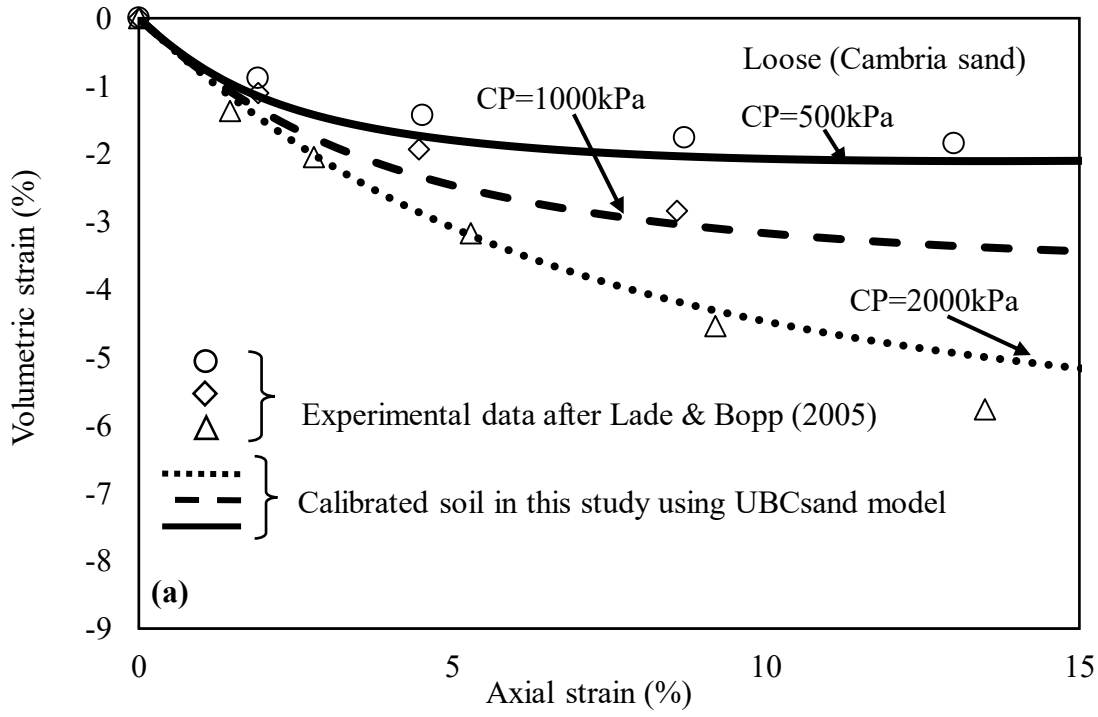

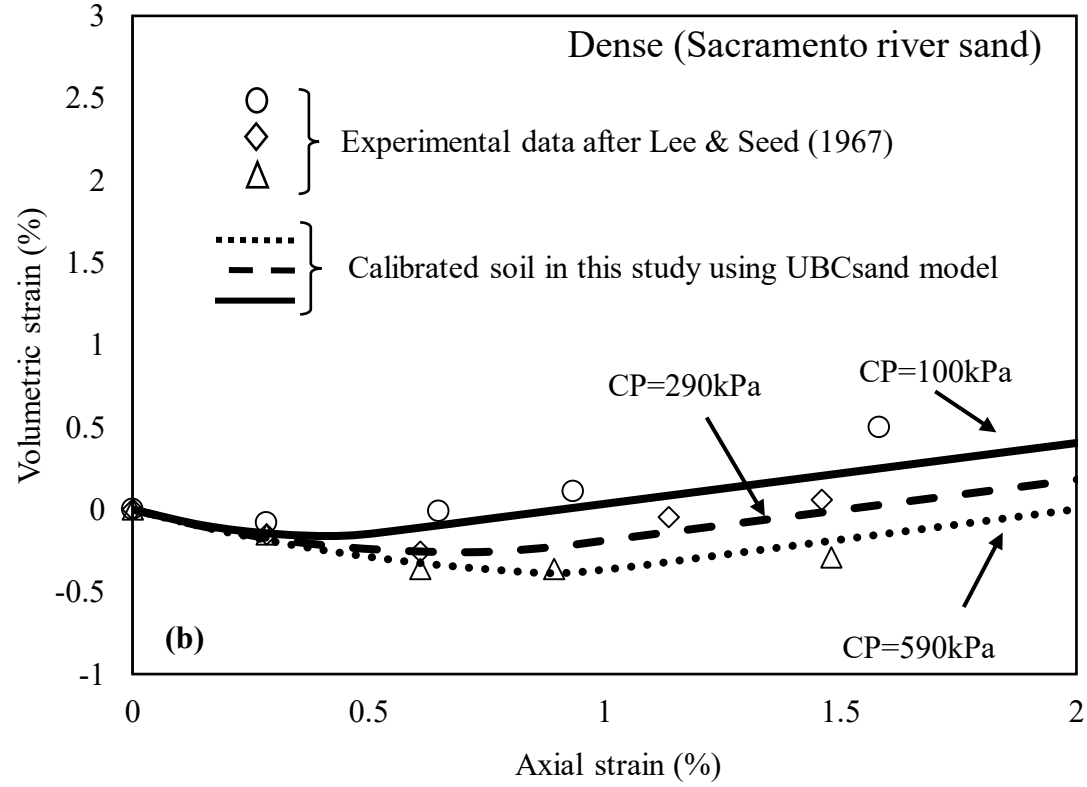

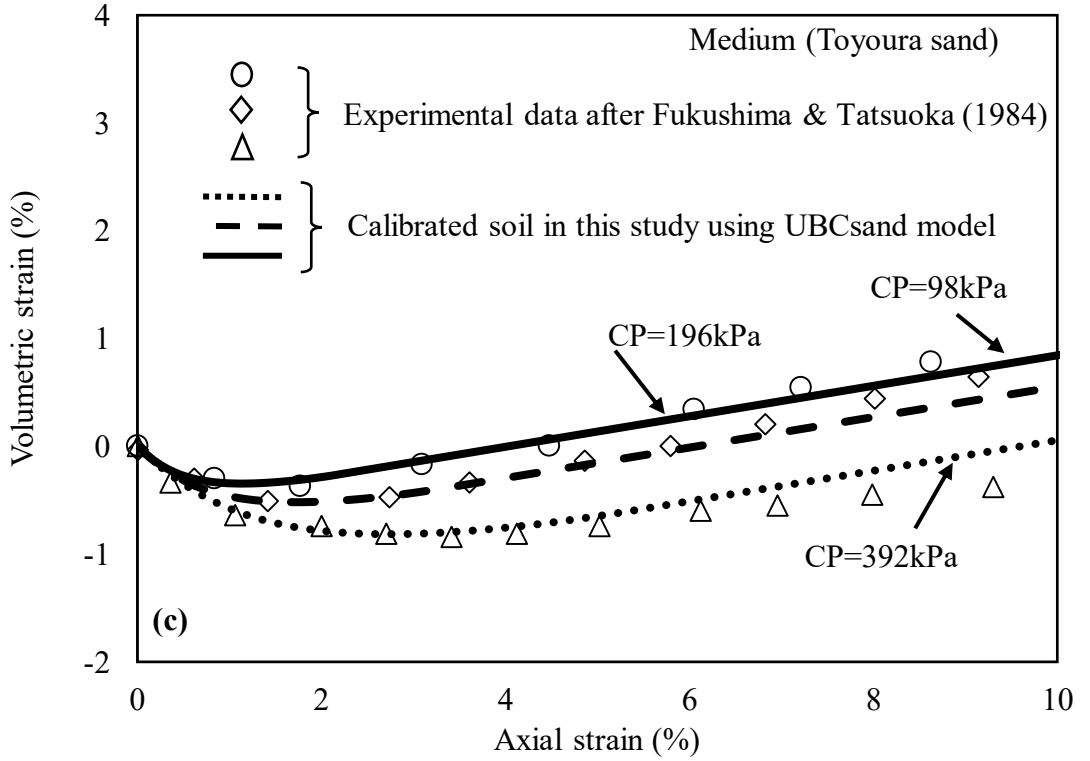

Figure 3.5. Comparison of (volumetric strain vs axial strain) data and numerical calibration for various confining pressures of drained triaxial compression tests on isotropically consolidated, (a) Loose Cambria sand, data taken from Lade & Bopp (2005), (b) Medium Toyoura sand, data taken from Fukushima & Tatsuoka (1984), (c) Dense Sacramento River sand, data taken from Lee & Seed (1967)

As evident, a good agreement between measurements and predictions were perceived, confirming suitability of the adopted constitutive model and calibrated model parameter in predicting the stress-strain response of the adopted soils. Summary of calibrated model parameters for loose sand (Cambria), medium dene sand (Toyoura) and dense sand (Sacramento River) are presented in

Table 3.2.

Table 3.2. Sandy soil properties obtained from soil calibration exercise using UBC sand model

Soil Parameters	Parameter Values		
	Loose	Medium	Dense
k_B^e	150	300	700
k_G^e	300	400	800
k_G^p	330	420	900
me	0.25	0.4	0.5
ne	0.25	0.4	0.5
np	0.25	0.4	0.5
ϕ_{cv}	31	30	30
ϕ_p	32	35	41
c	0	0	0
R_f	0.98	0.93	0.8
f_{dens}	0.3	0.6	1
γ_{unsat}	15.3	16	17
γ_{sat}	19.3	19.3	20
$(N_1)_{60}$	5	20	50

Chapter 4

Analytical and Numerical Approaches to Attain the Optimum Tapering Angle for Axially Loaded Bored Piles in Sandy Soils

4.1 Introduction

Obtaining the accurate bearing capacity of foundations have always been a matter of concern among geotechnical engineers considering different methods, such as limit equilibrium, limit (or bound) theorems of classical plasticity, or through load-displacement diagrams (Kalourazi et al. 2019; Shafaghat et al. 2018; Wu et al. 2019; Xie et al. 2019; Yang et al. 2019; Zhou et al. 2019). Therefore, several methods have been developed to predict the bearing capacity of foundations, particularly for deep foundations based on experimental or numerical studies such as optimised machine learning approach (Abdlrahem & El Naggar 2020; Almallah et al. 2020; Han et al. 2020; Jiang et al. 2020; Kardani et al. 2020).

Furthermore, due to the growing demand for designing more efficient and cost-effective foundations, including tapered piles, determining the optimum tapering angle in which tapered piles can provide more capacity (while having less settlement) is in demand. Besides, new developments of piling machinery have permitted installation of large-scale bored piles having different shapes at lesser costs (Lee et al. 2009; Paik

et al. 2013; Rybnikov 1990). Straight-wall cylindrical bored piles (i.e. constant circular cross-section along the pile) have been regularly adopted in practice.

Alternatively, tapered bored piles with variable cross-sectional area along the pile length (i.e. a larger pile head diameter and a smaller pile toe diameter) have not been as common as cylindrical piles due to different installation procedures and lack of current design standards. However, tapered piles have a great potential to be used as a cost effective alternative with enhanced performance. Indeed, geotechnical activities in undesirable soil conditions drive geotechnical engineers to design optimized foundation types, which require less material usage while yet not compromising safety. The idea of tapered piles accordingly can contribute to saving material usage such as concrete and reinforcement bars in pile foundations which in turn can be an environmentally friendly approach (Poulos & Davis 1980; Shafaghat & Khabbaz 2020b). Referring to Poulos & Davis (1980), in loose sand, pile axial force reduces from top to bottom and thus, a larger pile top cross-section is perceived to be more preferable as is in tapered piles. This efficient geometry of tapered piles can bring substantial benefits in terms of transferring structural loads to stronger strata.

In this study, initially a set of mathematical formulations are developed to determine the axial bearing capacity of bored tapered piles. The proposed bearing capacity equation captures the toe resistance, shaft friction and additional vertical resistance from the shaft, which is due to the inclination of tapered pile shaft. However, several model parameters are introduced which need to be calibrated against results from rigorous numerical modelling or comprehensive large scale experiments. Hence, a rigorous finite element modelling is conducted to find the aforementioned model parameters via plotting the axial bearing capacity predictions versus the tapering angle, and subsequently attaining the optimum tapering angles. The numerical modelling captures the nonlinear elasto-plastic response of the soil adopting UBCSAND constitutive model, calibrated against laboratory experimental results, and the results are compared with the proposed analytical formulations mentioned earlier.

Finally, a simple empirical equation is proposed to obtain the optimum tapering angle of piles with different slenderness ratios and in different types of sands. This optimum

tapering angle should be selected in order to use less material, while not compromising safety and performance.

4.2 Analytical development for ultimate axial bearing capacity of bored tapered piles in sand

Based on Terzaghi (1943) ultimate bearing capacity theorem and Meyerhof (1963) method for calculation of pile bearing capacity, cylindrical piles can provide capacities through their shaft and base, which are known as frictional bearing and toe bearing components, respectively. However, there is an additional capacity component for tapered piles, which is due to the inclination of the body (Figure 4.1). This extra component, which is the normal resistance through the pile body surface, is due to the fact that tapered piles can resist against an upward vertical force as a result of the inclination of their body.

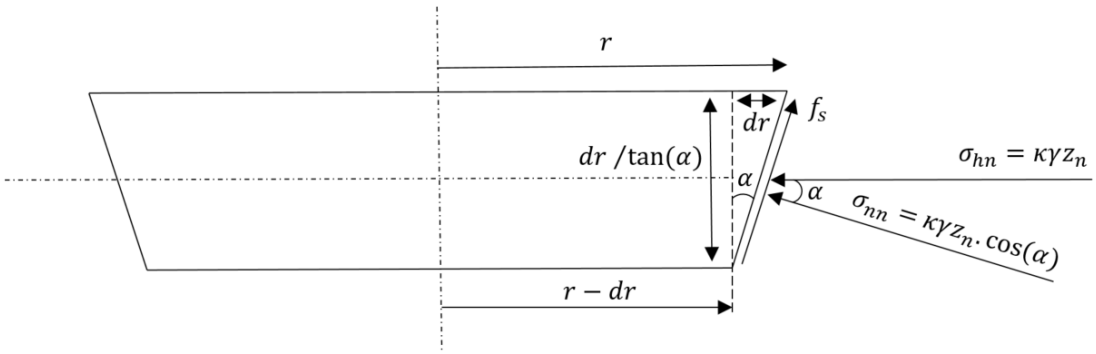

Figure 4.1. Free body diagram of shaft resistance force component of an element

Referring to existing state of practice for bearing capacity of the piles (Meyerhof 1963; Terzaghi 1943; Terzaghi et al. 1996), the toe (base) resistance, q_b, and the frictional (skin) resistance, q_s, of a single pile can be calculated as:

$$q_b = \sigma'_b N_q A_b \tag{4.1}$$

$$q_s = k\sigma'_m tan(\delta) A_s \tag{4.2}$$

where, σ'_b and σ'_m are the effective stresses at the toe and the mid-length of the pile, respectively; A_b and A_s are the pile toe area and the lateral surface area, respectively; N_q, δ and k are the bearing capacity factor, the pile-soil interface friction angle, and the lateral earth pressure coefficient, respectively. In this study, the effect of pile tapering on the lateral earth pressure coefficient has been taken into consideration using a taper coefficient (K_t), which is a function of the pile tapering angle and the soil internal friction angle. This taper coefficient is multiplied by the at rest lateral earth pressure coefficient (K_0) in Equation 4.2, to obtain the frictional resistance of tapered piles.

When using conventional bearing capacity equations to obtain the shaft resistance of a cylindrical pile (as expressed by Equation 4.2), at rest lateral earth pressure coefficient (K_0) is used. However, for tapered piles embedded in sand, the adjacent soil will be densified as the pile moves downward (see Figure 4.2) which is due to the mobilization of a portion of soil passive earth pressure in the vicinity of pile shaft. In this study, this effect has been taken into consideration as a taper coefficient (K_t), which is a function of the tapering angle and the soil internal friction angle, and will be multiplied by the K_0.

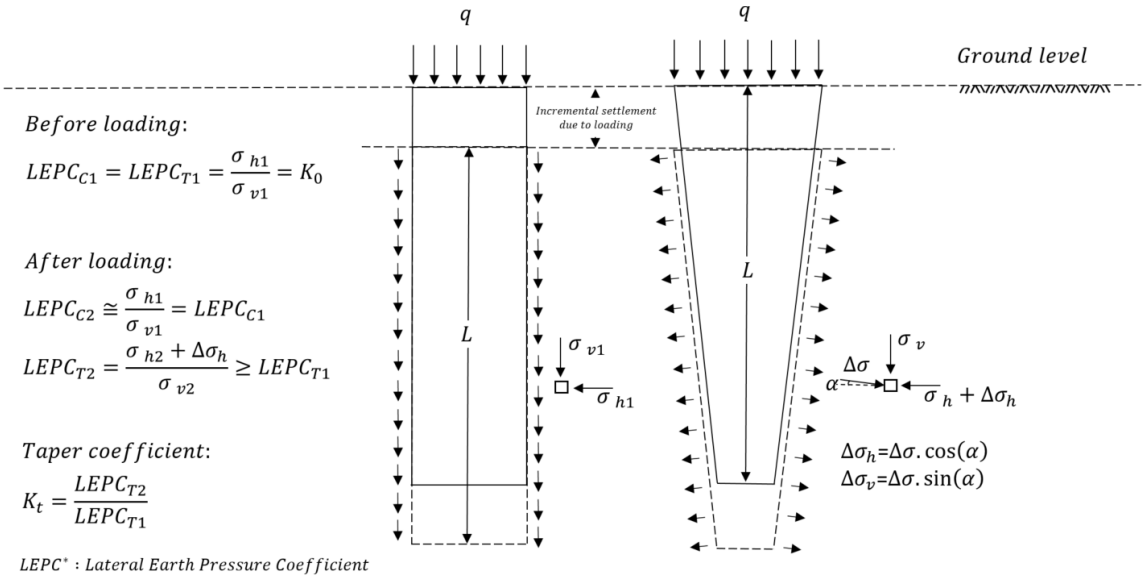

Figure 4.2. Schematic diagram of the stress state for an element adjacent to pile shaft for both bored cylindrical and tapered piles embedded in sand (before and after loading)

Figure 4.2 illustrates that considering two elements of soil in vicinity of pile shafts at the same level, the one that is adjacent to the tapered pile will resist against an additional horizontal force component due to the inclination of pile's body. Hence, by considering the equilibrium state, the ratio of the horizontal stress to the vertical stress for the tapered pile will increase.

Accordingly, by increasing the tapering angle, the taper coefficient increases. In other words, for a pile having a tapering angle of 0°, this coefficient will be equal to 1 (representing the condition for obtaining shaft resistance for a cylindrical pile), and for α=90°, the value of K_t would be equal to $\frac{K_p}{K_0}$ (representing the condition for obtaining friction beneath the pile toe surface), where K_p is the passive earth pressure coefficient. However, since in this study the comparisons have been made for piles having the same volume, the tapering angle will not exceed the maximum available tapering angle ($\alpha_{max} = tan^{-1}(\frac{\sqrt{3}r_c}{L})$). Hence, the taper coefficient values for tapered piles ($0 < \alpha < \alpha_{max}$) in this study will not be either equal to the maximum level ($K_t = \frac{K_p}{K_0}$), or the minimum level ($K_t = 1$).

The previously developed analytical equation by El Naggar and Wei (2000) was used as the reference model to derive an equation that predicts the taper coefficient as a function of soil internal friction angle and the pile tapering angle. The aforementioned reference model is a function of various parameters that are constant in this study, such as the pile displacement to diameter ratio (S_r) and the stress level at pile toe (σ_V), which the former considered 0.1 (as the criterion used to define the ultimate bearing capacity) and the latter mainly depends on the pile length (15 m). It should be noted that in this study the analytical equations were used to find the optimum tapering angle based on the ultimate bearing capacity. For investigating the serviceability settlement criterion, the optimum tapering angles can be obtained through load-settlement diagrams (through numerical analysis). For the serviceability criterion, the vertical settlement of 10% of the pile diameter can be considered similar to the assumption for the diameter ratio (S_r) above. Using other criterion (serviceability criterion) to find

the optimum tapering angle might have minor effect on the results (Hataf & Shafaghat 2015a, 2015b). Hence, in order to capture the optimum tapering angle, a new simplified mathematical equation was proposed as a function of soil internal friction angle, pile tapering angle, and a model parameter. The model parameter ζ represents the gradient at which the taper coefficient approached from 1 to $K_{t.max}$ for tapered piles and was obtained 100, using regression analysis. The new proposed K_t was plotted against the tapering angle for three different soil types (Loose Cambria sand, medium Toyoura sand and dense Sacramento River sand).

It is reasonable to assume that the vertical effective stresses increase linearly with depth in a uniform soil medium, while the cross-sectional area of the tapered pile decreases exponentially with depth (i.e. order 2 exponent). The third component of the axial bearing capacity of a tapered pile, which is the vertical bearing resistance stemming from the body of a tapered pile (q_{sv}), can be established using a mathematical integration of effective normal stresses distributed along the pile body. Hence, by dividing the tapered pile into infinitesimal segments as shown in Figure 4.3, this extra resistance component (i.e. q_{sv}) can be obtained using Equation 4.3.

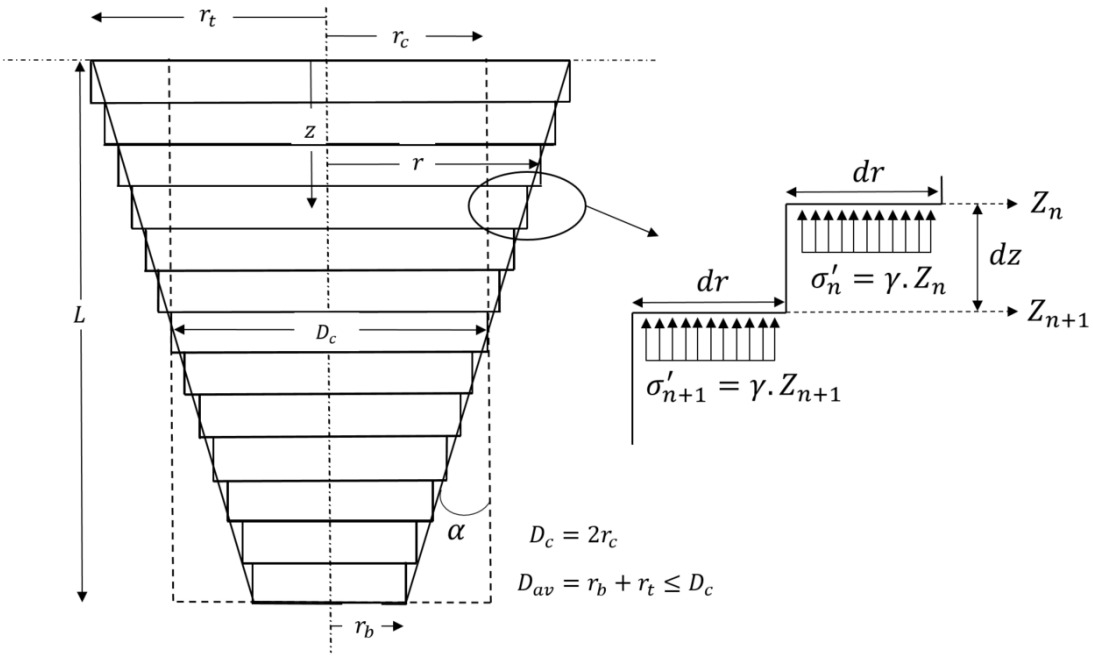

Figure 4.3. The schematic shape of a tapered pile divided into segments and the ledge force component (r_c,D_c are radius and the diameter of the reference cylindrical pile with the same volume)

$$q_{sv} = \sum_{n=1}^{n=\infty} N_t \sigma'_{bn} A_{bn} \quad 4.3$$

where, N_t is the bearing capacity factor for tapered piles, A_{bn} and σ'_{bn} are the projected area of the ledge of the segment (see Figure 4.4) and the effective vertical stress at the middle of the n^{th} segment, respectively, and can be determined using Equations 4.4 and 4.5, correspondingly.

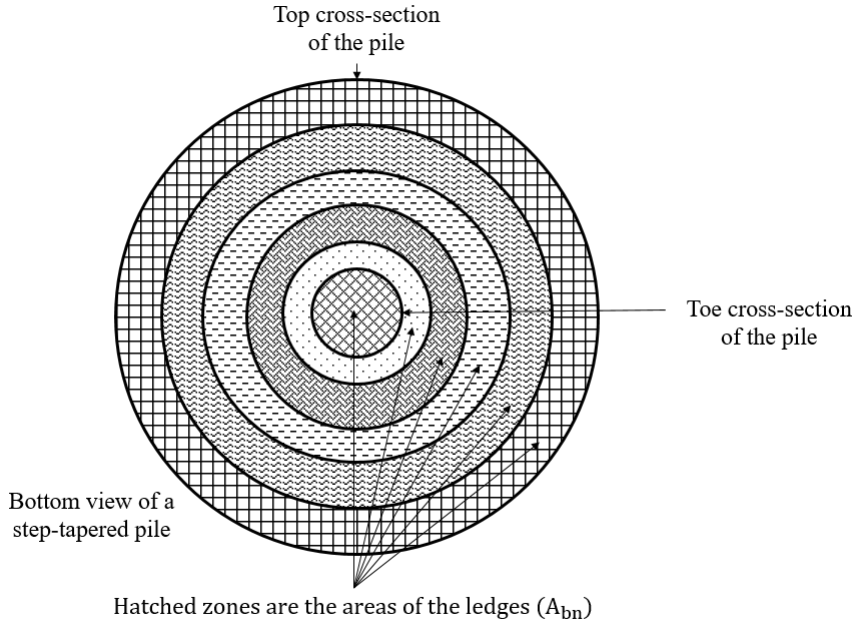

Figure 4.4. Schematic bottom perspective of a step-tapered pile with six ledges

$$A_{bn} = \pi(r_n^2 - (r_n + dr)^2) \quad 4.4$$

$$\sigma'_{bn} = \gamma z_{mn} \quad 4.5$$

where, z_{mn} is the mid-elevation of the n^{th} segment and can be defined using Equation 4.6.

$$z_{mn} = \frac{1}{2}(z_n + z_{n+1}) \quad 4.6$$

Where, z_n and z_{n+1} are the mid elevations of two consecutive segments. Indeed, the correlation between the depth (z) and the tapered pile geometrical characteristics can be presented as below:

$$z = \frac{(r_t - r)L}{(r_t - r_b)} \quad 4.7$$

In this study, the effective stress at mid-height of each pile's segment at depth z have been utilized (as presented in Equation 4.7 and depicted in Figure 4.3) to derive the mathematical equations.
Equation 4.2 has been used for each element of a segmented tapered pile separately at various depths from the pile head to pile toe. Hence, the equations developed in this study, including those used for obtaining the shaft resistance components, are based on more accurate stress states depending on depth z and not only one average number as the stress level at mid-height of pile.

The mathematical derivation for correlating z with the tapered pile geometries was performed based on keeping the volume of tapered piles identical to their counterpart cylindrical piles. Besides, since the radius of a tapered pile changes from head to toe, the variable r that represents the radius of a pile at depth z was considered as the primary variable in the equations of shaft resistance and the shaft vertical resistance component. Based on linear formulation (referring to Equation 4.7), the relationship between z and the radius of a pile at depth z was obtained, where z=0 represents the pile head elevation and z=L represents the pile toe elevation, as shown in Figure 4.3.

On the other hand, the correlation between the top and bottom radii of piles having a tapering angle of α with the radius of the cylindrical reference pile was developed based on equating the two equations obtaining the volume of a tapered pile (Equation 4.8) and the volume of the counterpart cylindrical pile (Equation 4.9).

$$V_t = \frac{1}{3}\pi L({r_t}^2 + {r_b}^2 + r_b.r_t) \quad 4.8$$

$$V_c = \pi L {r_c}^2 \quad 4.9$$

In the above equations, V_c is the volume of a cylindrical pile, V_t is the volume of a tapered pile, L is the length of pile, r_c is the radius of cylindrical reference pile, r_t and r_b are the top and bottom radii of tapered piles, respectively. Afterward, by substituting r_b in Equation 4.8 as a function of pile length and tapering angle ($r_b = r_t - Ltan(\alpha)$) yields Equation 4.10, which is the relationship between the radius of head of a tapered pile (r_t), having a tapering angle of α, with the radius of its counterpart same volume cylindrical pile (r_c).

Substituting Equations 4.4 to 4.7 into Equation 4.3, yields:

$$q_{sv} = \pi\gamma N_t \sum_{r=r_b}^{r=r_t} \frac{(2rdr)(r_t - r)L}{(r_t - r_b)} \quad 4.10$$

Equation 4.10 can be rewritten as a finite integral as follows:

$$q_{sv} = 2\pi\gamma N_t \int_{r_b}^{r_t} \frac{(r)(r_t - r)L}{(r_t - r_b)} dr \quad 4.11$$

On the other hand, the top and bottom radii of tapered pile (i.e. r_t and r_b) can be obtained as a function of the radius of the counterpart cylindrical pile with the same volume (i.e. r_c) and the tapering angle (α) as follows:

$$r_t = \frac{Ltan(\alpha) + \sqrt{4{r_c}^2 - (1/3)(Ltan(\alpha))^2}}{2} \quad 4.12$$

$$r_b = r_t - Ltan(\alpha) \quad 4.13$$

where, α is the tapering angle and L is the length of the pile. By introducing parameter D_{av} as the average pile diameter as below:

$$D_{av} = \sqrt{4{r_c}^2 - (1/3)(Ltan(\alpha))^2} \quad 4.14$$

Then by substituting Equations 4.12 to 4.14 into Equation 4.11, vertical bearing resistance stemming from the body of the tapered pile (q_{sv}) can be established as follows:

$$q_{sv} = \frac{1}{6}\gamma\pi N_t L^2 \, tan(\alpha) \, [3D_{av} - Ltan(\alpha)] \qquad 4.15$$

where, D_{av} denotes the average diameter of tapered pile which is defined via Equation 4.14. Similarly, for calculating the shaft resistance (q_{st}), Equation 4.2 can be rewritten as a summation of frictional resistances stemming from all elements as reported in Equation 4.16.

$$q_{st} = \sum k_t k_0 \gamma z cos(\alpha) tan(\delta) A_{sn} \qquad 4.16$$

The lateral surface area of an element, A_{sn} can be written as:

$$A_{sn} = (\frac{2\pi r_n}{sin(\alpha)})dr \qquad 4.17$$

Substituting Equations 4.7 and 4.17 into Equation 4.16, yields:

$$q_{st} = \sum_{r=r_b}^{r=r_t} \frac{k_t k_0 \gamma L cos(\alpha) tan(\delta)}{sin(\alpha)} \frac{2\pi r(r_t - r)}{(r_t - r_b)} dr \qquad 4.18$$

Referring to Figure 4.3, by a simple substitution of $r_t - r_b = Ltan(\alpha)$, and transforming the summation into a definite integration, Equation 4.16 can be rewritten as follows:

$$q_{st} = \int_{r_b}^{r_t} \frac{2\pi k_t k_0 \gamma cos^2(\alpha) tan(\delta)(r_t - r)r}{sin^2(\alpha)} dr \qquad 4.19$$

where, k_t is the taper coefficient for a tapered pile and δ is the pile-soil interface friction angle. Since the lateral earth pressure depends on the soil movement as a result of soil displacement surrounding the tapered pile, the taper coefficient, $k_t(\alpha)$, can be considered as a function of tapering angle, as presented in Equation 4.21. The taper

coefficient which has been presented in Equation 4.21, was obtained based on the Cavity Expansion Theory, proposed by El Naggar & Sakr (2000) in Equation 4.20. Since this study is focused on bored tapered piles at failure (for a settlement to diameter ratio of $U_p/d = 0.1$) the proposed simplified equation for the taper coefficient in this study captures only the effect of tapering angle and the soil internal friction angle. Figure 4.5 demonstrates the correlation between the two equations for the taper coefficient proposed by El Naggar & Sakr (2000) and this study.

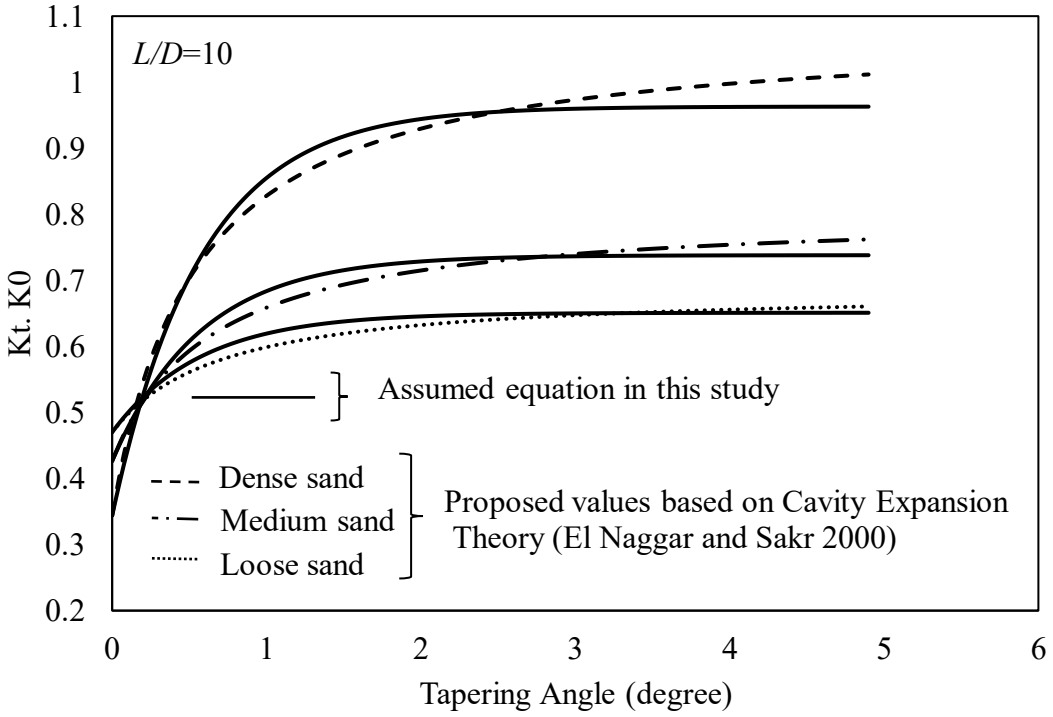

Figure 4.5. Correlation between the assumed simplified equation for the taper coefficient (kt) and the equation proposed by El Naggar and Sakr (2000) (Assuming Sr=Up/D=0.1)

$$k_{t_{Cv}}(\alpha) = \frac{tan(\alpha+\delta)cot(\delta)}{1+2\xi\, tan(\alpha)tan(\alpha+\delta)} + \frac{4Gtan(\alpha)\, tan(\alpha+\delta)cot(\delta)S_r}{[1+2\xi\, tan(\alpha)\, tan(\alpha+\delta)].K_0\sigma_v} \quad 4.20$$

$$k_t(\alpha) = 1 + (\frac{K_{max}-K_0}{K_0})\frac{1-exp(-\zeta\alpha)}{1-exp(-\zeta\alpha_{max})} \quad 4.21$$

Where, G is the shear stiffness of the soil and k_0 is the at rest lateral earth pressure coefficient, ξ is a coefficient depends on the radius of the pile and the extent where

the pressure bulb surrounding the pile assumes to be negligible ($2.5L(1\text{-}\nu)$), where L denotes the length of pile and ν denotes the Poisson's ratio, S_r is the ratio of pile displacement to its diameter ($S_r = U_p/D$). ζ is a correlation coefficient which represents the gradient at which taper coefficient approaches from 1 to $K_{t.max}$ for tapered piles and obtained 100. It should be noted that when the tapering angle is zero (i.e. $\alpha = 0$), Equation 4.21 converges to $k_t(\alpha) = 1$, which resembles the condition for conventional cylindrical piles in terms of at rest condition for the lateral earth pressure coefficient; while when $\alpha = \alpha_{max}$, then Equation 4.21 converges to a maximum lateral earth pressure $k_t(\alpha = \alpha_{max}) = K_{t.max}$, which is due to the mobilisation of a portion of passive earth pressure coefficient. In addition, α_{max} is the maximum tapering angle that a pile can practically hold, while keeping its volume identical to its counterpart cylindrical pile. This angle can be calculated based on Equation 4.22.

$$\alpha_{max} = tan^{-1}(\frac{\sqrt{3}r_c}{L}) \qquad 4.22$$

On the other hand, the bearing capacity factor, $N_t(\alpha)$ for tapered pile can be presented as in Equations 4.24 and 4.25. It should be noted that the bearing capacity factor (N_t) in this study is not the factor proposed by Terzaghi et al. (1996), but a modified factor based on Janbu (1976) proposed model of N_q and the tapering factor for base resistance of bored piles proposed by Paik et al. (2013). Since the increase in pile point resistance is not linear, the proposed N_t factor presented in Equation 4.24 was derived, considering three model parameters including, λ, β and ζ , to capture the effect of tapering angle on the vertical effective stress adjacent to the pile, and the gradient at which N_t approaches from N_{qc} for tapered piles. Figure 4.6 illustrates the correlation between the proposed equation for N_t in this study and the model proposed by Paik et al. (2013) in Equation 4.23 by assuming that TF_b is equivalent to the term ($\lambda - \beta.e^{-\frac{\pi\zeta\alpha}{180}}$).

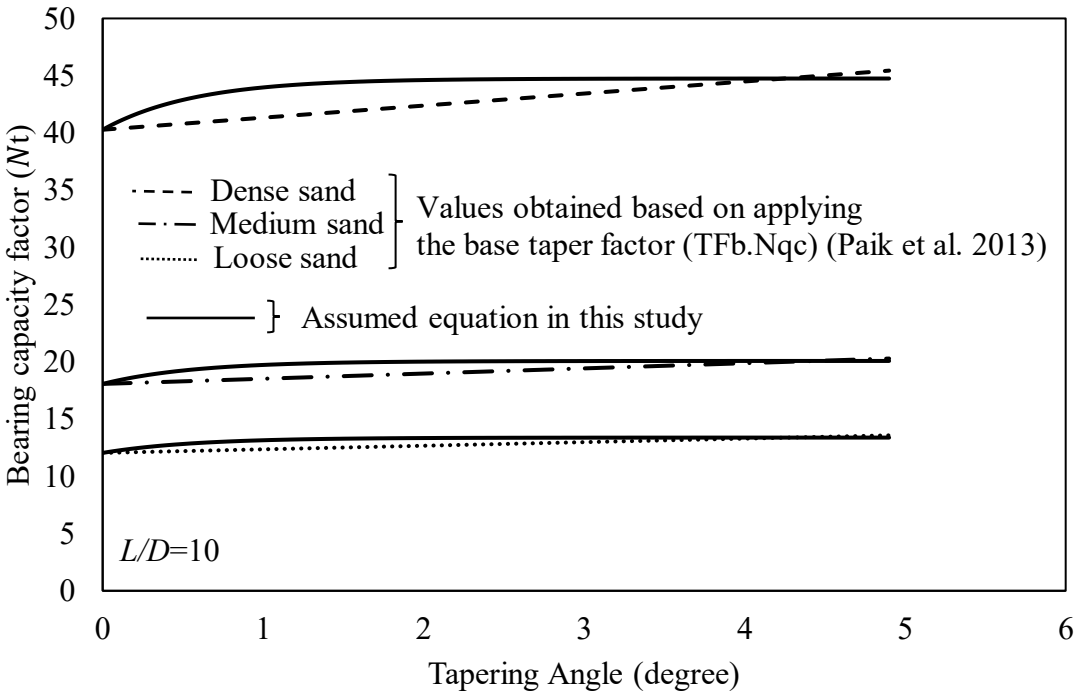

Figure 4.6. Correlation between the assumed simplified equation for the bearing capacity factor and the equation proposed by Paik et al. (2013)

$$TF_b(\alpha) = [1 + (0.0005Dr^{1.5}\ln(K_0) + 0.359).\alpha] \quad 4.23$$

$$N_t(\alpha) = \left(\lambda - \beta.e^{-\frac{\pi\zeta\alpha}{180}}\right).N_{qc} \quad 4.24$$

$$N_{qc} = [exp((\frac{\pi\psi}{90})tan(\phi))(tan(\phi) + \sqrt{1 + tan(\phi)^2})^2] \quad 4.25$$

Where, Dr is the relative density of sand, N_{qc} is the bearing capacity factor for the counterpart cylindrical pile recommended by Janbu (1976), ψ is a coefficient, corresponding to the soil relative density and its definition can be found in Figure 4.7, and can vary between 60° and 105° depending of the soil relative density as mentioned by Janbu (1976); ϕ is the friction angle of soil. In addition, λ and β are model parameters, capturing the effect of tapering angle on the vertical effective stress adjacent to the pile. Referring to Figure 4.6, their values were obtained to be equal to 1.11 and 0.11, respectively. It should be noted that the unit of ψ, ϕ and α in the above

equations is degree. It should also be noted that when the tapering angle is zero (i.e. $\alpha = 0$), Equation 4.24 is simplified to $N_t(\alpha = 0) = N_{qc}$ as expected.

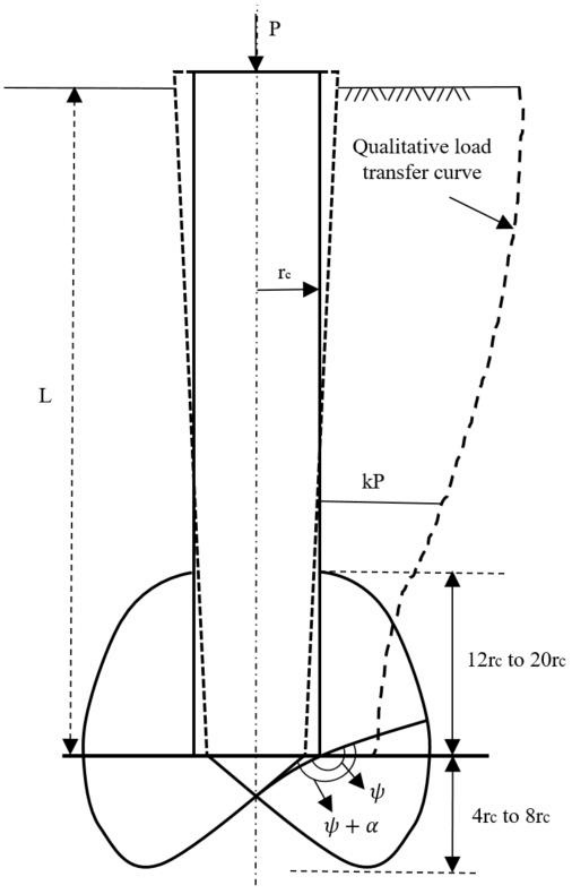

Figure 4.7. Schematic load transfer curve, the failure wedges beneath cylindrical and tapered piles and the ψ definition used in Nq factor (modified after Janbu 1976)

Substituting Equations 4.12 to 4.14 and Equation 4.21 into Equation 4.19 and expanding the integration yields:

$$q_{st} = \frac{\pi \gamma k_t k_0 L^2 \tan(\delta)}{6} [3D_{av} - L\tan(\alpha)] \qquad 4.26$$

As evident, the above-proposed equations (i.e. Equations 4.15 & 4.26) can capture the effects of the tapering angle on the shaft resistance and the shaft vertical resistance component, and obviously the lateral earth pressure varies nonlinearly with the tapering angle. In contrary to a cylindrical pile that the pile axial movement would not compress the soil surrounding the shaft (i.e. at rest condition is maintained), soil

compression around the pile shaft and gradual mobilisation of passive earth pressure in the case of tapered pile impacts the lateral earth pressure. Therefore, the frictional interaction between the tapered pile and the surrounding soil will be impacted too.

As mentioned earlier, the base area of the tapered pile can be written as a function of tapering angle and the radius of the counterpart cylindrical pile as presented in Equation 4.4. Hence, Equation 4.1 can be rewritten to obtain the base resistance of a tapered pile (q_{bt}):

$$q_{bt} = \frac{\pi L\gamma}{4} N_t [D_{av} - Ltan(\alpha)]^2 \qquad 4.27$$

The bearing capacity of a tapered pile (Q_T) is the summation of three resistance components, namely base resistance, q_{bt}, shaft resistance, q_{st}, and the shaft vertical resistance, q_{svt}, as presented in Equation 4.28.

$$Q_T = q_{bt} + q_{sv} + q_{st} \qquad 4.28$$

The term $D_b = [D_{av} - Ltan(\alpha)]$ can be introduced, which is representing the base diameter of a tapered pile and D_{av} is representing the average diameter of a tapered pile (refer to Equation (12)). Hence, by substituting Equations 4.15, 4.26 and 4.27 into 4.28, the total bearing capacity (Q_T) can be determined as:

$$Q_T = \frac{\pi\gamma L N_t}{4} {D_b}^2 + \frac{\pi\gamma L^2}{6} [k_t k_0 \, tan(\delta) + N_t \, tan(\alpha)][2D_{av} + D_b] \qquad 4.29$$

Equation 4.29 presents the axial bearing capacity of bored tapered piles embedded in sand considering three different components namely base resistance, shaft friction, and shaft vertical resistance. Equation 4.29 is a function of soil unit weight (γ), length of pile (L), tapering angle (α), taper coefficient (k_t), pile-soil interface friction angle (δ), bearing capacity factor for tapered pile (N_t), pile average diameter (D_{av}) and pile base diameter (D_b).

The differentiation of the Equation 4.29 with respect to tapering angle (α) is a complex practice, which includes a large number of terms. Hence, for a given set of parameters and performing a parametric study, the obtained Equations including (A.3), (A.4) and (A.5) can be solved (see Appendix A). The applied algorithm, shown in Figure 4.8, employed in the numerical solution, is based on Cauchy distribution and the initial guesses are real values and have a large spread of values on repeated calls, and Figure 4.9 can be generated.

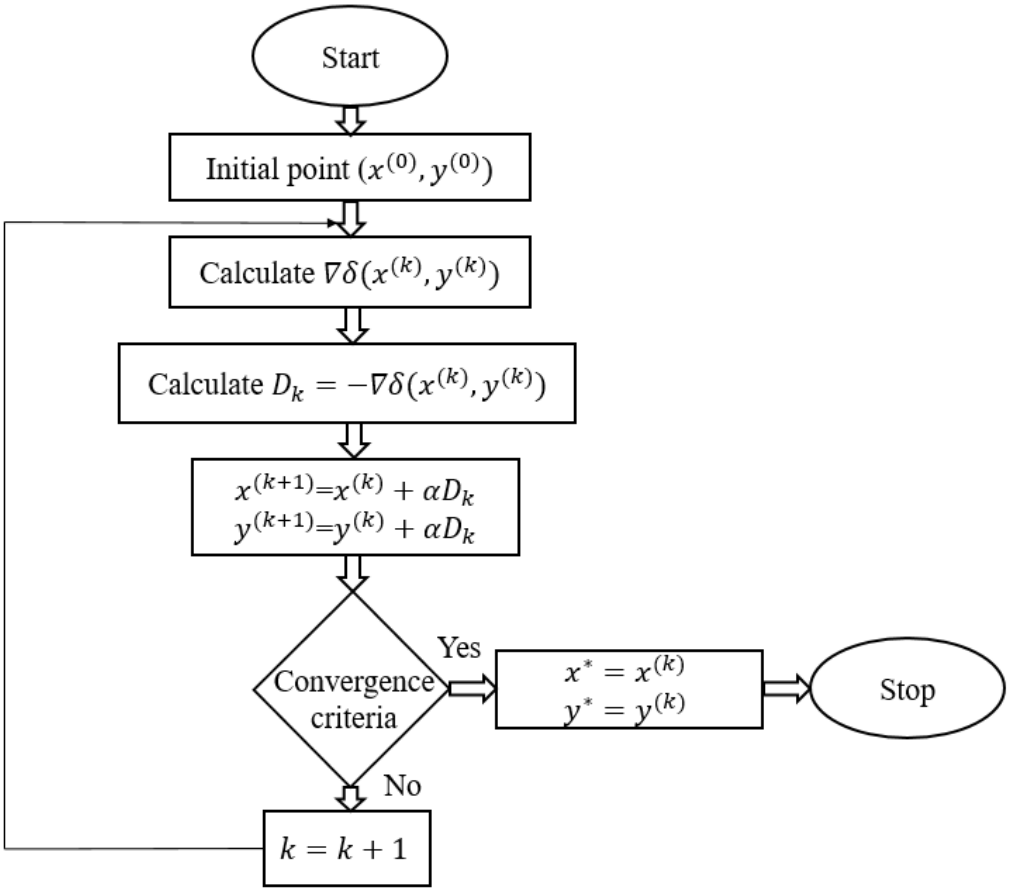

Figure 4.8. Flow chart of the applied algorithm in numerical solution based on Cauchy method (after Baesso et al. 2007)

The general formula of the Cauchy probability density function is as follows.

$$f(x) = \frac{1}{s\pi\left(1+\left(\frac{x-t}{s}\right)^2\right)} \qquad 4.30$$

Where, *s* is the scale parameter and *t* is the location parameter.

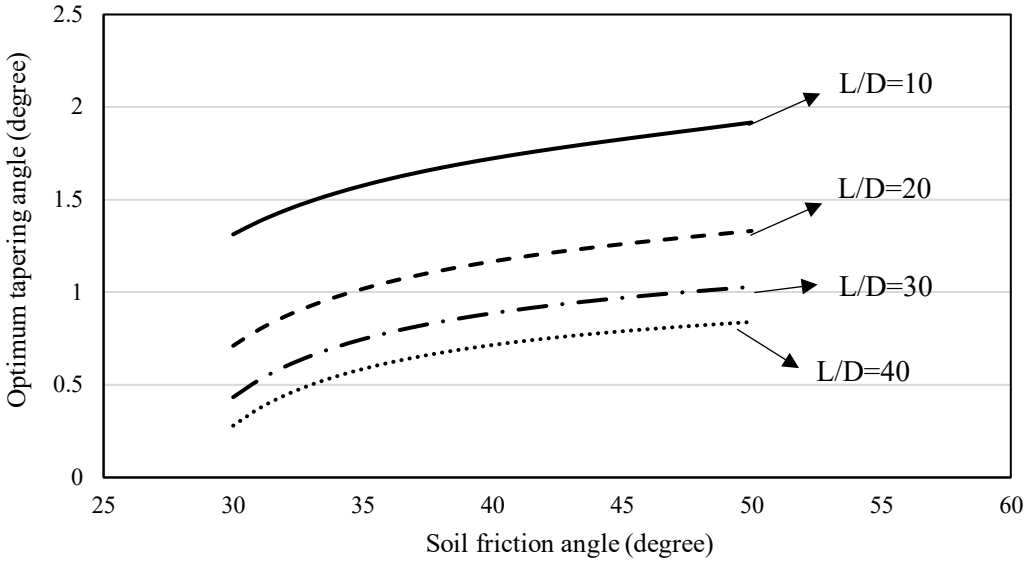

Figure 4.9. Variation of optimum tapering angle of piles having different L/D ratios embedded in different sands obtained from numerical solution

Figure 4.9 illustrates that based on a numerical solution, for different slenderness ratios and soil friction angles, an optimum tapering angle exists. The value of this angle is dependent on the type of sandy soil and the slenderness ratio of the pile as a geometry factor.

4.3 Numerical results and discussion

Figure 4.10 to Figure 4.13 demonstrate the axial load-displacement behaviour of the tapered piles with different tapering angles (including cylindrical pile corresponding to $\alpha = 0$) for piles with different *L/D* ratios of 10, 20, 30 and 40, respectively, for various compaction levels including loose, medium dense and dense.

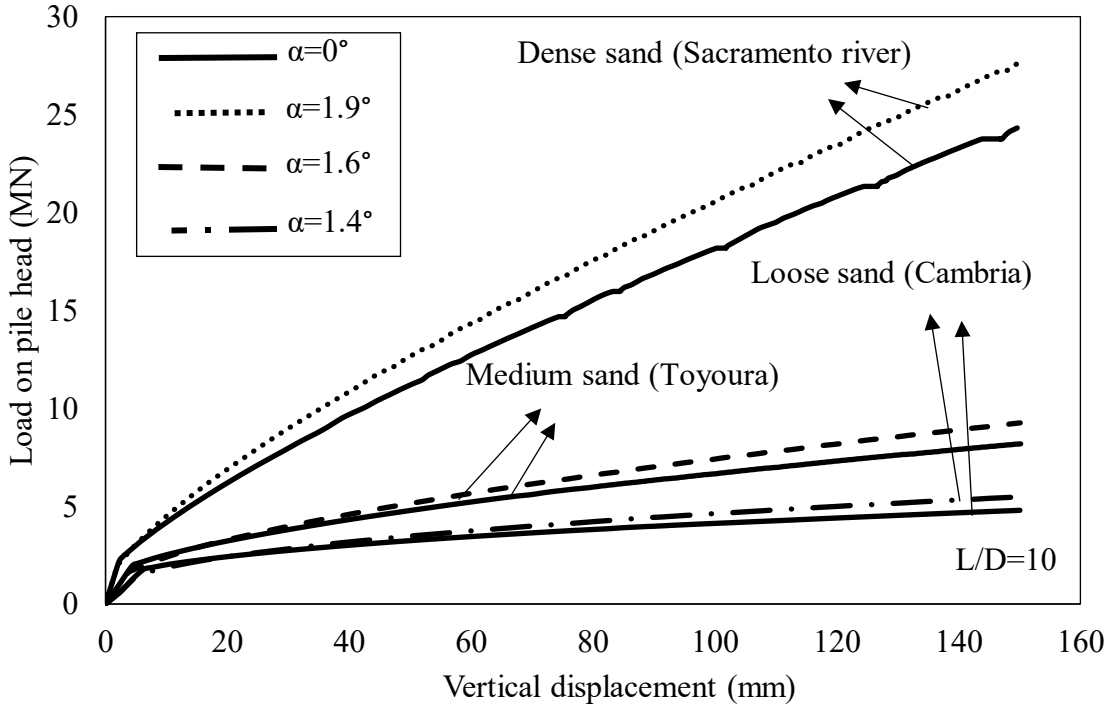

Figure 4.10. Load-displacement diagrams of tapered and straight-sided piles with L/D=10 in loose (Cambria), medium (Toyoura) and dense (Sacramento River) sands

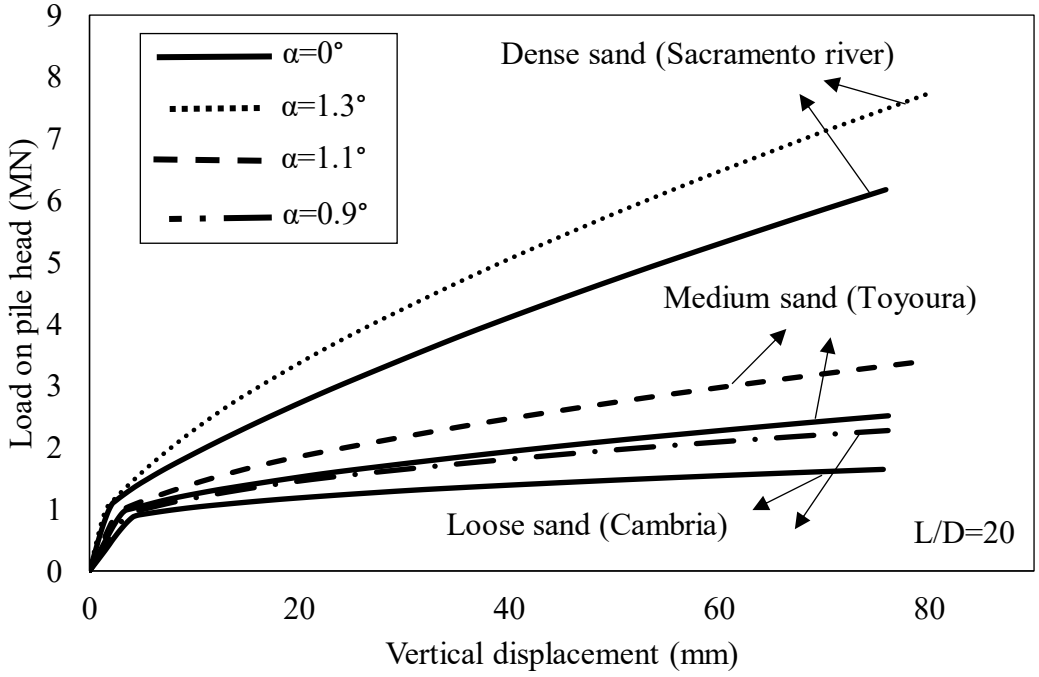

Figure 4.11. Load-displacement diagrams of tapered and straight-sided piles with L/D=20 in loose (Cambria), medium (Toyoura) and dense (Sacramento River) sands

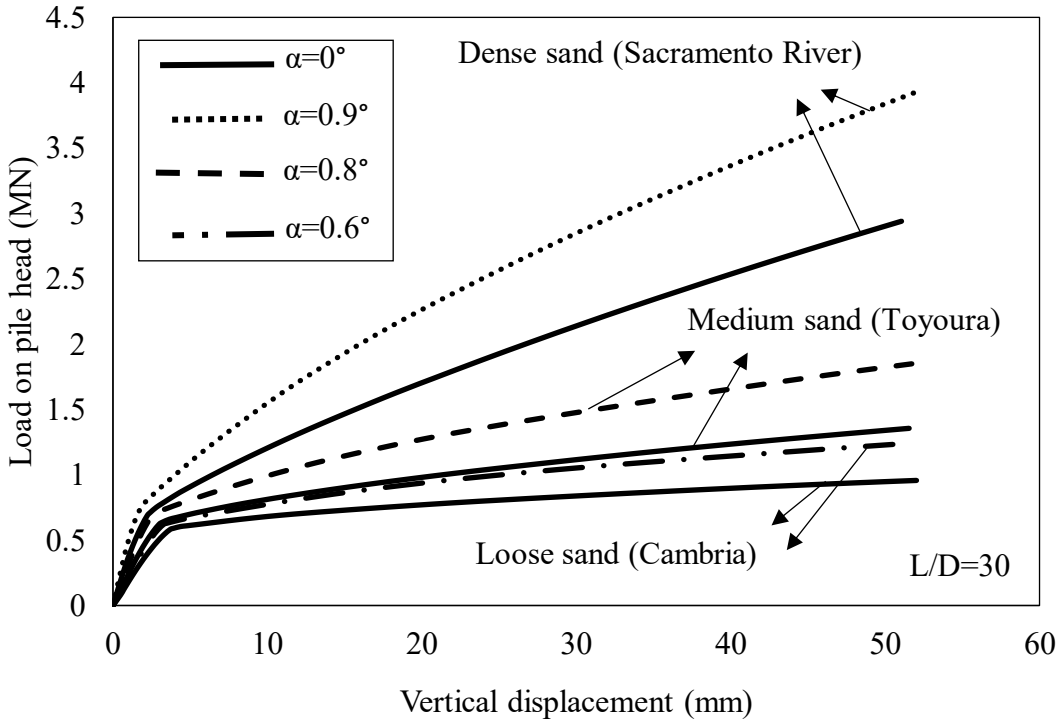

Figure 4.12. Load-displacement diagrams of tapered and straight-sided piles with L/D=30 in loose (Cambria), medium (Toyoura) and dense (Sacramento River) sands

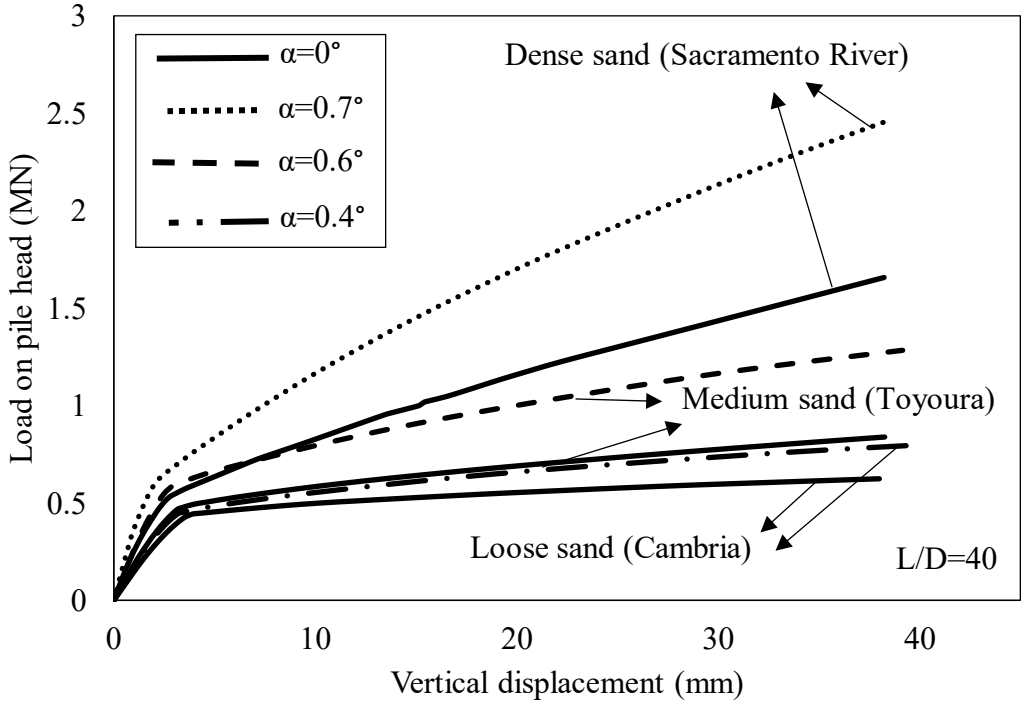

Figure 4.13. Load-displacement diagrams of tapered and straight-sided piles with L/D=40 in loose (Cambria), medium (Toyoura) and dense (Sacramento River) sands

Figure 4.10 to Figure 4.13 also suggest that as slenderness ratio (*L/D*) increased, the optimum tapering angle decreased, while as the soil relative density increased, the optimum tapering angle increased. It is also clear that the shaft resistance of piles experienced a peak point when the optimum tapering angle was observed. This is mainly due to reduction of the lateral surface area of piles by increasing the tapering angle. Nevertheless, the base resistance decreased and the shaft vertical resistance increases continuously as tapering angle increases. Therefore, the summation of three different bearing capacity components, resulting in the total bearing capacity, shows a specific optimum tapering angle for piles depending on the slenderness ratios and relative densities.

There are different techniques to interpret the axial load-displacement of piles to obtain the bearing capacity. As highlighted by Fellenius (2017); Fellenius (1991); Poulos & Davis (1980), the conventional methods in finding the bearing capacity through load-displacement curves such as double tangential method (Mansur & Kaufman 1956) or specific settlement method (based on 10% of the pile diameter) (EN 1997) would result in the serviceability bearing capacity. However, the analytical equations for bearing capacity similar to those reported in the previous section (see Equation 4.29) are representing the ultimate bearing capacity of piles since they adopt limit equilibrium theory, initially introduced by Coulomb in 1773.

The diagrams of different components of bearing capacities, including the vertical shaft bearing, the toe bearing and the shaft frictional resistances are plotted for piles having different tapering angles in Figure 4.14 andFigure 4.15. The results illustrate the variation of abovementioned capacity components of piles having *L/D* ratios of 10, 20, 30 and 40 in three different compaction levels, along with different tapering angles.

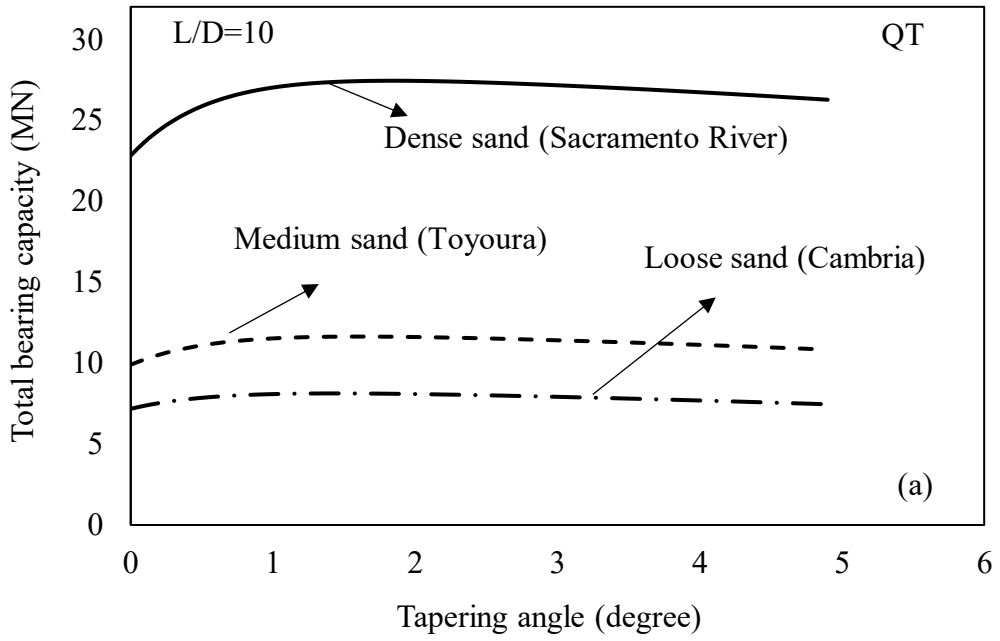
L/D=10
QT
Dense sand (Sacramento River)
Medium sand (Toyoura)
Loose sand (Cambria)
(a)
Total bearing capacity (MN)
Tapering angle (degree)
0
5
10
15
20
25
30
0
1
2
3
4
5
6

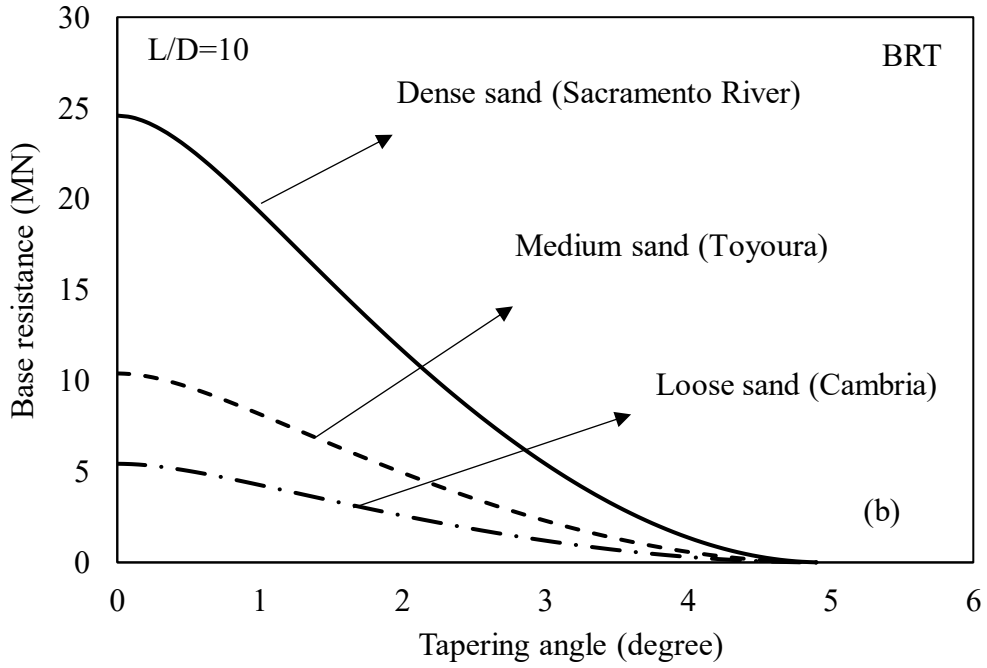
L/D=10
BRT
Dense sand (Sacramento River)
Medium sand (Toyoura)
Loose sand (Cambria)
(b)
Base resistance (MN)
Tapering angle (degree)
0
5
10
15
20
25
30
0
1
2
3
4
5
6

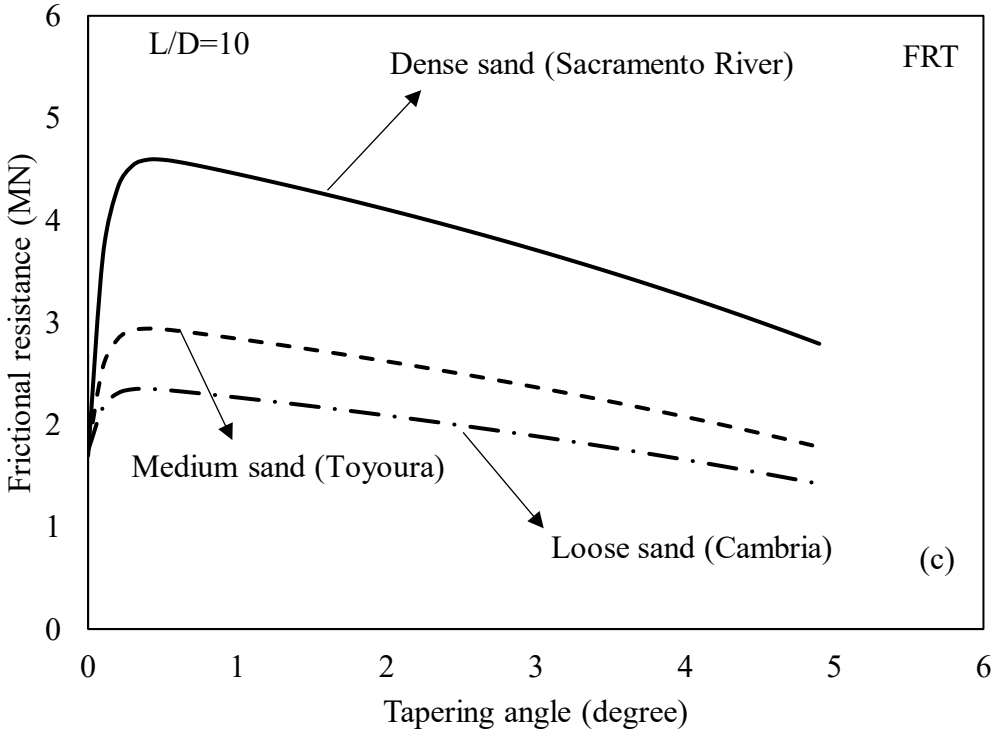
L/D=10
Dense sand (Sacramento River)
FRT
Medium sand (Toyoura)
Loose sand (Cambria)
(c)
Frictional resistance (MN)
Tapering angle (degree)
0
1
2
3
4
5
6

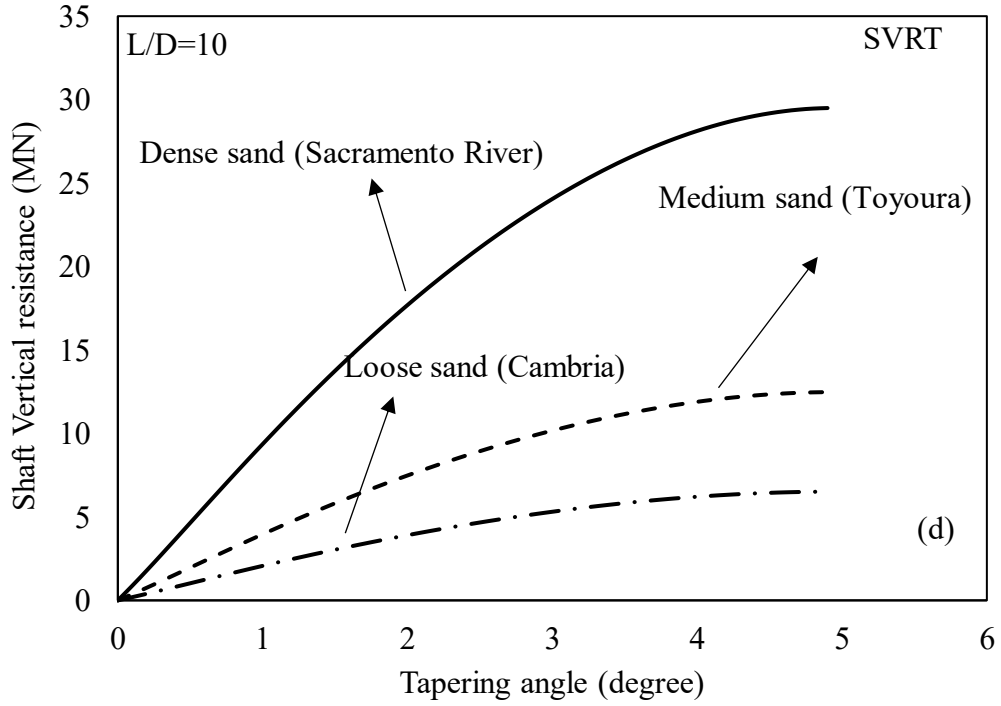
L/D=10
SVRT
Dense sand (Sacramento River)
Medium sand (Toyoura)
Loose sand (Cambria)
(d)
Shaft Vertical resistance (MN)
Tapering angle (degree)
0
5
10
15
20
25
30
35
1
2
3
4
6

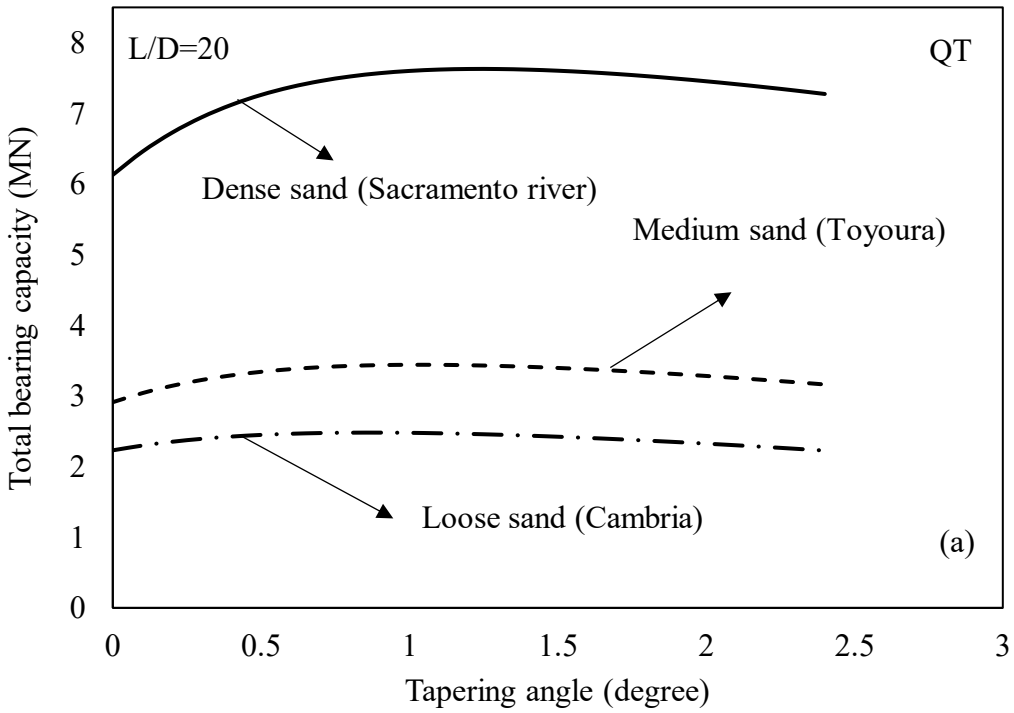
L/D=20
QT
Dense sand (Sacramento river)
Medium sand (Toyoura)
Loose sand (Cambria)
(a)
Total bearing capacity (MN)
Tapering angle (degree)
0
1
2
3
4
5
6
7
8
0
0.5
1
1.5
2
2.5
3

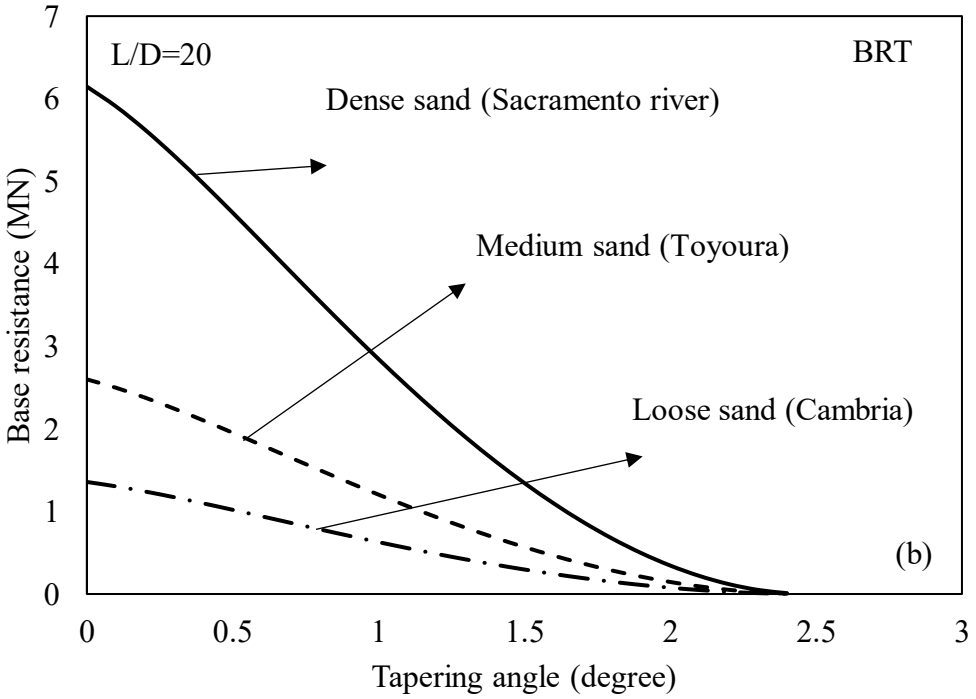
L/D=20
BRT
Dense sand (Sacramento river)
Medium sand (Toyoura)
Loose sand (Cambria)
(b)
Base resistance (MN)
Tapering angle (degree)
0
1
2
3
4
5
6
7
0
0.5
1
1.5
2
2.5
3

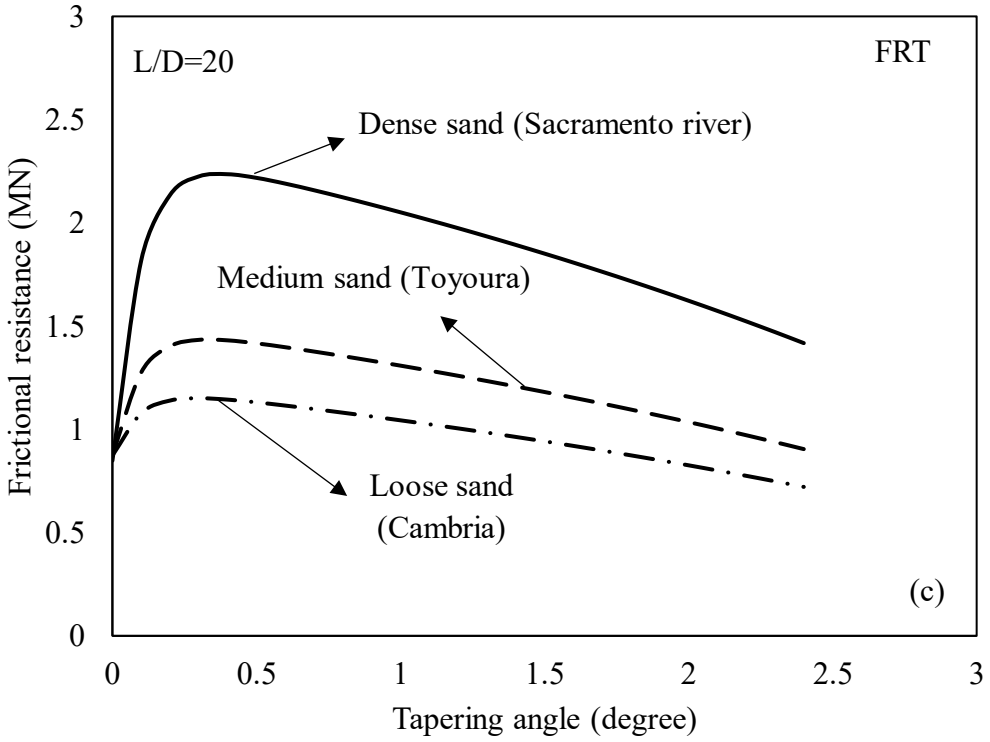

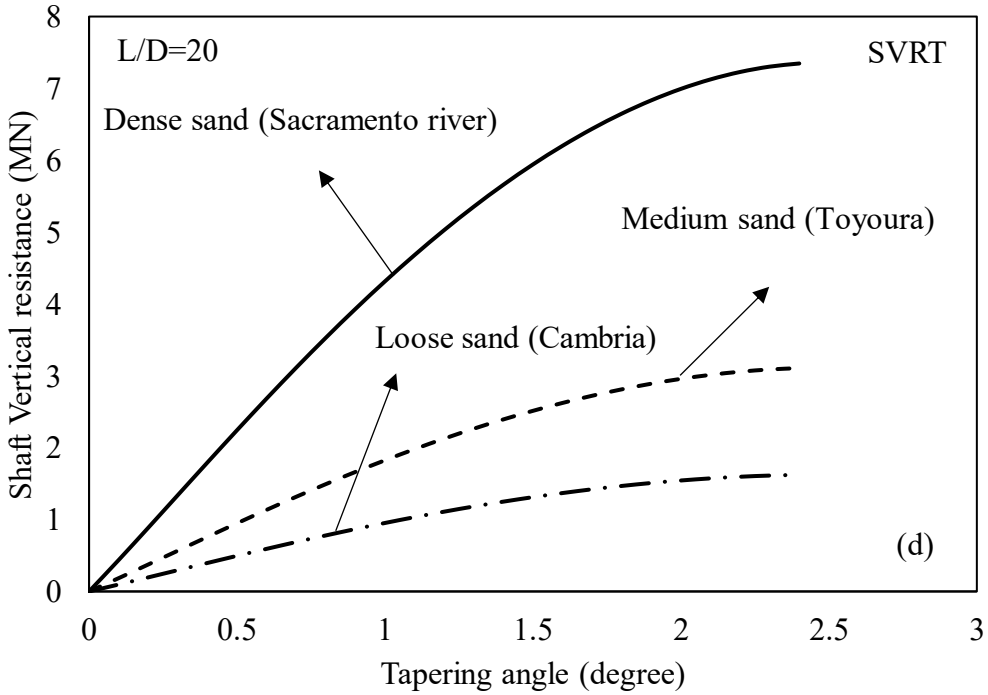

Figure 4.14. Variation of different components of ultimate bearing capacity for different tapering angels (L/D=10 & L/D=20) a) Total bearing (QT) b) Base resistance (BRT) c) Frictional resistance (FRT) d) Shaft Vertical resistance (SVRT)

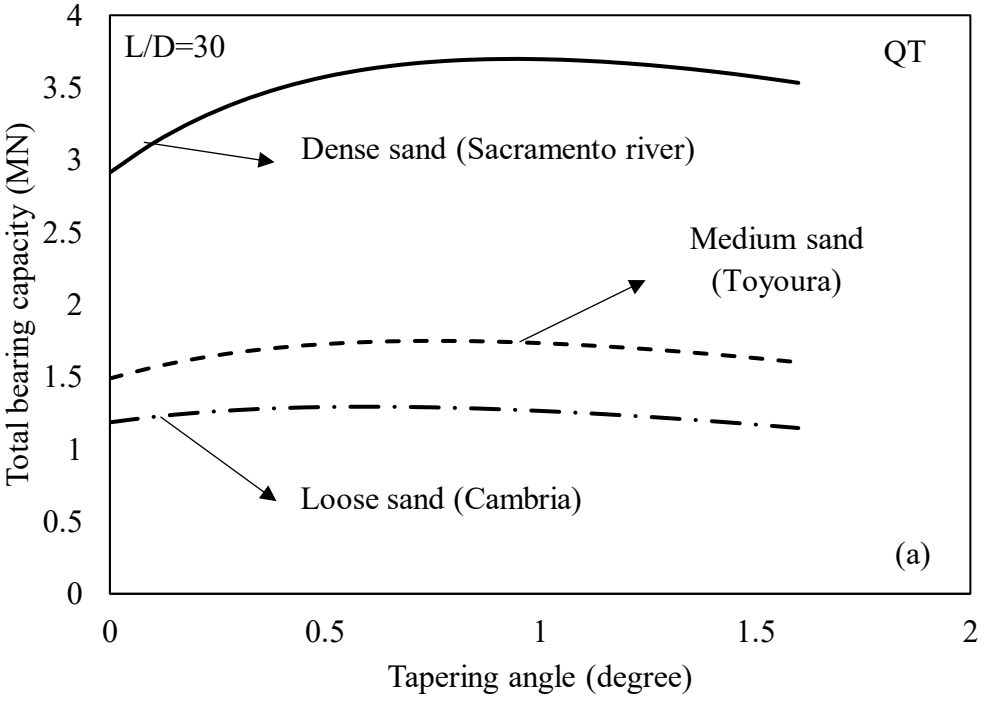
L/D=30
QT
Dense sand (Sacramento river)
Medium sand
(Toyoura)
Loose sand (Cambria)
(a)
Total bearing capacity (MN)
Tapering angle (degree)
0
0.5
1
1.5
2
2.5
3
3.5
4

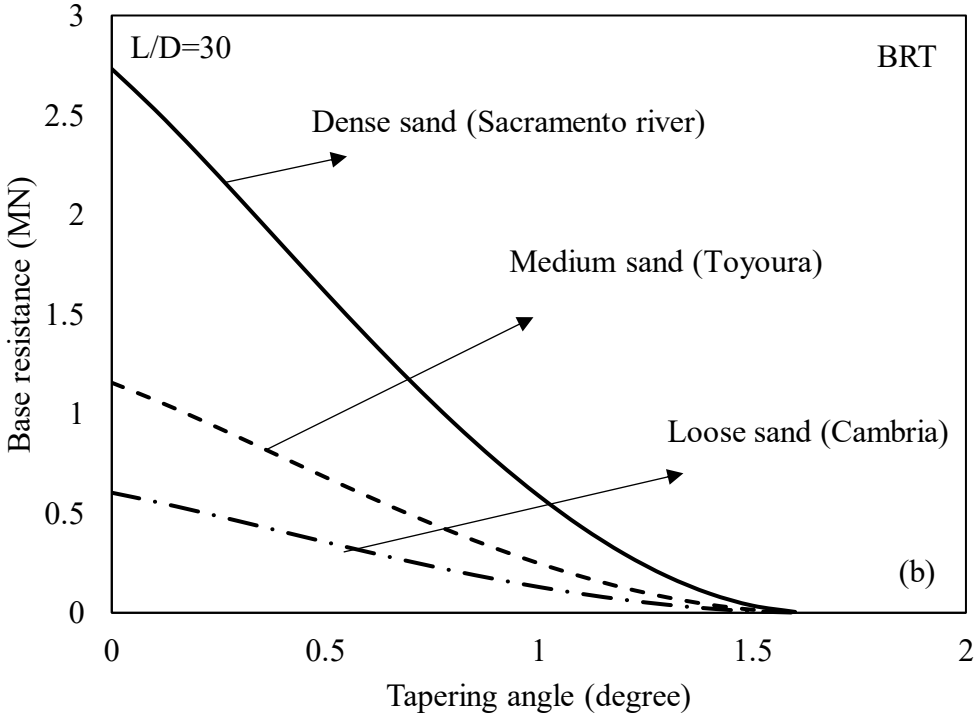
L/D=30
BRT
Dense sand (Sacramento river)
Medium sand (Toyoura)
Loose sand (Cambria)
(b)
Base resistance (MN)
Tapering angle (degree)
0
0.5
1
1.5
2
2.5
3

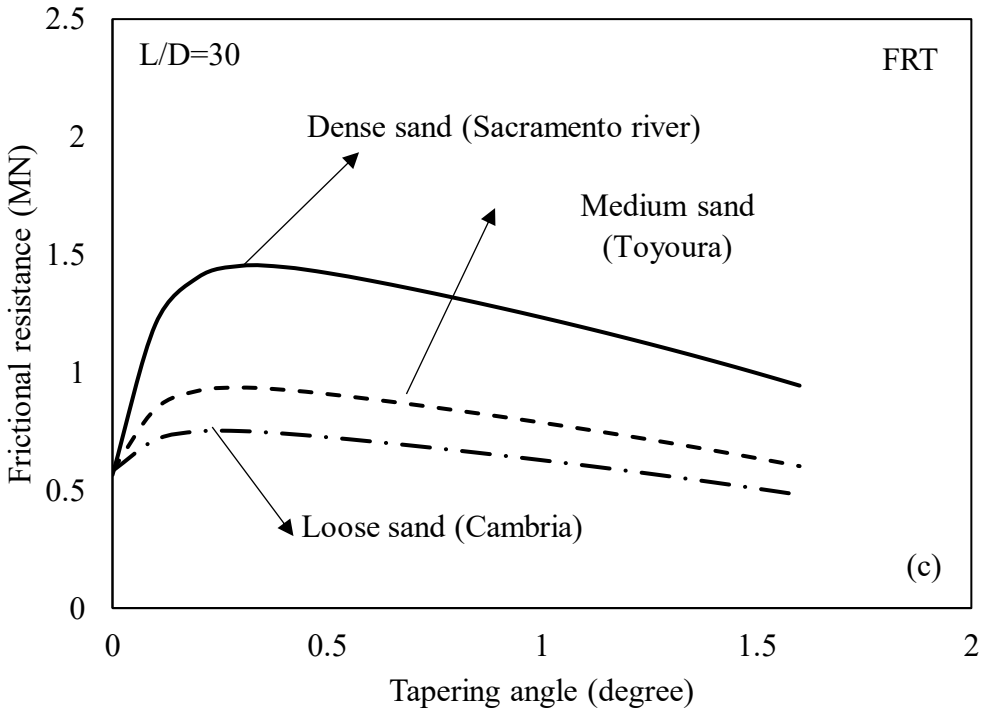
L/D=30
FRT
Dense sand (Sacramento river)
Medium sand
(Toyoura)
Loose sand (Cambria)
(c)
Frictional resistance (MN)
Tapering angle (degree)
0
0.5
1
1.5
2
2.5

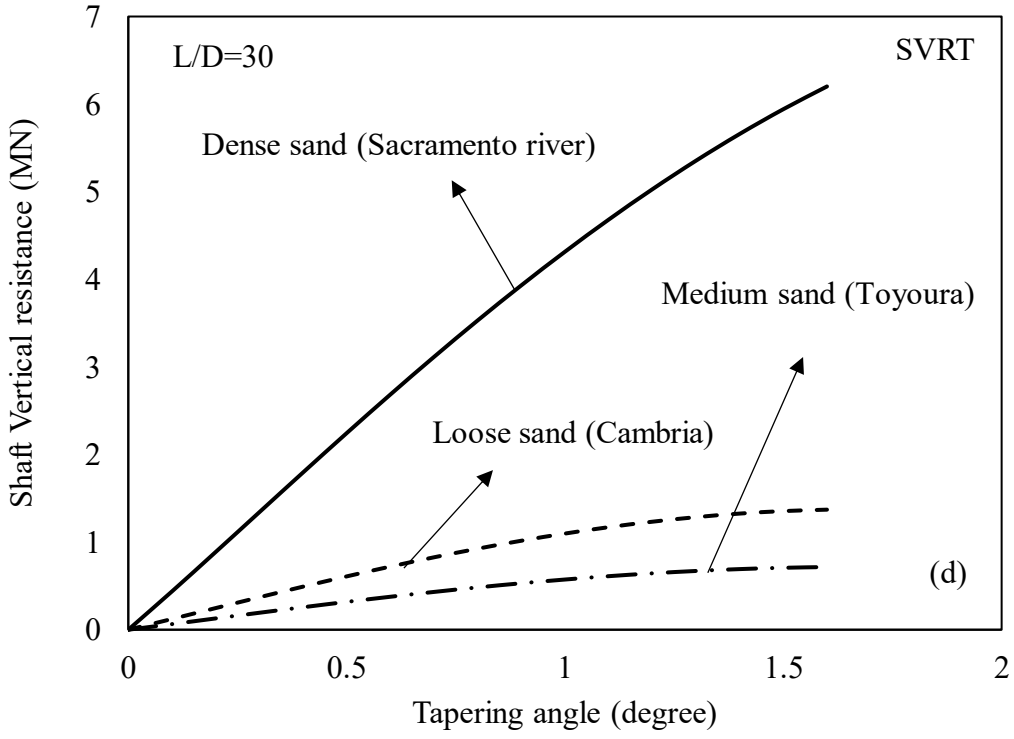
L/D=30
SVRT
Dense sand (Sacramento river)
Medium sand (Toyoura)
Loose sand (Cambria)
(d)
Shaft Vertical resistance (MN)
Tapering angle (degree)
0
1
2
3
4
5
6
7

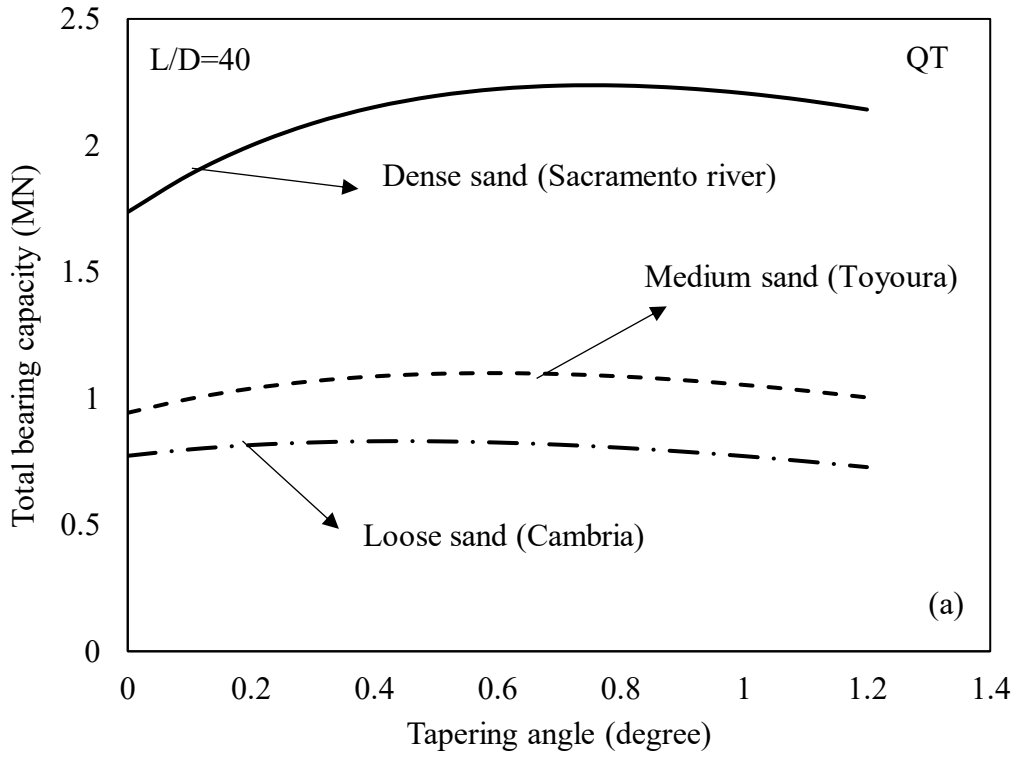
L/D=40
QT
Dense sand (Sacramento river)
Medium sand (Toyoura)
Loose sand (Cambria)
(a)
Total bearing capacity (MN)
Tapering angle (degree)
2.5
2
1.5
1
0.5
0
0
0.2
0.4
0.6
0.8
1
1.2
1.4

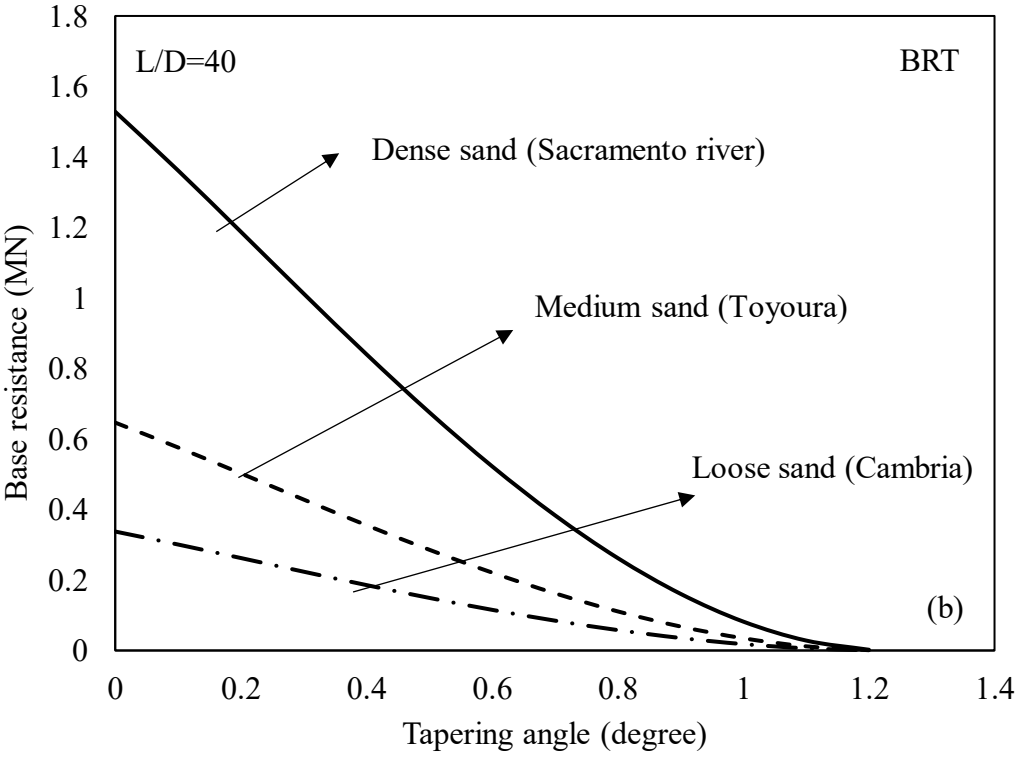
L/D=40
BRT
Dense sand (Sacramento river)
Medium sand (Toyoura)
Loose sand (Cambria)
(b)
Base resistance (MN)
Tapering angle (degree)
1.8
1.6
1.4
1.2
1
0.8
0.6
0.4
0.2
0
0
0.2
0.4
0.6
0.8
1
1.2
1.4

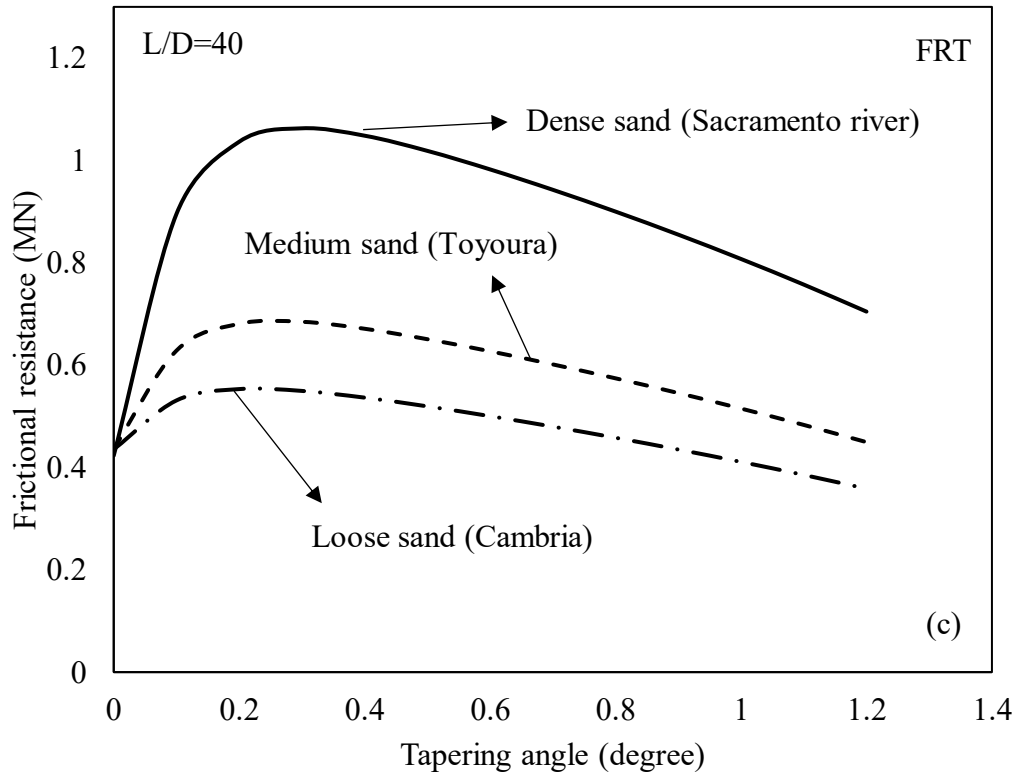

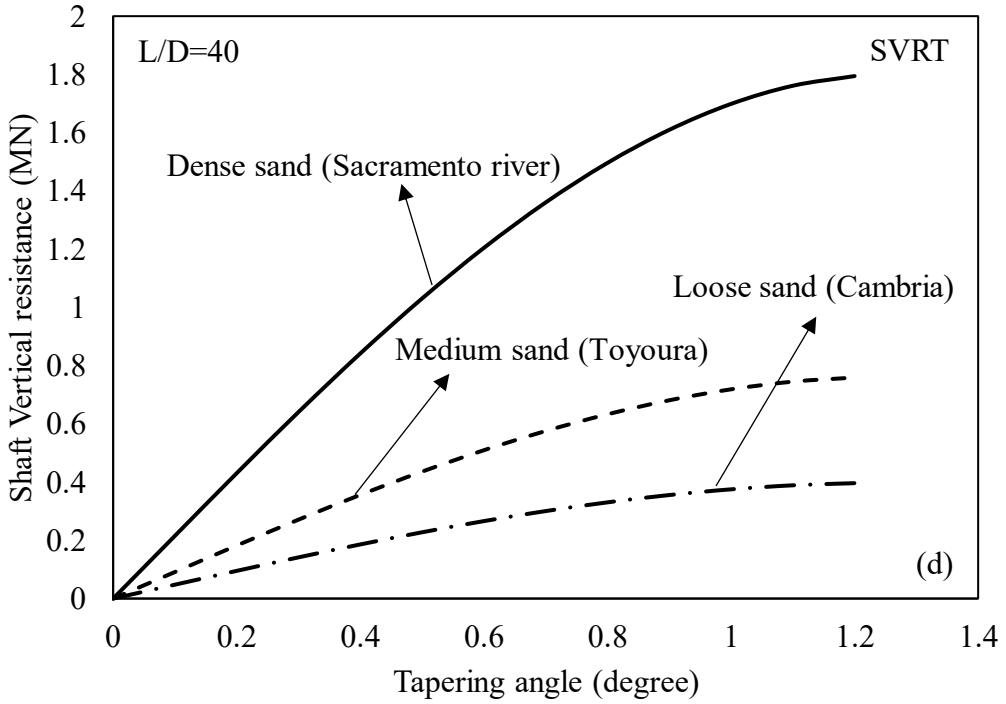

Figure 4.15. Variation of different components of ultimate bearing capacity for different tapering angels (L/D=30 & L/D=40) (a) Total bearing (QT) (b) Base resistance (BRT) (c) Frictional resistance (FRT) (d) Shaft Vertical resistance (SVRT)

As can be seen in Figure 4.14 and Figure 4.15, the total bearing capacity diagram versus tapering angle, which were plotted based on the mathematical developed formulas (Equations 4.15, 4.26, 4.27 and 4.29), experienced a peak point indicating that an optimum tapering angle exists. In addition, by increasing the tapering angle from 0°, the shaft resistance and the total bearing capacity increased, and the base resistance decreased. However, after reaching the optimum tapering angle, there was a slight decrease in the total bearing capacity, meaning that the effect of tapering angle still is an advantage comparing to the same volume counterpart cylindrical pile.

Figures 4.14 and 4.15 clearly indicate that by increasing the tapering angle, the shaft vertical resistance increased as the projected area of the shaft increased. However, the base resistance experienced a peak value when the pile had a zero tapering angle. Subsequently, due to the decrease in pile base area, the base resistance decreased, where at the maximum tapering angle it approached zero.

Figure 4.16 demonstrates the relative shear stresses around piles. As can be seen, larger relative shear stress bulbs have been developed surrounding the tapered piles. By increasing the tapering angle, the adjacent soil was densified and accordingly the lateral earth pressure and the stiffness of the soil increased, which in turn could affect the shear stresses around the pile. In addition, since for tapered piles having an optimum tapering angle, the developed shear bulb surrounding and beneath the toe covers a larger area, the equivalent vertical stress at the toe level is also higher. Indeed, this increase is taken into account in the adopted equation for the bearing capacity factor, N_t, as a function of tapering angle, expressed in Equation 4.24.

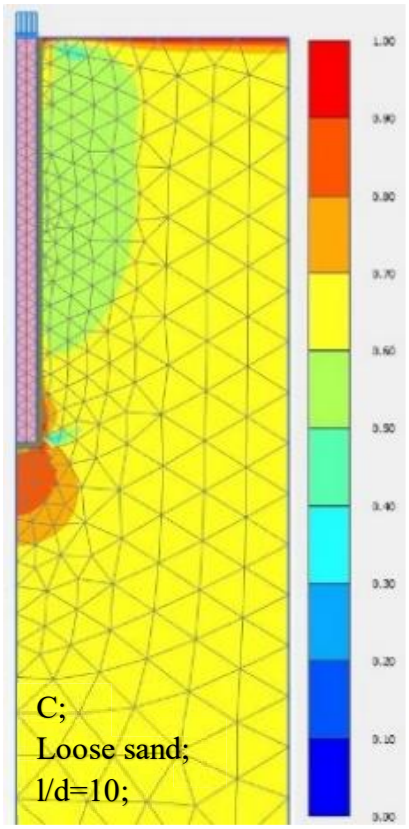
C;
Loose sand;
l/d=10;

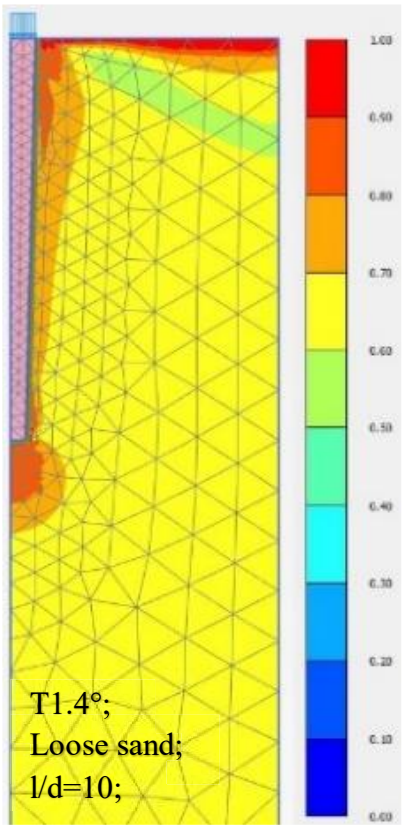
T1.4°;
Loose sand;
l/d=10;

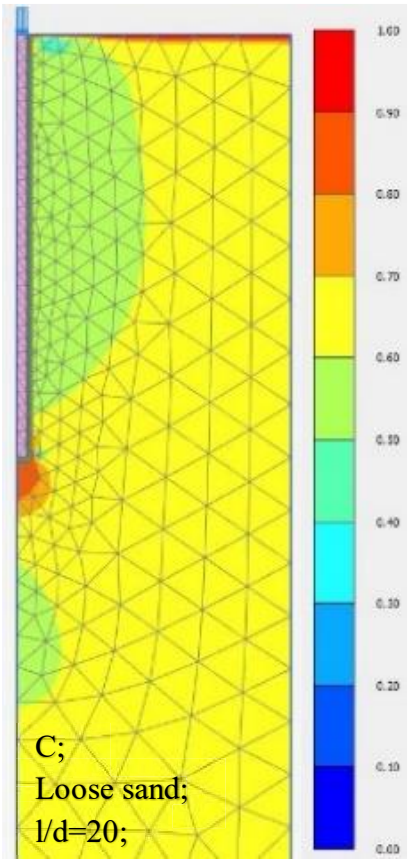
C;
Loose sand;
l/d=20;

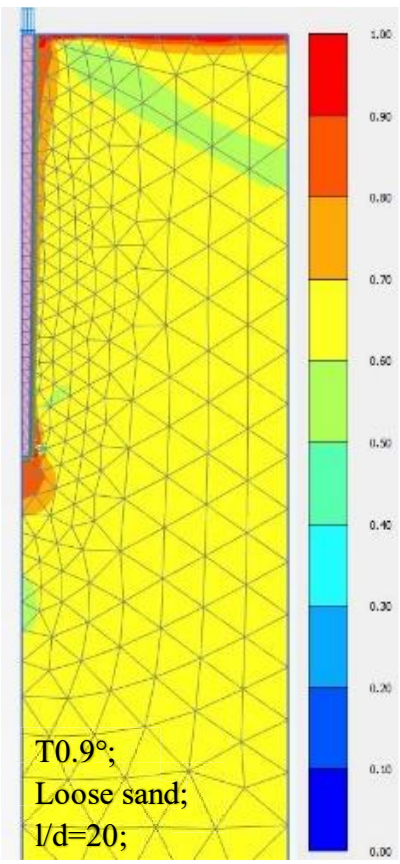
T0.9°;
Loose sand;
l/d=20;

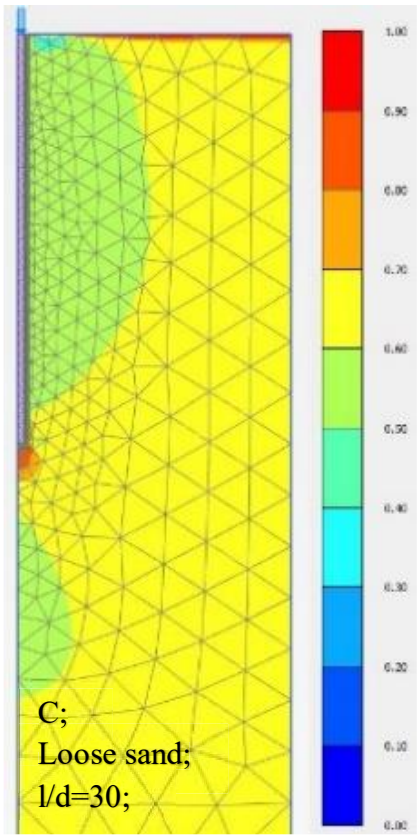
C;
Loose sand;
l/d=30;

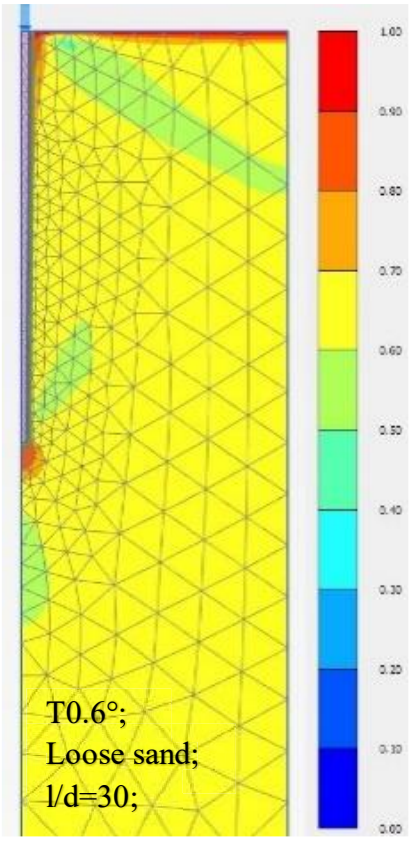
T0.6°;
Loose sand;
l/d=30;

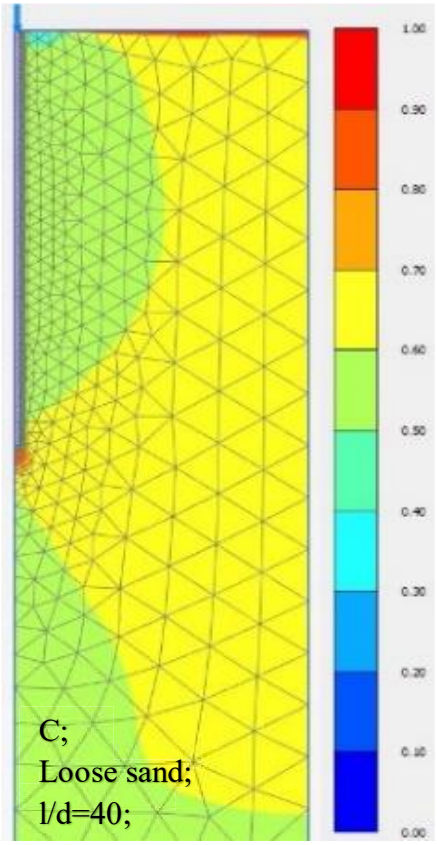
C;
Loose sand;
l/d=40;

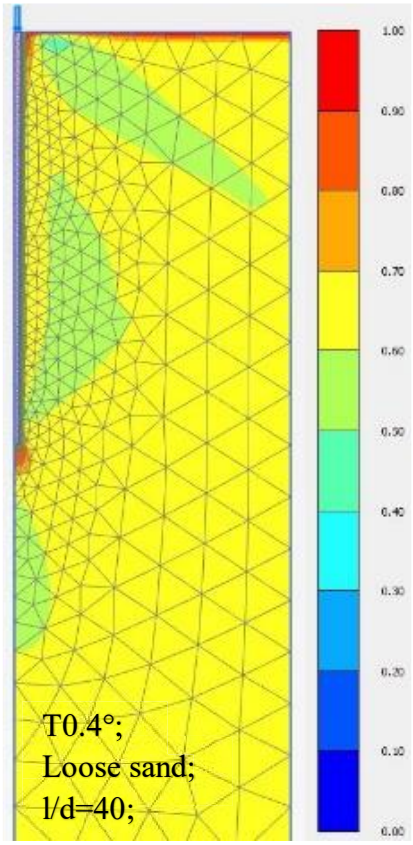
T0.4°;
Loose sand;
l/d=40;

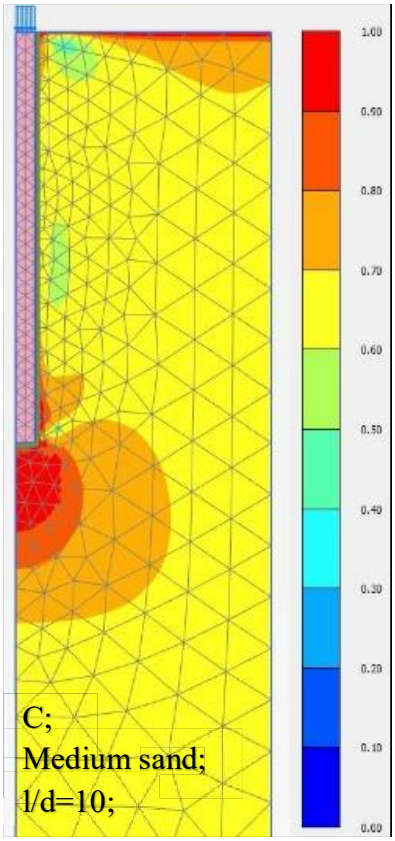
C;
Medium sand;
l/d=10;

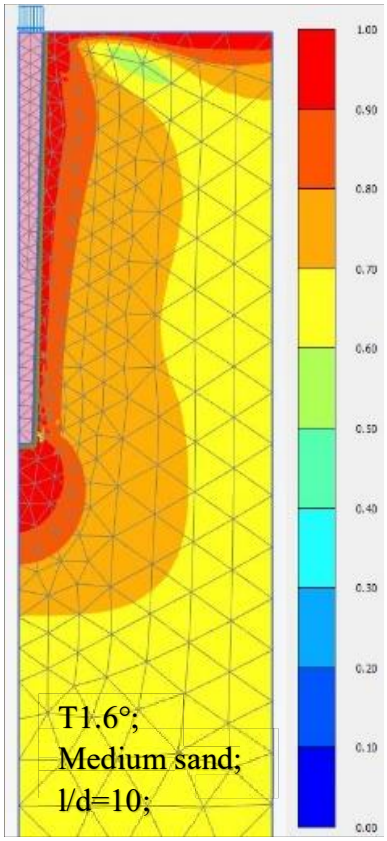
T1.6°;
Medium sand;
l/d=10;

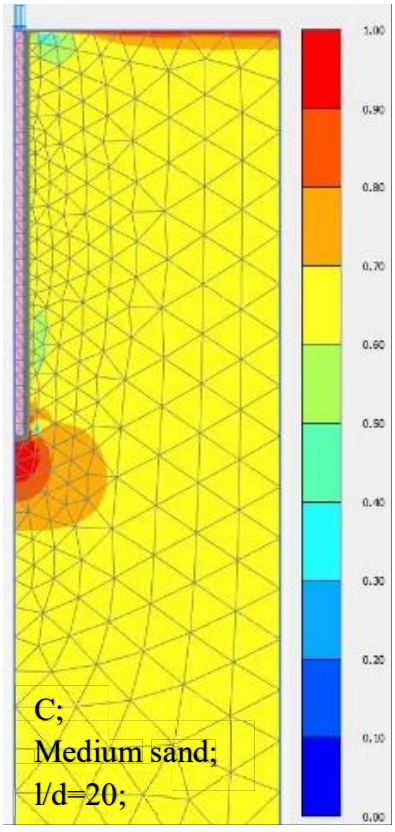
C;
Medium sand;
l/d=20;

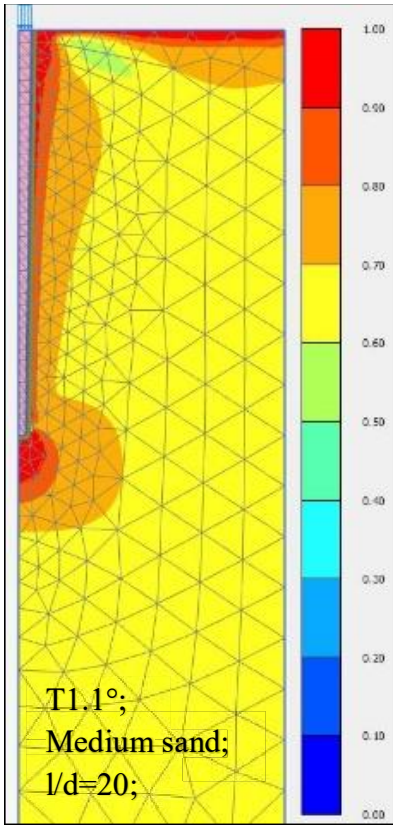
T1.1°;
Medium sand;
l/d=20;

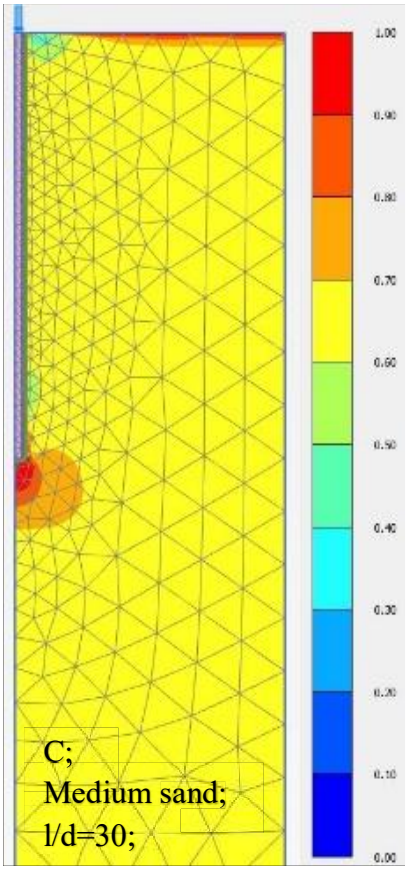
C;
Medium sand;
l/d=30;

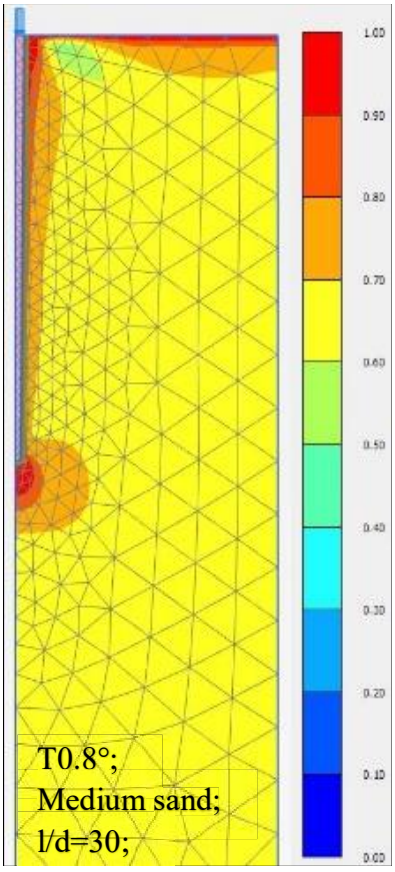
T0.8°;
Medium sand;
l/d=30;

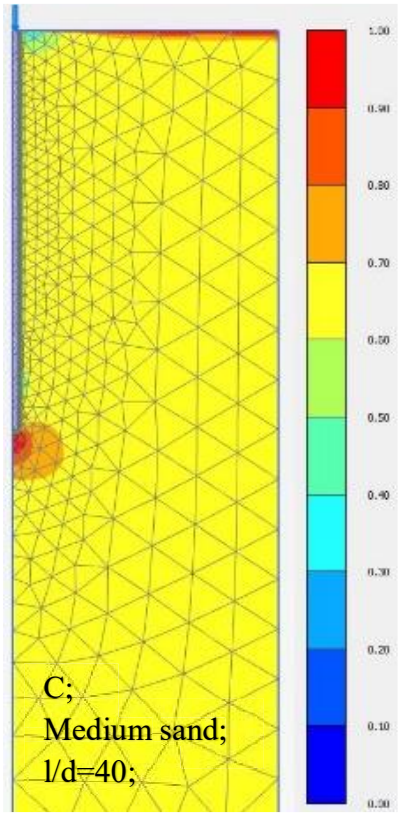
C;
Medium sand;
l/d=40;

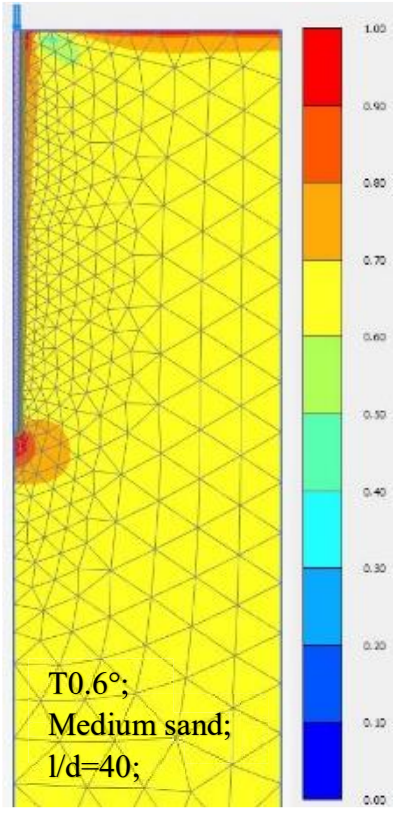
T0.6°;
Medium sand;
l/d=40;

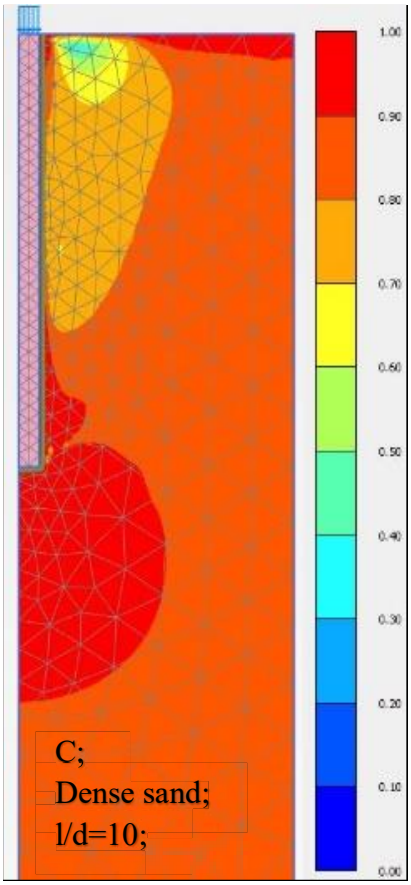
1.00
0.90
0.80
0.70
0.60
0.50
0.40
0.30
0.20
0.10
0.00
C;
Dense sand;
l/d=10;

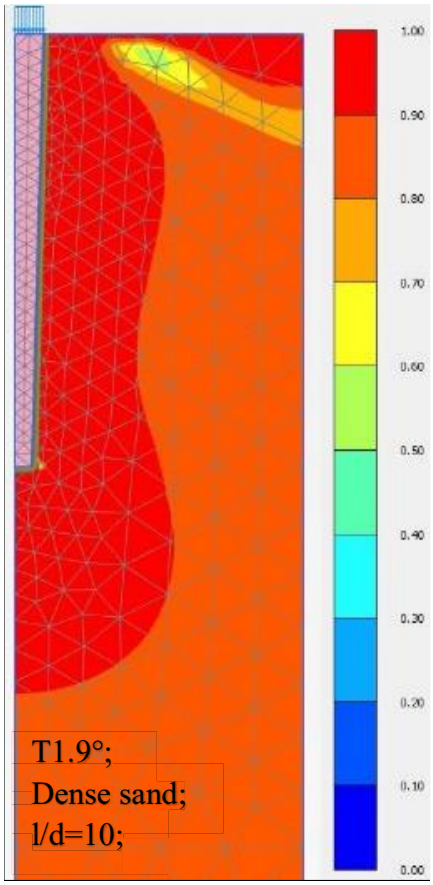
1.00
0.90
0.80
0.70
0.60
0.50
0.40
0.30
0.20
0.10
0.00
T1.9°;
Dense sand;
l/d=10;

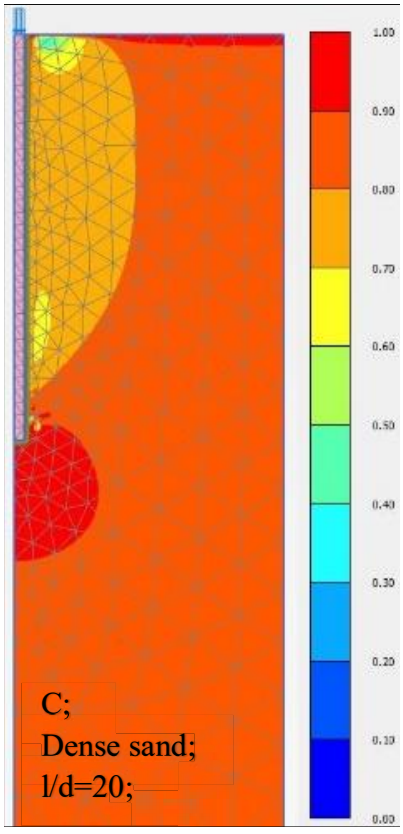
1.00
0.90
0.80
0.70
0.60
0.50
0.40
0.30
0.20
0.10
0.00
C;
Dense sand;
l/d=20;

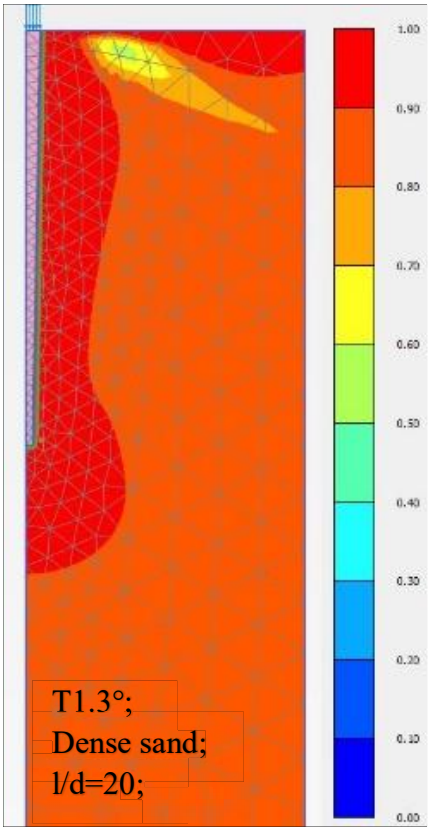
1.00
0.90
0.80
0.70
0.60
0.50
0.40
0.30
0.20
0.10
0.00
T1.3°;
Dense sand;
l/d=20;

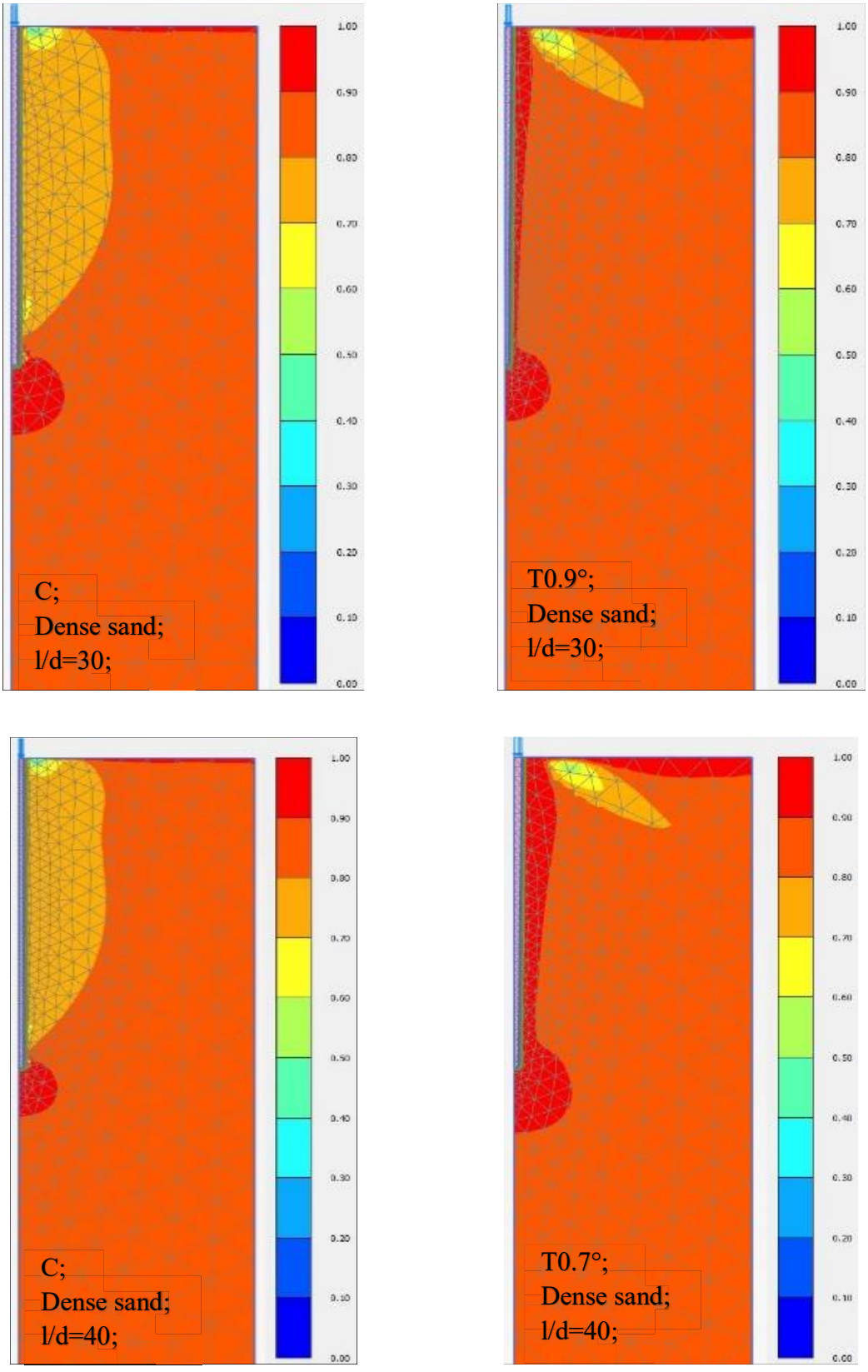

Figure 4.16. Relative shear stress distribution around piles with different slenderness ratios in sand with various relative densities (Loose Cambria sand, Medium Toyoura sand, and Dense Sacramento River sand), (C: Cylindrical, T: Tapered)

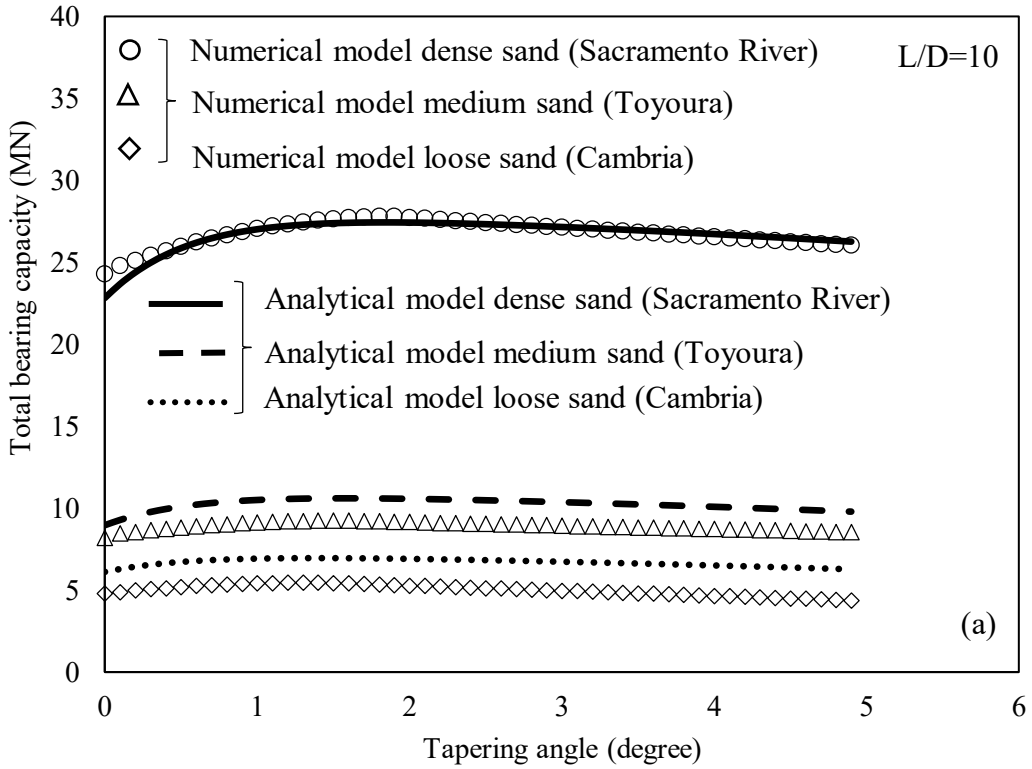
Numerical model dense sand (Sacramento River)
Numerical model medium sand (Toyoura)
Numerical model loose sand (Cambria)
L/D=10
Analytical model dense sand (Sacramento River)
Analytical model medium sand (Toyoura)
Analytical model loose sand (Cambria)
(a)
Total bearing capacity (MN)
Tapering angle (degree)
0
5
10
15
20
25
30
35
40
0
1
2
3
4
5
6

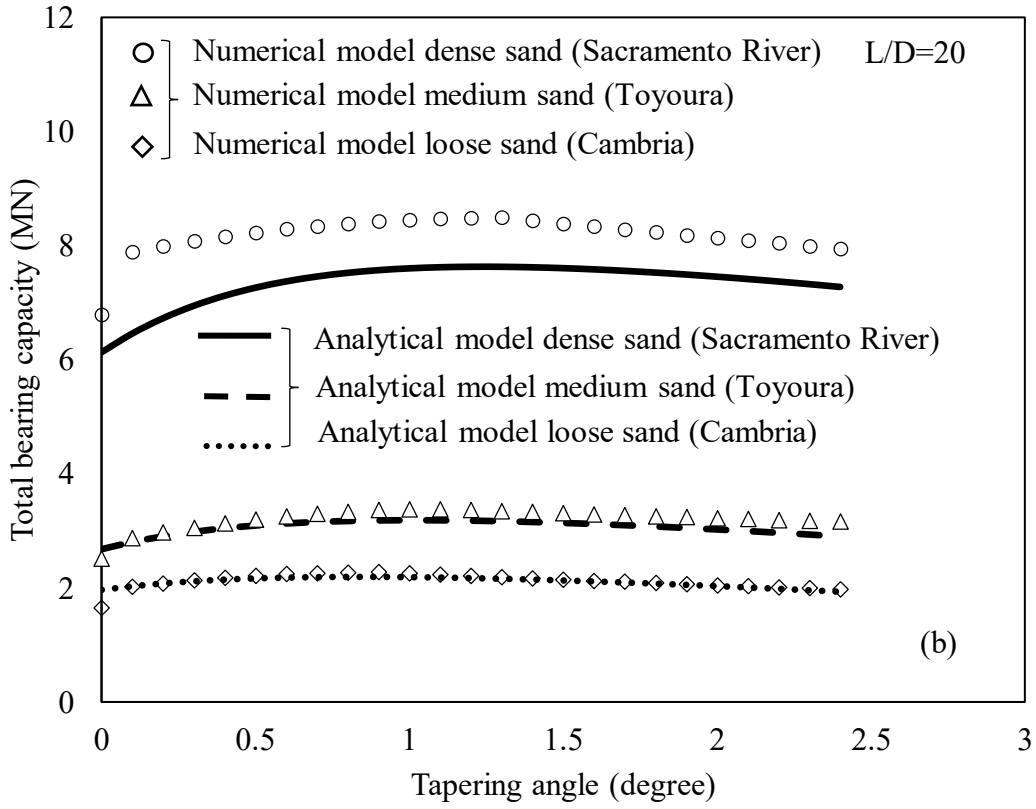
Numerical model dense sand (Sacramento River)
Numerical model medium sand (Toyoura)
Numerical model loose sand (Cambria)
L/D=20
Analytical model dense sand (Sacramento River)
Analytical model medium sand (Toyoura)
Analytical model loose sand (Cambria)
(b)
Total bearing capacity (MN)
Tapering angle (degree)
0
2
4
6
8
10
12
0
0.5
1
1.5
2
2.5
3

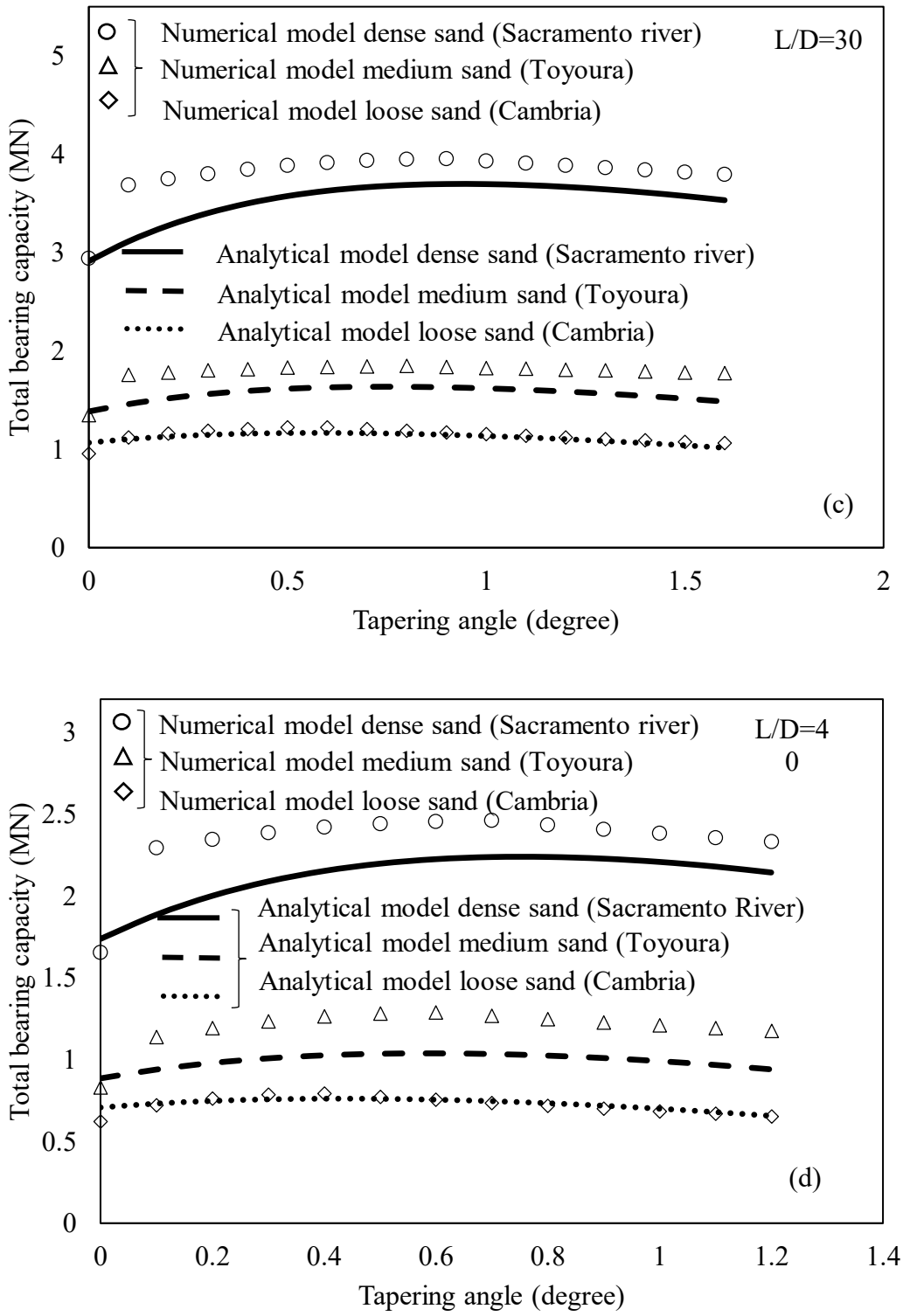

Figure 4.17. Validation of the proposed analytical model for obtaining the bearing capacity with numerical results for various L/D ratios and different types of sand (a) L/D=10, (b) L/D=20, (c) L/D=30, (d) L/D=40

4.4 Simplified equation for selecting optimum tapering angle

After generating the load-displacement curves from the numerical analysis, and obtaining the axial bearing capacity (i.e. load resistance at a certain settlement, s_e =10% of the pile diameter) for each series of analysis with a constant *L/D* ratio and various tapering angles, the angle with the highest pile axial capacity, is selected as the optimum tapering angle.

Figure 4.17 presents the comparison between analytical predictions adopting proposed Equation 4.29 and finite element predictions for the axial bearing capacity of the tapered pile under different soil characteristics and pile geometries. The developed analytical equations for piles result in the ultimate bearing capacity of piles (Terzaghi et al. 1996), and the numerical modelling presents the serviceability capacity based on the aforementioned criteria using load-displacement curves (capacity at the settlement equivalent to 10% of the pile diameter) (EN 1997). In fact, the numerical modelling takes the soil stiffness into account and it captures the nonlinear elasto-plastic response of the soil. However, in this study, the proposed analytical bearing capacity equation has been validated through a calibration process to obtain the model parameters based on the aforementioned settlement criterion.

Although there is a slight difference in validation diagrams of Figure 4.17, which is due to the non-linear behaviour of the calibrated soil using UBC sand model in the numerical modelling, the peak points that represent the optimum tapering angles obtained through both analytical and numerical models were matched. This proves the validity of not only the axial bearing capacity relationship as Equation 4.29, but also the optimum tapering angle.

Figure 4.18 illustrates the variation of the optimum tapering angle for different compaction conditions for sandy soil including loose, medium dense and dense and different *L/D* ratios of 10, 20, 30 and 40.

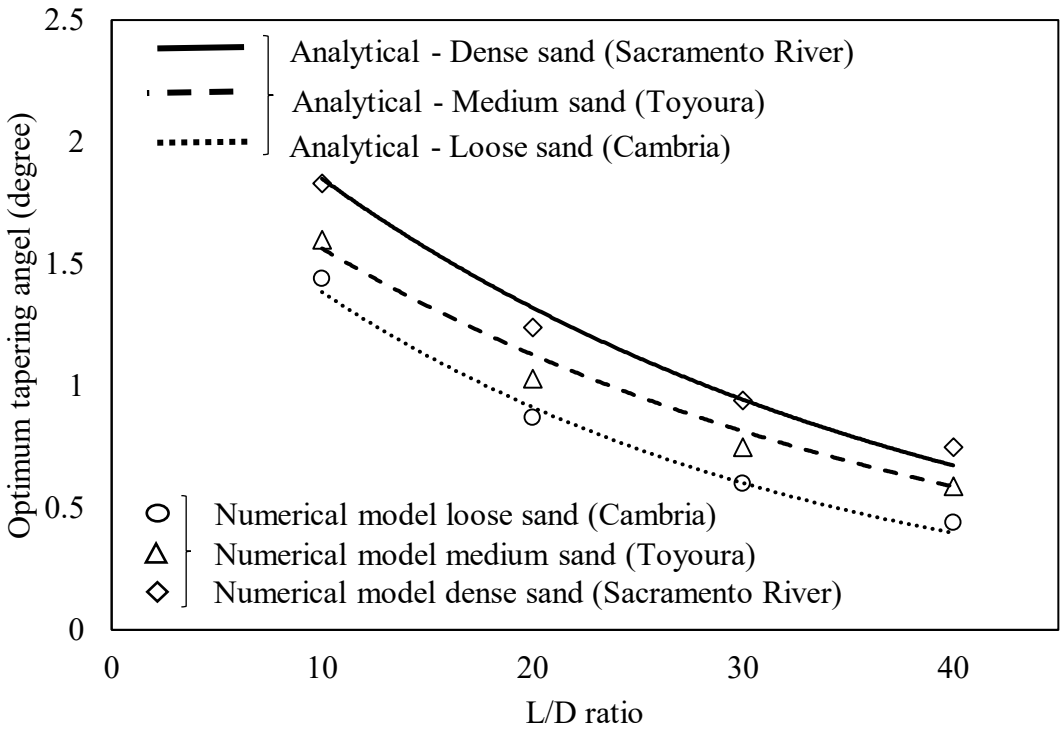

Figure 4.18. Variation of optimum tapering angel versus length to diameter ratio for loose sand (Cambria), medium sand (Toyoura), dense sand (Sacramento River) obtained from numerical analysis

Referring to Figure 4.18, the optimum tapering angle decreases as the pile becomes more slender (i.e. *L/D* increased). As Figure 4.18 shows, the relationship between the optimum tapering angle and the *L/D* ratio has a decreasing trend. However, the variation of the optimum tapering angle with respect to soil internal friction angle follows opposite pattern as evident in Figure 4.18. Referring to Figure 4.18, the impact of tapering angle on piles embedded in dense sand is quite notable. The reason can be related to the significant increase in both frictional and shaft vertical components. As captured in Equations 4.21 and 4.24, the increasing rate of soil lateral earth pressure coefficient by applying the taper coefficient k_t and the bearing capacity factor N_t with increasing tapering angle was more pronounced when internal friction angle of the soil increased. However, for more slender piles (i.e. increasing *L/D*), the effect of tapering angle was less noticed. Moreover, for a given *L/D*, a reduction in the optimum tapering angle was observed when soil compaction changed from dense toward loose sand. In other words, for a pile used in this study with *L/D* = 10, the optimum tapering angle decreased from 1.9° (corresponding to dense sand) to 1.4° (corresponding loose sand),

while this decrease as a result of changes in *L/D* was from 1.4° (corresponding to *L/D=10*) to 0.4° (corresponding to *L/D=40*) for piles embedded in loose sand.

The optimum tapering angles obtained from analytical calculations and numerical analyses are computed and compared in Table 4.1.

Table 4.1. Compared optimum tapering angels obtained from analytical and numerical methods

L/D	α_{Opt} Loose (Cambria sand)		α_{Opt} Medium (Toyoura sand)		α_{Opt} Dense (Sacramento River sand)	
	Analytical	Numerical	Analytical	Numerical	Analytical	Numerical
10	1.44°	1.4°	1.60°	1.6°	1.83°	1.9°
20	0.87°	0.9°	1.03°	1.1°	1.24°	1.3°
30	0.60°	0.6°	0.75°	0.8°	0.94°	0.9°
40	0.44°	0.4°	0.59°	0.6°	0.75°	0.7°

As can be seen, a good correlation exists between the predictions via analytical and the numerical methods in the obtained optimum tapering angles.

Based on the results presented in Figure 4.17 and Figure 4.18, and considering the factors captured in the analytical solution (Equations 4.15, 4.26, 4.27 and 4.29), simplified Equation 4.31 is proposed to predict the optimum tapering angle for bored tapered piles as a function of friction angle of soil ϕ, length of pile *L,* and diameter of the reference equivalent cylindrical pile *D*. Indeed, the proposed equation represents the normalised optimum tapering angle as the ratio between the optimum tapering angle to the maximum feasible tapering angle of tapered piles ($\alpha_r = \frac{\alpha_{opt}}{\alpha_{max}}$).

$$\alpha_r = tan^2(\phi)\left(\frac{a}{e^{\sqrt{\frac{D}{L}}}} - b.tan^2(\phi)\, e^{\sqrt{\frac{D}{L}}}\right) \quad 4.31$$

where, a and b are two model parameters, calibrated to be 1.43 and 0.51, respectively, using the result summarised in Figure 4.18 and Table 4.1. It should be mentioned that the maximum tapering angle (α_{max}) can be calculated using Equation 4.22.

Equation 4.31 is a simplified approximation to obtain the optimum tapering angle based on the soil and pile characteristics and can be used readily by practicing engineers to select the most efficient tapering angle for bored piles.

4.5 Validation of the numerical model with field test results

There is a limited number of field pile load tests on large scale bored tapered piles in sand to capture the beneficial effects of tapered piles and observing the optimum tapering angle. In this study, two bored piles embedded in sand were used to validate the numerical results and the developed mathematical relationships. The selected cases were two bored piles including one cylindrical and one tapered with a tapering angle of 1.2°, tested by Lee et al. (2009) at Iksan City in the southern area of the Republic of Korea.

According to the in situ test results, the groundwater table is 8 m beneath the ground level. In addition, the representative NSPT value at the pile base and along the pile shaft were obtained as 10 and 12, respectively. Besides, the representative cone resistance, q_c, was reported 4.35 MPa along the pile shaft and 5.25 MPa for the pile base. It should be noticed that before installing the piles, the top 2 m layer of silty clay has been removed. The geometry properties of piles used in the field pile load tests conducted by Lee et al. (2009) can be seen schematically in Figure 4.19.

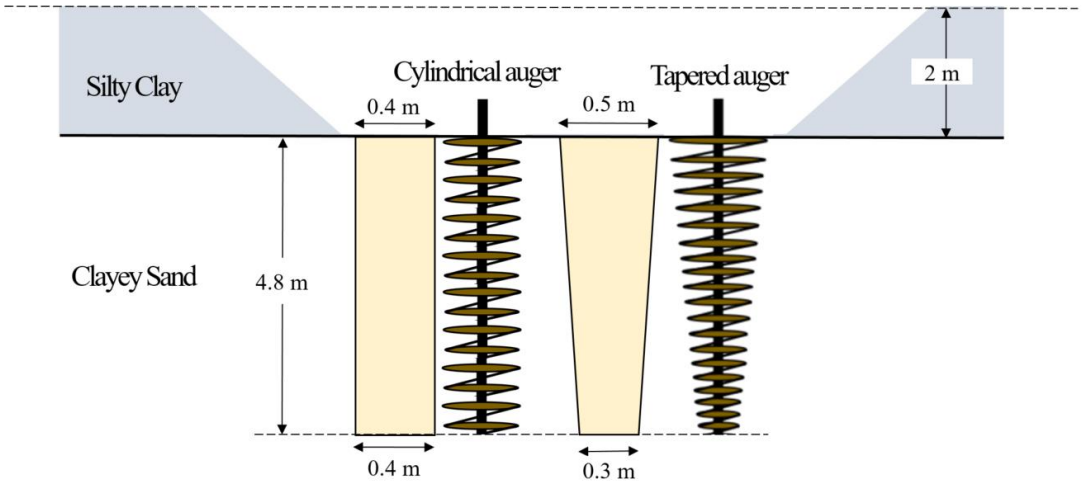

Figure 4.19. Schematic of bored piles along with the manufactured augers by Lee et al. (2009) for installing and testing piles at Iksan City in the southern region of the Republic of Korea

Figure 4.19, illustrates that two layers of soil consisted of 2 m of silty clay overlaying a deep clayey sand layer exist at the site of investigation and the soil parameters are presented in Table 4.2.

Table 4.2. Soil properties at the site of Iksan City in the southern region of the Republic of Korea (after Lee et al. 2009)

Soil type based on USCS	Soil parameters				
	γ_d (kN/m3)	γ_t (kN/m3)	ϕ_p	ϕ_{cs}	*Dr (%)*
SC	14.5	18.1	35.48°	31.08°	55

A numerical analysis containing modelling of both piles, which have been tested at site, was performed and the load-displacement behaviour of piles obtained. A comparison was made for the load-displacement diagrams of piles obtained from field tests and numerical models, as shown in Figure 4.20.

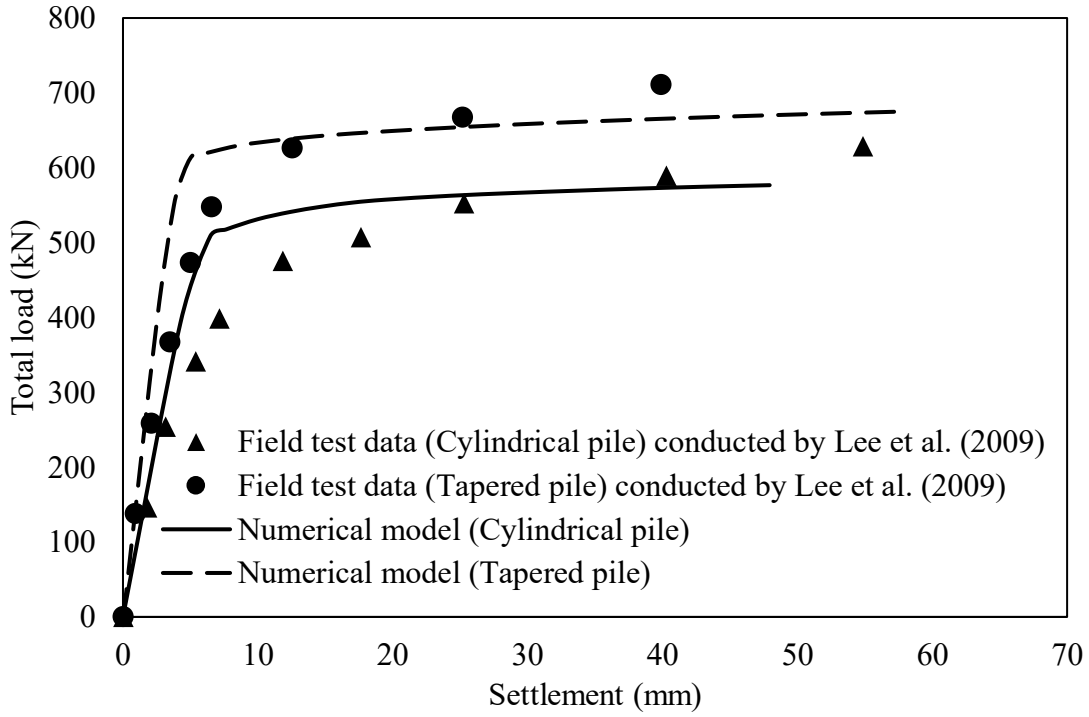

Figure 4.20. Comparison between the load-displacement diagrams obtained from numerical modelling and pile load tests conducted by Lee et al. (2009)

Figure 4.20 illustrates that the numerical model can predict accurate load-displacement behaviour for cylindrical and tapered piles. The criterion for obtaining piles' ultimate bearing capacity in this study was based on the specific pile settlement to diameter ratio ($S_r = 0.1$). Since the diameter of the cylindrical reference pile tested at the site was 400 mm, the specific settlement of 40 mm was used to acquire piles' ultimate bearing capacity.

On the other hand, using the proposed mathematical relationships (Equations 4.21, 4.24 and 4.29), taper coefficient (k_t), the bearing capacity factor (N_t), and the total load capacity of piles (Q_T) can be obtained as presented in Table 4.3. It should be noticed that since the soil at the site contains about 30% clay, the coefficient ψ of Equation 4.25 was assumed to be 100° for both piles. Table 4.3, summarizes the model parameters and bearing capacity factors obtained from the analytical approach and the total bearing capacities obtained from three different methods.

Table 4.3. Comparison of bearing capacity results obtained from various methods

Calculation method	Bearing capacity factors and model parameters					
	Cylindrical Pile: C ($\alpha = 0°$)					
	ζ	λ	β	k_t	N_t (N_{qc})	Q_T (kN)
Analytical model result	100	1.11	0.11	1.0	48.6	578
Numerical modelling result	-	-	-	-	-	585
Field test result	-	-	-	-	-	598
Calculation method	Tapered Pile:T ($\alpha = 1.2°$)					
	ζ	λ	β	k_t	N_t	Q_T (kN)
Analytical model result	100	1.11	0.11	1.76	53.4	661
Numerical modelling result	-	-	-	-	-	670
Field test result	-	-	-	-	-	708

Table 4.3 indicates that the proposed mathematical relationships and the numerical analyses can predict the bearing capacity of bored cylindrical and tapered piles with a reasonable degree of accuracy. Hence, these new relationships can be used by practicing engineers to make a quick comparison between the load capacities of these two types of piles with the same amount of material.

4.6 Summary

This study numerically proved that there is an optimum tapering angle for piles embedded in sand where the unit load capacity approaches to its maximum level.
Firstly, a governing equation to obtain the axial bearing capacity of bored tapered piles in sand was developed analytically. Then, the acquired bearing capacity equation was differentiated with respect to the tapering angle, and solved numerically using the

Cauchy algorithm for a given set of model parameters. The roots of the solved equation proved the existence of the optimum tapering angle for piles, where the maximum bearing capacity was provided. Afterwards, the calibrated aforementioned model parameters of the analytical model were obtained against the results of comprehensive numerical modelling.

An empirical equation for obtaining the optimum tapering angle for bored piles was presented, which practicing engineers can readily apply. The presented equation is a function of slenderness ratio of piles and the soil internal friction angle, and it is normalized to the maximum available tapering angle that a pile can have with the same volume of material.

Both the total bearing capacity and the optimum tapering angle equations have been validated with numerical analysis using UBC sand model in three different soil models including loose Cambria, medium Toyoura and dense Sacramento River sands. The soil parameters were obtained through a calibration exercise using the UBC sand constitutive model. An optimum tapering angle was obtained for various sand types including loose, medium, and dense sand.

The proposed analytical equation can predict the ultimate bearing capacity of a tapered pile based on the tapering angle and the diameter of the cylindrical reference pile with the same volume. While the bearing capacity of pile increases with increasing the tapering angle until reaching the optimum tapering angle, a tapered pile can provide up to 40% higher axial capacity comparing to its counterpart cylindrical pile.

As the tapering angle exceeds the optimum value, the bearing capacity of tapered piles decreases gradually. However, those piles, having larger tapering angles, can still provide higher carrying capacities compared to their counterpart cylindrical piles.

Chapter 5

Developing an Efficiency Equation for Tapered Pile Groups in Sand Using Mathematical and Numerical Analyses

5.1 Introduction

Capturing the behaviour of pile groups using numerical modelling, needs a three dimensional analysis which is a time-consuming effort. Hence, proposing an equation for predicting the bearing capacity of piles considering the important parameters such as the slenderness ratio, the pile spacing, the tapering angle, the sand internal friction angle and the number of piles, is of great significance. Although, several group efficiency equations have been proposed to date, to the best of authors' knowledge, the effect of tapering angle has not been considered in the developed equations. On the other hand, most of the investigations on tapered piles are specified for isolated single piles rather than pile groups, relating to the complication assessment of pile group behaviour. The two main problems associated with pile group design are the pile group efficiency (η) and the settlement factor (S_f), which are defined as Equations 2.19 and 2.20 in Chapter 2.

According to Equation 2.19, if the group capacity is equal to the sum of all individual pile capacities, then the group efficiency (η) will be equal to 1. The ASCE Committee

on Deep Foundations (CDF) suggests that friction piles in cohesionless soils embedded at the usual spacing of s = 2D to 3D can have a group efficiency $\eta > 1$ (ASCE 1984). The reason assumed is that in frictional soil, the pile displacement along with driving vibrations increases the soil density in a vicinity zone of the pile. This effect is more significant in driven piles. However, considering friction piles in cohesive soils, the group capacity can be obtained as the summation of the point bearing along with block shear of the group. In this condition, the group capacity rarely can be more than the summation of single piles capacities.

The presence of pile cap also plays a significant role in pile group capacity as well as the pile group efficiency. For instance, if the pile cap is laying on the ground, the pile group will settle with the soil as the piles will also settle that much. For a free standing cap, the group bearing capacity of cylindrical piles would be the sum of the individual point capacities and block perimeter shear. While, for tapered piles, an additional shaft vertical bearing component should be taken into account. Hence, for tapered pile groups, the corresponding bearing ratio will affect the group efficiency, particularly for piles having larger angles (Shafaghat & Khabbaz 2020b).

Most of the developed relationships and guidelines are regarding to straight-sided wall piles. However, the attempt of this study is to investigate the characteristics of tapered piles featuring the effect of tapering angle. For this purpose, based on the mathematical definition of group efficiency factor, a new formula for a group of tapered piles is presented. The predicted relationship can be a function of a number of important parameters, as expressed in Equation 5.1.

$$\eta = f(m, n, s, L, d, \alpha, \phi) \qquad 5.1$$

In the above equation, m is the number of piles in a row of a group, n is the number of piles in a column of a group, S is the spacing between piles, d is the average diameter of piles (equivalent to the same volume counterpart straight-sided wall pile diameter), α is the tapering angle of piles, L is the length of piles, and ϕ is the internal friction angle of the granular soil.

Afterwards, an array of numerical analyses is performed to model the single bored cylindrical and tapered piles as well as pile groups with the same volume of material. Thereafter, the load-displacement diagrams of single and group of tapered piles are obtained through numerical survey and the mathematical developed efficiency relationship is verified. The constitutive model for sand, developed by the University of British Columbia, known as UBC sand constitutive model (Beaty & Byrne 2011), is used for the numerical analysis of piles in loose Cambria sand.

5.2 Existing group efficiency equations

There are several relationships to predict the group efficiency for conventional cylindrical piles. Some relationships are established for group of piles in sand and some can predict the efficiency in clay. Besides, based on the pile cap condition of pile group, the efficiency coefficients can be divided into two categories including, pile group with a cap laying on the ground and pile group with a free-standing cap. In Chapter 2.6 of this study, an overview of some of the well-known efficiency equations for cylindrical pile foundations was presented. Most of the equations provide the efficiency of pile groups with a free-standing cap. As can be seen, the effect of tapering angle has not been taken into consideration in obtaining the pile group efficiency.

As described in Section 2.6 in Chapter 2, the most common parameters in predicting the pile group efficiency are the pile spacing, the pile diameter and the number of piles in each row and column. Even though, other factors, such as the interaction factor between the piles within a group, play a significant role in obtaining the efficiencies.

Several other equations have been proposed to predict the efficiency of pile groups considering different parameters (Randolph 1994; Rao 2010; Tuan 2016a; Zhao 1999). However, these relationships are only applicable for straight-sided wall pile groups and to the best of authors' knowledge, none of the above equations can capture the effect of all above-mentioned parameters simultaneously.

5.3 Analytical approach

The analytical solution is routed from the basic definition of efficiency coefficient, which is as Equation 2.19. In Equation 2.19, Q_s is the bearing capacity of single pile and Q_g is the bearing capacity of the group. The load Q_s is conventionally divided into three components of shaft (skin) resistance (Q_f), the base (tip) resistance (Q_b), and the vertical component of bearing along the length of tapered pile due to inclination of their body (Q_{sv}). Figure 5.1 illustrates a tapered pile group along with separated resistance forces.

$$Q_s = Q_f + Q_b + Q_{sv} \qquad 5.2$$

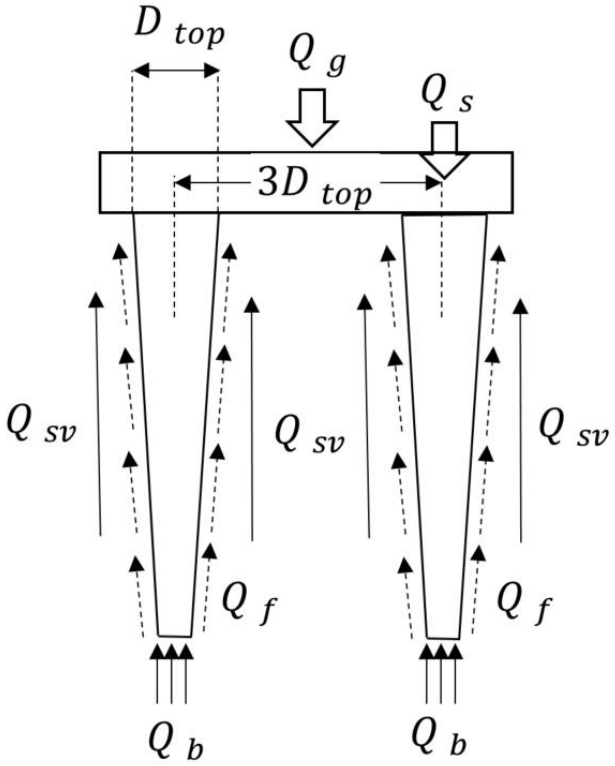

Figure 5.1. Tapered pile group and the separated resistance forces

Vesic (1967) and Chellis (1969) have suggested that for piles embedded in sand, the group effect can be taken into consideration only for the shaft bearing component. According to this assumption, the group bearing capacity can be written as:

$$Q_g = \sum Q_b + \eta_{sv} \cdot \sum Q_{sv} + \eta_s \cdot \sum Q_f \quad 5.3$$

where, the parameter η_s is the shaft load efficiency which is similar to what has been suggested by Sayed & Bakeer (1992), but with a slight modification to consider the effect of tapering angle. In addition, η_{sv} is the shaft vertical load efficiency, which is derived similar to the former load efficiency and can be written as:

$$\eta_s = \eta'_s \cdot K \quad 5.4$$

$$\eta_{sv} = \eta'_{sv} \cdot K \quad 5.5$$

where, η'_s is the geometric efficiency coefficient and *K* is the group interaction factor. Substituting Equations 5.3 to 5.5 in Equation 2.19 yields:

$$\eta_g = \frac{\eta'_s \cdot K \cdot \sum Q_f}{\sum Q_s} + \frac{\eta'_{sv} \cdot K . \sum Q_{sv}}{\sum Q_s} + \frac{\sum Q_b}{\sum Q_s} \quad 5.6$$

Vesic (1980) has recommended that for a group having m × n piles, the ratio of $\frac{\sum Q_f}{\sum Q_s}$ is equal to the ratio of $\frac{Q_f}{Q_s}$ for a single pile. Hence, by assuming that the ratio of $\frac{\sum Q_{sv}}{\sum Q_s}$ is equal to the ratio of $\frac{Q_{sv}}{Q_s}$ for a single pile in sandy soil, the efficiency equation for a pile group in sand can be written as,

$$\eta_g = 1 + (\eta'_s \cdot K - 1) \cdot \frac{Q_f}{Q_s} + (\eta'_{sv} \cdot K - 1) \cdot \frac{Q_{sv}}{Q_s} \quad 5.7$$

In addition, η'_s is defined in Equation 5.8 (Sayed & Bakeer 1992) and η'_{sv} is derived similar to the friction geometric efficiency coefficient as presented in Equation 5.9.

$$\eta'_s = \frac{P_g}{\sum P_s} \quad 5.8$$

$$\eta'_{sv} = \frac{A_p}{\sum A_b + \sum A_{sv}} \quad 5.9$$

where, P_g is the perimeter of the pile group, A_p is the area of the end surface of the block of pile group (as an equivalent large pile), $\sum P_s, \sum A_b$, and $\sum A_{sv}$ are the summations of the single piles lateral perimeter, the summation of base area of single piles, and the summation of shaft horizontal projected area corresponding to the vertical load bearing of single piles, respectively, as illustrated in Figure 5.2.

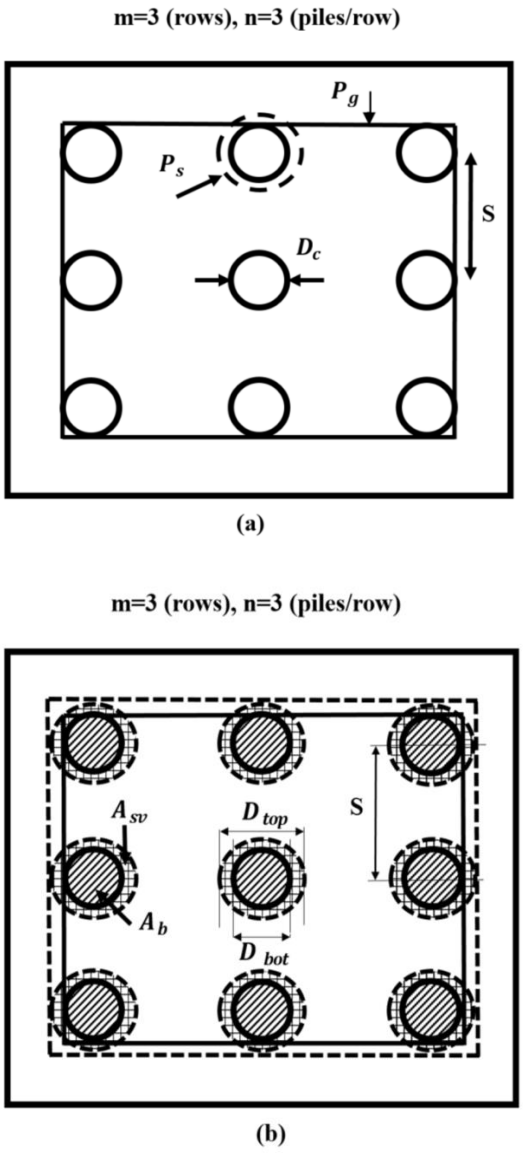

Figure 5.2. Bottom view of a typical pile group pattern and the geometry efficiency coefficients definition a) shaft geometry efficiency (η'_s) b) shaft vertical bearing geometry efficiency (η_{sv})

Accordingly, knowing that $A_{sv} + A_b = \frac{\pi}{4} D_{top}^2$ and for a circular pile group, η'_s and η'_{sv} can be defined as:

$$\eta'_s = 2 \times \left[\frac{[(m-1)\times s + D_{av}] + [(n-1)\times s + D_{av}]}{\pi \times n \times m \times D_{av} \times \cos(\alpha)}\right] \quad 5.10$$

$$\eta'_{sv} = 4 \times \left[\frac{[(m-1)\times s + D_{bot}].[(n-1)\times s + D_{bot}]}{\pi \times n \times m \times D_{top}^2}\right] \quad 5.11$$

Hence, the final mathematical model for the efficiency of bored tapered pile groups in sand can be derived by Equation 5.12.

$$\left\{\eta_g = 1 - \left(1 - 2 \times \left[\frac{[(m-1)\times s + D_{av}] + [(n-1)\times s + D_{av}]}{\pi \times n \times m \times D_{av} \times \cos(\alpha)}\right].K\right) \cdot \frac{Q_f}{Q_s} - \right.$$
$$\left. (1 - 4 \times \left[\frac{[(m-1)\times s + D_{bot}].[(n-1)\times s + D_{bot}]}{\pi \times n \times m \times D_{top}^2}\right].K) \cdot \frac{Q_{sv}}{Q_s}\right\} \quad 5.12$$

where, K can be obtained through existing data reported by Sayed & Bakeer (1992). Equation 5.12 gives the pile group efficiency by considering pile geometry parameters, including tapering angle and the sandy soil properties. It should be noted that for finding the total bearing capacity of piles using load-displacement diagrams, the load on pile heads corresponding to $0.05D_{av}$ of pile settlement (which is 75mm) is used. Moreover, for a single pile (assuming m=n=1), the geometry efficiency coefficients should be modified as the pile cross-sections were assumed to be circular, but the arrangements assumed to be square. While, for a single pile the geometry efficiency coefficients must be equal to 1. It is also worth mentioning that by increasing the spacing to large values, the group interaction factor approaches to zero. Hence, the group interaction factor has an inverse relationship with the pile spacing. Hence, the terms $\eta'_s K$ and $\eta'_{sv} K$ approach 1 for large spacing values.

5.4 Three-dimensional finite element modelling and overview of the numerical models

The numerical modelling conducted in this study includes two sets of pile group models and two sets of single pile models with different geometries, but identical volume of material. Piles were modelled using a finite element software package, PLAXIS 3D (Brinkgreve et al. 2002), and the interface elements were used for shaft and toe of piles. In this analysis, piles with circular cross-section were embedded in an elasto-plastic ground and a monotonic compressive axial load was applied on their heads. It should be noticed that piles in each group were loaded individually with the same amount of loading as single pile models. Hence the results of this study can represent a free standing cap situation, where each pile in group partakes equal amount of loading. A summary of geometrical properties of piles considered in the numerical modelling with different tapering angles and various top and bottom radii are presented in Table 5.1.

Table 5.1. Geometry of the piles used in the numerical analyses

L/D	Piles	Tapering angle (Degrees)	Top radius (mm)	Bottom radius (mm)	Length (m)	Volume ($\boldsymbol{m^3}$)
10	CL	0	750	750	15	26.5
	TL	1.4	925	559	15	26.5

The enhanced meshing system was applied surrounding each pile, where the pile and soil interact through the interface plane as shown in Figure 5.3. This refinement could improve the mesh quality and consequently contribute to more accurate results. Piles were modelled as solid elements and volumetric objects to consider the tapering effect and to capture the stress states surrounding them.

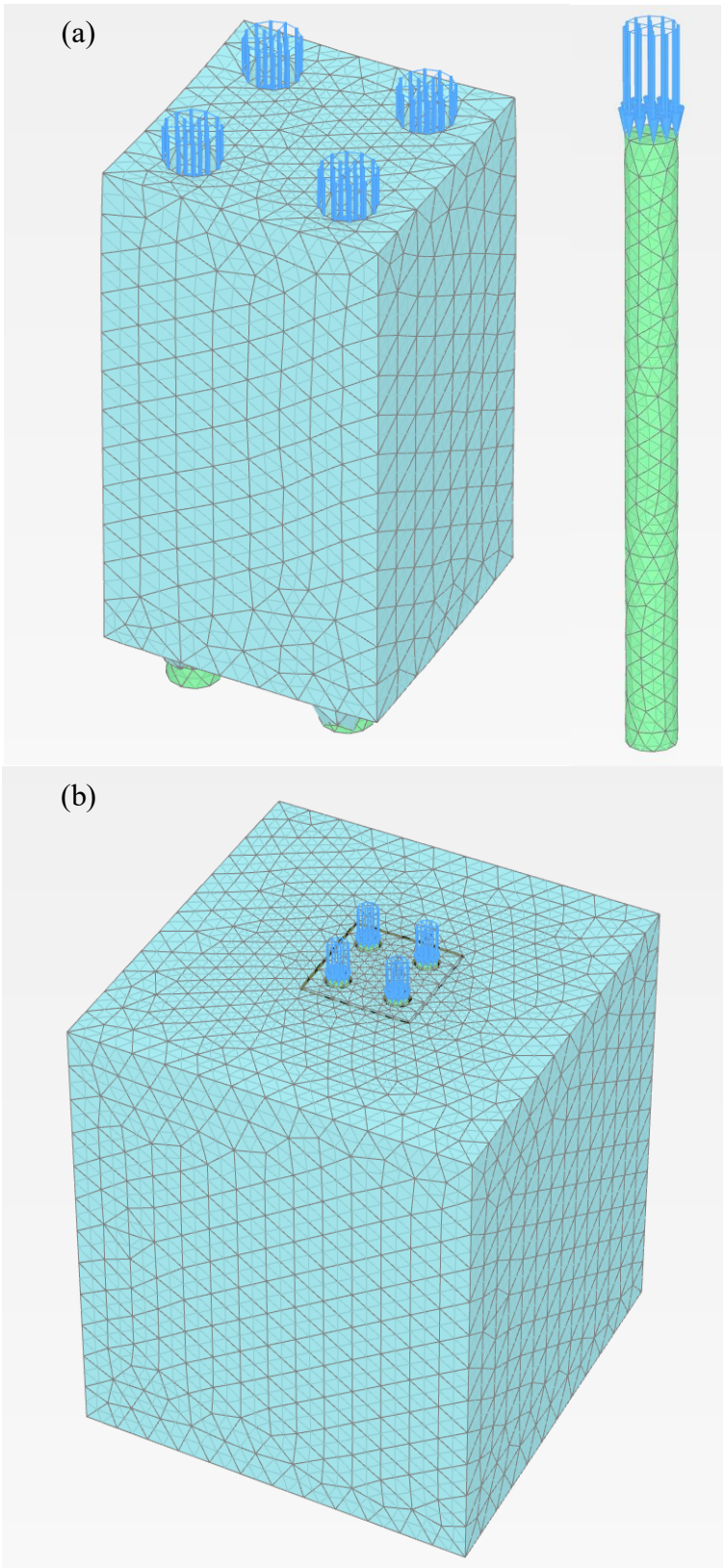

Figure 5.3. Enhanced meshed system used for piles in 3D numerical analyses, (a) Single pile and group of four piles, (b) Pile group along with the adjacent soil used in numerical analysis

The interface elements between pile and the adjacent soil were considered and the reduction factor (R_f) of 0.7 was used. This factor applies to the strength and stiffness parameters of soil as captured in Equations 3.5 and 3.6.

In the abovementioned equations, ϕ_i is the internal friction angle of the interface, ϕ_{soil} is the internal friction angle of the soil, G_i is the shear modulus of the interface, and G_{soil} is the shear modulus of the soil. Figure 5.4 illustrates the three-dimensional model of piles embedded in soil along with the interfaces surrounding the piles as well as interfaces around pile group blocks.

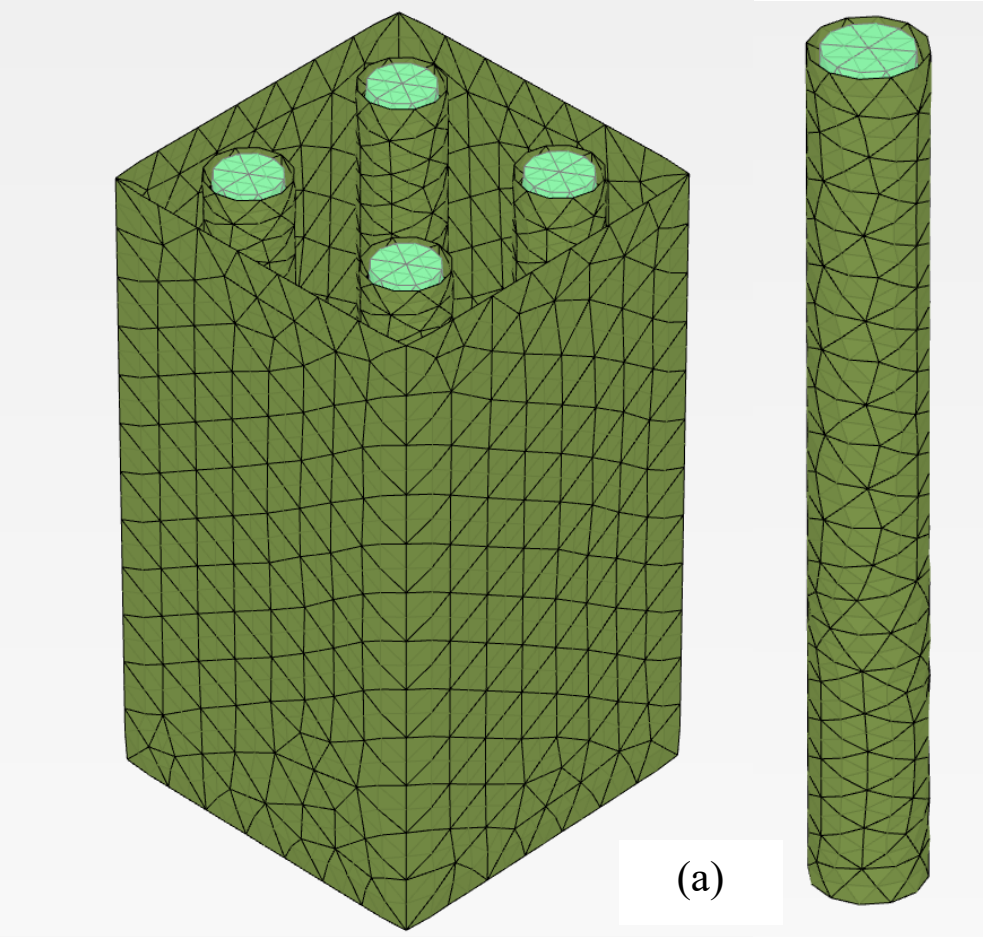

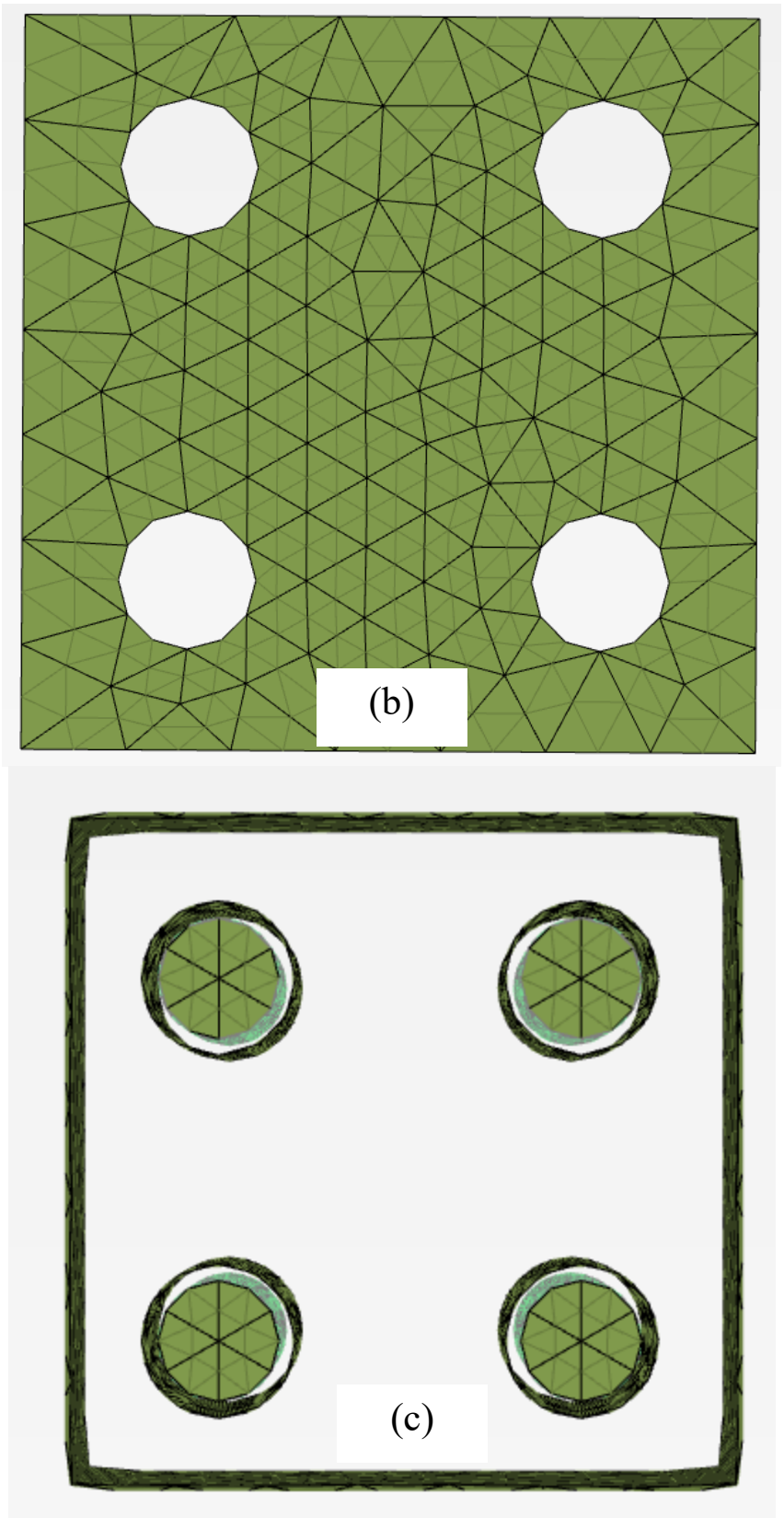

Figure 5.4. Interfaces surrounding the individual piles and at the lateral and bottom faces of pile blocks (a) Pile block along with the single pile and the interfaces (b) The interface of pile group below the pile block (bottom view) (c) Pile toe interfaces (bottom view)

5.5 Validation of the obtained efficiency equation using 3D FEM numerical analysis

The load-displacement behaviour of modelled piles are considered as reference data to calculate the bearing capacities (Q_f, Q_{sv}, Q_s) using numerical integration of vertical effective stress on the base surface area of piles (Hataf & Shafaghat 2015a, 2015b; Shafaghat & Khabbaz 2020a; Shafaghat et al. 2018). Therefore, these load-displacement diagrams for a single pile and group of piles are extracted as a result of three dimensional numerical modelling, as shown in Figure 5.5 andFigure 5.6.

Both single piles and pile groups with an arrangement of 2×2 and slenderness ratio of $\frac{L}{D_c} = 10$ (where D_c is the diameter of the reference same volume cylindrical pile) are modelled in loose Cambria sand. It can be noted that the UBC sand model is used for the numerical analysis. The pile model material parameters including the Poisson's ratio, Young's modulus, unit weight and its behavioural model are presented in Table 5.2, respectively. The spacing of $S = 3D_{top}$ is used to model the piles in groups for this study as it is perceived to be the optimum spacing of piles to have efficient interaction in group (Poulos 1979; Poulos & Davis 1980). The reference settlement of piles for interpreting different components of bearing capacity is assumed to be as $\delta_{ref} = 0.05D_{av}$. Moreover, concerning the group interaction factor (K), which is a function of pile spacing, the method of pile installation, and type of soil, its values ranging from 0 to 1 (Hanna et al. 2004; Sayed & Bakeer 1992). According to the relative density of the target sand, and based on the recommendations in the literature (Hanna et al. 2004), the group interaction factor (*K*) for a 2×2 bored pile group, embedded in loose sand, is *K*=0.5.

Table 5.2. Pile material parameters

Parameters	$\gamma(\frac{kN}{m^3})$ (Unit weight)	ν (Poisson's ratio)	E (GPa) (Elastic modulus)	Material model
Values	24	0.15	25	Linear-Elastic

Table 5.3 represents the input parameters of soil properties used in the numerical modelling based on the UBC sand model.

Table 5.3. Sandy soil properties adopted for numerical analysis based on UBC sand model (loose Cambria sand)

k_B^e	150
k_G^e	300
k_G^p	330
me	0.25
ne	0.25
np	0.25
ϕ_{cv}	31°
ϕ_p	32°
c	0
R_f	0.98
f_{dens}	0.3
$\gamma_{unsat}(\frac{kN}{m^3})$	15.3
$\gamma_{sat}(\frac{kN}{m^3})$	19.3
$(N_1)_{60}$	5

In Table 5.3, k_B^e is the elastic bulk modulus factor, k_G^e is the elastic shear modulus factor, k_G^p is the plastic shear modulus factor, *me* is the rate of stress-dependency of elastic bulk modulus, *ne* is the rate of stress-dependency of elastic shear modulus, np is the rate of stress-dependency of plastic shear modulus, ϕ_{cv} is the constant volume friction angle, ϕ_p is the peak friction angle, c is the cohesion, R_f is the failure ratio, f_{dens} is the densification factor and $(N_1)_{60}$ is the corrected SPT value.

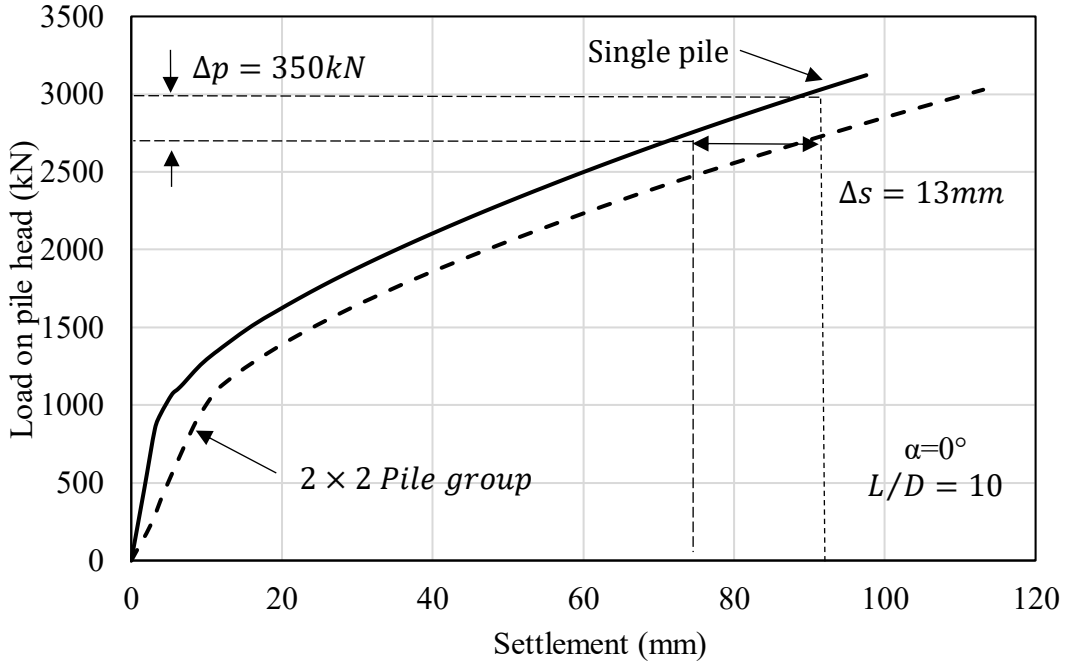

Figure 5.5. Load-displacement curves for single and group of cylindrical pile modellings, (Loose Cambria sand)

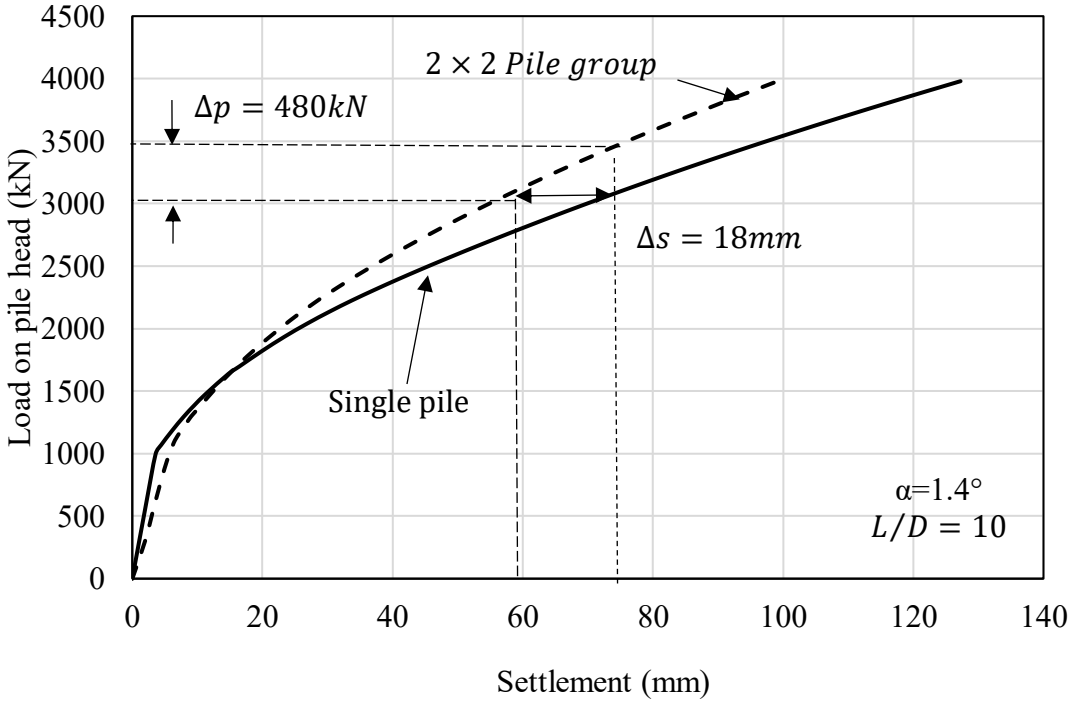

Figure 5.6. Load-displacement curves for single and group of tapered pile modellings, (Loose Cambria sand)

According to the load-displacement results of Figure 5.5 andFigure 5.6 obtained from the three-dimensional numerical modelling, and based on the numerical calculation techniques used to find the various components of resistances (Hataf & Shafaghat

2015a), the friction bearing ratio and the shaft vertical bearing ratio are obtained and presented in Table 5.4.

Table 5.4. Bearing capacity ratios of a single same volume cylindrical and tapered piles

Bearing capacity ratios	Cylindrical pile	Tapered pile with α=1.4°
Shaft bearing ratio ($\frac{Q_f}{Q_s}$)	0.23	0.27
Shaft vertical bearing ratio ($\frac{Q_{sv}}{Q_s}$)	0	0.35

According to Figure 5.5 andFigure 5.6 and using Equation 2.19 the pile group efficiencies of both 2×2 cylindrical and tapered piles are 0.90 and 1.1, respectively. On the other hand, using Equation 5.12, the pile group efficiencies are obtained 0.91 and 1.06, which shows the presented efficiency equation can simply predict the pile group efficiency while considering the tapering angle with a reasonable accuracy. Figure 5.7 andFigure 5.8 illustrate the relative shear stress state and the vertical displacement of piles at the end of the block of cylindrical and tapered groups, respectively.

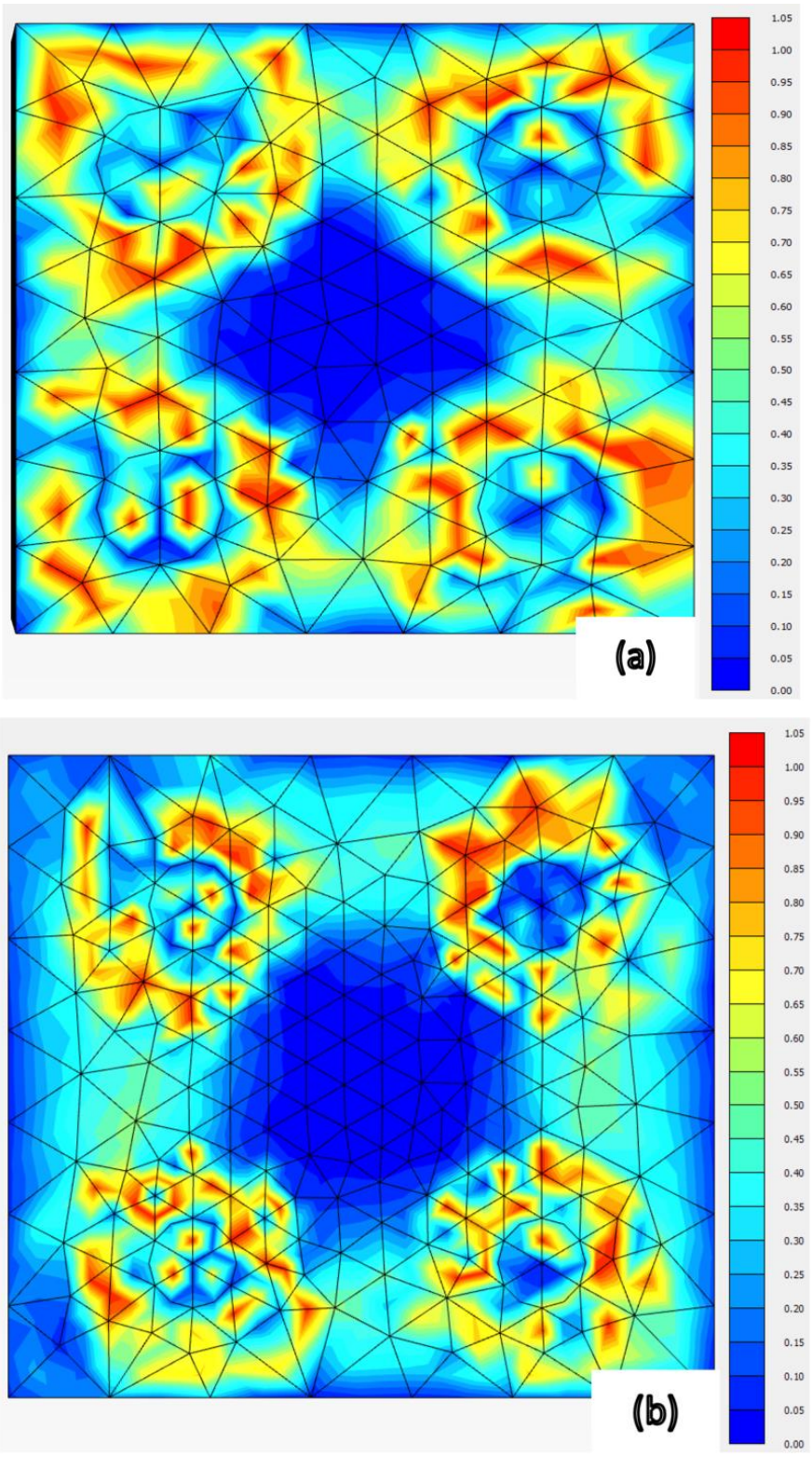

Figure 5.7. Relative shear stress state on the end surface of the block of pile groups (bottom view), (a) Cylindrical pile group, (b) Tapered pile group (α=1.4°)

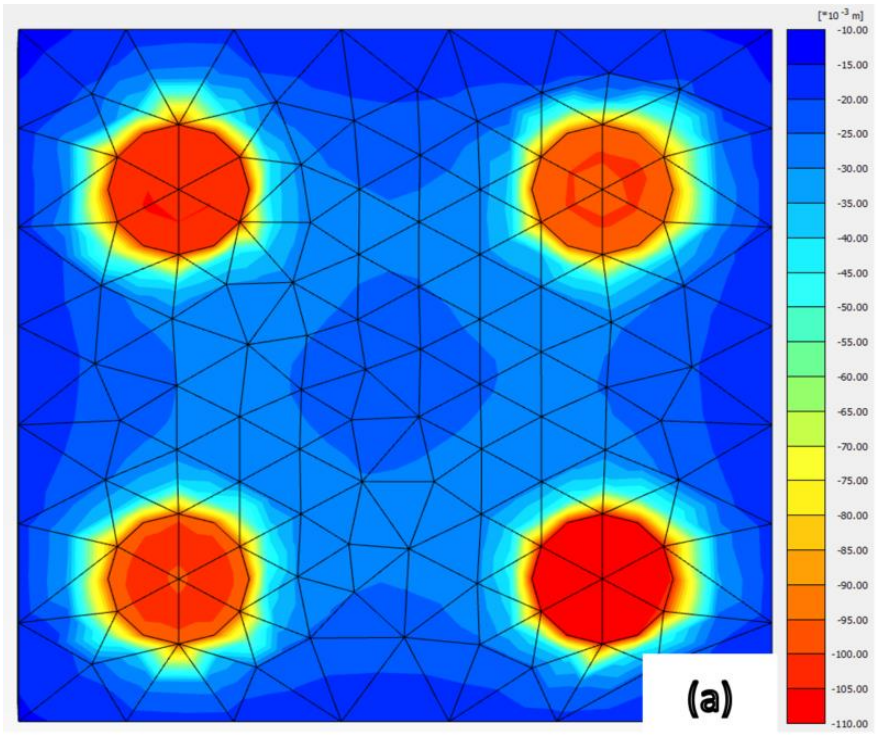

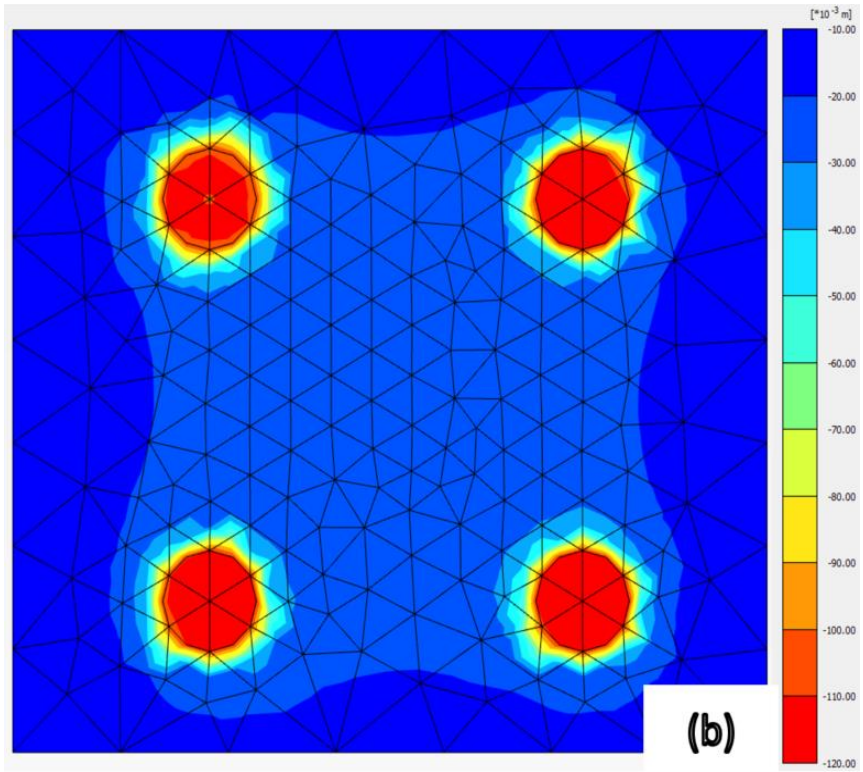

Figure 5.8. Vertical displacement state on the end surface of the block of pile groups (bottom view), (a) Cylindrical pile group, (b) Tapered pile group (α=1.4°)

Figure 5.8 illustrates that the vertical displacement of the soil at the centre part of the tapered pile group is more uniform comparing to the vertical displacement of the cylindrical pile group. This is due to the shaft inclination of tapered piles which makes the upper cross-section bigger than the toe. In other words, the tapering effect can compact the surrounding soil downward, which in turn densifies the adjacent soil while the pile experiences incremental settlement. Hence, for tapered piles embedded in sand, the lateral earth pressure coefficient will increase by each incremental settlement of pile. This will lead to increase in both the shaft friction resistance as well as the shaft vertical resistance component. Accordingly, single tapered piles provide more bearing capacity comparing to their counterpart same volume cylindrical piles, and will improve the efficiency when used in a group.

5.6 Validation of the obtained efficiency equation using field test data

In order to validate the proposed mathematical model for predicting the efficiency of bored pile groups, a set of experimental tests as well as field tests conducted by several researchers was used (Brown et al. 1988; McVay et al. 1995; Ruesta & Townsend 1997; Shibata et al. 1989). The field tests have been conducted for groups with 3x3 arrangement and various spacing to diameter ratios from 2 to 5. Table 5.5 presents the efficiency values obtained from the proposed model of this study and values obtained from other sources, including numerical, theoretical and experimental investigations.

Table 5.5. Comparison between pile group efficiencies achieved from the proposed model of this study and values obtained from other sources, including numerical, theoretical and experimental investigations

Reference	Method	S/D					
		2	3	5	6	8	10
Mathematical model of this study	Mathematical	0.81	0.84	0.86	0.91	0.96	1.0
Numerical analysis of this study	Numerical	0.85	0.95	-	-	-	-
Brown et al. (1988)	Full scale field load test	-	0.75	-	-	-	-
Sayed & Bakeer (1992)	Mathematical	0.66	0.81	0.89	0.96	1.0	1.0

McVay et al. (1995)	Experimental (Centrifuge)	-	0.73	0.92	-	-	-
Ruesta & Townsend (1997)	Full scale field load test	-	0.80	-	-	-	-
Shibata et al. (1989)	Experimental (Centrifuge)	0.58	-	1.0	-	-	-
Tuan (2016b)	Mathematical	0.65	0.82	0.87	1.0	1.0	1.0
Converse-Labarre (Bolin (1941))	Mathematical	0.60	0.73	0.83	0.86	0.89	0.92

5.7 Summary

This study presents a new simple equation for prediction of pile group efficiency considering the effect of tapering angle in cohesionless soil under vertical loading. Firstly, a simple analytical relationship based on the mathematical definition of the pile group efficiency is developed. However, the effect of tapering angle is captured by defining a new geometry efficiency coefficient associated with the shaft vertical bearing component of tapered piles. Thereafter, a mathematical equation is developed by taking into account the shaft vertical bearing ratio and the new geometry efficiency coefficient. On the other hand, a numerical analysis is performed for modelling a single bored cylindrical pile and a tapered pile with the same volume as well as bored tapered pile groups to validate the proposed mathematical equation. The UBC sand constitutive model is adopted for the modelling of piles in loose Cambria sand. Subsequently, the load-displacement diagrams of single and group of piles are obtained. Then, the bearing capacities of cylindrical and tapered bored piles both as single and group are computed and compared, using a specific settlement criterion. Besides, the friction resistance ratio and the shaft vertical bearing ratio are separated, applying numerical methods. Having calculated the ratios of various components of bearing capacity, pile group efficiencies can be obtained from both numerical and mathematical models. The results show that the proposed equation can predict the pile group efficiency incorporating the tapering angle as well as other influencing parameters as a simple and novel relationship.

Chapter 6

Numerical Evaluation of Bearing Capacity of Step-tapered Piles Using p-y Curves Analysis

6.1 Introduction

Step-tapered piles can provide bearing capacity through their shaft, base, and the end surface of stepped section. This specific kind of deep foundation has a larger upper diameter (for an assigned pile length) and smaller diameters in the lower parts. Step-tapered piles have a more efficient distribution of material through their body. As the upper sections endure higher forces compared to the lower parts, accumulation of material distribution in the upper part is more efficient to resist against greater forces.

Most of the relationships, developed for predicting the behaviour of piles, are associated with the conventional cylindrical piles or prismatic ones, while for step-tapered piles, there are limited analytical solutions. By and large, in the last three decades, the growing tendency to investigate the behaviour of tapered and step-tapered piles has made it inevitable to conduct more research in this area. Figure 1 demonstrates some different bored cast piles having various shapes (Bowles 1996).

Referring to Figure 1.1 (h), a step-tapered pile is demonstrated schematically. This study aims to investigate the behaviour of these piles installed in sand. The load-displacement diagram of each model is obtained separately, and a detailed comparison is made to quantify the behaviour of piles with different shapes, but having the same volume. By altering the stepped length of the pile, the stress contours developed around the shaft will change due to changes in the stress level and the lateral earth pressures.

6.2 Modelling in PLAXIS 2D

In this study, the width of the cluster is considered to be at least ten times greater than the pile diameter, equal to 6m, and the depth of the cluster is considered to be at least three times greater than the pile length, equal to 30m. After creating a soil cluster, the state of underground water level is determined and also some properties of the soil are attributed to this cluster. The level of underground water is placed at a depth of 20m from the ground. The meshing of the entire soil cluster and pile volume is performed using the properties given in Table 6.1.

Table 6.1. Meshing properties used in modelling

Elements type	15-node
Number of soil elements	1381
Number of nodes	11332
The average of elements size (m)	0.57

The meshing of the model is refined at the pile-soil interface. Since piles are considered bored cast in situ, the analysis is performed in three stages; the first stage is the initial condition, which resembles the soil without any structural element in it, the second and the third stages include placing of the pile in the soil and loading on the pile head, respectively. For loading on piles, an estimated load of almost twice the capacity of a pile bearing capacity is used; hence, the obtained load-settlement diagrams will advance enough to apply different methods for bearing capacity calculations.

6.3 Calculation of bearing capacity of piles

In order to obtain the bearing capacity of each pile, two loading series are required to be applied. Each pile is initially subjected to a vertical loading that is approximately twice the estimated capacity through analytical solutions. By the completion of the analysis, the load-settlement diagram of the model is obtained. Then, by employing a MATLAB code, written by the authors, and using the double tangential method, the bearing capacity of each pile is calculated. Thereafter, the pertained pile is analysed under the obtained load capacity once again, so that the actual stress distribution proportional to the bearing capacity of each model at the end of the pile or around the pile walls can be observed. Likewise, in order to obtain end the bearing capacity of each pile, the effective stress distribution perpendicular to the end surface elements are acquired and by the use of appropriate mathematical methods the amount of end bearing capacity of the pile is estimated. The frictional resistance of piles can also be calculated by subtracting the two last values from the total bearing capacity. However, that end bearing capacity due to the stepping of piles should be calculated similarity according to the number of steps. According to Figure 6.1 and applying Equations 6.1 to 6.5), the value of end bearing capacity of step-tapered piles can be calculated.

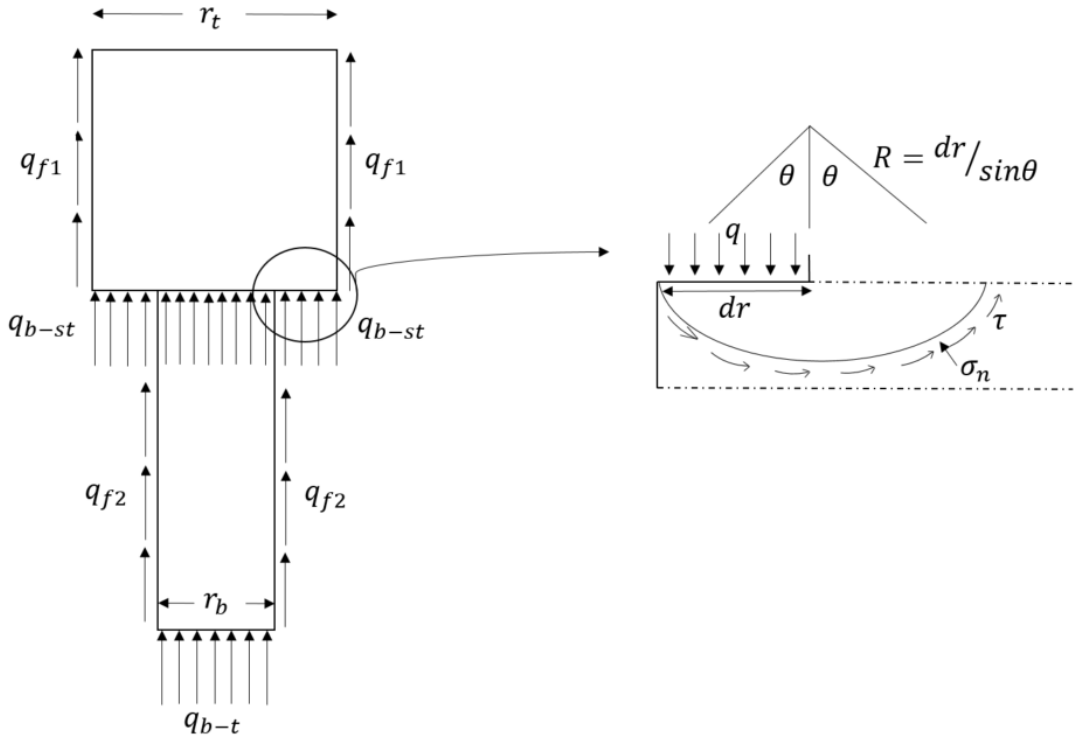

Figure 6.1. The schematic shape of a step-tapered pile and the failure zone beneath the ledge

The area of the end surface of the pile stepped section is calculated by:

$$A_{st} = \pi r_t^2 - \pi {r_b}^2 \qquad 6.1$$

where, r_t and r_b are the radii of upper and lower parts of the pile, respectively.
The area of the pile end surface is:

$$A_b = \pi r_b^2 \qquad 6.2$$

The end bearing capacity due to the stepped section is obtained using:

$$q_{b-st} = q_{st}.(\pi r_t^2 - \pi {r_b}^2) \qquad 6.3$$

where q_{b-st} is the end bearing of stepped section and q_{st} is the effective normal stress on the stepped section. The end bearing capacity of the pile at its toe is:

$$q_{b-t} = q_b.(\pi r_b^2) \quad 6.4$$

where, q_{b-t} is the end bearing of the pile toe and q_b is the effective normal stress on the pile toe. Hence, the total end bearing capacity is obtained by:

$$q_V = q_{b-st} + q_{b-t} \quad 6.5$$

6.4 Model properties selection

In this study, three series of piles are analysed separately. Each series consists of five pile models with different geometries. Within each series, all variables of sand are constant, and each five series of piles are analysed under the same loading condition. The first series is examined in loose sand with a friction angle of $\phi = 33°$, a dilation angle of $\psi = 3°$, elastic modulus of 30MPa and a lateral pressure coefficient of $K_0 = 0.45$. The key properties of 3 series of soils, implemented in the numerical analysis, are summarised in Table 6.2.

Table 6.2. Different considered conditions for modelling in sand

Set 1 (loose sand)	Set 2 (medium sand)	Set 3 (dense sand)
ϕ=33°	ϕ=37°	ϕ=41°
E=30MPa	E=45MPa	E=60MPa
ψ=3°	ψ=7°	ψ=11°
K=0.45	K=0.40	K=0.33

Three series of pile models in sand with different ϕ, ψ, elastic modulus and different at rest lateral earth pressure coefficients are analysed and compared. Then comparison is made for models within a series and also for series with each other. To illustrate the point, consider the first series of piles, which consisted of five piles, including a cylindrical pile and four step-tapered piles that can be compared to each other. Pile models are selected and made in a way to be practically applicable in real scale. Stepped models with a cylindrical reference model are possible to be made in two ways. The first method is to maintain the upper cross-section of pile constant and

reduce the lower cross-section of the pile. The volume of step-tapered piles constructed with this method in comparison with the cylindrical reference pile is reduced. Therefore, this method is out of the scope of this research. The second method is to consider a cylindrical reference pile and change the upper and lower section of pile simultaneously. Hence, the smaller lower cross-section and the larger upper cross-section of pile are made and by a change in the length of the upper part of the pile, different models of piles having the same volume are made. Since the purpose is to make a comparison of load-displacement diagrams of step-tapered piles with their counterpart cylindrical ones having the same volume, the research is focused on the second method. The length of the cylindrical reference model is considered 10m, and its diameter is selected 0.6 m. Hence, by changing the length and the diameter of the upper part of the pile, different pile models are created. The properties of different step-tapered models are presented in Table 6.3.

Table 6.3. Properties of step-tapered piles having the same volume as cylindrical reference piles

Pile	$L' = {h_i}/{h} * 100$	r_t	r_b	L_t	L_b	h (m)	V (m^3)
C	100	0.3	0.3	10	-	10	2.8
ST1	20	0.45	0.25	2	8	10	2.8
ST2	30	0.4	0.25	3	7	10	2.8
ST3	40	0.36	0.25	4	6	10	2.8
ST4	50	0.34	0.25	5	5	10	2.8

In Table 6.3, h_i is the length of the upper part of the step-tapered pile, h is the total length of the pile and h_i/h *100 is the ratio of the length of the upper part to the total length of the pile, or in other words it is the percentage of the total length of the pile with a greater diameter. L_t and L_b are the height of the upper and lower sections of the stepped section, r_t and r_b are the radii of the upper and lower parts of the pile respectively and V is the total volume of the pile. In this study in order to make stepped models of the same volume, the diameter of the lower part of the pile for all models is

considered constant and equal to 0.5m and the diameter of the upper part of the pile changes. Therefore, there can be different pile models as shown in Figure 6.2.

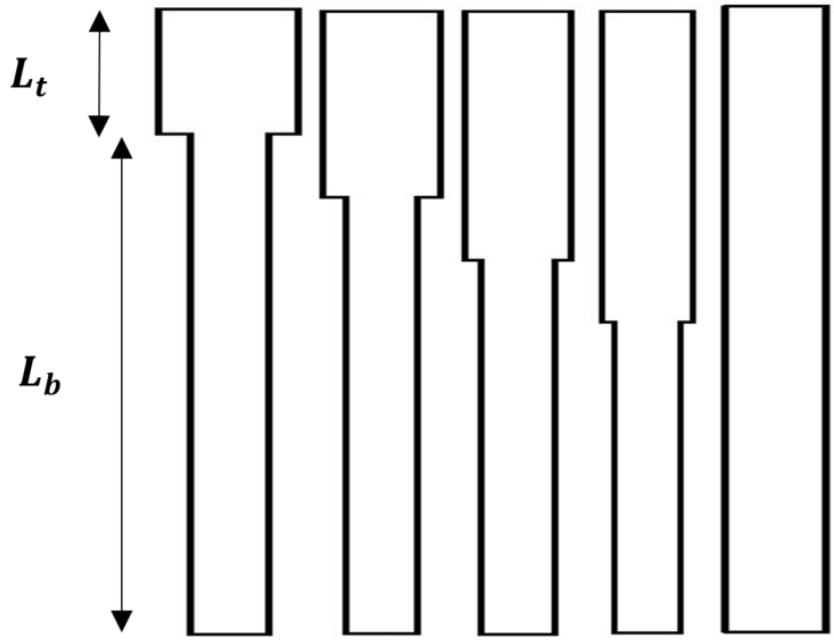

Figure 6.2. The schematic shape of step-tapered along with their cylindrical reference pile

Pile models of the study are made of concrete material and a linear elastic model has been designated for piles. The assigned properties of concrete, used in simulations, are given in Table 6.4.

Table 6.4. Properties of used concrete in modelling

Material	Concrete
Material Model	Linear Elastic
Drainage Type	Non-Porous
$\gamma(\frac{kN}{m^3})$	27
$E(\frac{kN}{m^2})$	31×10^6
ν	0.15

Since soil-facing mechanical interactions play a significant role in obtaining the pile bearing capacity, numerical analysis of pile foundations entails the use of interface elements between different component materials to analyse the soil-structure

interactions and to observe the shear transfer and normal stresses through the discontinuities. When adopting finite element analysis using PLAXIS, soil-structure interactions can be simulated using “zero-thickness” interface elements between the two different components of soil and the structure. The elements of the interface use a strength reduction factor which directly affects the soil strength parameters in the interface zone. In order to consider the interaction effect between the soil and concrete interface, the strength value in this study is considered as $R_{inter} = 0.7$ as suggested by Brinkgreve et al. (2002). Figure 6.3 illustrates the step-tapered pile (ST3) model embedded in sand along with the point load on pile head and the pile-soil interface.

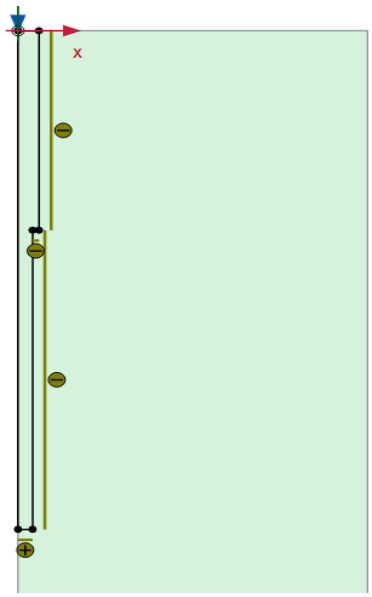

Figure 6.3. Step-tapered pile model in Plaxis 2D along with the pile-soil interface

6.5 The properties of used soil

Soil selection for the purpose of modelling has been made so that the results can be verified with a practical case. For this purpose, the results of three common types of sandy soil (loose, medium, and dense) were evaluated and compared. In sandy soil, more focus is on the internal friction angle, dilation angle and the lateral pressure coefficient of the soil. The soil properties are selected and shown in Table 6.5.

Table 6.5. Properties of used sand in modelling

Material model	γ $(\frac{kN}{m^3})$	γ_{sat} $(\frac{kN}{m^3})$	E (MPa)	ϕ' (degree)	ψ	$K_\circ$	$\boldsymbol{\upsilon}$	C′ (kPa)	R_{INTER}
Hardening soil (Drained)	15	18	30	33°	3°	0.45	0.2	0	0.7
	17	19	45	37°	7°	0.4	0.2	0	0.7
	18	20	60	41°	11°	0.33	0.2	0	0.7

As mentioned, for the purpose of sensitivity analysis, the internal friction angle (ϕ), the dilation angle (ψ), and the lateral pressure coefficient (K) are considered as three variables.

6.6 Results and discussion

The load-displacement diagrams of models are obtained and finally to determine the effectiveness of step-tapered piles a comparison is made.

6.6.1 Results of bearing capacity and settlement

After conducting several numerical analyses, the p-y curve of each straight-sided wall pile and step-tapered pile obtained. Figure 6.4 illustrates the load-settlement curves of piles in sand with an internal friction angle of 33º.

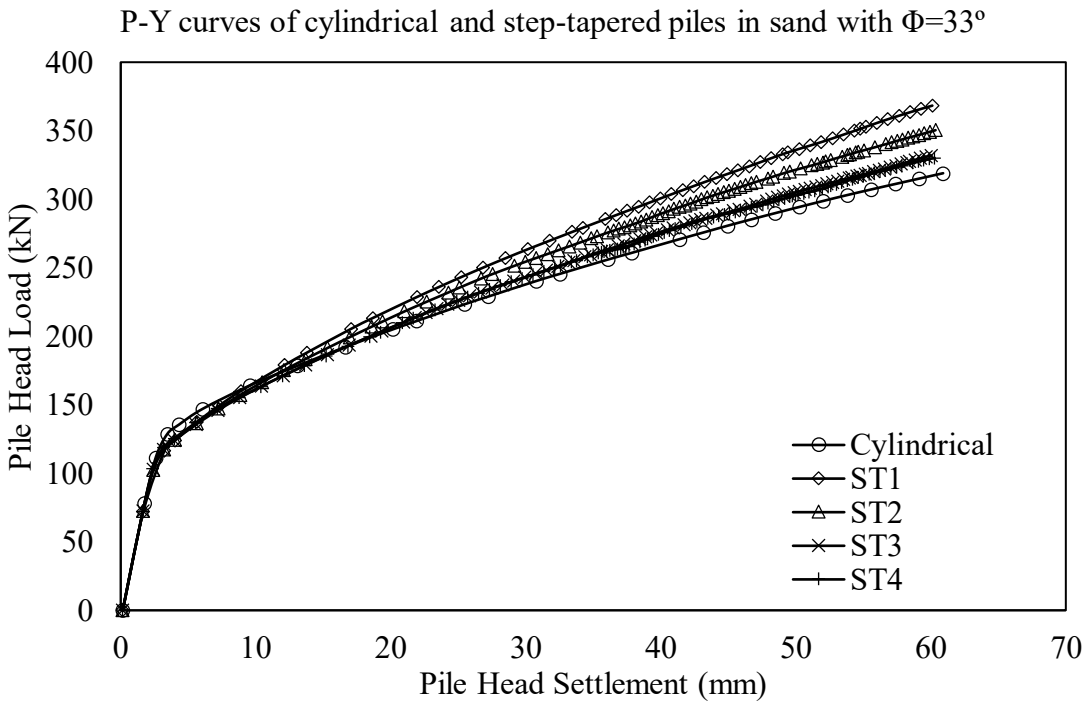

Figure 6.4. The P-Y curves of cylindrical reference pile and step-tapered piles in sand with Φ=33º

End bearing capacity of each pile is assessed using numerical integration of effective normal stress on the pile toe and stepped toe as well. Then frictional resistance of piles is calculated by subtracting the end bearing component from total resistance of pile. It should be noted that the bearing capacity of step-tapered piles is the sum of the three values: 1- The friction values of the body; 2-End bearing of the pile toe; 3-End bearing of the stepped part of the pile.

6.6.2 Stress states and plastic points around piles

According to Figure 6.5 and Figure 6.6, for cylindrical piles under axial load, the stress direction and plastic points are beneath the pile toe. A straight-sided wall pile has a larger toe cross-sectional area than that of its counterpart same volume step-tapered pile. Hence, the end bearing capacity provided by cylindrical piles is only at the base and is more than that of step-tapered piles. However, for step-tapered piles, the end resistances is achieved by mobilising the soil beneath the toe and the stepped part as well. Indeed, due to the soil densification beneath the stepped part, the shaft resistance boosts. As can be seen in Figure 6.6, the soil beneath the stepped part densifies the soil adjacent to the pile. Therefore, the lateral earth pressure coefficient of the soil

increases, and consequently, the effective lateral pressure and shaft resistance of pile are boosted.

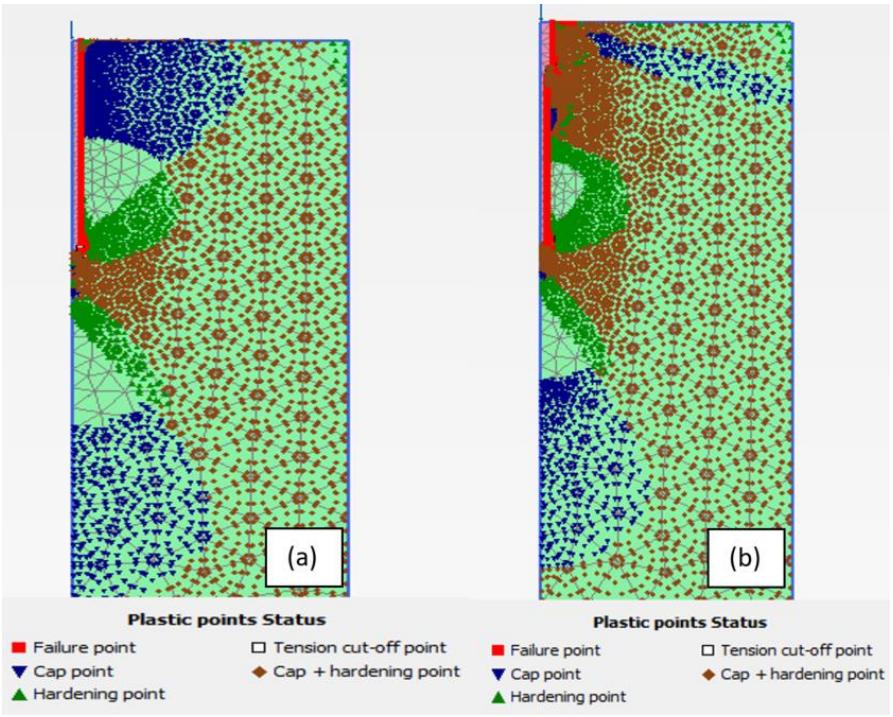

Figure 6.5. Distribution of plastic points around the piles (a) Cylindrical pile, (b) Step-tapered pile ST1

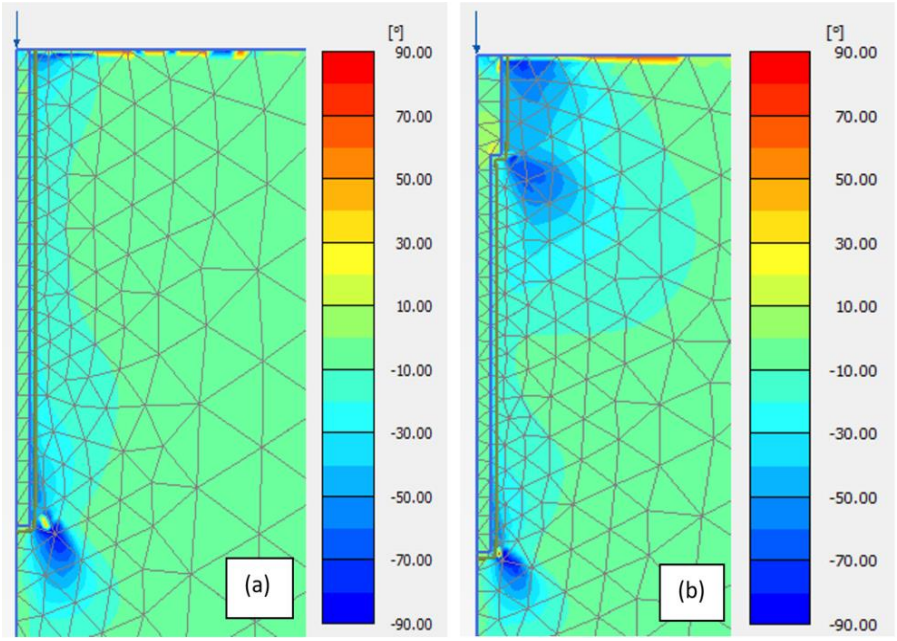

Figure 6.6. Principal stress directions around (a) Cylindrical pile (b) Step-tapered pile ST1

As Figure 6.5 and Figure 6.6 suggest, the stepped part of the step-tapered piles can provide the shaft with higher resistances. The distribution of plastic points illustrates that cylindrical piles are not using all the potential shaft capacity as a larger area around the shaft is still in the elastic zone. Hence, existing a step on the pile body can increase the pile resistance by providing more capacity through more hardening and cap points. Table 6.6 to 6.8, illustrate some differences between the bearing capacity of step-tapered piles and their counterpart cylindrical piles with the same volume for three different series of models. Since the ledge section of the ST1 pile has a longer shaft beneath (comparing to the rest of step-tapered piles), the densification of the soil in the vicinity of pile allow pile to provide a higher shaft friction. In other words, the ledge section in the ST1 applies an additional confined stress to a longer depth of the soil elements adjacent to the pile, while for ST4 this soil mobilisation applies to a less depth.

Table 6.6. Comparison between the bearing capacities of same volume piles in loose sand (Set 1)

Piles	End bearing capacity (kN)	Friction bearing capacity (kN)	Total bearing capacity (kN)
C	170	54	224
ST1	192	69	261
ST2	181	57	238
ST3	176	56	232
ST4	174	55	229

Table 6.7. Comparison between the bearing capacities of same volume piles in medium sand (Set 2)

Piles	End bearing capacity (kN)	Friction bearing capacity (kN)	Total bearing capacity (kN)
C	457	152	609
ST1	500	203	703
ST2	520	173	693
ST3	495	165	660
ST4	465	155	620

Table 6.8. Comparison between the bearing capacities of same volume piles in dense sand (Set 3)

Piles	End bearing capacity (kN)	Friction bearing capacity (kN)	Total bearing capacity (kN)
C	716	306	1022
ST1	803	373	1176
ST2	769	329	1098
ST3	740	317	1057
ST4	731	313	1044

6.6.3 The state of stress on the end surface of the pile (base)

The state of shear stress on the pile shaft is indicated in Figure 6.7 for two cylindrical and step-tapered (ST4) piles. According to Figure 6.7, it can be perceived that for cylindrical piles, the shear stress state is relatively high at the pile toe, while for step-tapered piles the shear stress state is higher at both the stepped part and pile toe. As can be seen, providing higher shear stresses beneath the stepped part can increase the shaft capacity of the pile. Hence, this proves that step-tapered piles have the potential to be used in granular soil or even layered soil.

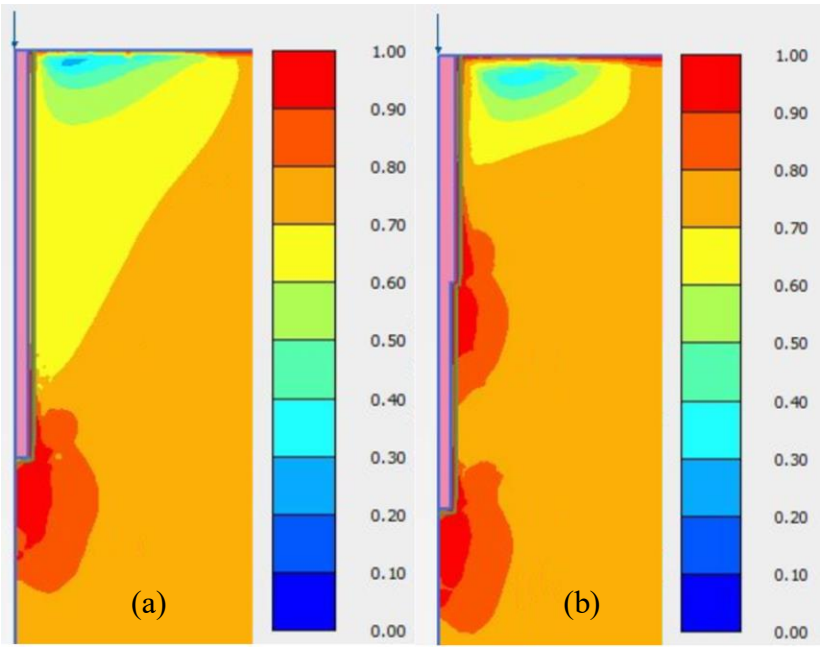

Figure 6.7. Relative shear stress distribution on the pile shaft
a) Cylindrical pile b) Step-tapered pile

6.7 Summary

Step-tapered piles are those with a larger top diameter, and a smaller diameter at lower sections as the body gets slender stepwise from top to toe in one or some steps. This study aimed to investigate the behaviour of step-tapered piles having only one step under axial loading condition. Three series of piles embedded in sand were examined numerically using the three-dimensional finite element method. Each set consists of five piles, including one reference straight sided wall pile and four step-tapered piles having the same volume. Different internal friction angles of 33°, 37°, 41° (to represent loose, medium and dense sands, respectively) and corresponding elastic modulus and lateral earth pressure coefficients were considered to observe their effect on the bearing capacity and settlement of piles. The load-displacement diagram of each pile was obtained, and accordingly, the frictional and end bearing resistances were calculated using conventional methods. A code was developed using MATLAB software to acquire the numerical data and carry out the calculations. Moreover, the normal and shear stress states, plastic points, and deformations around the step and toe of piles were computed and compared. According to the results, the advantages of step-tapered piles over their counterpart cylindrical ones in terms of bearing capacity and settlement were discussed. Finally, the optimum stepped length of the pile was determined.

Chapter 7

Conclusions and Ideas for Future Research on Tapered Piles

7.1 Summary

The main aim of this study has been establishing a relationship for estimating the optimum tapering angle of bored tapered piles associated with sand properties (varying with the relative density) and the pile geometry. The optimum tapering angle is associated to the maximum axial resistance of piles, while keeping the volume of material in the tapered pile the same as their counterpart cylindrical one. Analytical formulations were derived to obtain the axial resistance of bored tapered piles embedded in sand. The developed governing equations can estimate the shaft vertical bearing component of the tapered pile, which is related only to tapered piles and varies nonlinearly with the tapering angle. After differentiating the acquired bearing capacity relationship with respect to the tapering angle, the optimum tapering angle for that specific condition (specific sand type and pile geometry including the slenderness ratio) can be achieved.

The finite element method was used to perform the numerical modelling and to calibrate the model parameters of the derived analytical equation, considering the soil nonlinear behaviour and the pile-soil interaction. UBC sand behavioural model was adopted to simulate the soil behaviour adjacent to the tapered pile and the model parameters were calibrated against laboratory test results for sandy soils with various relative densities. Thereafter, a numerical approach was adopted to acquire the results. Consequently, the load-displacement curves of the tapered piles were obtained through numerical calculations, and the optimum tapering angle, resulting in the maximum axial capacity was attained.

Additionally, a simple equation to obtain the group efficiency of bored piles incorporating the tapering angle was developed. A new geometry efficiency coefficient was developed for the shaft vertical bearing component of tapered piles. This new factor has a significant effect on calculating the pile group efficiency as this bearing component increases by increasing the tapering angle. The proposed equations can be employed by practicing engineers to predict the behaviour of cylindrical and tapered pile groups embedded in sand in a simple and time saving manner.

Moreover, the bearing capacity of step-tapered piles under axial load were analysed and compared with their counterpart same volume straight piles. The behaviour of step-tapered piles under axial loading showed that they have the potential to provide more bearing capacity in some conditions (depending on soil type and stepped length). Hence, they might also be an efficient type of deep foundation in layered soil (which requires more research in the area) where the stepped section can be design to be located on top of each layer to increase the vertical effective stress adjacent to the pile. Where the pile body faces a cohesive soil, the stepped section can increase the end resistance and where the body interacts with a non-cohesive soil, the shaft resistance can provide capacity.

7.2 Concluding remarks

It was concluded that the optimum tapering angle is a function of soil properties and the geometry of piles, particularly the soil relative density and the pile slenderness ratio. From loose to dense sand, the optimum tapering angle increases for piles, having the same *L/D* ratio. However, this increase is small, particularly for more slender piles with *L/D*>20. On the other hand, considering one type of sand, the optimum tapering angle significantly decreases as *L/D* ratio increases, where it tends to reach approximately a constant value, when the value of *L/D* is greater than or equal to 40. Accordingly, for a pile used in this study with *L/D* = 10, the optimum tapering angle decreased from 1.9° (corresponding to dense sand) to 1.4° (corresponding loose sand), while this decrease as a result of changes in *L/D* was

from 1.4° (corresponding to *L/D=10*) to 0.4° (corresponding to *L/D=40*) for piles embedded in loose sand.

On the other hand, according to the efficiency values for a 2×2 pile group, it is obvious that the tapering angle can significantly affect the bearing capacity of piles when arranged in a group. If the tapering angle increases from 0° to 1.4°, the efficiency will enhance more than 15%. The load-displacement diagrams of single piles in the elastic zone represent a more stiff behaviour than piles in a group (for settlements less than $0.01D_{av}$). However, for a group of tapered piles and for settlements more than $0.01D_{av}$, the load-displacement diagram locates above the load-settlement diagram of a single pile, which in turn can contribute to higher efficiency values.

Moreover, by increasing the tapering angle, the friction bearing and the shaft vertical bearing ratios increase. This increase is mainly due to the decrease in the end surface area of the piles and the increase of shaft horizontal projected area. Accordingly, there should be an increase in the group interaction factor by increasing the tapering angle. Field test data is required to investigate this finding more precisely.

Furthermore, step-tapered piles provide more end bearing capacity through the base and stepped section, thus these piles can be an alternative to conventional straight-sided wall piles. The maximum bearing capacity was provided from the stepped pile which had the shortest step (ST1) with the bearing capacity ratio of around 1.15 with respect to its counterpart same volume cylindrical pile.

For step-tapered piles placed in sand, due to the soil densification and compaction beneath the stepped section lateral earth pressure coefficient of the soil increases and consequently the shaft resistance and finally total bearing capacity increase.

7.3 New directions and ideas for future research on tapered pile foundations

Based on the detailed review of the efforts conducted to shed light on the behaviour of tapered and step-tapered piles, the following directions and ideas for future research on tapered piles are presented:

Firstly, it is clear that the majority, if not all of the studies surveyed in this review, were carried out on small scale model tests and do not represent prototype conditions. Hence, the real data gap in this regard is the lack of field data from instrumented prototype tapered piles.

According to the literature, to develop proper input parameters for analytical models of tapered piles, pressure-meter tests (PMT) can be useful, as there are strong theoretical relationships between them. To minimize the costs, it is not necessary to make the whole length of a pile to be tapered. Since in some situations, it might be efficient to optimize the pile tapering length for design purposes and a specific project application.

There is an optimum tapering angle for tapered piles, which can provide higher values of capacity and less settlements (as proved in this study). This angle can be a function of internal friction angle of soil, lateral earth pressure coefficient, dilation angle of soil, the ratio of length to diameter of pile, and pile-soil interface material. So far, limited investigations have been conducted to obtain and clarify this angle, and if not all, most of the researchers concluded that by increasing tapering angle the bearing capacity increases, which may not be accurate. There is a gap area to investigate this optimum tapering angle experimentally by considering other important factors such as type of soil (cohesive soils) and soil elastic modulus. Besides, the cross-section geometry of tapered and step-tapered piles can be considered circular, triangular, hexagonal, etc.

The effect of tapering angle in a group of piles needs to be investigated through experimental investigation methods. Particularly, when this tapering angle can

directly influence the stress zone around the pile, which in turn can significantly affect the interaction factor of the group. There are several relationships to predict the group efficiency for conventional cylindrical piles as discussed in this study. Some of the relationships concerning group of piles in sand with a free-standing cap or laying cap have been investigated (Chellis 1969; Kishida 1965; Poulos & Davis 1980; Vesic 1967). Although a large number of empirical and analytical equations have been developed to predict the efficiency of cylindrical pile groups, the effect of the tapering angle has not been taken into consideration. To investigate the impact of tapering angle on pile group efficiency and pile-soil-pile interaction factor, experimental, analytical and numerical analysis based on the finite element method using available software packages is recommended (Brinkgreve et al. 2002).

Although there are a few generic methodologies for calculating the bearing capacity of bored and driven tapered piles in cohesionless soil, analytical relations that have been developed to predict the bearing capacity and settlement of tapered piles are complex or impractical. In addition, for the implementation of the equation developed by Kodikara & Moore (1993), software needs to be developed and to be commercially available. Hence, investigating the behaviour of driven tapered piles having various type of materials through experiments and numerical modellings is required. For step-tapered piles, a practical relationship needs to be presented as well to predict the settlement and bearing capacity of the piles.

Most of the equations presented are associated with the application of tapered piles in coarse-grained soils. However, in cohesive frictional soils and under high confining pressures, the vertical component of force along the pile length can increase the compression capacity significantly.

The effect of time on the bearing capacity of tapered piles should be taken into consideration for tension and compression loadings, particularly in the emerging analytical methods. Since by each incremental settlement of tapered piles, the adjacent soil will be compacted and accordingly, the lateral earth pressure and finally shaft resistance will increase. Then, the analytical model might precisely be verified with the actual load-displacement measurements.

As an assessment of the present and because of the proceeding demonstrations and discussion, it seems that taper coefficient needs to be calculated using some field test results. It is found that the taper coefficient, presented in Canadian Foundation Engineering Committee (1978), needs to be modified and classified based on the pile installation method. Since the fact that whether the pile is installed using driving method or as bored cast-in-place will have a significant effect on shaft capacity of pile.

Due to several important signs of progress in recent years, the technology of tapered piles has the potential to be recognized worldwide. Moreover, the application of tapered pile groups can be investigated for inshore and offshore structures facing massive lateral forces. Finally, tapered pile groups having a cap laying on the ground or having free-standing cap should be examined experimentally and numerically.

Numerical modelling of various types of structures constructed on tapered pile groups under seismic loading conditions such as earthquake loading, can lead to have a better insight into their response. In fact, due to the concentration of the material on the upper portions of these cone shaped piles, the induced base shear arising from the seismic loading might be greater comparing to the case of having cylindrical same volume pile group. Hence, push-over analysis is recommended for examining the drift of high-rise buildings constructed on tapered pile foundations.

Tapered piles have the ability to mobilize a portion of passive earth pressure coefficient adjacent to their shaft. Hence, when subjected to axial harmonic loadings such as machine foundation loading, these piles might provide more bearing capacity. However, conducting experimental or field tests under axial and lateral dynamic loading condition can be of great importance to prove the aforementioned presumption.

Effects of scouring on stiffness and damping coefficients of tapered piles have not been analysed whether analytically, experimentally or numerically. Because of the tapering angle, which causes a non-uniform material distribution along tapered piles

and due to the inclined body, the stiffness and damping parameters for these piles can change considerably, which need further analysis.

References

Abdlrahem, M.A. & El Naggar, M.H. 2020, 'Axial performance of micropile groups in cohesionless soil from full-scale tests', *Canadian Geotechnical Journal*, no. 999, pp. 1-19.

Almallah, A., El Naggar, H. & Sadeghian, P. 2020, 'Axial Behavior of Innovative Sand-Coated GFRP Piles in Cohesionless Soil', *International Journal of Geomechanics*, vol. 20, no. 10, p. 04020179.

ASCE, D.F.C. 1984, 'Practical Guidelines for the Selection, Design and Installation of Piles', *USA, ASCE Deep Foundation Committee*, vol. 5, p. 7.

Bakholdin, B. 1971, 'Bearing capacity of pyramidal piles', pp. 507-10.

Beaty, M.H. & Byrne, P.M., *UBCSAND constitutive model version 904aR*, University of British Columbia, 2011.

Bhushan, K. & Askari, S. 1984, 'Lateral-load tests on drilled pier foundations for solar plant heliostats', *Laterally Loaded Deep Foundations: Analysis and Performance*, ASTM International.

Bhushan, K. & Haley, S. 1980, 'Development of computer program using PY data from load test results for lateral load design of drilled piers', *Woodward-Clyde Consultants Professional Development Committee, San Francisco, Calif*, vol. 1183.

Bhushan, K., Lee, L.J. & Grime, D.B. 1981, 'Lateral load tests on drilled piers in sand', ASCE, pp. 114-31.

Bolin, H. 1941, 'The pile efficiency formula of the Uniform Building Code', *Building Standards Monthly*, vol. 10, no. 1, pp. 4-5.

Bowles, L.E. 1996, *Foundation analysis and design*, McGraw-Hill.

Brinkgreve, R., Swolfs, W. & Engine, E. 2002, 'Plaxis users manual', *Balkema, Rotterdam (The Neetherlands)*.

Brown, D.A., Morrison, C. & Reese, L.C. 1988, 'Lateral load behavior of pile group in sand', *Journal of Geotechnical Engineering*, vol. 114, no. 11, pp. 1261-76.

Bryden, C., Arjomandi, K. & Valsangkar, A. 2018a, 'Dynamic axial stiffness and damping parameters of tapered piles', *International Journal of Geomechanics*, vol. 18, no. 7, p. 06018014.

Bryden, C., Arjomandi, K. & Valsangkar, A. 2018b, 'Effect of material damping on the dynamic axial response of pile foundations'.

Bryden, C., Arjomandi, K. & Valsangkar, A. 2020, 'Dynamic Axial Response of Tapered Piles Including Material Damping', *Practice Periodical on Structural Design and Construction*, vol. 25, no. 2, p. 04020001.

Budhu, M. & Davies, T.G. 1987, 'Nonlinear analysis of laterality loaded piles in cohesionless soils', *Canadian Geotechnical Journal*, vol. 24, no. 2, pp. 289-96.

Byrne, P.M., Park, S.-S., Beaty, M., Sharp, M., Gonzalez, L. & Abdoun, T. 2004, 'Numerical modeling of liquefaction and comparison with centrifuge tests', *Canadian Geotechnical Journal*, vol. 41, no. 2, pp. 193-211.

Chellis, R.D. 1969, *Pile foundations.*, 2nd Ed edn, McGraw-Hill, Inc., New York, N.Y.

Committee, C.G.S.F. 1978, *Canadian foundation engineering manual*, Canadian Geotechnical Society.

D'Appolonia, E. & Hribar, J. 1963, 'Load transfer in a step-taper pile', *Journal of the Soil Mechanics and Foundations Division*, vol. 89, no. 6, pp. 57-80.

De Nicola, A. & Randolph, M.F. 1993, 'Tensile and compressive shaft capacity of piles in sand', *Journal of Geotechnical Engineering*, vol. 119, no. 12, pp. 1952-73.

Dehghanpoor, A. & Ghazavi, M. 2012, 'Response of tapered piles under lateral harmonic vibrations', *Int. J. of GEOMATE*, vol. 2, no. 2, p. S1.

Dougherty, J.J. 2017, *The Development of the TAPERTUBE® PILE, DFP Foundation Products, LLC*, viewed 19 December 2018, <http://www.pilelineonline.com/devtt.htm>.

Dutta, S. 1986, 'Influence of surface taper and shape of pile on ultimate load and uplift capacities', *Indian Geotechnical Journal*, vol. 16, pp. 167-80.

El-Marsafawi, H., Han, Y. & Novak, M. 1992, 'Dynamic experiments on two pile groups', *Journal of geotechnical engineering*, vol. 118, no. 4, pp. 576-92.

El Naggar, M.H. & Sakr, M. 2000, 'Evaluation of axial performance of tapered piles from centrifuge tests', *Canadian Geotechnical Journal*, vol. 37, no. 6, pp. 1295-308.

El Naggar, M.H. & Sakr, M. 2002, 'Cyclic response of axially loaded tapered piles', *International Journal of Physical Modelling in Geotechnics*, vol. 2, no. 4, pp. 01-12.

El Naggar, M.H. & Wei, J.Q. 1999a, 'Axial capacity of tapered piles established from model tests', *Canadian Geotechnical Journal*, vol. 36, no. 6, pp. 1185-94.

El Naggar, M.H. & Wei, J.Q. 1999b, 'Response of tapered piles subjected to lateral loading', *Canadian Geotechnical Journal*, vol. 36, no. 1, pp. 52-71.

El Naggar, M.H. & Wei, J.Q. 2000a, 'Cyclic response of axially loaded tapered piles', *Geotechnical Testing Journal*, vol. 23, no. 1, pp. 100-15.

El Naggar, M.H. & Wei, J.Q. 2000b, 'Uplift behaviour of tapered piles established from model tests', *Canadian Geotechnical Journal*, vol. 37, no. 1, pp. 56-74.

Elkasabgy, M. & El Naggar, M.H. 2013, 'Dynamic response of vertically loaded helical and driven steel piles', *Canadian Geotechnical Journal*, vol. 50, no. 5, pp. 521-35.

EN, B. 1997, '1 (2004). eurocode 7: Geotechnical design-part 1: General rules', *British Standards, UK*.

Fahmy, A. & El Naggar, M.H. 2017, 'Axial performance of helical tapered piles in sand', *Geotechnical and Geological Engineering*, vol. 35, no. 4, pp. 1549-76.

Fellenius, B. 2017, 'Basics of foundation design', Series Basics of foundation design Electronic Edition, <www.Fellenius.net>.

Fellenius, B.H. 1991, 'Pile foundations', *Foundation engineering handbook*, Springer, pp. 511-36.

Fellenius, B.H. & Altaee, A. 1999, 'Experimental study of axial behaviour of tapered piles: Discussion', *Canadian Geotechnical Journal*, vol. 36, no. 6, pp. 1202-3.

Fellenius, B.H., Brusey, W.G. & Pepe, F. 2000, 'Soil set-up, variable concrete modulus, and residual load for tapered instrumented piles in sand'Performance Confirmation of Constructed Geotechnical Facilities Amherst, Massachusetts, United States, pp. 98-114.

Fukushima, S. & Tatsuoka, F. 1984, 'Strength and deformation characteristics of saturated sand at extremely low pressures', *Soils and Foundations*, vol. 24, no. 4, pp. 30-48.

Ghazavi, M. 2000a, 'Lateral analysis of tapered piles subjected to earthquake loading and supporting lifelines', pp. 127-32.

Ghazavi, M. 2000b, 'Theoretical and experimental aspects of tapered piles subjected to static loads', vol. 1, pp. 84-92.

Ghazavi, M. 2003, 'Behaviour of tapered piles subjected to dynamic loads', vol. 7, pp. 469-76.

Ghazavi, M. 2006, 'Bearing Capacity of Tapered and Step-tapered Piles Subjected to Axial Compressive Loading, Proceedings of 7-th International Conference On Coastal, Ports & Marine Structures, KN Toosi University of Technology, Iran, Vol. 6'.

Ghazavi, M. 2007, 'Analysis of kinematic seismic response of tapered piles', *Geotechnical and Geological Engineering*, vol. 25, no. 1, p. 37.

Ghazavi, M. 2008, 'Response of tapered piles to axial harmonic loading', *Canadian geotechnical journal*, vol. 45, no. 11, pp. 1622-8.

Ghazavi, M., Ahmadi-Bidgoli, H. & Hashemolhosseini, H. 2003, 'Numerical studies of tapered piles subjected to axial harmonic vibrations', vol. 5, pp. 239-46.

Ghazavi, M., Barkhordari, K. & Mahbod, A. 2007, 'DYNAMIC ANALYSIS OF PILE DRIVING FROM VARIOUS HAMMERING LOCATIONS ALONG PILE SHAFT'.

Ghazavi, M. & Dehghanpour, A. 2010, 'Dynamic Analysis of Piles under Lateral Harmonic Vibration'.

Ghazavi, M. & Etaati, M. 2001, 'Analysis of tapered piles under axial loading using finite element method', pp. 443-9.

Gotman, A. 2000, 'Finite-element analysis of tapered piles under combined vertical and horizontal loadings', *Soil Mechanics and Foundation Engineering*, vol. 37, no. 1, pp. 5-12.

Gupta, P.S.K., Rajagopal, K. 2015, 'Review of research on taper and stepped piles', paper presented to the *The 6th International Geotechnical Symposium on Disaster Mitigation in Special Geoenvironmental Conditions Chennai*, India.

Han, K., Seo, M.J., Hong, W.-T. & Lee, J.-S. 2020, 'End-Bearing Capacity of Embedded Piles with Inclined-Base Plate: Laboratory Model Tests', *Journal of Geotechnical and Geoenvironmental Engineering*, vol. 146, no. 8, p. 04020063.

Han, Y. & Novak, M. 1988, 'Dynamic behaviour of single piles under strong harmonic excitation', *Canadian Geotechnical Journal*, vol. 25, no. 3, pp. 523-34.

Hanna, A.M., Morcous, G. & Helmy, M. 2004, 'Efficiency of pile groups installed in cohesionless soil using artificial neural networks', *Canadian Geotechnical Journal*, vol. 41, no. 6, pp. 1241-9.

Hataf, N. & Shafaghat, A. 2015a, 'Numerical comparison of bearing capacity of tapered pile groups using 3D FEM', *Geomechanics and Engineering*, vol. 9, no. 5, pp. 547-67.

Hataf, N. & Shafaghat, A. 2015b, 'Optimizing the bearing capacity of tapered piles in realistic scale using 3D finite element method', *Geotechnical and Geological Engineering*, vol. 33, no. 6, pp. 1465-73.

Horvath, J.S. & Trochalides, T. 2004, 'A half century of tapered-pile usage at the John F. Kennedy International Airport', paper presented to the *5th International Conference on Case Histories in Geotechnical Engineering.*, Missouri University of Science and Technology, USA.

Horvath, J.S., Trochalides, T., Burns, A. & Merjan, S. 2004a, 'Axial-compressive capacities of a new type of tapered steel pipe pile at the John F. Kennedy International Airport', paper presented to the *5th International Conference on Case Histories in Geotechnical Engineering.* , Missouri University of Science and Technology, USA.

Horvath, J.S., Trochalides, T., Burns, A. & Merjan, S. 2004b, 'A New Type of Tapered Steel Pipe Pile for Transportation Applications', *Geotechnical Engineering for Transportation Projects*, pp. 1299-308.

Horvath, J.S., Trochalides, T., Burns, A., Merjan, S. 2004a, 'A new analytical method for the axial-compressive static capacity of tapered driven piles in coarse-grain soil', paper presented to the *International e-Conference on Modern Trends in Geotechnical Engineering: Geotechnical Challenges and Solutions*, Missouri University of Science and Technology, USA.

Horvath, J.S., Trochalides, T., Burns, A., Merjan, S. 2004b, 'Tapered driven piles new directions for an old concept', paper presented to the *International e-Conference on Modern Trends in Geotechnical Engineering: Geotechnical Challenges and Solutions*, Missouri University of Science and Technology, USA.

Ismael, N.F. 2001, 'Axial load tests on bored piles and pile groups in cemented sands', *Journal of geotechnical and geoenvironmental engineering*, vol. 127, no. 9, pp. 766-73.

Ismael, N.F. 2003, 'Load tests on straight and step tapered bored piles in weakly cemented sand: Nabil F. Ismael', *Field Measurements in Geomechanics*, CRC Press, pp. 142-9.

Ismael, N.F. 2006, 'Analysis of Lateral Load Tests on Step Tapered Bored Piles in Calcareous Sands', *GeoCongress 2006: Geotechnical Engineering in the Information Technology Age*, pp. 1-6.

Ismael, N.F. 2009, 'Behavior of step tapered bored piles in sand under static lateral loading', *Journal of geotechnical and geoenvironmental engineering*, vol. 136, no. 5, pp. 669-76.

Jain, M., Rastogi, P. & Bhandari, R. 2013, 'Comparative Behavior of Tapered and Uniform Diameter Piles in Loose Sands', *Indian Jeotechnical Journal*, pp. 154-62.

Janbu, N. 1976, 'Static Bearing Capacity of Friction Piles', vol. 1.2, pp. 479-88.

Jiang, C., Zhang, Z. & He, J. 2020, 'Nonlinear analysis of combined loaded rigid piles in cohesionless soil slope', *Computers and Geotechnics*, vol. 117, p. 103225.

Kalourazi, A.F., Izadi, A. & Chenari, R.J. 2019, 'Seismic bearing capacity of shallow strip foundations in the vicinity of slopes using the lower bound finite element method', *Soils and Foundations*, vol. 59, no. 6, pp. 1891-905.

Kardani, N., Zhou, A., Nazem, M. & Shen, S.-L. 2020, 'Estimation of bearing capacity of piles in cohesionless soil using optimised machine learning approaches', *Geotechnical and Geological Engineering*, vol. 38, no. 2, pp. 2271-91.

Khan, M.K., El Naggar, M.H. & Elkasabgy, M. 2008, 'Compression testing and analysis of drilled concrete tapered piles in cohesive-frictional soil', *Canadian Geotechnical Journal*, vol. 45, no. 3, pp. 377-92.

Kishida, H. 1965, 'Bearing capacity of pile groups under eccentric loads in sand', *Proc. 6th ICSMFE, Montreal*, vol. 2, pp. 270-4.

Kodikara, J., Kong, K. & Haque, A. 2006, 'Numerical evaluation of side resistance of tapered piles in mudstone', vol. *Géotechnique,* 56, no. 7, pp. 505-10.

Kodikara, J.K. & Moore, I.D. 1993, 'Axial response of tapered piles in cohesive frictional ground', *Journal of Geotechnical Engineering*, vol. 119, no. 4, pp. 675-93.

Kong, G.Q., Yang, Q., Liu, H.L. & Liang, R.Y. 2013, 'Numerical study of a new belled wedge pile type under different loading modes', *European Journal of Environmental and Civil Engineering*, vol. 17, no. sup1, pp. s65-s82.

Kurian, N.P. & Srinivas, M.S. 1995, 'Studies on the behaviour of axially loaded tapered piles by the finite element method', *International journal for numerical and analytical methods in geomechanics*, vol. 19, no. 12, pp. 869-88.

Lade, P.V. & Bopp, P.A. 2005, 'Relative density effects on drained sand behavior at high pressures', *Journal of the Japanese Geotechnical Society: soils and foundation*, vol. 45, no. 1, pp. 1-13.

Lee, J., Paik, K., Kim, D. & Hwang, S. 2009, 'Estimation of axial load capacity for bored tapered piles using CPT results in sand', *Journal of geotechnical and geoenvironmental engineering*, vol. 135, no. 9, pp. 1285-94.

Lee, J.K., Jeong, S. & Kim, Y. 2018, 'Buckling of tapered friction piles in inhomogeneous soil', *Computers and Geotechnics*, vol. 97, pp. 1-6.

Lee, K.L. & Seed, H.B. 1967, 'Drained strength characteristics of sands', *Journal of Soil Mechanics & Foundations Div*, vol. 93, no. 6, pp. 117-41.

Liu, J., He, J., Wu, Y. & Yang, Q. 2012, 'Load transfer behaviour of a tapered rigid pile', vol. *Géotechnique,* 62, no. 7, p. 649.

Livneh, B. & El Naggar, M.H. 2008, 'Axial testing and numerical modeling of square shaft helical piles under compressive and tensile loading', *Canadian Geotechnical Journal*, vol. 45, no. 8, pp. 1142-55.

Mahmoud, M. & Burley, E. 1994, 'Lateral load capacity of single piles in sand', *Proceedings of the Institution of Civil Engineers-Geotechnical Engineering*, vol. 107, no. 3, pp. 155-62.

Majumder, M. & Chakraborty, D. 2018, 'Bearing capacity of tapered piles in clay under undrained condition', *International Journal of Geotechnical Engineering*, pp. 1-7.

Manandhar, S. & Yasufuku, N. 2012, 'Analytical model for the end-bearing capacity of tapered piles using cavity expansion theory', *Advances in Civil Engineering*, vol. 2012.

Manandhar, S. & Yasufuku, N. 2013, 'Vertical bearing capacity of tapered piles in sands using cavity expansion theory', *Soils and Foundations*, vol. 53, no. 6, pp. 853-67.

Manna, B. & Baidya, D. 2009, 'Vertical vibration of full-scale pile—analytical and experimental study', *Journal of geotechnical and geoenvironmental engineering*, vol. 135, no. 10, pp. 1452-61.

Mansur, C.I. & Kaufman, R.I. 1956, 'Pile Tests, Low-Sill Structures, Old River, La', *Journal of the Soil Mechanics and Foundations Division*, vol. 82, no. 4, pp. 1-33.

McVay, M., Casper, R. & Shang, T.-I. 1995, 'Lateral response of three-row groups in loose to dense sands at 3D and 5D pile spacing', *Journal of Geotechnical Engineering*, vol. 121, no. 5, pp. 436-41.

Meyer, B.J. & Reese, L.C. 1979, *Analysis of single piles under lateral loading*, Center for Highway Research, University of Texas at Austin TX.

Meyerhof, G., Sastry, V. & Yalcin, A. 1988, 'Lateral resistance and deflection of flexible piles', *Canadian Geotechnical Journal*, vol. 25, no. 3, pp. 511-22.

Meyerhof, G.G. 1963, 'Some recent research on the bearing capacity of foundations', *Canadian Geotechnical Journal*, vol. 1, no. 1, pp. 16-26.

Nordlund, R. 1963, 'Bearing capacity of piles in cohesionless soils', *Journal of the Soil Mechanics and Foundations Division*, vol. 89, no. 3, pp. 1-36.

Norris, G. 1986, 'Theoretically based BEF laterally loaded pile analysis', Navtes, pp. 361-86.

Novak, M. 1974, 'Dynamic stiffness and damping of piles', *Canadian Geotechnical Journal*, vol. 11, no. 4, pp. 574-98.

Novak, M. 1977, 'Vertical vibration of floating piles', *Journal of the Engineering Mechanics Division*, vol. 103, no. 1, pp. 153-68.

Novak, M. & Aboul-Ella, F. 1978, 'Impedance functions of piles in layered media', *Journal of the Engineering Mechanics Division*, vol. 104, no. 3, pp. 643-61.

Novak, M. & F. Grigg, R. 1976, 'Dynamic experiments with small pile foundations', *Canadian Geotechnical Journal*, vol. 13, no. 4, pp. 372-85.

Paik, K., Lee, J. & Kim, D. 2010, 'Axial response and bearing capacity of tapered piles in sandy soil', *Geotechnical Testing Journal*, vol. 34, no. 2, pp. 122-30.

Paik, K., Lee, J. & Kim, D. 2013, 'Calculation of the axial bearing capacity of tapered bored piles', *Proceedings of the Institution of Civil Engineers-Geotechnical Engineering*, vol. 166, no. 5, pp. 502-14.

PETAJA, J. 1981, *Experiences of Tapered Friction Piles*, IPT Foundation Consultants, Ltd, Helsinki, Finland.

Pise, P.J. 1984, 'Lateral response of free-head pile', *Journal of Geotechnical Engineering*, vol. 110, no. 12, pp. 1805-9.

Poulos, H.G. 1971, 'behavior of Laterally Loaded Piles: I-Single Piles. Journal of the Soil Mechanics and Foundations Division', vol. 97.

Poulos, H.G. 1979, 'Group factors for pile-deflection estimation', *Journal of Geotechnical and Geoenvironmental Engineering*, vol. 105, no. (ASCE 15032)

Poulos, H.G. 1982, 'Single pile response to cyclic lateral load', *Journal of Geotechnical and Geoenvironmental Engineering*, vol. 108, no. GT3.

Poulos, H.G. & Davis, E.H. 1980, *Pile foundation analysis and design*.

Puri, V. 1988, 'Observed and predicted natural frequency of a pile foundation'.

Randolph, M. 1994, 'Design methods for pile group and piled rafts', vol. 5, pp. 61-82.

Randolph, M.F. 1981, 'The response of flexible piles to lateral loading', *Geotechnique*, vol. 31, no. 2, pp. 247-59.

Rao, N.K. 2010, *Foundation design: theory and practice*, John Wiley & Sons.

Reddy, A.S. & Ramasamy, G. 1973, 'Analysis of an axially and laterally loaded tapered pile in sand', *Soils and Foundations*, vol. 13, no. 4, pp. 15-27.

Ruesta, P.F. & Townsend, F.C. 1997, 'Evaluation of laterally loaded pile group at Roosevelt Bridge', *Journal of Geotechnical and Geoenvironmental Engineering*, vol. 123, no. 12, pp. 1153-61.

Rybnikov, A. 1990, 'Experimental investigations of bearing capacity of bored-cast-in-place tapered piles', *Soil Mechanics and Foundation Engineering*, vol. 27, no. 2, pp. 48-52.

Saha, S. & Ghosh, D. 1986, 'Vertical vibration of tapered piles', *Journal of geotechnical engineering*, vol. 112, no. 3, pp. 290-302.

Sakr, M. & El Naggar, M.H. 2003, 'Centrifuge modeling of tapered piles in sand', *Geotechnical testing journal*, vol. 26, no. 1, pp. 22-35.

Sakr, M., El Naggar, M.H. & Nehdi, M. 2005, 'Lateral behaviour of composite tapered piles in dense sand', *Proceedings of the Institution of Civil Engineers-Geotechnical Engineering*, vol. 158, no. 3, pp. 145-57.

Sakr, M., Naggar, M.H.E. & Nehdi, M. 2004, 'Load transfer of fibre-reinforced polymer (FRP) composite tapered piles in dense sand', *Canadian Geotechnical Journal*, vol. 41, no. 1, pp. 70-88.

Sayed, S.M. & Bakeer, R.M. 1992, 'Efficiency formula for pile groups', *Journal of geotechnical engineering*, vol. 118, no. 2, pp. 278-99.

Shafaghat, A. 2013, 'Numerical comparison of bearing capacity of tapered and cylindrical pile groups with three-dimensional finite element method', Shiraz University, Iran.

Shafaghat, A. & Khabbaz, H. 2020a, 'Numerical Evaluation of Bearing Capacity of Step-Tapered Piles Using PY Curves Analysis', *Advancements in Geotechnical Engineering*, Springer, pp. 200-12.

Shafaghat, A. & Khabbaz, H. 2020b, 'Recent advances and past discoveries on tapered pile foundations: a review', *Geomechanics and Geoengineering*, vol. 15, pp. 1-30.

Shafaghat, A., Khabbaz, H., Moravej, S. & Shafaghat Ah 2018, 'Effect of Footing Shape on Bearing Capacity and Settlement of Closely Spaced Footings on Sandy Soil', *International Journal of Geotechnical and Geological Engineering*, vol. 12, no. 11, pp. 676-80.

Shibata, T., Yashima, A. & Kimura, M. 1989, 'Model tests and analyses of laterally loaded pile groups', *Soils and foundations*, vol. 29, no. 1, pp. 31-44.

Society, C.G. 1978, *Canadian foundation engineering manual*, Canadian Geotechnical Society.

Spronken, J.T. 1998, 'Bearing capacity of tapered piles', University of Calgary.

Tabaroei, A., Abrishami, S. & Hosseininia, E.S. 2017, 'Comparison between two different pluviation setups of sand specimens', *Journal of Materials in Civil Engineering*, vol. 29, no. 10, p. 04017157.

Tavasoli, O. & Ghazavi, M. 2018, 'Wave propagation and ground vibrations due to non-uniform cross-sections piles driving', *Computers and Geotechnics*, vol. 104, pp. 13-21.

Tavasoli, O. & Ghazavi, M. 2020, 'Effect of tapered and semi-tapered geometry on the offshore piles driving performance', *Ocean Engineering*, vol. 201, p. 107147.

Terzaghi, K. 1943, 'Theoretical Soil Mechanics. JohnWiley & Sons', *New York*, pp. 11-5.

Terzaghi, K., Peck, R.B. & Mesri, G. 1996, *Soil mechanics in engineering practice*, John Wiley & Sons.

Tuan, P. 2016a, 'A simplified formular for analysis group efficiency of piles in granular soil', *International Journal of Scientific & Engineering Research*, vol. 7, no. 7, pp. 15-21.

Tuan, P.A. 2016b, 'A simplified formular for analysis group efficiency of piles in granular soil', *International Journal of Scientific & Engineering Research*, vol. 7, no. 7, pp. 15-21.

Vali, R., Mehrinejad Khotbehsara, E., Saberian, M., Li, J., Mehrinejad, M. & Jahandari, S. 2019, 'A three-dimensional numerical comparison of bearing capacity and settlement of tapered and under-reamed piles', *International Journal of Geotechnical Engineering*, vol. 13, no. 3, pp. 236-48.

Vesic, A. 1980, 'Predicted behavior of piles and pile group at the Houston site'.

Vesic, A.S. 1967, 'A Study of Bearing Capacity of Deep Foundations', Final Report Project B-169 Engineering experiment station.

Vesic, A.S. 1977, 'Design of pile foundations', *NCHRP synthesis of highway practice*, no. 42.

Wei, J. & El Naggar, M.H. 1998, 'Experimental study of axial behaviour of tapered piles', *Canadian Geotechnical Journal*, vol. 35, no. 4, pp. 641-54.

Wei, J.Q. 1998, 'Experimental investigation of tapered piles', University of Western Ontario.

Wei, J.Q. & El Naggar, M.H. 1999, 'Experimental study of axial behaviour of tapered piles: Reply', *Canadian Geotechnical Journal*, vol. 36, no. 6, pp. 1204-5.

Wu, Y., Zhou, X., Gao, Y., Zhang, L. & Yang, J. 2019, 'Effect of soil variability on bearing capacity accounting for non-stationary characteristics of undrained shear strength', *Computers and Geotechnics*, vol. 110, pp. 199-210.

Xie, J. & Vaziri, H.H. 1991, 'Vertical vibration of nonuniform piles', *Journal of engineering mechanics*, vol. 117, no. 5, pp. 1105-18.

Xie, Y., Leshchinsky, B. & Han, J. 2019, 'Evaluation of bearing capacity on geosynthetic-reinforced soil structures considering multiple failure mechanisms', *Journal of Geotechnical and Geoenvironmental Engineering*, vol. 145, no. 9, p. 04019040.

Yang, S., Leshchinsky, B., Cui, K., Zhang, F. & Gao, Y. 2019, 'Unified approach toward evaluating bearing capacity of shallow foundations near slopes',

Journal of Geotechnical and Geoenvironmental Engineering, vol. 145, no. 12, p. 04019110.

Zhan, Y.-g., Wang, H. & Liu, F.-c. 2012, 'Numerical study on load capacity behavior of tapered pile foundations', *Electronic Journal of Geotechnical Engineering*, vol. 17, pp. 1969-80.

Zhao, Y.J., Stolarski, H.K. 1999, 'Stability of Pile Groups. Technical report documentation, No. MN/RC-31', University of Minnesota.

Zhou, H., Zheng, G., Yang, X., Li, T. & Yang, P. 2019, 'Ultimate seismic bearing capacities and failure mechanisms for strip footings placed adjacent to slopes', *Canadian Geotechnical Journal*, vol. 56, no. 11, pp. 1729-35.

Appendix A – Differentiations with respect to tapering angle

This appendix presents the differentiation of the axial bearing capacity of tapered pile (i.e. Equation 4.29) in an attempt to show the presence of optimum tapering angle and identifying the parameters impacting the optimum tapering angle. Hence, the derivation of Equation 4.29 with respect to tapering angle α can be written as follows:

$$\frac{\partial Q_T}{\partial \alpha} = \frac{\partial q_{bt}}{\partial \alpha} + \frac{\partial q_{sv}}{\partial \alpha} + \frac{\partial q_{st}}{\partial \alpha} \tag{A.1}$$

Then by solving the following equation, the optimum tapering angle can be achieved. Hence:

$$\frac{\partial q_{bt}}{\partial \alpha} + \frac{\partial q_{sv}}{\partial \alpha} + \frac{\partial q_{st}}{\partial \alpha} = 0 \tag{A.2}$$

Referring to Equations 4.15, 4.26 and 4.27 and by differentiating each component, Equations (A.3) to (A.5) can be obtained. For the sake of concise presentation, however, since these equations are long and complex, it has broken into smaller equations defined as f functions.

$$\left\{\frac{\partial q_{bt}}{\partial \alpha} = \frac{11}{7}\left(\gamma L tan(\phi) f_1 f_2 f_3 f_5^2 + \gamma L f_1 f_2 f_3 f_5 \left(L f_4 + \frac{L^2\, tan(\alpha) f_4}{3 f_6}\right)\right) + \frac{11}{14}\gamma\beta L e^{-\alpha\beta} f_1 f_2 f_5^2\right\} \tag{A.3}$$

$$\left\{\frac{\partial q_{sv}}{\partial \alpha} = -\frac{9}{17}\left(\gamma L^2\, tan(\alpha)\, f_1 f_2 f_3 \left(L f_4 + \frac{L^2\, tan(\alpha) f_4}{f_6}\right) + \gamma L^2 f_1 f_2 f_3 f_4 f_7 + \gamma\beta L^2 e^{-\alpha\beta}\, tan(\alpha)\, f_1 f_2 f_7\right) - \frac{22}{21}\gamma L^2\, tan(\alpha)\, tan(\alpha) f_1 f_2 f_3 f_7\right\} \tag{A.4}$$

$$\begin{cases} \frac{\partial q_{st}}{\partial \alpha} = \frac{22}{21}\Big(\gamma L^2\, tan(\alpha)\, tan(\delta)\, sec(\alpha)^2\, f_8 f_9 + \\ \qquad \frac{\gamma L^2 \zeta\, tan(\delta)\, sin(\phi)(sin(\phi)-3)\, sec(\alpha)^2 f_9 f_{11}}{(sin(\phi)-1) f_{13}}\Big) + \\ \qquad \frac{9}{17}\Big(\frac{\gamma L^3 \tan(\delta)\Big(f_{12}+\sqrt{3}Ltan(\alpha)\Big)\big(1+tan(\alpha)^2\big)\sec(\alpha)^2 f_8}{f_{12}}\Big) \end{cases} \quad \text{(A.5)}$$

$$f_1 = e^{tan(\phi)(2\alpha+\frac{10\pi\psi}{9})} \quad \text{(A.6)}$$

$$f_2 = \left(tan(\phi) + \sqrt{1 + tan(\phi)^2}\right)^2 \quad \text{(A.7)}$$

$$f_3 = \lambda - e^{-\alpha\beta} \quad \text{(A.8)}$$

$$f_4 = 1 + tan(\alpha)^2 \quad \text{(A.9)}$$

$$f_5 = Ltan(\alpha) - f_6 \quad \text{(A.10)}$$

$$f_6 = \sqrt{4{r_c}^2 - \frac{L^2 tan(\alpha)^2}{3}} \quad \text{(A.11)}$$

$$f_7 = Ltan(\alpha) - 3f_6 \quad \text{(A.12)}$$

$$f_8 = sin(\phi) + \frac{sin(\phi)(sin(\phi)-3)}{f_{10}} - \frac{f_4 sin(\phi)(sin(\phi)-3)}{f_{10}} - 1 \quad \text{(A.13)}$$

$$f_9 = Ltan(\alpha) - \sqrt{3} f_{12} \quad \text{(A.14)}$$

$$f_{10} = (sin(\phi) - 1) f_{13} \quad \text{(A.15)}$$

$$f_{11} = e^{-2\alpha\zeta} \quad \text{(A.16)}$$

$$f_{12} = \sqrt{12{r_c}^2 - L^2\, tan(\alpha)^2} \quad \text{(A.17)}$$

$$f_{13} = e^{-\pi\zeta} - 1 \tag{A.18}$$

Due to the complexity of the above equations to establish the optimum tapering angle analytically, Equations A.3 to A.5 were developed and solved numerically using MATHEMATICA and MATLAB software packages.

Appendix B – Developed MATLAB codes

Generated code for obtaining the bearing capacity components of tapered bored piles in sand as well as optimum tapering angle:

```
Clear
clc
close all
%-------------------------------------------------------------------------
% Importing the data from the excel file containing the optimum tapering
angles obtained through the numerical modelling for the comparison
Aopt_Plaxis=xlsread('Ed3-Optimum tapering angles','B4:E6');
 %-------------------------------------------------------------------------
%% The code can be used based on the requested input data from user
% syms G A L D K RC
%w2=input ('Enter the number of variations for pile tapering angle?=');
% RC1=input ('Enter the value for the radius of counterpart same volume
cylindrical pile (meter)? RC=');
% A2=input ('Enter the tapering angle of the pile? Alpha=');
% %K1=input ('Enter the value for the lateral earth pressure coefficient
of the soil? K=');
% G1=input ('Enter the value for the soil density (kN/m^3)? G=');
% L1=input ('Enter the value for length of pile (meter)? L=');
% phi1=input ('Enter the value for the soil internal friction angle
(degree)? phi=');
% Dr1=input ('Enter the value for soil relative density (percent)? Dr=');
%K1=input ('Enter the value for the lateral earth pressure coefficient of
the soil? K=');
%-------------------------------------------------------------------------
syms phiz Jz Az RCz Dz Lz Gz Drz
% w3z is the maximum tapering angle can be defined based on the referenced
cylindrical pile (having the same volume)
w3z=atan(3^0.5*RCz./Lz);
% K0z is the at rest lateral earth pressure coefficient
K0z=1-sin(phiz);
% Kpz is the passive lateral earth pressure coefficient
Kpz=(1+sin(phiz))./(1-sin(phiz));
% Ktz is the taper coefficient which applies to the earth pressure
coefficients (Jz is a model parameter)
```

```
Ktz=[-1.*((0.2*Kpz-K0z)./(1-exp(-3.*Jz.*2*w3z))).*exp(-
6.*Jz.*Az)+K0z+((0.2*Kpz-K0z)./(1-exp(-3.*Jz.*2*w3z)))];
% Nqc0z is the bearing capacity factor for cylindrical piles based on
Janbu (1976)
Nqc0z=(((tan(phiz)+(1+(tan(phiz)).^2).^0.5).^2.*exp(2*(((100).*Drz.*pi/180
)+0).*tan(phiz))));
% Nqz is the bearing capacity factor for tapered piles (Az is tapering
angle)
Nqz=[(2-0.2*exp(-100.*Az))].*Nqc0z/1.8;
% SVRz is the Shaft Vertical Resistance component of tapered piles
SVRz =-(3537115888337719*Gz.*Lz.^2.*Nqz.*tan(Az).*(Lz.*tan(Az) -
3.*(4*RCz.^2 - (Lz.^2.*(tan(Az)).^2)/3).^(1/2)))./6755399441055744;
% BRTz is the Base Resistance component of piles
BRTz =(3537115888337719*Gz.*Lz.*Nqz.*(Lz.*tan(Az) - (4*RCz.^2 -
(Lz.^2.*(tan(Az)).^2)./3).^(1/2)).^2)./4503599627370496;
% FRTz is the Frictional Resistance component of piles
FRTz =-(3537115888337719*Gz.*Ktz.*Lz.^2.*tan(Dz).*(Lz.*tan(Az) -
3*(4*RCz.^2 -
(Lz.^2.*(tan(Az)).^2)./3).^(1/2)))./(6755399441055744*cos(Az).^2);
QTz=SVRz+BRTz+FRTz.*cos(Az);
diffrentiation1z=diff(QTz,Az);
DIFz=simplify(diffrentiation1z,'Steps',50);
%--------------------------------------------------------------------------
% G1 is the soil unit weight
G1=17;
% RC2 is the radius of the reference cylindrical pile
RC2=0.75;
% L1 is the pile length
L1=15;
% n is the number of piles
n=1;
M=ones(3,4);
M2=ones(3,4);
Manalytical=sym('Manalytical',[3,4]);
psi1=1;
% J is the model parameter which has been calibrated
J=100/6;
% flag=0;
% while flag~=1;
for ii=-1:1;
    phi3=32;
    phi4=phi3+(ii+1)^2*3^(ii+1)*2^(-1*ii*(ii+1));
    psi3=1;
    psi4=phi4-30;
```

```
for i=1:4;
    RC1=RC2./(i)
    phi1=phi4
    phicv1=30;
    psi1=psi4;
if  phi1==32;
    psi1=phi1-31;
end
% Dr1 is the soil relative density and Dr3 is the model parameter defined
by Janbu (1976)
if  phi1==32;
    Dr1=0.3;
    Dr3=0.6;
elseif phi1==35;
    Dr1=0.4;
    Dr3=0.65;
    elseif phi1==41;
    Dr1=1;
    Dr3=0.75;
end
% w and w3 are the maximum tapering angles of piles corresponding to the
reference cylindrical pile (in degrees and radians, respectively)
w=(180/pi)*atan(3^0.5*RC1./L1);
w3=atan(3^0.5*RC1./L1);
% A2 is the tapering angles increments by 0.05 degree, as a vector
A2=0:0.05:w;
w1=size(A2);
w2=w1(1,2);
G=sym('G',[1,w2]);
N=sym('N',[1,w2]);
A=sym('A',[1,w2]);
L=sym('L',[1,w2]);
D=sym('D',[1,w2]);
K=sym('K',[1,w2]);
RC=sym('RC',[1,w2]);
Dr=sym('Dr',[1,w2]);
if min(RC1)*min(L1)*min(G1)*min(phi1)==0;
    clear
    clc
    ANS='Restart'
elseif RC1>0
    if max(size(RC1))==1;
    RC1=RC1*ones([1,w2]);
    end
```

```
    if max(size(A2))==1;
        A2=A2*ones([1,w2]);
    end
    if max(size(G1))==1;
        G1=G1*ones([1,w2]);
    end
    if max(size(L1))==1;
        L1=L1*ones([1,w2]);
    end
    if max(size(phi1))==1;
        phi1=phi1.*ones([1,w2]);
    end
     if max(size(phicv1))==1;
         phicv1=phicv1.*ones([1,w2]);
     end
    if max(size(psi1))==1;
        psi1=psi1.*ones([1,w2]);
    end
     J1=J*ones([1,w2]);
    LD=max(L1./(2.*RC1));
    A1=pi*A2./180;
    phi2=pi.*phi1./180;
    phicv2=pi.*phicv1./180;
    psi2=pi.*psi1./180;
    D1=(0.7).*phi2;
    if max(size(D1))==1;
        D1=D1.*ones([1,w2]);
end
%-------------------------------------------------------------------------
    K0=1-sin(phi2);
    if max(size(K0))==1;
        K0=K0.*ones([1,w2]);
    end
    Kp=(1+sin(phi2))./(1-sin(phi2));
    if max(size(Kp))==1;
    Kp=Kp.*ones([1,w2]);
    end
Kt=[-1.*((0.2*Kp-K0)./(1-exp(-3.*J.*2*w3))).*exp(-6.*J.*A1)+K0+((0.2*Kp-
K0)./(1-exp(-3.*J.*2*w3)))];
    if max(size(Kt))==1;
       Kt=Kt*ones([1,w2]);
    end
    Kc=min(Kt)*ones([1,w2]);
%-------------------------------------------------------------------------
```

```
% In case the bearing capacity factor proposed by Terzaghi () is required
%     a1=cos((A2)*pi/180);
%     a2=exp((tan(phi1*pi/180)).*(360-4*phi1-4*(-1)*A2)*pi/180);
%     a4=tan((45-0.5*phi1)*pi/180);
%     a3=tan((45-0.5*phi1)*pi/180);
%     a4=cos((phi1+A2)*pi/180);
%     Nqc0=[(a1.*a2)./(a3.*a4)].*(2-exp(-1000.*A1))
%     Nq=((exp(pi+2*A2*pi/180)).*(tan((45+phi1./2+A2)*pi/180)).^2);
%     1.*[((1+2.*A1.*Kt)./3).*(3+A1)./(1+2.*A1)];
%-------------------------------------------------------------------------
Nqc0=(((tan(phi2)+(1+(tan(phi2)).^2).^0.5).^2.*exp(2*(((100).*Dr3.*pi/180)
+0).*tan(phi2))));
Nq=[(2-0.2*exp(-100.*A1))].*Nqc0/1.8;
Nqc=Nq(1,1);
Nqc=Nqc*ones([1,w2]);
%-------------------------------------------------------------------------
SVR =-(3537115888337719*G.*L.^2.*N.*tan(A).*(L.*tan(A) - 3.*(4*RC.^2 -
(L.^2.*(tan(A)).^2)/3).^(1/2)))/6755399441055744;
SVRx=eval(subs(SVR,[G,L,N,RC,A],[G1,L1,Nq,RC1,A1]));
BRT =(3537115888337719*G.*L.*N.*(L.*tan(A) - (4*RC.^2 -
(L.^2.*(tan(A)).^2)./3).^(1/2)).^2)./4503599627370496;
BRTx=eval(subs(BRT,[G,L,N,RC,A],[G1,L1,Nq,RC1,A1]));
FRT =-(3537115888337719*G.*K.*L.^2.*tan(D).*(L.*tan(A) - 3*(4*RC.^2 -
(L.^2.*(tan(A)).^2)./3).^(1/2)))./(6755399441055744*cos(A).^2);
FRTx=eval(subs(FRT,[G,L,RC,D,K,A],[G1,L1,RC1,D1,Kt,A1]))
BRC =(3537115888337719*G.*L.*N.*RC.^2)./1125899906842624;
BRCx=eval(subs(BRC,[G,L,N,RC],[G1,L1,Nqc,RC1]));
FRC =(3537115888337719*G.*K.*L.^2.*RC.*tan(D))/1125899906842624;
FRCx=eval(subs(FRC,[G,L,RC,D,K],[G1,L1,RC1,D1,Kc]));
DIFx1=subs(DIFz,[phiz,Jz,RCz,Dz,Lz,Gz,Drz],[phi2(1,1),J1(1,1),RC1(1,1),D1(
1,1),L1(1,1),G1(1,1),Dr3(1,1)]);
QT=(SVRx+BRTx+FRTx.*cos(A1));
QC=BRCx+FRCx;
Ratio=(SVRx+BRTx+FRTx.*cos(A1))./(BRCx+FRCx);
%-------------------------------------------------------------------------
syms z;
P1=polyfit(A2,QT,4);
QTeq=P1(1,1).*z.^4+P1(1,2).*z.^3+P1(1,3).*z.^2+P1(1,4).*z.^1+P1(1,5);
q3=diff(QTeq,z);
q4=eval(simplify(solve(q3==0, z,'maxdegree',3,'Real',true),'steps',50));
q5=min(q4);
M(ii+2,i)=q5.*M(ii+2,i);
Manalytical(ii+2,i)=DIFx1;
q6=(vpasolve(Manalytical(ii+2,i)==0, Az));
```

```
q6=min(q6);
q6=(180./pi).*q6
M2(ii+2,i)=q6.*M2(ii+2,i);
errorNumerical=Aopt_Plaxis-M;
%-------------------------------------------------------------------------
figure('Position',[100,100,800,600])
subplot(2,2,1)
plot(A2,SVRx)
subplot(2,2,2)
plot(A2,BRTx)
hold on;
subplot(2,2,2)
plot(A2,BRCx)
% hold off;
subplot(2,2,3)
plot(A2,FRTx.*cos(A1))
hold on;
subplot(2,2,3)
plot(A2,FRCx)
% hold off;
subplot(2,2,4)
plot(A2,QT)
hold on;
subplot(2,2,4)
plot(A2,QC)
% hold off;
end
end
end
M2
M
errorNumerical;
ERR=abs(abs(max(max(errorNumerical)))+abs(min(min(errorNumerical))));
%-------------------------------------------------------------------------
```

Generated code based on double-tangential method to obtain the bearing capacity of piles based on p-y curve:

```
%-------------------------------------------------------------------------
%% Double tangent to obtain the bearing capacity of piles based on p-y curve
%-------------------------------------------------------------------------
clc, clear
%% Input data
AB=xlsread('Cylindrical-groups-p-y');
ABS=size(AB);
ABS1=ABS(1,2);
odd=1:2:ABS1;
even=2:2:ABS1;
Q=AB(:,even);
S=AB(:,odd);
a=[1,1];
ABS2=ABS1/2;
aa=ones(1,ABS2);
for ii=1:ABS2
QQ=Q(:,ii);
SS=S(:,ii);
for i=1:119
if isnan(QQ(i,1));isnan(SS(i,1));
QQ(i,1)=0;SS(i,1)=0;
end
end
Qx1=size(QQ);
Qx2=Qx1(1,1);
Qx3=Qx2-3;
Qx4=Qx2-2;
Qx6=QQ(Qx2,1);
Sx1=size(SS);
Sx2=Sx1(1,1);
Sx3=Sx2-3;
Sx4=Sx2-2;
Sx6=SS(Sx2,1);
while Qx6<0.000001
Qx2=Qx2-1;
Sx2=Sx2-1;
Qx3=Qx2-3;
Qx4=Qx2-2;
Sx3=Sx2-3;
Sx4=Sx2-2;
```

```
Qx6=QQ(Qx2,1);
Sx6=SS(Sx2,1);
C=[SS(Qx3,1),QQ(Qx3,1)];
D=[SS(Qx4,1),QQ(Qx4,1)];
A=[SS(2,1),QQ(2,1)];
B=[SS(3,1),QQ(3,1)];
end
m1=(A(1,2)-B(1,2))/(A(1,1)-B(1,1));
m2=(C(1,2)-D(1,2))/(C(1,1)-D(1,1));
L1=[m1 A(1,2)-m1*A(1,1)];
L2=[m2 C(1,2)-m2*C(1,1)];
U=[1 -m1;1 -m2];
T=[L1(1,2);L2(1,2)];
AAA=U\T;
AAA=AAA';
BB=AAA.*a;
F=BB(1,1);
aa(1,ii)=F.*aa(1,ii);
end
display (aa)
%-------------------------------------------------------------------------
```

Generated code for obtaining the pile group efficiency considering the tapering effect:

```
%-------------------------------------------------------------------------
% Find the pile group efficiency considering the tapering effect
%-------------------------------------------------------------------------

clear
clc
close all
G1=17;
RC2=0.75;
L1=15;
n=1;
M=ones(3,4);
M2=ones(3,4);
Eff=ones(3,4);
Manalytical=sym('Manalytical',[3,4]);
psi1=1;
J=100/6;
for i=1:1;
RC1=RC2./(i)
end
phi1=32;
Dr1=0.3;
Dr3=0.6;
G1=17;
L1=15;
w=(180/pi)*atan(3^0.5*RC1./L1);
w3=atan(3^0.5*RC1./L1);
A2=0;
w1=size(A2);
w2=w1(1,2);
G=sym('G',[1,w2]);
N=sym('N',[1,w2]);
A=sym('A',[1,w2]);
L=sym('L',[1,w2]);
D=sym('D',[1,w2]);
K=sym('K',[1,w2]);
RC=sym('RC',[1,w2]);
Dr=sym('Dr',[1,w2]);
if max(size(RC1))==1;
RC1=RC1*ones([1,w2]);
end
```

```
if max(size(A2))==1;
A2=A2*ones([1,w2]);
end
if max(size(G1))==1;
G1=G1*ones([1,w2]);
end
if max(size(L1))==1;
L1=L1*ones([1,w2]);
end
if max(size(phi1))==1;
phi1=phi1.*ones([1,w2]);
end
phi2=pi.*phi1./180;
J1=J*ones([1,w2]);
LD=max(L1./(2.*RC1));
A1=pi*A2./180;
D1=(0.7).*phi2;
if max(size(D1))==1;
D1=D1.*ones([1,w2]);
end
%-------------------------------------------------------------------------
K0=1-sin(phi2);
if max(size(K0))==1;
K0=K0.*ones([1,w2]);
end
Kp=(1+sin(phi2))./(1-sin(phi2));
if max(size(Kp))==1;
Kp=Kp.*ones([1,w2]);
end
Kt=[-1.*((0.2*Kp-K0)./(1-exp(-3.*J.*2*w3))).*exp(-6.*J.*A1)+K0+((0.2*Kp-
K0)./(1-exp(-3.*J.*2*w3)))];
if max(size(Kt))==1;
Kt=Kt*ones([1,w2]);
end
Kc=min(Kt)*ones([1,w2]);
%-------------------------------------------------------------------------
Nqc0=(((tan(phi2)+(1+(tan(phi2)).^2).^0.5).^2.*exp(2*(((100).*Dr3.*pi/180)
+0).*tan(phi2))));
Nq=[(2-0.2*exp(-100.*A1))].*Nqc0/1.8;
Nqc=Nq(1,1);
Nqc=Nqc*ones([1,w2]);
SVR=-(3537115888337719*G.*L.^2.*N.*tan(A).*(L.*tan(A)    -    3.*(4*RC.^2    -
(L.^2.*(tan(A)).^2)/3).^(1/2)))/6755399441055744;
SVRx=eval(subs(SVR,[G,L,N,RC,A],[G1,L1,Nq,RC1,A1]));
```

```
BRT=(3537115888337719*G.*L.*N.*(L.*tan(A)        -        (4*RC.^2        -
(L.^2.*(tan(A)).^2)./3).^(1/2)).^2)./4503599627370496;
BRTx=eval(subs(BRT,[G,L,N,RC,A],[G1,L1,Nq,RC1,A1]));
FRT=-(3537115888337719*G.*K.*L.^2.*tan(D).*(L.*tan(A)    -    3*(4*RC.^2    -
(L.^2.*(tan(A)).^2)./3).^(1/2))./(6755399441055744*cos(A).^2);
FRTx=eval(subs(FRT,[G,L,RC,D,K,A],[G1,L1,RC1,D1,Kt,A1]));
BRC =(3537115888337719*G.*L.*N.*RC.^2)./1125899906842624;
BRCx=eval(subs(BRC,[G,L,N,RC],[G1,L1,Nqc,RC1]));
FRC =(3537115888337719*G.*K.*L.^2.*RC.*tan(D))/1125899906842624;
FRCx=eval(subs(FRC,[G,L,RC,D,K],[G1,L1,RC1,D1,Kc]));
Az,'maxdegree',3,'Real',true),'steps',50)));
QT=(SVRx+BRTx+FRTx.*cos(A1));
QT2=(SVRx+BRTx+FRTx);
QC=BRCx+FRCx;
Ratio=(SVRx+BRTx+FRTx.*cos(A1))./(BRCx+FRCx);
%-------------------------------------------------------------------------
% Efficiencies
D_ave=(4.*RC1.^2-(1/3).*(L1.^2).*(tan(A1)).^2).^0.5;
D_top=D_ave+L1.*(tan(A1));
D_bot=D_ave-L1.*(tan(A1));
m=3; n=3;
sf1=2:0.5:10;
S=D_top.*sf1;
IF_K=0.35;
Eff_1=2.*(((m-1).*S+D_ave)+((n-1).*S+D_ave))./(pi.*m.*n.*D_ave.*cos(A1))
Eff_2=4.*(((m-1).*S+D_bot).*((n-1).*S+D_bot))./((pi.*m.*n.*D_top.^2))
Friction_factor=FRTx./QT2;
Base_factor=(SVRx)./QT2;
Eff_friction=1-(Friction_factor).*(1-Eff_1.*IF_K)-(Base_factor).*(1-
Eff_2.*IF_K)
Eff_base_component=(Base_factor).*(1-Eff_2.*IF_K)
Eff_friction_component=(Friction_factor).*(1-Eff_1.*IF_K)
%-------------------------------------------------------------------------
```